PROCEEDINGS

OF

SIXTEENTH DEFENSE CONFERENCE ON NONDESTRUCTIVE TESTING

26 - 28 SEPTEMBER 1967

DEPARTMENT OF DEFENSE
PLASTICS TECHNICAL EVALUATION CENTER
PICATINNY ARSENAL, DOVER, N. J.

UNITED STATES NAVAL ORDNANCE LABORATORY
WHITE OAK, MARYLAND

*MSG DI4 DROLS PROCESSING-LAST INPUT IGNORED

-- 1 OF 4
-- ***DTIC DOES NOT HAVE THIS ITEM***
-- 1 - AD NUMBER: D423153
-- 5 - CORPORATE AUTHOR: NAVAL ORDNANCE LAB WHITE OAK MD
-- 6 - UNCLASSIFIED TITLE: PROCEEDINGS OF THE SIXTEENTH DEFENSE
-- CONFERENCE ON NONDESTRUCTIVE TESTING.
--11 - REPORT DATE: SEP 26, 1967
--12 - PAGINATION: 267P
--20 - REPORT CLASSIFICATION: UNCLASSIFIED
--21 - SUPPLEMENTARY NOTE: PROCEEDINGS: '16TH DEFENSE CONFERENCE ON
-- NONDESTRUCTIVE TESTING', 26-28 SEP 67, U.S. NAVAL ORDNANCE
-- LABORATORY, WHITE OAK, SILVER SPRING, MARYLAND. (SEE PL-26885 - PL-
-- 26886).
--22 - LIMITATIONS (ALPHA): APPROVED FOR PUBLIC RELEASE; DISTRIBUTION
-- UNLIMITED. AVAILABILITY: U.S. NAVAL ORDNANCE LAB., WHITE OAK,
-- SILVER SPRING, MARYLAND 20910.
--33 - LIMITATION CODES: 1

-- END Y FOR NEXT ACCESSION END
111111
Alt-Z FOR HELP3 ANSI 3 HDX 3 3 LOG CLOSED 3 PRINT OFF 3 PARITY

PROCEEDINGS OF THE

SIXTEENTH DEFENSE CONFERENCE ON NONDESTRUCTIVE TESTING

26, 27 and 28 September 1967

U. S. NAVAL ORDNANCE LABORATORY
White Oak, Silver Spring, Maryland

FOREWORD

It has been a pleasure for NOL(WO) to host the Sixteenth Defense Conference on Nondestructive Testing. Meetings such as this permit open discussion of problems and their solutions, thereby enabling each of us to benefit from the experience of others. Through the years these conferences have stimulated the initiation of research and developmental projects, have provided an open forum for early discussion of research work through information papers, and have offered a means of direct contact through the distribution list.

This Conference was successful through the cooperative efforts of many persons. I acknowledge with thanks the contributions made by the members of the Steering Committee, The Staff of the NOL X-ray Laboratory - D. Polansky, L. V. Burt, C. H. Dyer, W. R. Maddy, J. Somers and R. A. Youshaw - and my secretary, Mrs. Headlee.

E. L. Criscuolo

E. L. CRISCUOLO
Host Chairman

PURPOSE OF DEFENSE CONFERENCE ON NONDESTRUCTIVE TESTING

SCOPE

The coordination of the development and the application of nondestructive methods for the testing and inspection of materials and assemblies for the Department of Defense.

OBJECTIVES

1. To provide for an effective dissemination of information pertaining to nondestructive methods and applications among members and their respective establishments in the Department of Defense.

2. To provide for the utilization of the knowledge, skills and experiences of specialists in the various branches of the Department of Defense for the attack and solution of problems within the Military establishment.

3. To encourage (wherever applicable) uniform practices in the application of nondestructive testing methods.

FUNCTIONS

1. Development of a common report and information distribution list. (Emphasis on individuals rather than on organizations).

2. Development and distribution of a current bibliography of defense establishments and/or contractors' reports, going back at least to 1946.

3. Development and distribution of abstracts of present and projected programs (Research, Development and Engineering).

4. Compilation and distribution of useful information such as location, work specialties, staff and facilities of:

   a. Government laboratories or other installations active in the development and utilization of nondestructive testing methods.

   b. Commercial laboratories or installations active in the field of interest.

   c. Consultants and Contractors active in the field of interest.

5. Evaluation of problems and proposed solutions in conference. The steps which are likely to be taken are:

a. Analysis of the problem in terms of design, engineering, production, inspection and testing history. Such an analysis may be partial before presentation, but should be as complete as possible before specific solutions are detailed.

b. Presentation of problem to conference as a whole or conference panel qualified in nondestructive testing inspection.

c. Liaison between the group in which the problem arises and those qualified, as indicated by conference discussion, to provide assistance in the solution. (Once liaison is effected, the two groups proceed without channeling through the conference).

d. Report to conference (for the record) the degree of success of the approach taken. If a solution has been reached, the formulation of requirements should be presented.

ORGANIZATION

1. Members - Employees of the Defense Establishment concerned with nondestructive testing, inspection, or evaluation, having confidential security clearance.

2. Officers - A secretarial board of not less than three, or not more than seven, who shall be elected yearly by a majority of the conference. This group will serve to receive and transmit information, to act as a steering group, and will elect one of their number as chairman (formerly executive secretary).

3. Meetings - The conference shall meet at least once a year at various establishments, as agreed upon between representatives of the establishment and the steering group. The presiding officer at such meetings shall be the conference member whose establishment is acting as host.

LOCATIONS AND DATES OF PREVIOUS CONFERENCES

Organizational Meeting	3-4 Oct 1951	Watertown Arsenal Watertown, Massachusetts
2nd Conference	23-24 Jan 1952	Frankford Arsenal Philadelphia, Pennsylvania
3rd Conference	19-20 Nov 1952	U.S. Naval Gun Factory Washington, D. C.
4th Conference	17-18 Mar 1954	Army Res. & Dev. Labs Fort Belvoir, Virginia
5th Conference	16-17 Mar 1955	Naval Ordnance Plant Indianapolis, Indiana
6th Conference	9-10 Apr 1956	Detroit Arsenal Centerline, Michigan
7th Conference	19-20 Feb 1957	U. S.Naval Ordnance Test Sta. China Lake, California
8th Conference	4-5 Dec 1957	SAAMA, Kelly Air Force Base, Texas
9th Conference	15-16 Oct 1958	Army Ballistics Missile Agency Redstone Arsenal, Alabama
10th Conference	6-7 Oct 1959	Naval Air Material Center Philadelphia, Pennsylvania
11th Conference	13-15 Sep 1960	OCAMA, Tinker Air Force Base, Oklahoma
12th Conference	28-30 Aug 1961	Army Natick Laboratories Natick, Massachusetts
13th Conference	25-27 Sep 1962	Naval Ammunition Depot Concord, California
14th Conference	25-27 Aug 1964	Robins Air Force Base, Georgia
15th Conference	4-6 Oct 1966	U.S. Army Materials Res. Agency Watertown, Massachusetts

12484

TABLE OF CONTENTS

TABLE OF CONTENTS (Continued)

TABLE OF CONTENTS (Continued)

CHAIRMAN'S COMMENTS -

I take this opportunity to thank all the members of the Steering Committee for all their help in getting the 16th Conference ready. I also extend my thanks to the Problem Coordinators and Technical Consultants, who made very real contributions to the conference.

Also important to the success of the Conference were the excellent arrangements provided by our hosts. On behalf of the Conference I extend a hearty thanks.

Finally of course, my thanks to the people who came. The lively floor discussions on the problems and papers showed that everybody came to contribute. I hope that everyone was able to take back something - a new idea, a new bit of information. I know of one man who brought a problem in personnel certification. There were people at the Conference who were able to help him, and he returned to California with his problem solved. This is an example of the intangible benefits of a conference of this type; the opportunity for people to talk things over, to share knowledge and acquire information aside from that offered by the program.

In conclusion, I congratulate David Gamache on his election to the chairmanship of the steering committee for the 17th Conference. Every chairman expects to do better than the last. I wish Dave all success.

Stephen D. Hart

1967 Steering Committee

Stephen D. Hart, Chairman, U. S. Naval Research Laboratory

Lt. Col. W. F. Bennett, Kelly Air Force Base, Texas

Ernest H. Rodgers, Army Materials & Mechanics Research Agency

John G. Turbitt, Naval Torpedo Station, Keyport, Washington

James Peale, Warner Robins Air Force Base, Georgia

David Gamache, Army Tank-Automotive Command

David M. Moses, Defense Supply Agency, Washington

E. L. Criscuolo, Naval Ordnance Laboratory, Silver Spring, Md.

Problem Coordinators

James A. Holloway, Physicist, Processing and NDT Branch (MAMN)
Air Force Materials Laboratory, Wright-Patterson AFB, Ohio

Robert L. Huddleston, Chief, Materials Evaluation Section
STEAP-DS-EP, U.S. Army Development & Proof Services,
Aberdeen Proving Ground, Maryland

Eugene Ashton, Aerospace Engineer, Naval Plant Representative
Office, Lockheed Missile & Space Company, Sunnyvale, California

Maurice J. Curtis, Staff Engineer, Code 5503, Naval Weapons
Center, China Lake, California

Michael Stellabotte, Physical Metallurgist, Code MAMM,
Naval Air Development Center, Johnsville, Warminster, Pa.

William H. Baer, Senior Metallurgist, U. S. Army Mobility
Equipment Research & Development Center, Fort Belvoir, Va.

Bernard Boisvert, AFLC NDI Program Manager, Hq. SAAMA(SANTEP)
Kelly Air Force Base, Texas

Technical Consultants

Radiography - B. J. Brunty, Supervisory Inspector (Metals)
Head, Test Operation Section, NWS, Concord, Cal.

Eddy Current- Harold P. Hatch, Physicist, U. S. Army Materials &
Mechanics Research Center, Watertown, Massachusetts

Ultrasonics - Donald Gallagher, Materials Treatment Processes
Inspection Specialist, San Francisco Bay Naval
Shipyard, Vallejo, California

Penetrants & Magnetic Particle - E. W. McKelvey, Materials Engineering Technician,
Air Force Materials Laboratory, Wright-Patterson
Air Force Base, Ohio

REPORT ON BUSINESS MEETINGS

Tuesday Meeting

Two suggestions of the Steering Committee were proposed and accepted:

1. To change the title of the Executive Secretary to Chairman.

2. To change the method of electing the chairman. He will now be elected by the Steering Committee from among the four who have served two years. This will have the effect of increasing the Steering Committee to nine members starting next year. The change is not effective this year because none of the two year members could accept it if elected.

New business was deferred to Wednesday.

Wednesday Meeting

The first item of business was election of four new members of the steering committee. The Chairman had appointed Messrs. Goldspiel, Kress, Boisvert and Britt as a nominating committee. The new members elected were:

Air Force -	Captain Elee W. Tyler, Randolph AFB
Army -	Emmett Barnes, Picatinny Arsenal
Navy -	M. J. Curtis, Naval Weapons Center, China Lake
DSA -	John Britt, DCAS, Boston

A motion was made by Mr. Moses "To form a committee composed of members from the services and DSA to effect a standardization of documents relating to inspection certification and qualification of procedures, equipment and personnel." In discussion, a question was raised as to the authority of the Conference to undertake this task. A further question was raised as to whether the Conference ought to engage in policy matters. It was also pointed out that something along this line was already being worked on at AMMRAC. In spite of these contrary arguments the feeling was that this is important enough to try to accomplish something, and the motion passed. Mr. Moses accepted chairmanship and will proceed to form the committee.

Thursday Meeting

It was announced that David Gamache of Army Tank-Automotive Command was elected chairman of the Steering Committee for the 17th Conference.

STEERING COMMITTEE FOR 1968

David Gamache, Chairman
AMSTA-QED
Army Tank-Automotive Command
Michigan Army Missile Plant
Warren, Michigan 48090

Autovon 925-2548
Comm. 313 264-1100 x2548

David M. Moses
DSAH-FQES
Defense Supply Agency
Cameron Station
Alexandria, Virginia 22314

Autovon 224-7141
Comm. 202 974-7141

James Peale
WRMA(WRNEAS)
Warner Robins Air Force Base
Georgia 31093

Autovon 468- 6274
Comm. 912 926- 6274

John G. Turbitt, Code 3345
Naval Torpedo Station
Keyport, Washington 98345

Autovon 554-1510 x8874
Comm. 206 478-8874/8873

Captain Elee W. Tyler
ATC(ATMME-A)
Randolph Air Force Base
Texas 78248

Autovon 360-4663/3663

John F. Britt
Defense Contract Admin. Services
666 Summer Street
Boston, Massachusetts 02210

Autovon 744-1698

Emmett Barnes
SMUFA N1-5, Bldg. 908
Picatinny Arsenal
Dover, New Jersey 07801

Autovon 552-1530 x3964

Maurice J. Curtis, Code 5503
U. S. Naval Weapons Center
China Lake, California 93555

Autovon 898-1700
Comm. 714 3752-1411
ext 71720/72802

CONFERENCE HIGHLIGHT

On Wednesday, September 27, the Aerospace Presentations Team from the Air University, Maxwell Air Force Base, Alabama brought to the Conference their presentation of "The United States Space Program".

This team consisted of Lt. Col. James S. Wall, Major Robert K. Potter and Captain David L. Frederick. They highlighted the activities of the space program, presenting a fast-moving, articulate picture of what has been done, is being done, and will be done in space. Many of the color slides and movie clips used to illustrate the presentation were made in space.

In addition to the Conference attendees, this program was opened to the employees of the Naval Ordnance Laboratory. A capacity crowd filled the Auditorium and the presentation was well received.

We are indebted to Lt. Col. Bennett of the Steering Committee for arranging for the visit of this team.

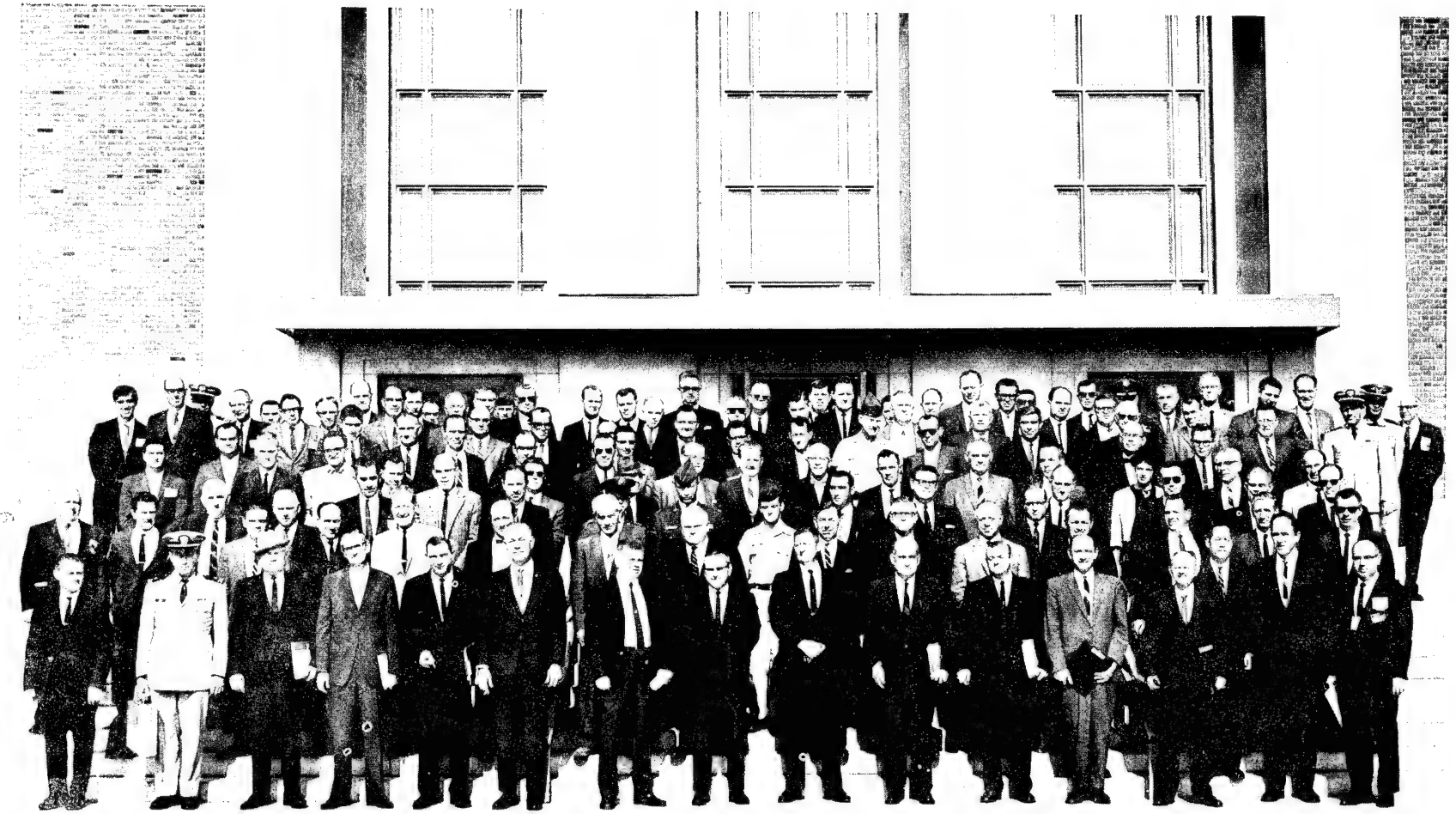

ATTENDEES
16th DOD CONFERENCE ON NDT
Total Registration 182

Attendance
Tuesday - 165
Wednesday - 161
Thursday - 135

PROBLEM No. 1

NONDESTRUCTIVE TESTING OF THE STRUCTURAL INTEGRITY OF ELECTRO-MECHANICAL VARIABLE DEPTH SONAR TOWCABLES

Naval Applied Sciences Laboratory
Brooklyn, New York

By S. Goldspiel

Name of Product to be Evaluated - Electro-mechanical towcable used for variable depth sonar.

Kind of Material Involved - The towcable consists of an electrical core surrounded by two helical layers of galvanized (improved plow) steel wires with reversed lay.

Type of Process Involved in Manufacture of Product - This is not applicable, as product to be tested in completed form as used on Naval vessels.

Design of Product - Figures 1 and 2 show the cable with and without fairing. The length of an average cable is 600 ft. Normally it is payed out and retrieved by means of a drum. For expediency during NDT, the portion under test will have the fairing removed.

Quantity Involved in NDT Evaluation - In the immediate future the quantity involves field inspection of cables in about 200 ships. Each ship, in turn, has about 600 feet of cable, which are at the present replaced on an arbitrary basis every 18 months. Testing may actually be confined to about 50 feet of free portion of the cable, which receives the severest flexural and fatigue loading. If the method proves successful, it may be carried over to testing of similar cables, which have no electrical conductors and are used for towing. In that case, the numbers involved would be greater by several orders of magnitude.

Kind of Quality Characteristic to be Evaluated - It is desired to detect a single broken strand in the inner (second) layer of the armor wire.

Magnitude of Quality Characteristic Needed for Satisfactory Services - In actual practice it has been learned that when a cable fails a number of strands are usually broken in the inner helical armor. However, it is considered that for absolute safety, failure of a single strand should be detectable at the earliest possible time.

Basis of Judging Reliability - Reliability of method will be judged on its ability for early detection of failure of a single strand. This would help arrest catastrophic failures, which entail loss of sonar transducers.

Urgency - Loss of gear at sea interferes with use of sonar equipment, which may be of urgent importance. In addition, arbitrary replacement on basis of time in service is wasteful. Replacement of good cables entails a loss of about $15,000 (exclusive of labor). On the other hand, breakage in use produces a loss of about $50,000 for the electronic gear involved.

Feasibility of Redesign - This has not been considered, because there are too many installations of the type described in service.

Present Inspection Method - Visual inspection on outer layer of armor wire is made at monthly intervals. These are not very effective because failures generally start with inner (second) annular layer wires. Conventional radiography or fluoroscopy, though applicable for diagnostic checking during method development, is not practical under field conditions. Limited attempts to use Eddy Current methods were unsuccessful because field perturbations from inner layer wire failures are shielded by the relatively heavy outer layer wires. Optimization of frequencies and use of null methods to increase signal to noise ratios have as yet not been tried.

Limitations of Test Equipment - The main features should be portability and ruggedness for use on actual ships near the cable installation. In addition, it should be readily operable by normal nontechnical Naval shipboard personnel. No serious space limitations are anticipated if, as is expected, a decision will be made to remove fairing from the portion of cable under test.

Security Classification - Unclassified.

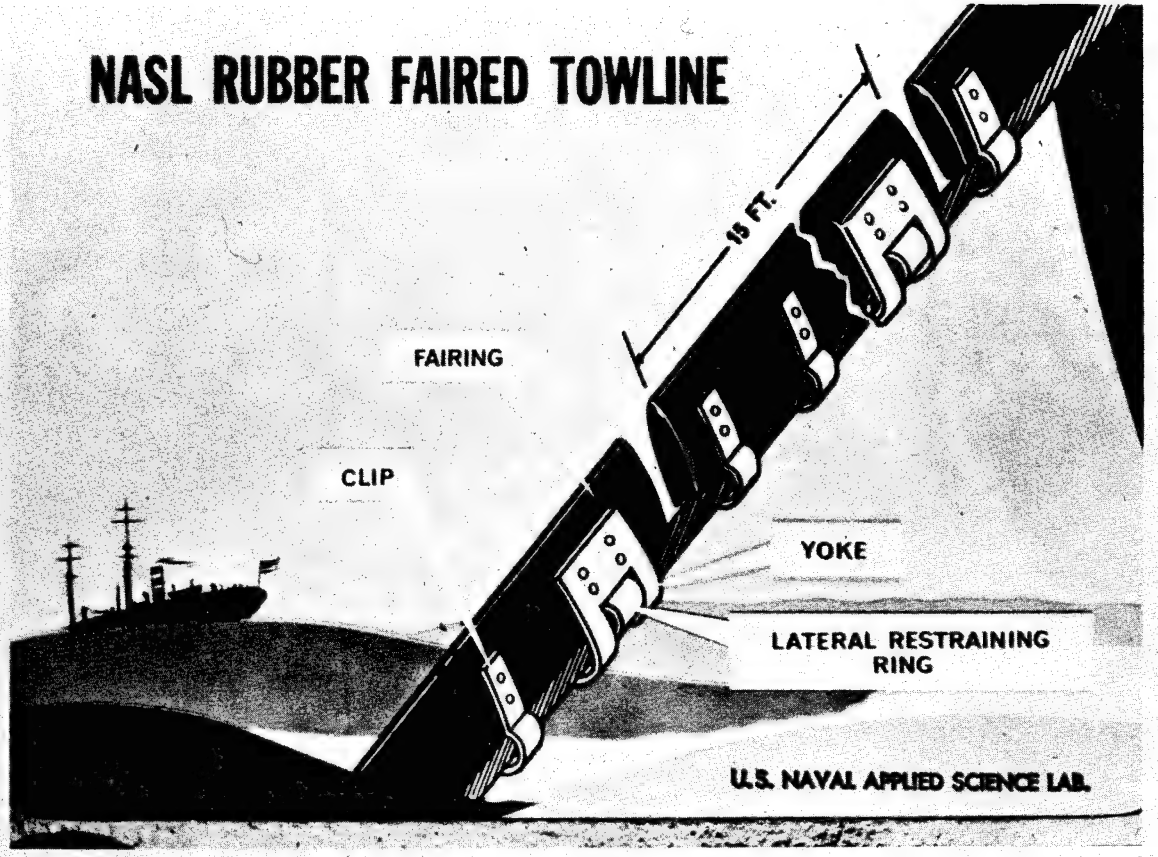

FIGURE 1. OVERALL VIEW OF ELECTRO-MECHANICAL VARIABLE DEPTH TOWCABLE

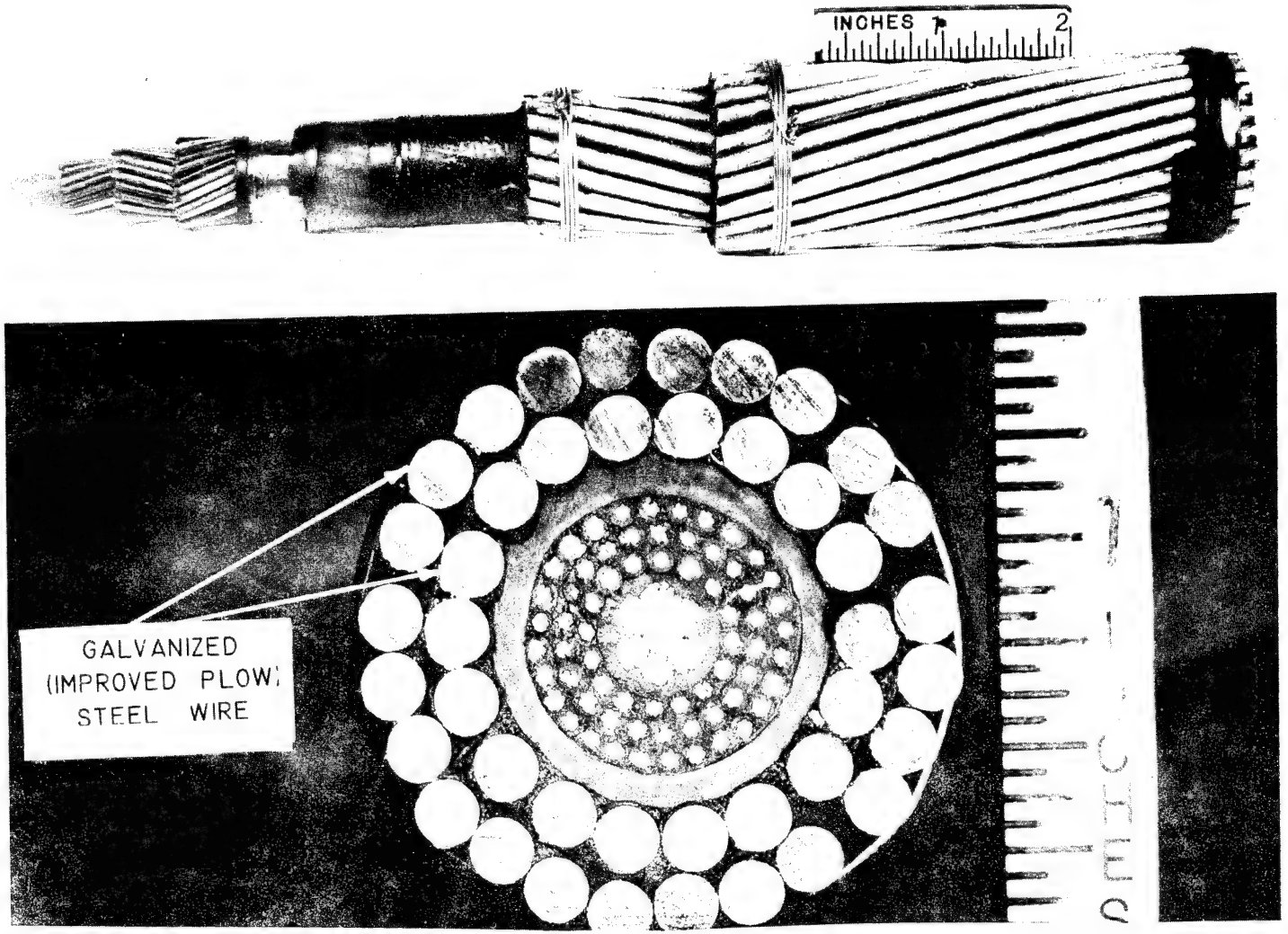

FIGURE 2. DETAIL VIEWS OF $1\frac{3}{8}$" O.D. TOWCABLE. TOP: LONGITUDINAL; BOTTOM: CROSS SECTION.

SUMMARY REPORT OF PROBLEM NO. 1

NONDESTRUCTIVE TESTING OF THE STRUCTURAL INTEGRITY OF ELECTRO-MECHANICAL VARIABLE DEPTH SONAR TOWCABLES

James A. Holloway
Problem Coordinator

The technical consultants and meeting attendees after considering the problem, i.e., the detection of a single broken strand in the second layer of the galvanized "plow steel" cable, suggest a magnetic method as the most promising solution. The technique would involve either a single or double coil encircling the cable which would be used to establish a magnetic field in the cable. An additional coil would be required to monitor the magnetic flux in the cable. Preliminary laboratory experiments should establish the sensitivity of the technique for detecting a broken strand as well as the perturbations of the magnetic field caused by cable lay up. If this latter factor is significant, a dual detector coil may be a solution for compensating the change in the signal caused by cable lay up.

Supplemental information concerning this technique should be available from Republic Steel Corporation who use a magnetic NDT method to inspect bridge cable. It is further suggested that tangential radiography be used to verify any indications obtained with the magnetic technique. An additional suggestion which may be applicable is to reverse the attachment ends of the cable. Since failure is located within 50 feet of the sonar gear, reversing attachment ends periodically should increase the life of the cables. Also attachment of an additional cable from the sonar gear to a point several feet past the area of failure would save the gear when the cable breaks.

PROBLEM No. 2

DEVELOPMENT OF ACCEPTANCE STANDARDS FOR SHIP PROPELLERS AND NDT INSPECTION METHODS FOR DETERMINATION OF ACCEPTABILITY TO THE STANDARDS DEVELOPED

Presented by

Joseph E. Costello
Quality Assurance Division, Philadelphia Naval Shipyard

Introduction

A ship propeller is a device which converts torque into thrust. When torque is transmitted to the propeller, its configuration creates a region of high pressure in back of itself and a region of low pressures in front of itself. Consequently, the ship is pulled and pushed forward through the water by the differential in pressure of these two regions. This thrust is transmitted to the ship itself through the fillet areas at the root of each propeller blade into the hub and finally through the propeller shafting to the ship. It is readily apparent that the principal region of stress in this drive train is in the propeller blade-fillet areas adjacent to the hub. In practice, it has been found that the catastrophic failures which have occurred have been principally in this area of the propeller. A careful study of failures and near-failures of propellers by various naval facilities has shown the failure mode to be fatigue failure. The origins of these failures have been found to be due to both surface and internal discontinuities present in the propeller castings. At the present time the nondestructive testing of naval propellers is limited to a surface inspection employing the liquid penetrant test method.

Problem

A nondestructive test method is needed which will determine the presence of internal discontinuities in bronze propellers and acceptance standards need to be developed to evaluate test findings. The materials presently being used in casting naval propellers are manganese bronze, nickel magnanese bronze, nickel aluminum bronze and manganese nickel aluminum bronze or Superston. Magnetic particle inspection cannot be used on these nonferrous materials; in addition, magnetic particle inspection is still basically a surface inspection method. Liquid penetrant inspections do a very adequate job of revealing discontinuities in propeller

surfaces but there is no positive correlation between surface indications and propeller failures due to internal discontinuities. In the radiography of these hub to blade fillet areas the complexities of casting geometry, constantly changing thicknesses, high density and large thickness of material require that high energy X- or gamma ray sources be used in lengthy exposures of very limited coverage. These many interrelated factors reduce sensitivity of the radiographic inspection method to the point which makes it impossible to produce the desired results, i.e., discontinuities small in size, but significant in terms of fatigue failure, cannot be revealed. At the present time the ultrasonic test method has not been able to surmount the many problems inherent in attempting to test these fillet areas. The principal areas of difficulty are large grain size of the material and the curving geometry of the surfaces.

SUMMARY REPORT OF PROBLEM NO. 2

DEVELOPMENT OF ACCEPTANCE STANDARDS FOR SHIP PROPELLERS AND NDT INSPECTION METHODS FOR DETERMINATION OF ACCEPTABILITY TO THE STANDARDS DEVELOPED

Robert L. Huddleston
Problem Coordinator

This problem concerns the need for NDT methods which will detect defects which have caused the failure of ship propellers. These are cast bronze propellers, inspected for surface defects by liquid penetrant inspection under MIL-STD-278. Service failures have been found to result from fatigue cracking, originating at near-surface and other internal discontinuities.

Attempts to inspect the propellers by NDT techniques in addition to liquid penetrant have not proven successful. Cobalt 60 has been used for radiography without success, apparently because of the test item shape and mass. Shape and most particularly metallurgical inhomogeneity have defeated attempts to use ultrasonics.

At a meeting with the technical consultants, the problem was discussed in more detail. It was suggested that etching might remove "flowed-over" metal and enable the liquid penetrant to better locate surface porosity. The presenter did not think that surface finish requirements would permit this.

It was concluded that MIL-STD-278 is not adequate to insure the interior soundness required to prevent propeller failures. The inspection requirements should be re-evaluated in the light of failure experience.

It was further concluded that supervoltage radiography should permit adequate inspection of the propellers for interior soundness. Such equipment is available at a number of Government and industrial facilities.

It was also suggested that shot peening be considered for improving fatigue resistance at the surface.

As problem coordinator, I wish to thank Mr. Costello for his presentation and Mr. Summey for his contributions during the discussion. I also wish to thank the technical consultants and all those who contributed to the discussion.

PROBLEM No. 3

STEAM STOP VALVES

Presented by

Ralph P. Petraglia
Inspection Specialist
Boston Naval Shipyard

Problem

Steam boilers on naval vessels are required to undergo a hydrostatic test to prove the tightness of all parts of the boiler, including valves, gaskets and fittings. In performing this test, the water used is at the same temperature as the boiler and fireroom, and maintained at this temperature throughout the test. It is required that a water pressure equal to the design pressure be employed. A drop of 1.5 percent of test pressure in one hour is the maximum acceptable leakage.

During the test, all joints are inspected and visible leaks are remedied. If necessary, boiler tubes are re-rolled in the tube sheet. After correction of visible leaks in these accessible areas, any further losses of pressure are caused by leaky stop valves connected to the boiler. The problem is to ascertain which of the valves is at fault and in need of repair or overhaul. Since six or more valves are involved in a boiler, it would be costly to remove all valves when only one may be the actual leaker. The valves are welded into the piping system, and removal is an expensive procedure.

The valves in question are conventional gate valves. Leakage of water past the internal valve seat may be the result of wear, corrosion, or mechanical misfit. Since the leakage flow is usually only a slow internal trickle, the problem of detecting the leakage by external means is a challenging one.

Most of these valves are of the 3" to 5" size, and have a heavy steel body approximately 1" thick. Composition is usually 2-1/4% Chromium - 1% Molybdenum, but in some instances plain carbon steel is employed. See Figures 1 and 2.

Sonic pick-up devices have been tried without success to detect the internal flow past the valve seat.

The device used did not possess sufficient sensitivity to detect the internal flow.

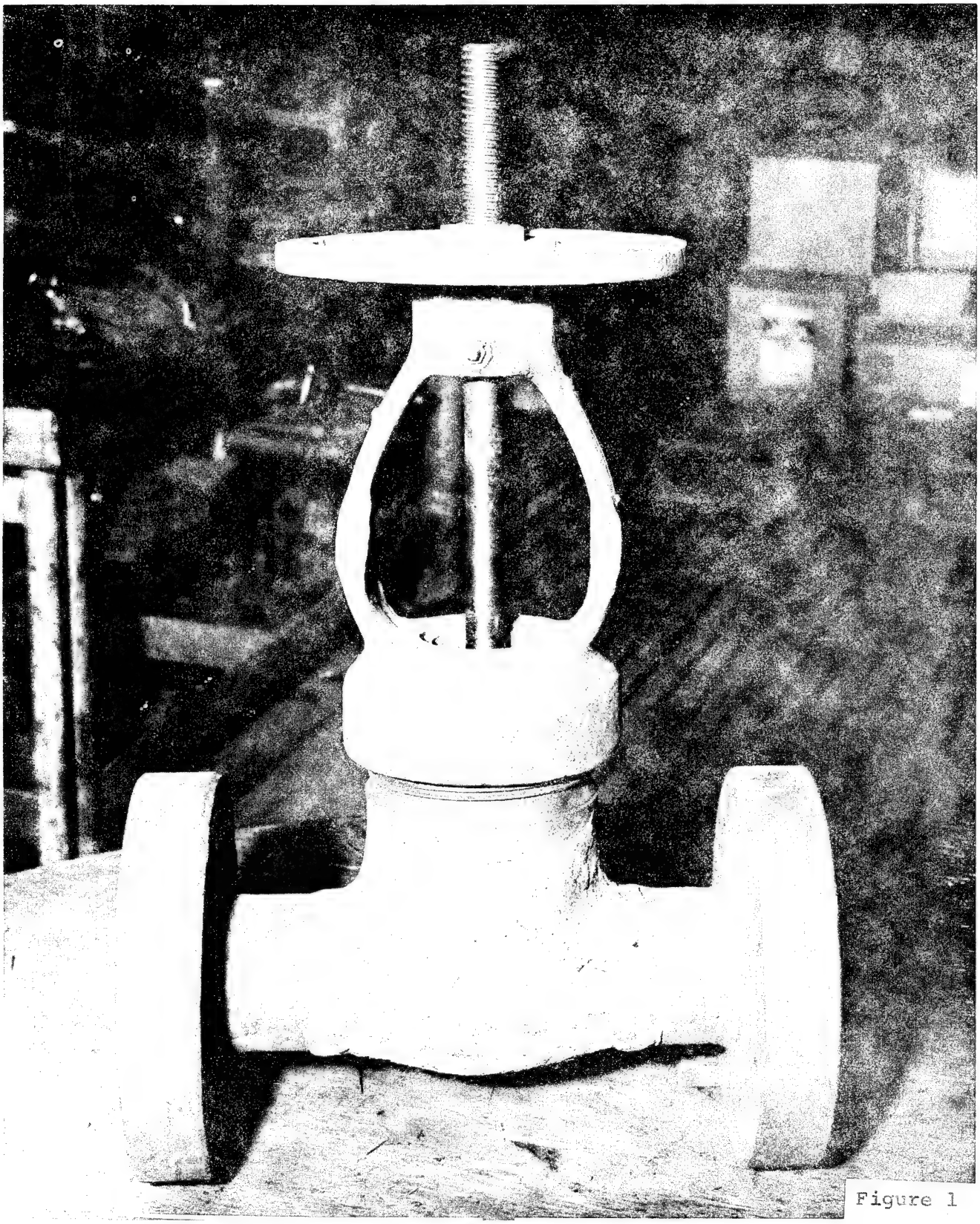

Figure 1

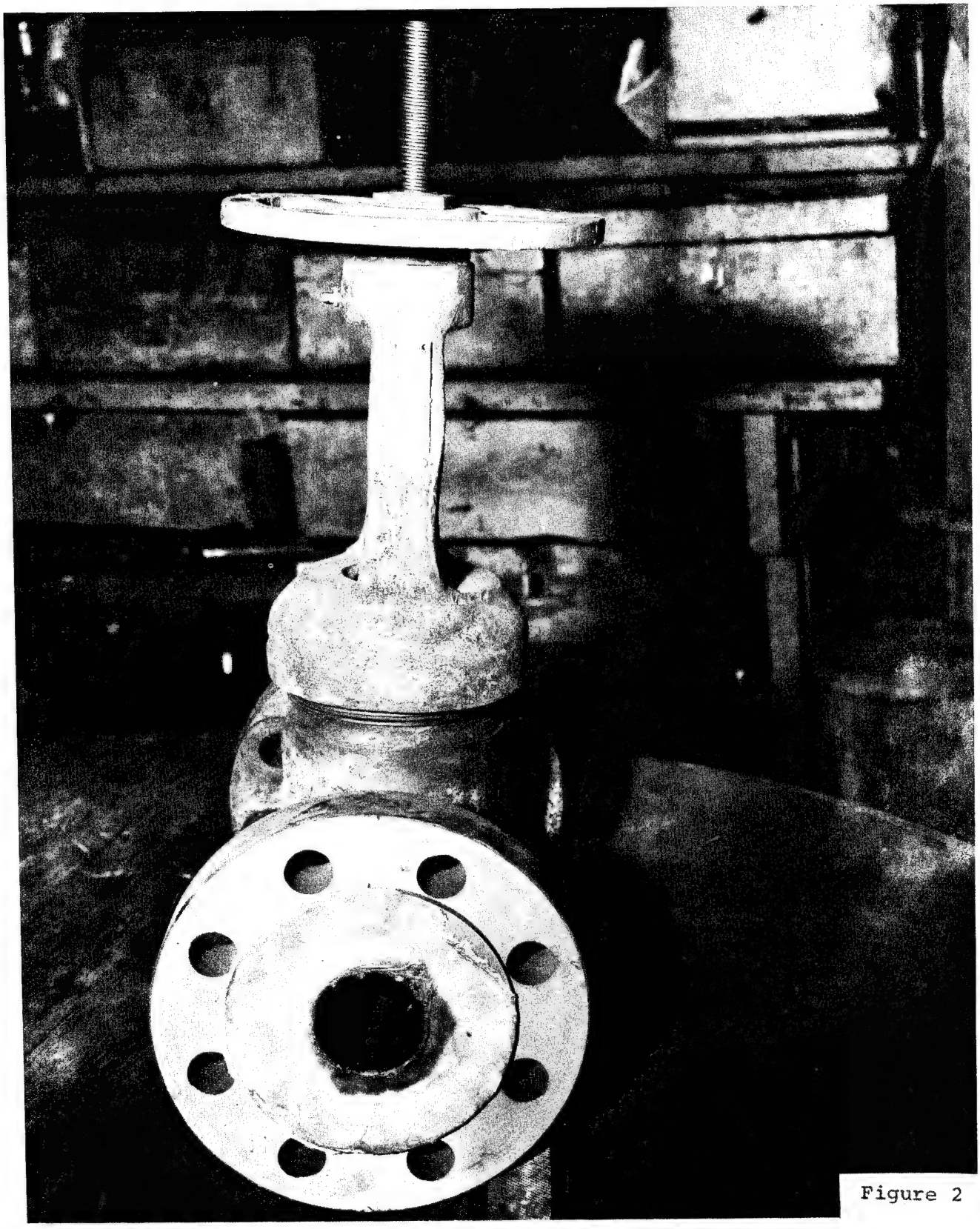

Figure 2

SUMMARY REPORT OF PROBLEM NO. 3

STEAM STOP VALVES

Eugene Ashton
Problem Coordinator

On the face of it, the problem is very simple: Find the leaking valve in a set of eight during hydrotest of a boiler. The difficulty arises in that only a very slight leak (1-1/2% pressure drop in one hour) can be tolerated. Working pressure is 1500 psi. Valves are 3-5" in diameter with 1" to 1-1/4" walls. Mr. Petraglia reported that sonic pickups had been tried without success. Ultrasonics had also been tried unsuccessfully. Radiography has been successful in detecting the puddle that forms downstream during leakage, but it is too expensive. At present the defective valve is found by replacing them one by one until leakage stops. As the valves are welded in place this is also an expensive operation.

Of the many suggestions made from the floor, the following were considered by the panel to be the most promising:

a. Try chilling an area immediately downstream and observe the thaw-out characteristic.

b. Try sonic (or low ultrasonic) detection again, using a highly amplified detector.

c. Introduce a gas, such as air, and detect sonically.

d. Use x-radiation through-transmission gauging.

e. Use ultrasonic flaw detection system before and after pressurizing to detect puddling.

f. Remove only the valve bonnet rather than the entire valve for inspection.

PROBLEM No. 4

FAILURE OF ADHESIVE-BONDED ALUMINUM HONEYCOMB PANELS

Presented by
John G. Gurtowski
Naval Air Systems Command

Problem

Aluminum, adhesive-bonded aircraft honeycomb failures have been a continuing problem. The incidence of failures is increasing even apart from F-4 troubles which have involved persistent failures on a large scale. It appears reasonable to conclude that demands of high performance aircraft, in more critical applications, may be pushing to the limit the honeycomb state-of-art as practiced and that deficiencies or selection of materials employed, fabrication, quality control, design and testing are becoming significant factors, tending to limit the usefulness of bonded honeycomb as a structural material. The relative importance of these various factors and their individual contributions to the problem are difficult to assess, due to lack of basic information as to failure causes. Investigations conducted to date have not provided the necessary information, partly because of the inability to resolve the question of structural adequacy or isolate it from materials considerations. Also, product improvement efforts are hampered by lack of information on structural requirements and lack of reliable nondestructive test procedures for determining the stresses that develop in the adhesive when the panels are subjected to mechanical loading (compressive, tension, shear, etc.), to thermal cycling and for predicting the useful life of new panels in service.

Enclosures 1 through 9 are partial examples of in-service failures of bonded honeycomb panels.

Enclosure 1

Enclosure 2

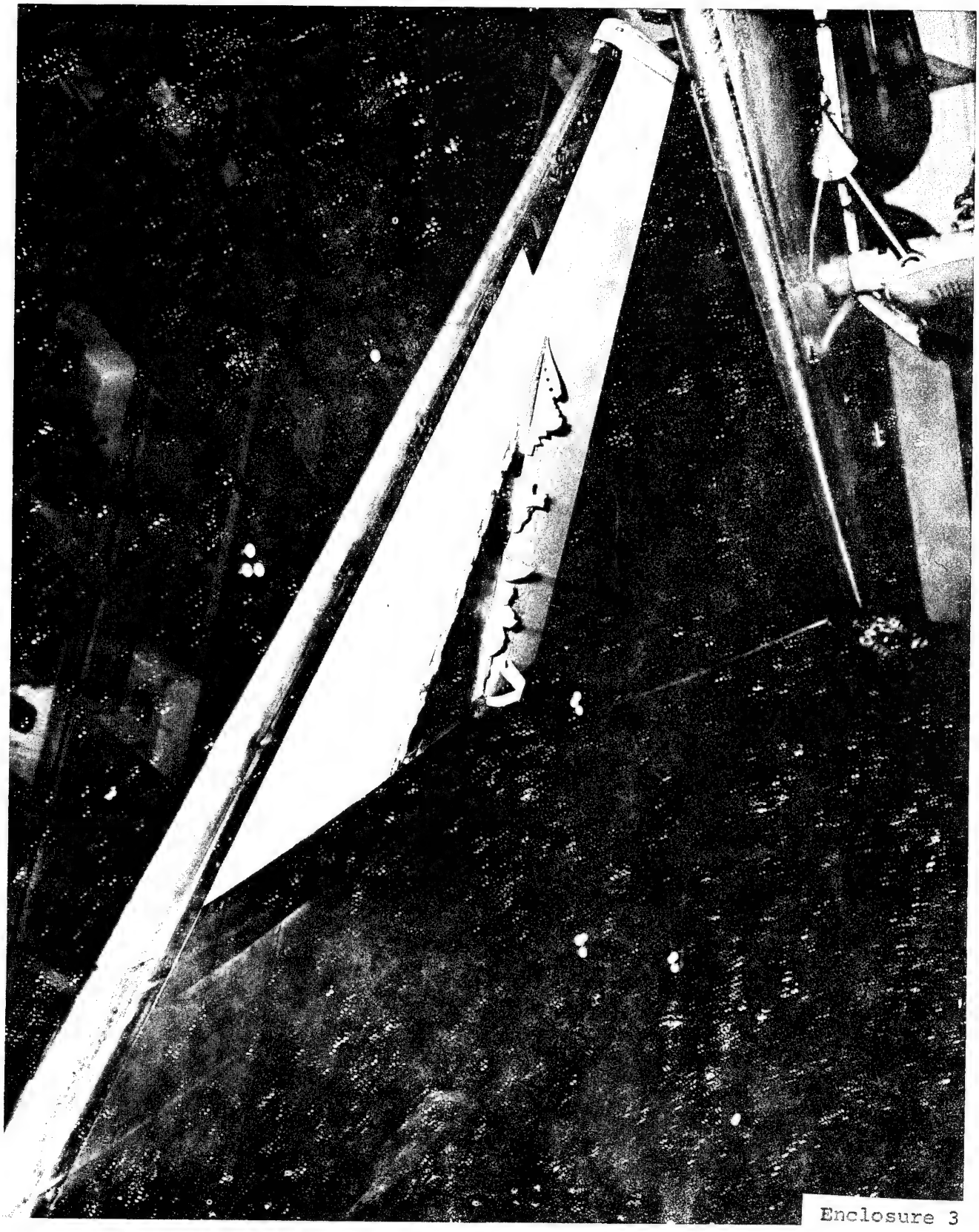

Enclosure 3

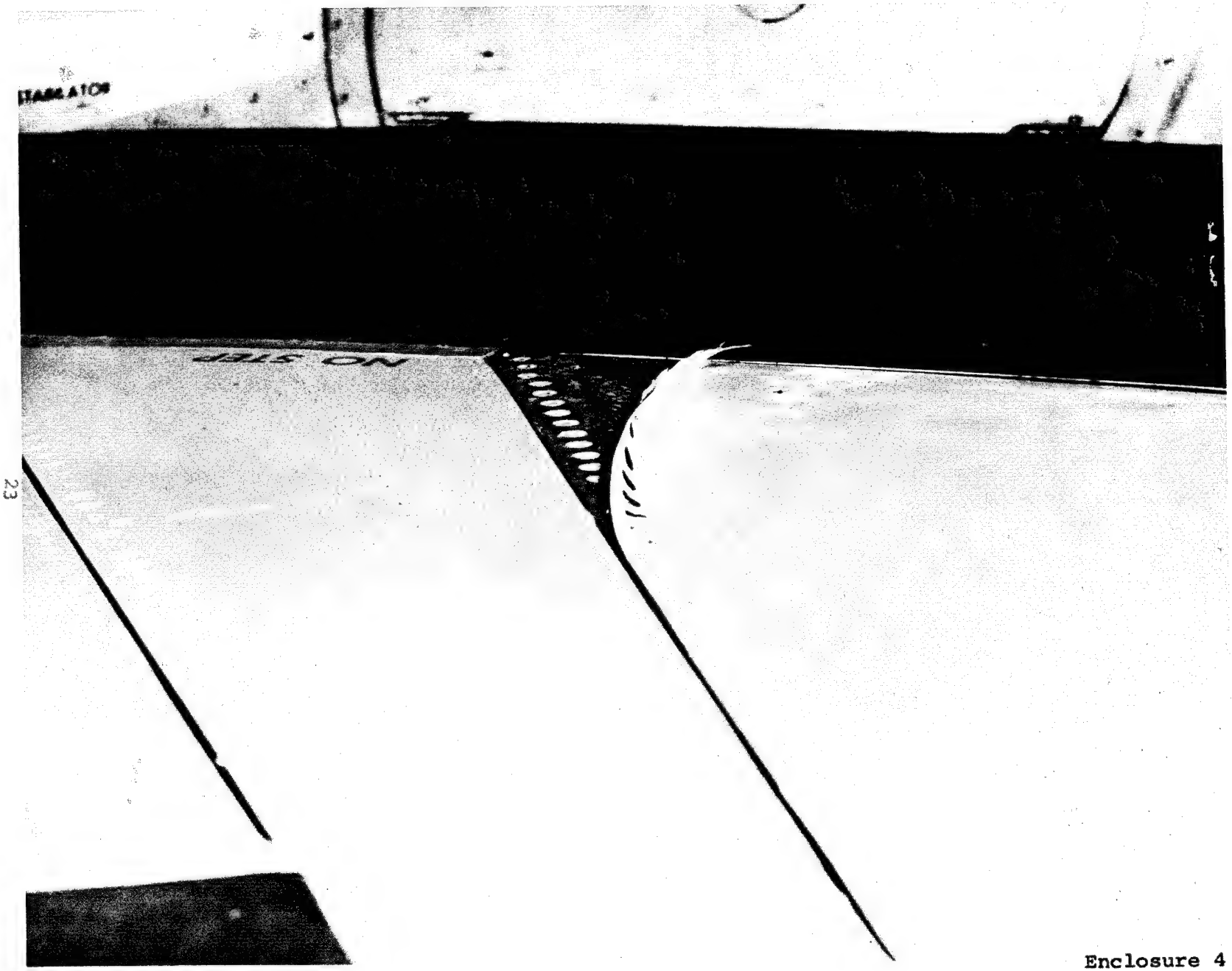

Enclosure 4

Enclosure 5

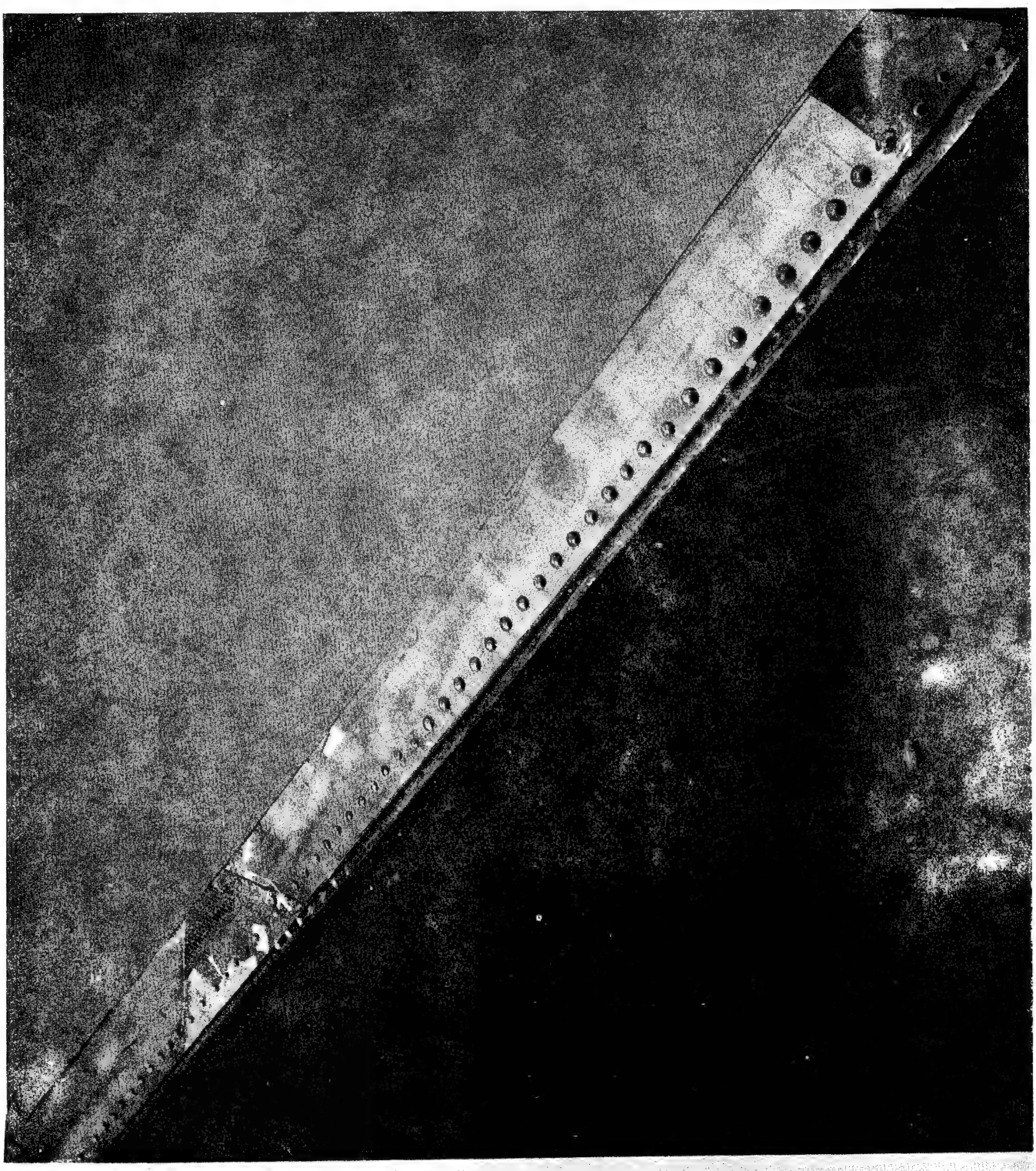

INBOARD EDGE OF PANEL 150491 R/H SHOWING EXTERNAL SURFACE OF FACING

PHOTO NO: CAN-378660(L)-10-66

Enclosure 6

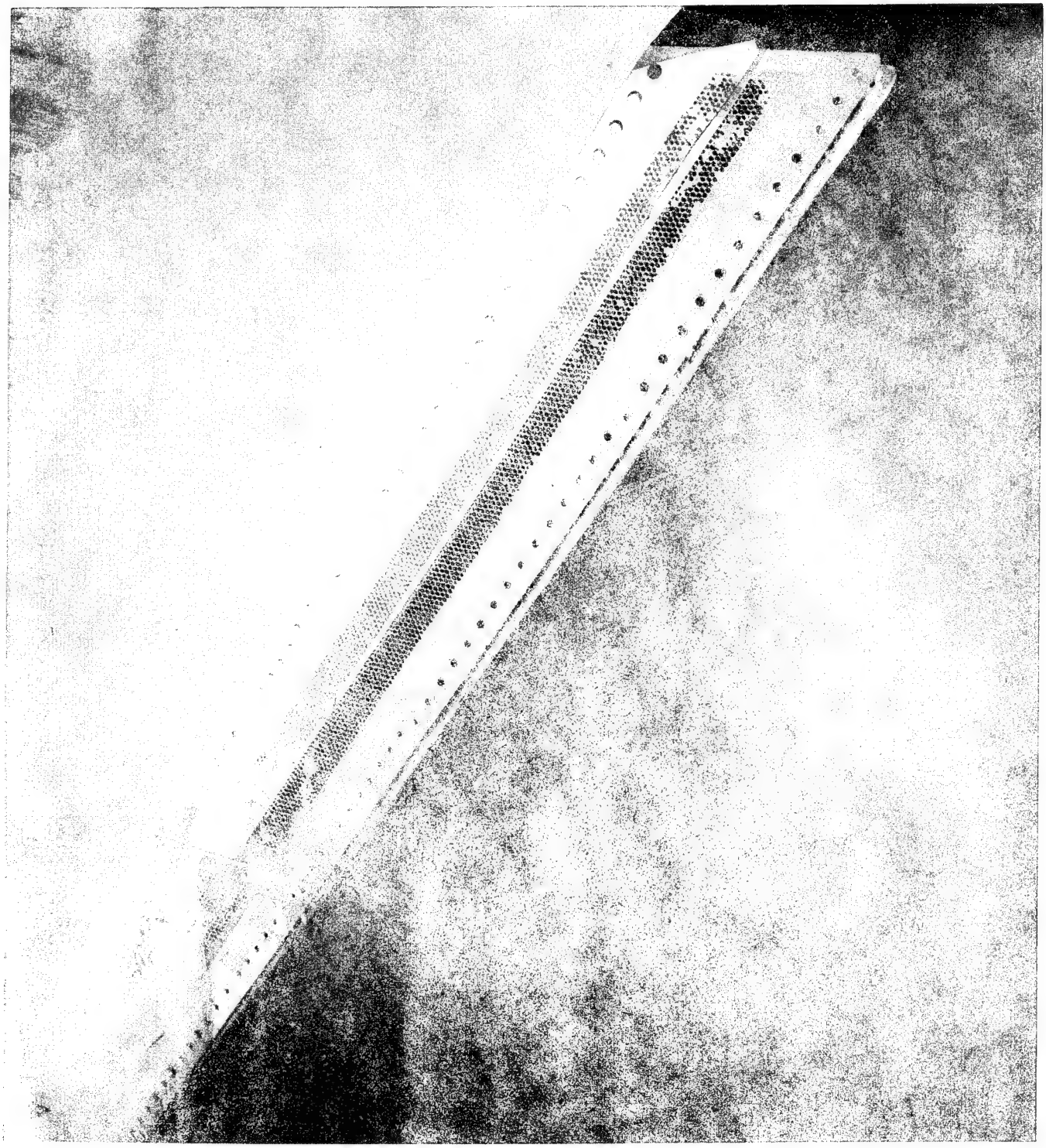

INBOARD EDGE OF PANEL 150491 R/H SHOWING THE INNER SURFACE OF THE DOUBLER AND THE UPPER SURFACE OF THE SPAR AND ADJACENT HONEYCOMB

PHOTO NO: CAN-378659(L)-10-66

Enclosure 7

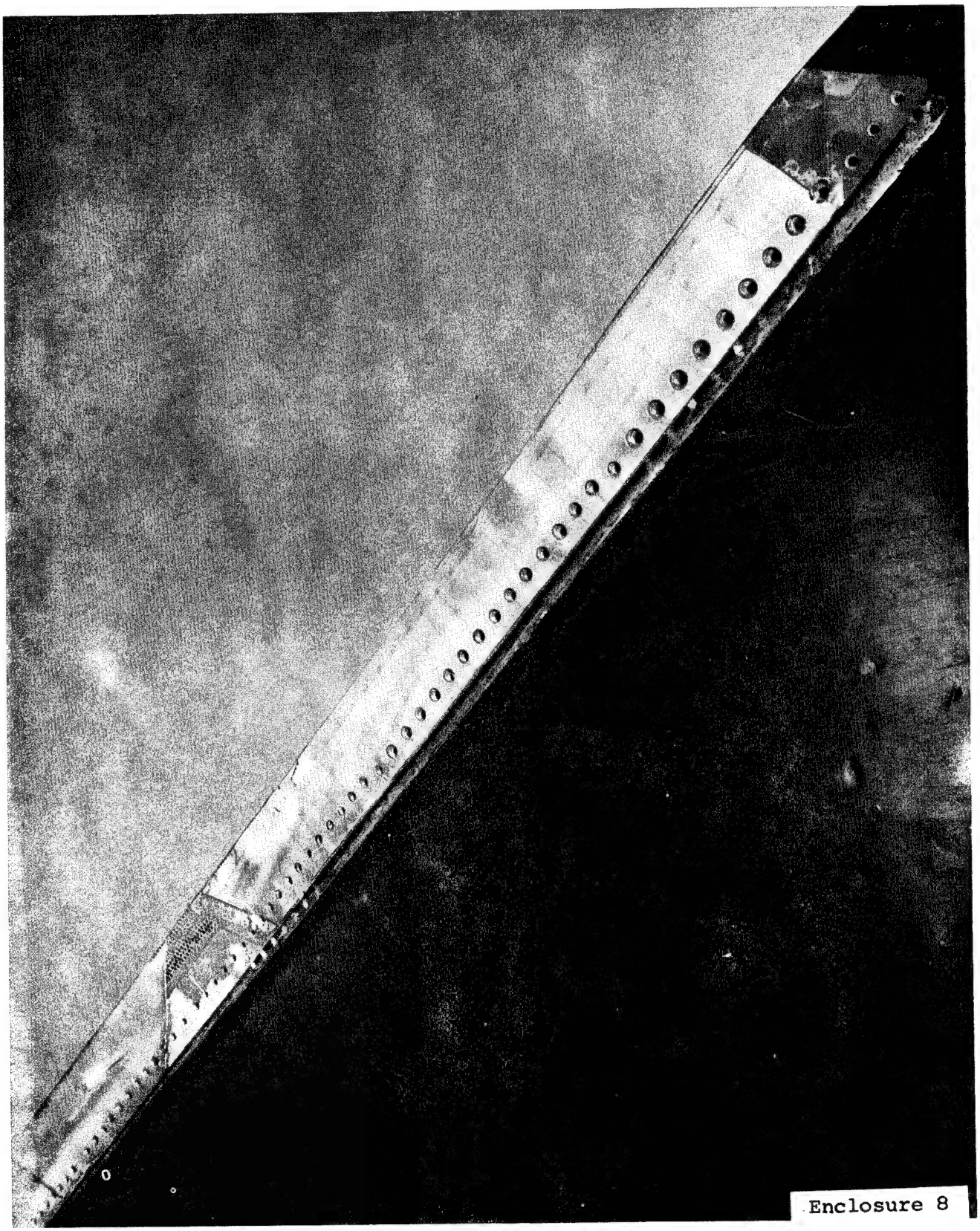

Enclosure 8

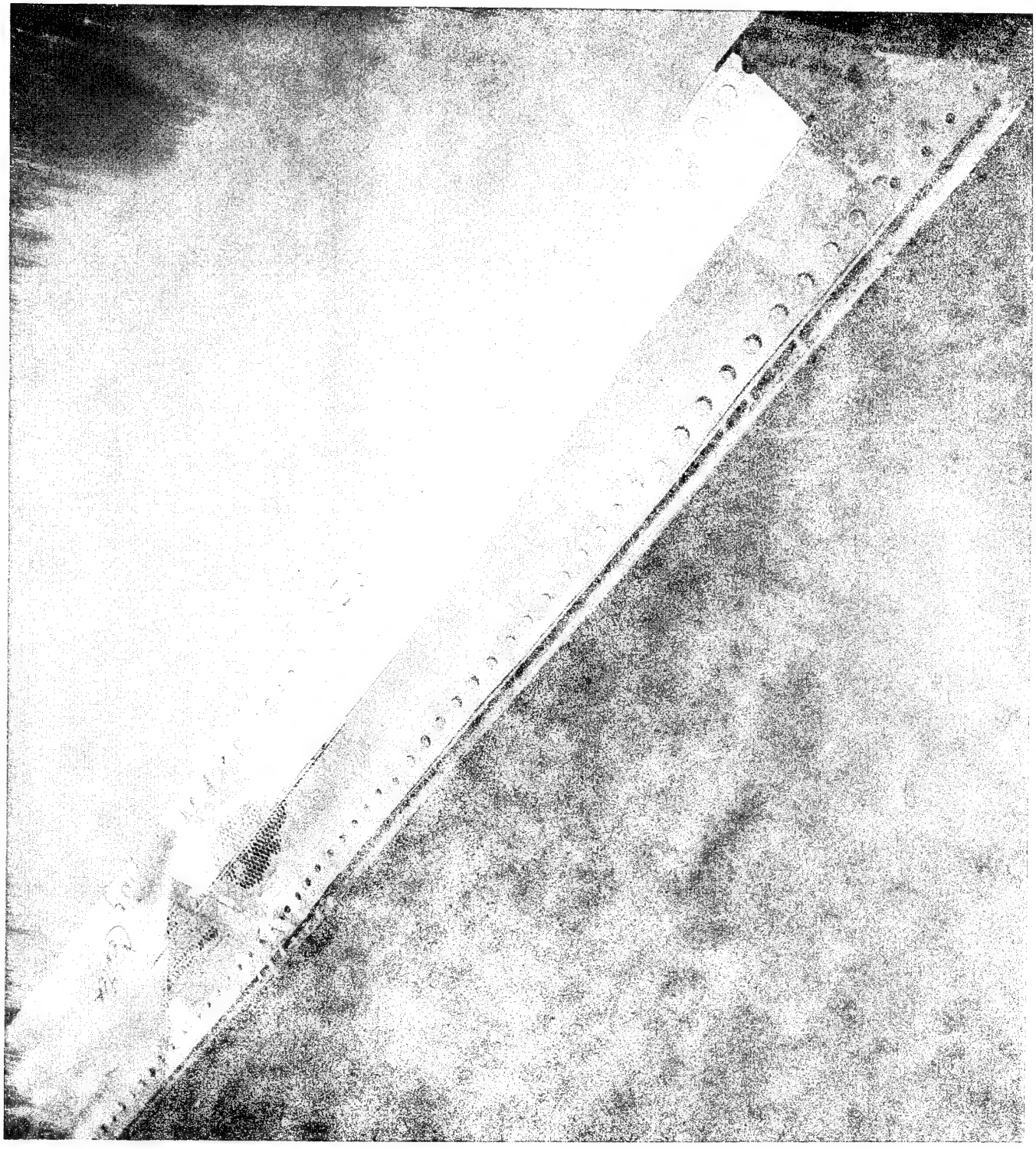

INBOARD EDGE OF PANEL 150491 R/H SHOWING THE INTERIOR SURFACE OF THE FACING AND THE UPPER SURFACE OF THE DOUBLER

PHOTO NO: CAN-378657(L)-10-66

Enclosure 9

SUMMARY REPORT OF PROBLEM NO. 4

INVESTIGATION OF ADHESIVE-BONDED ALUMINUM HONEYCOMB CONSTRUCTION

Maurice J. Curtis
Problem Coordinator

Characteristics Sought

Adhesion Corrosion Voids Delaminations	NDT techniques can probably provide data for these characteristics
Strength of bond Predicted life service Time to failure	Current NDT techniques are unlikely to provide data for these characteristics

Current Practice

X-ray, ultrasonics and coin tapping are stated in the Program to be in use. However, it was stated orally that ultrasonics is not satisfactory, that beta scatter was frequently limited because of skin thickness, and that tapping with a coin was the only acceptable present practice.

I would remind the problem presenter that Problem No. 6 reported in the minutes of the 15th Conference, discussed tapping with specially designed, standard-shaped hammers.

Lt.Col. Bill Bennett, Kelly AFB, suggested pulse echo. Warren Inglis, Frankford Arsenal, suggested the Fokker bond tester and Ed McKelvey, Wright-Patterson, indicated that although it requires considerable skill and calibration it nevertheless gives valid data on aluminum honeycomb. Both Inglis and McKelvey favored the North American Aviation Sonic Test System which is comprised of the Sonic Resonator and the Eddy-Sonic techniques. This system which has been recently developed, permits inspection of composite structures when access is limited to one surface only. (Mr. Curtis gave technical data on this system to Ed Criscuolo for forwarding to Mr. Gurtowski.) Mr. D. Ballard of Sandia stated that the nondestructive testing profession currently lacks a technique that will provide quantitative data on adhesive strength. Only from such data could service life or time-to-failure be predicted.

Mr. J. Johnson, NARF, San Diego, considered that manual tapping would be of doubtful value because of human variables such as a head cold, lack of interest because of family problems, etc. He favors the Fokker Bond Tester; this tester is capable of giving reproducible results in the hands of different operators at different plants and with different machines, when the technique is standardized. He suggested contacting Miss Eleanor Vadala of NAEC who has had experience with the Fokker Bond Tester.

Lt. Colonel Bennett, Kelly AFB, indicates that in AFLC a nondestructive testing program on F-111 test panels successfully located near-side unbond areas of less than 0.1 square inch reliably. He offered Mr. Gurtowski copies of reports on this testing program.

The Wednesday problem discussion meeting developed two additional ideas. The use of cholesteric liquid crystals was discussed. The group believed that Paper No. 7 which was to be presented Thursday would contain ideas of value to Mr. Gurtowski. Mr. B. J. Brunty, NWS, Concord, California, suggested the use of a portable vacuum suction cup to be placed on a few selected and correlated areas (if such can be defined). A transparent window in the cup would permit viewing changes in a photostress coating applied to these selected areas. Perhaps other strain sensing or deflection indicating devices could be used rather than the photostress coating. If the bond between the skin and core had failed, the skin would deflect differently when a vacuum was applied than would skin over an area whose bond had not failed.

The use of Eddy Sonic testing seems to be in disfavor because a panel that had undergone 7,000 hours of simulated environmental exposure appeared satisfactory to the eddy sonic tests. However, a mate to that panel failed on an aircraft after 327 hours of actual service. As is frequently encountered, we have the question - i.e., was simulation realistic or is the eddy sonic tester inadequate? More study is required before this paradox can be answered with engineering assurance.

(Subsequent to the meeting the Problem Coordinator read with interest "Research on Exploratory Development of Nondestructive Methods for Crack Detection", Technical Report AFML-TR-67-167, in which favorable test results on honeycomb structures are reported. The system involves an electronically driven vibrator and an accelerometer pickup. Such a system would be far more consistent in output and response than the currently favored coin tapping and human ear. A copy of the technical report has been sent to Mr. Gurtowski).

PROBLEM No. 5

CONTROL OF EQUIPMENT VARIABLE IN ULTRASONIC INSPECTION OF BRAZED JOINTS

Presented by

Joseph Stea
Philadelphia Naval Shipyard

Background

The evaluation of the percent of bond present in a brazed pipe joint, as required by NAVSHIPS Document 0900-001-7000 (250-634-6), is determined by ultrasonic pulse-echo inspection. Brazed joints are to be inspected by the straight beam method for determining transmission to and reflection from the inside diameter of the fitting for unbond, and from the inside diameter of the pipe for bond. Joints are accepted when the average bond of the brazed joint is 60 percent or more.

Problem

Differences of average bond percentages, (within 15) obtained by operators inspecting the same brazed joint, were disclosed in auditing. A higher bond average (within 15%) than that obtained by ultrasonic inspection was disclosed by visual peel examination of brazed joints. These variances of bond percentages are inherent in the present process, which allows for a 15% reproducibility limit. The equipment and operator variables of the presently available procedures and equipment result in such low reproducibility that operators inspecting a 60% bonded joint will evaluate it by ultrasonic inspection, at from 45 to 75% bond.

Discussion

In establishing the 60% bonded acceptance requirement of NAVSHIPS 0900-001-7000 for brazed pipe joints, a factor of 15% was included for the operator, equipment and beam divergence variables. On the assumption that operator and beam divergence variables cannot be controlled or eliminated because of the human element and the curved geometry of the joint, a study was conducted solely on equipment variables. The intent of the study was to determine if equipment variables could be eliminated to improve the inspection process reliability and thereby decrease the 15% reproducibility factor.

The ultrasonic inspection of brazed pipe joints is based on the premise that bond and unbond portions of a joint beneath the area of a transducer will reflect signal amplitudes proportionately. A portion of a joint considered to be 50% bonded beneath the area of a transducer will theoretically reflect signals of equal amplitude (See Fig. 1). However, since all testing is performed in the Fresnel zone, or near field, a 50% bonded area need not reflect signals of equal amplitude. A typical distance amplitude curve for bronze joint material discloses that amplitudes increase unpredictably with distance in the near field (See Fig. 2).

If that part of the curve representing unbond and bond thickness can be altered and controlled by equipment adjustment so equal amplitude signals can be produced, a 50% bonded area would produce signals of equal amplitude (See Fig. 3).

Experimental Results

An investigation was conducted to determine how to control relative signal amplitudes in the near field zone. The parameters involved were equipment circuitry, frequency employed and distribution of transducer sensitivity.

At present the only reference block required by 0900-001-7000 for the ultrasonic inspection of brazed pipe joints is a standard type time base step block. This standard type block is limited in that only one time base line signal can be displayed at any one time. A relative response reference standard, which permits the simultaneous display on the cathode ray tube of the two signals, representing the unbond and bond conditions, was designed and manufactured (See Fig. 4). An ultrasonic system composed of a Model 50A Sonoray Flaw Detector and a 3/8-inch diameter transducer were employed for the investigation. The tests were conducted at frequencies: 2.25 MHZ and 5 MHZ.

The transducer was positioned on the newly designed relative response block so that 50% of the transducer area was active on the 3/8-inch thickness and 50% active on the 1/2-inch thickness, (See Fig. 4). The combination of thicknesses was selected at random; however, the combination of thicknesses used as a standard should correspond to the respective brazed joint thickness being tested. The two signals obtained from the relative response block were displayed on the cathode ray tube. While maintaining a constant pressure upon the transducer, various equipment controls were manipulated and a change of relative amplitude of the two signals was noted. Results of the tests are presented in Table 1.

TABLE I

Relative Response				Equipment Control Adjustments		
2.25 MHZ		5 MHZ				
3/8"	1/2"	3/8"	1/2"	Filter	Suppression	Pulse Length
10	4-1/2	10	7	In	Normal*	Normal*
10	5	10	7	In	Normal	Maximum
10	1	10	9	In	Normal	Minimum
10	5	10	9-1/2	In	Maximum	Normal
10	3-1/2	10	6	In	Minimum	Normal
10	1	10	10	In	Maximum	Minimum
10	4-1/2	10	5	In	Minimum	Maximum
10	7	10	10	In	Maximum	Maximum
10	3-1/2	10	6	In	Minimum	Minimum
10	6	10	10	Out	Normal	Normal
10	8	10	10	Out	Normal	Maximum
10	2	10	9	Out	Normal	Minimum
10	4	10	10	Out	Maximum	Normal
10	7-1/2	10	9	Out	Minimum	Normal
10	2	10	8	Out	Maximum	Minimum
10	7	10	10	Out	Minimum	Maximum
10	10	10	10	Out	Maximum	Maximum
10	7	9-1/2	10	Out	Minimum	Minimum

*Adjusted for the most clear signal presentation

It is important to note that since the test results were related to the transducer employed, it was necessary to determine if the transducer was uniformly active over the area of the face. The use of a transducer whose sensitivity is not equally distributed over the face area will result in non-proportional amplitude signals. A transducer can be verified to be uniformly active by repositioning the transducer on the relative amplitude block. A transducer of uniform activity will display constant relative signal amplitudes no matter how the transducer is repositioned.

Conclusions:

The results of the experimental investigation indicate that variation of suppression, pulse length and/or frequency of the ultrasonic instrument can alter the representative brazed joint unbond-bond signals. Relative amplitude of unbond-bond signals becomes erratic when produced by a transducer whose activity is not uniformly distributed.

A revision of the present ultrasonic inspection procedure requirements of NAVSHIPS Document 0900-001-7000 (250-634-6) is indicated. The revision should include employing the recommended relative response calibration standard as follows:

1. The transducer should be verified as being uniformly active by repositioning the transducer on the standard for assurance of constant responses.

2. Using the recommended relative response calibration standard, position the transducer on the standard corresponding to the two thicknesses being tested and adjust the equipment to display the relative response signals of the unbond and bond, as nearly equally as possible.

The consideration of the proposed procedure will ultimately lead to this principal consideration: Can the elimination of such equipment variables lead to a lowered bond value for acceptance, and if so, to what extent? Extended investigation of the proposed procedure is warranted.

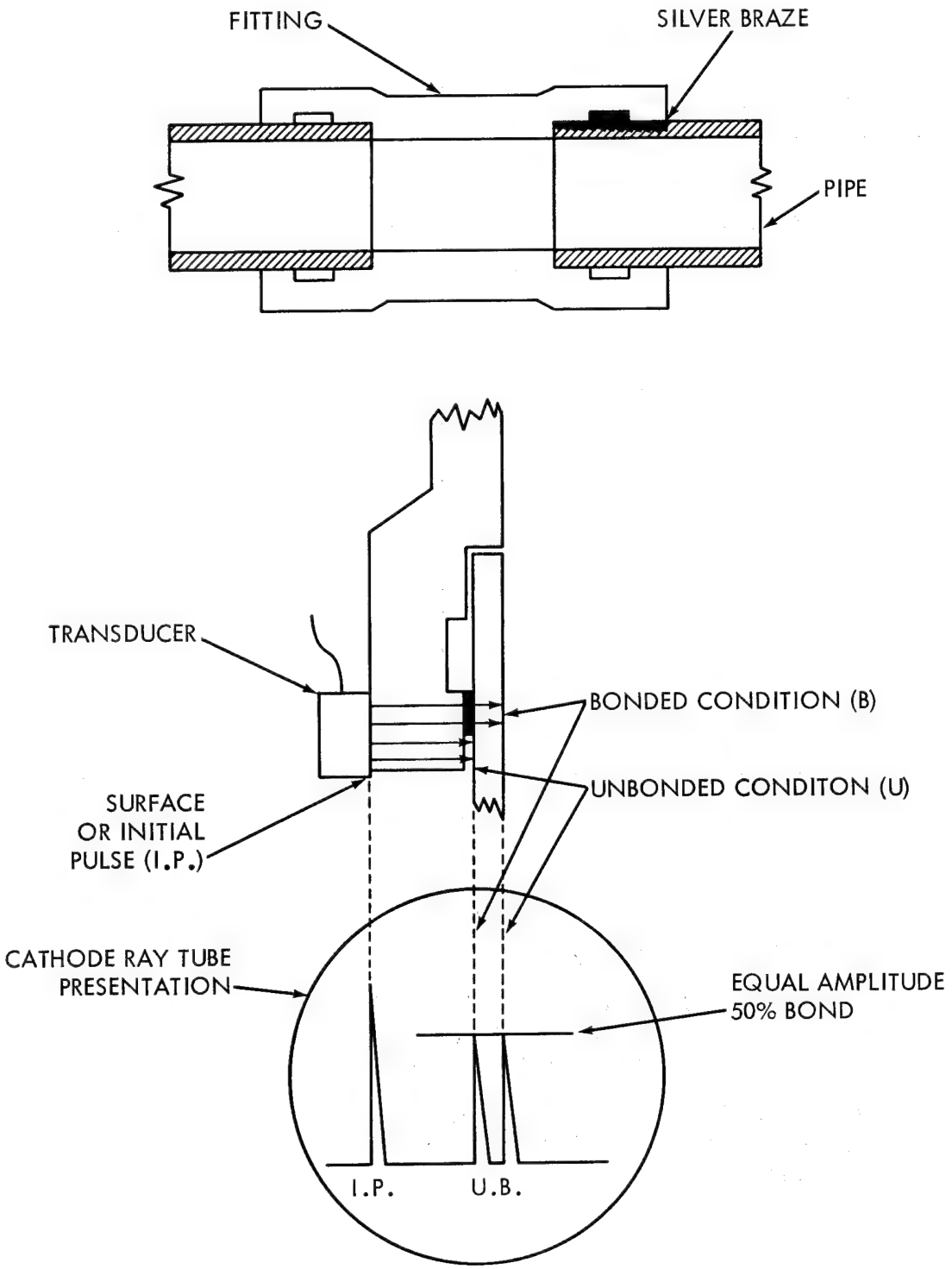

FIG.1 BASIC PRINCIPLE OF ULTRASONIC INSPECTION OF BRAZED PIPE JOINTS

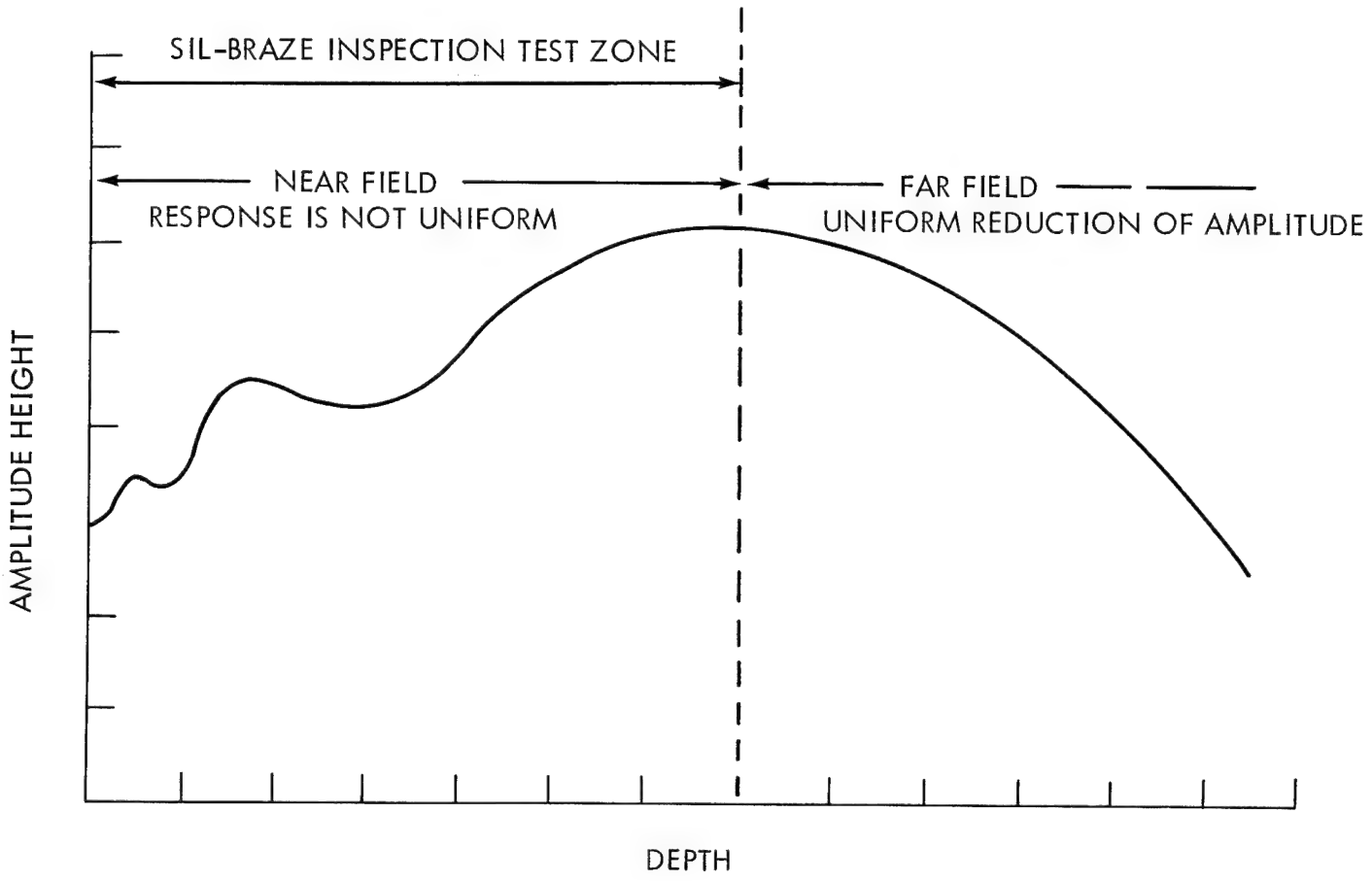

NEARFIELD IS DEPENDENT ON $N = 0.25\ D^2 f/c$ WHERE:

D = DIAMETER OF TRANSDUCER
f = SOUND FREQUENCY
c = ACOUSTIC VELOCITY

THE CALCULATED NEAR FIELD FOR BRONZE, EMPLOYING A 3/8" DIAMETER, 2.25 MHZ TRANSDUCER IS APPROXIMATELY 0.570 INCH.

FIG.2 TYPICAL ULTRASONIC RESPONSE CURVE

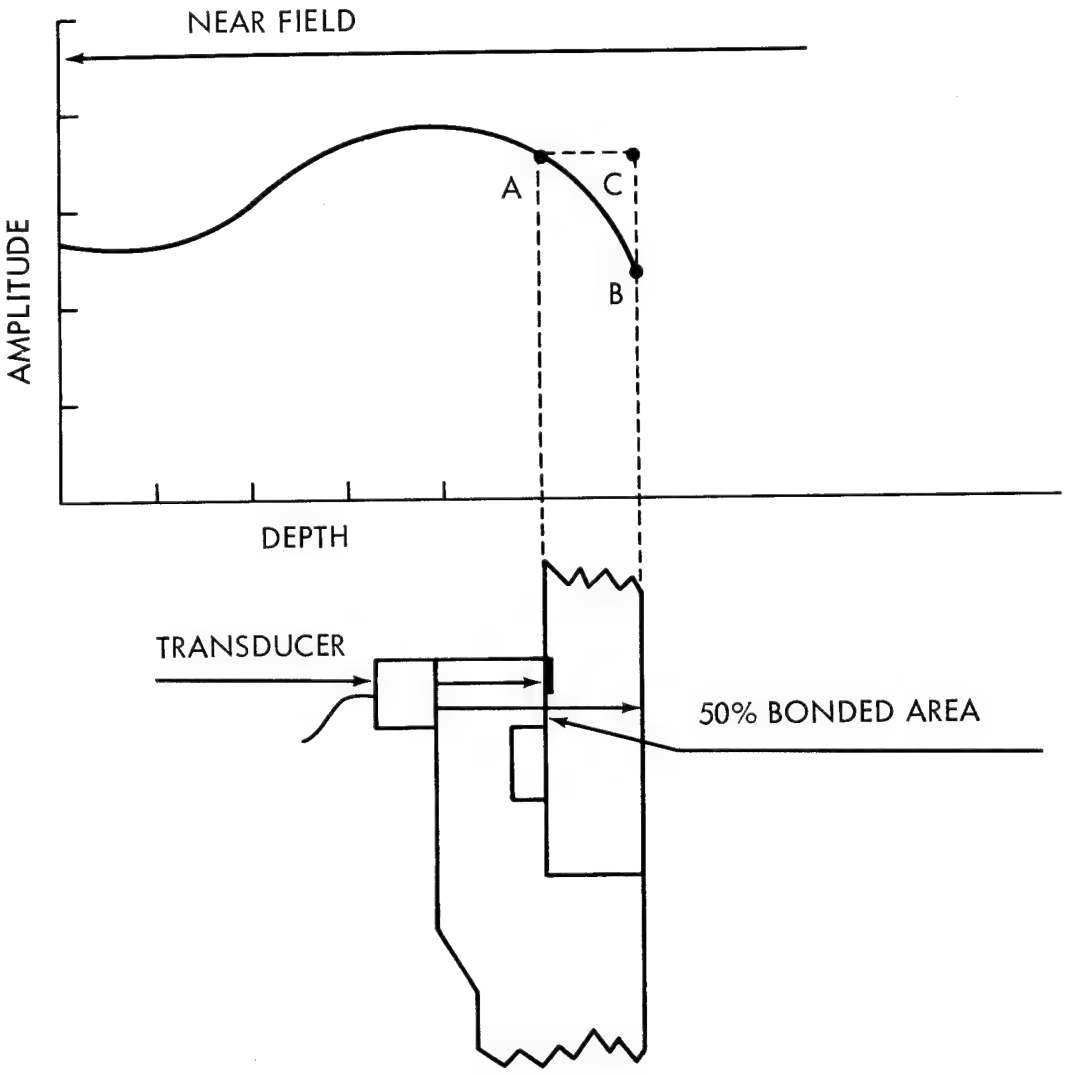

AB CURVE-NOT CONTROLLED-RESULTS IN UNEQUAL RELATIVE RESPONSE

AC CURVE-CONTROLLED-RESULTS IN EQUAL RELATIVE RESPONSE

FIG.3 EFFECT OF CONTROLLED RESPONSE CURVE

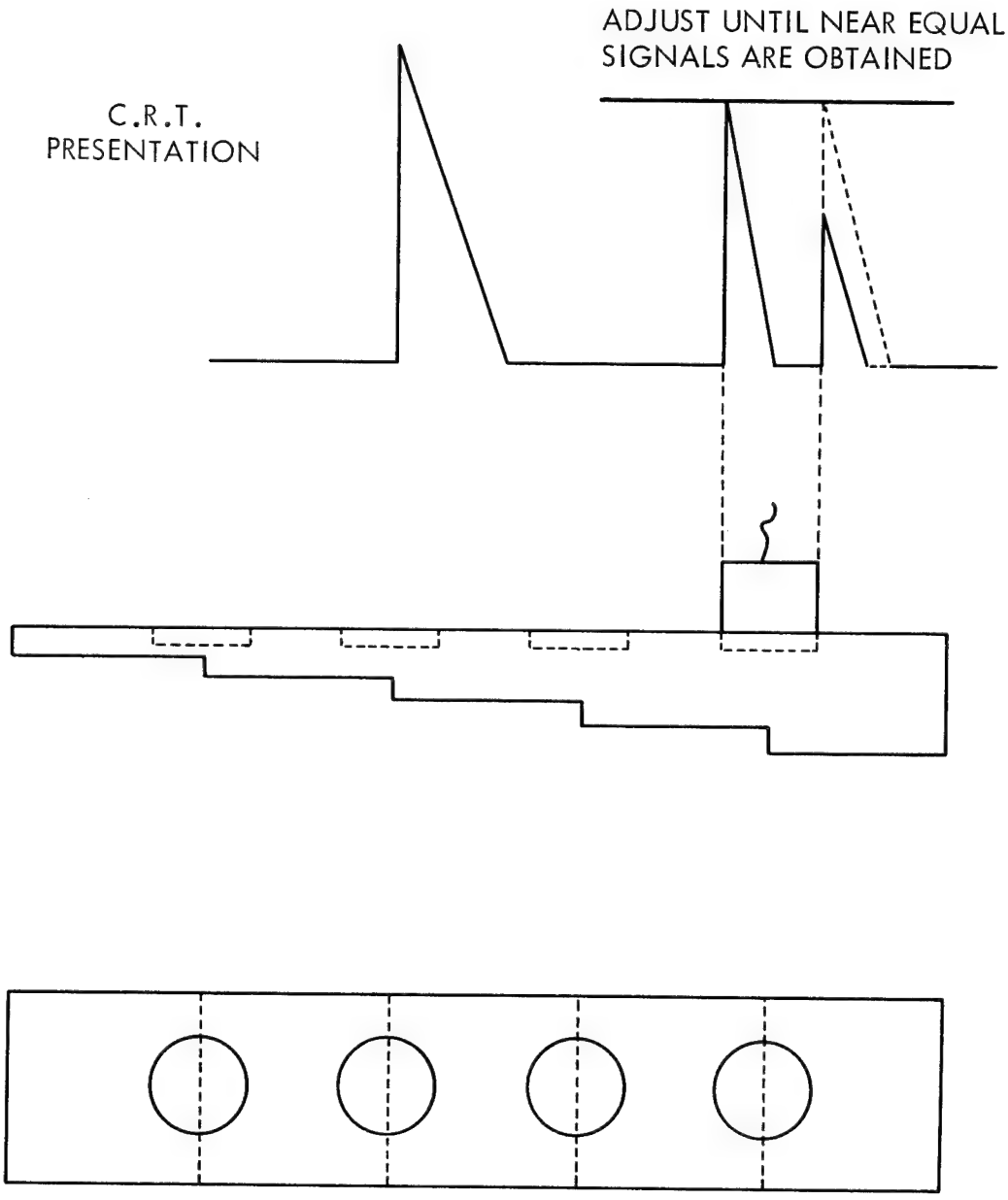

SELECT RELATIVE STEPS CORRESPONDING TO COMBINATION OF THICKNESSES REPRESENTING UNBOND AND BOND. STANDARD TO BE MADE OF ACOUSTICALLY SIMILAR MATERIAL TO THAT BEING TESTED.

FIG.4 RECOMMENDED RELATIVE RESPONSE REFERENCE STANDARD

SUMMARY REPORT OF PROBLEM NO. 5

EQUIPMENT VARIABLES AND THEIR EFFECTS IN THE ULTRASONIC INSPECTION OF BRAZED JOINTS

Michael Stellabotte
Problem Coordinator

With all due respect for the presenter, his organization, and the Committee responsible for the selection of papers and/or problems, I believe the item under discussion should have been presented, after more complete study, as a paper in support of the Philadelphia Naval Shipyard's request for a modification or revision of NAVSHIPS Document 0900-001-7000 (250-634-6).

The material submitted indicates that the existing operator and equipment variables are such that during the inspection of a 60% bond brazed joint (the minimum quality acceptable) the values obtained varied from 45% bond to 75% bond. In order to improve the inspection process reliability, the author suggests the following:

a. construction and use of a "relative response" reference standard simulating a 50% bond condition in flat material.

b. a procedure, utilizing the above standard, for checking, rapidly and in the field, the uniformity of activity over the face area of the transducer employed. Data obtained with a particular ultrasonic system and the "relative response" standard indicate that variation of each of three instrument control settings can significantly alter the relative response ratio of the bond to unbond signals.

Comments

I, quite frankly, do not fully understand just what Mr. Stea desired from this conference. I believe, however, that the report submitted has made a very good start at a procedure for developing reference standards for brazed joints although this may not have been the original intent. The following simple procedure (perhaps extremely over-simplified) seems to suggest itself:

a. Procure a transducer which is "uniformly active over the area of the face".

b. Following the suggestion of Mr. Warren Inglis of the Frankford Arsenal, affirm the quality of the transducer by laboratory methods. These methods are apparently known to Mr. Stea.

c. Following the suggestion of Mr. Louis Cardinal of the Naval Research Laboratory, manufacture a 50% bond, "modified relative response" standard, i.e., one that is curved as opposed to the present flat one. Further, the curvature of future reference standards should match that of the material to be tested.

d. Repeat the experimental work reported on above to determine if the same results hold true. If so, determine the settings necessary to produce a bond to unbond signal ratio of one, i.e., adjust the equipment to display the relative response signals as nearly equally as possible.

e. Investigate to see if other degrees of bond can now be more accurately determined by the "standardized instrument".

I hope that my interpretation of the material discussed has been correct, and that it has, perhaps, clarified the problem area in the minds of the other conferees. More importantly, I hope the comments and suggestions reported herein stimulate Mr. Stea into an extended investigation along the lines indicated. Mr. Stea requested that other activities give consideration to the performance of similar experiments and inform him as to any results obtained.

PROBLEM No. 6

SHAPED CHARGE LINER FOR ARTILLERY AMMUNITION

Saul Schiff
Picatinny Arsenal

INTRODUCTION

The product is a flanged hollow cone used in an anti-tank ammunition item to shape and line the high explosive charge. The performance of the item is related to the grain structure in the finished liner and it is desired to monitor the grain structure of liners during production without functionally destroying them.

HISTORY

The shaped charge effect is the notable increase in penetrating power of a high explosive charge when it is hollowed on the surface facing the target. Hollowing out the surface serves to direct the explosive wave along the axis of the hollowed portion and to focus the detonation force toward a single area on the target.

Although the phenomenon was observed prior to 1800 in Germany and Norway it first became known of in this country during the 1880's through the work of Dr. Charles Munroe, an American explosives chemist. Dr. Munroe discovered that if a block of guncotton were to have letters cut into a surface and then placed with the lettered surface against a steel plate and detonated, the letters would be indented into the surface of the steel. Because of his formal work in this field he is usually credited with the discovery of the shaped charge effect and the term is sometimes referred to as the "Munroe effect".

From the time of Munroe's discovery until about 1940 there was very little heard of the subject in this country, but World War II provided the impetus to develop anti-tank ammunition with a high armor defeat capability, and intensive research was begun into the application of the Munroe principle for this purpose. The research studies were probably instigated by the action of a Swiss engineer, H.A. Mohaupt, in bringing to this country the idea of a projectile carrying a high explosive charge in the form of a hollow cavity. The cavity was lined with a thin walled steel cone. The liner served not only to form and maintain the shape of the cavity but also greatly aided penetration by contributing the material for the formation of a high velocity metallic jet. Much research was devoted to improvement of the liner.

FUNCTIONING

A typical shaped charge missile has a steel body fitted at the forward end with a thin walled, cone-shaped metal liner whose apex extends backward into the body cavity. The high explosive fills the remainder of the body cavity except for a portion at the base which is taken up by the fuze. A hollow ogive head is screwed to the forward end to provide the desired flight characteristics and to maintain the design standoff distance from cone base to target.

When the projectile strikes the target, the fuze detonates the HE charge and the detonation wave moves forward; the liner collapses and erupts into a long, narrow jet of atomized cone material and explosion gases. The jet velocity is very high (from 10,000 to greater than 40,000 feet per second) and it impinges on the target exerting pressures up to 250,000 atmospheres (3,700,000 pounds per square inch). As a result, the target material is pushed aside from the axis of the jet and is penetrated by it.

THE PROBLEM

The ammunition item in question is fin stabilized - which implies that no rotation of the missile is required for it to maintain stable flight. However, some rotation is imparted to it by the gun rifling and although this rotation is kept relatively slow, by fitting the shell body with a free-turning obturator band, it nevertheless gives the jet particles sufficient tangential velocity to cause the jet to spread and break up prematurely; thereby lessening penetration. Fortunately the tendency of the jet to break up can be counteracted, and full penetration capability restored, by manufacturing the liner (hereafter referred to as the cone) in such a way that the individual material grains of the sidewall are aligned in the exact direction necessary to impart an equal counter-rotation to the jet. The achievement of the proper grain orientation needed to counteract a given rate of missile rotation is called "spin compensation" and, during manufacture of the cones, it is necessary to duplicate the required degree of spin compensation in cone after cone throughout the entire contract quantity. To maintain this kind of control, the method of examining material texture by X-Ray Diffraction is used. But there are certain disadvantages to the present application of this method; namely, that special preparation of the cone is required prior to inspection and the preparation renders the cone unserviceable.

The specific problem then, is the need for a technique which can be used to predict spin compensation by examining a cone without destroying it.

MANUFACTURE

The cone material is cold rolled, annealed copper of electrolytic quality. The material is purchased in rolled strip and blanked into discs which are then lightly dished and cupped in a mechanical press. The blank is then formed into a hollow truncated cone by the rotary extrusion process, the flange trimmed by punch press, and the truncated end drawn to form a short cylindrical cup (Fig 1).

Rotary extrusion is performed on Lodge and Shipley Flo-Turn machines. In this operation the cupped disc is clamped between the end of a vertical, rotating mandrel and a live center (Fig 2). A tool, moving parallel to the mandrel surface, plastic flows the material over the mandrel. The process differs from the standard metal-spinning technique in that all tool motions are completely mechanized; whereas metal spinning is predominantly a manual

operation. Production rate is 400 cones per machine per shift and, for the present quantity of approximately 160,000 units the unit cost for the finished cone is estimated to be $2.80.

During flo-turning, the material grains are rotated and their crystal slip planes are brought into alignment at an angle with the cone axis as continuous deformation of the copper blank takes place along these planes of slip. The alignment angle can be varied by changing the machine feed and speed relationship. Factors which affect final grain orientation during cone manufacture are:

1. Shape of forming tool edge
2. Speed of rotation of mandrel
3. Feed rate of forming tool
4. Hardness and type of copper blank
5. Original blank thickness
6. Direction of machine speed and feed relationships

GRAIN STRUCTURE INSPECTION

The present inspection procedure was developed through the work of Drs. M. Gainer and C. Glass at Aberdeen Proving Ground under the technical cognizance of Frankford Arsenal. The method replaced an earlier one which estimated spin compensation by scribing lines through the center of a blank and measuring the angle of twist undergone by the lines after forming the cone (Fig 3). The improved method measures the grain orientation by recording the varying intensity levels of a diffracted X-Ray beam. Inspection is as follows:

A one inch wide band is machined and acid etched in the sidewall of the cone to a total depth of .035 inches. The cone is placed in a fixture with its forward sidewall in the vertical plane and then slowly rotated in this plane while an X-Ray beam is focused at a point on the prepared surface. The beam is diffracted by the crystal lattices of the sidewall grains and back-reflected to a Geiger tube. The equipment records the varying intensities about the projected cone of diffraction in terms of scintillations (or counts) per second. The difference between two intensity peaks which appear about the diffraction cone is a measure of the mean grain orientation at the point of measurement and is relatable to the material texture throughout the cone sidewall (Fig 4).

INSPECTION CRITERIA

Fifty samples are taken from each production lot of approximately 5,000 cones and subjected to the diffraction test. The difference readings taken at four points around the sample periphery are averaged and the

average for all samples must fall within the allowable limits established by a set of cones of known performance, which are used as standards. Prior to production a pilot sample of 35 projectiles containing cones made to these limits are detonated while suspended vertically above a target and spun about the longitudinal axis at various spin rates. The pilot samples must pass requirements for penetration at a specified spin rate before the limits set by the standard cones are adopted for subsequent production.

The pilot sample firing which is expensive, time consuming, and completely destructive is performed only once, at the beginning of the contract, to affirm that proper spin compensation is achieved or to provide information for corrective manufacturing changes. Once established as correct, the limits set by the standard cones are the criteria for cone lot acceptance.

Because the cone is destroyed in preparation for taking diffraction readings the actual readings of the cones used in the firing test are not known, so that optimum limits are never accurately determined and the cones used in the test are only assumed to have been representative of the lot, even though they may not actually be. This is all the more apparent when it is known that diffraction averages from consecutive cones of the same lot may vary 50% or more of the established allowable range.

CONCLUSION

Although it is hoped (and expected) that this committee can offer a workable solution to the problem posed, there is no intention of abandoning the present method of inspection without making every effort to overcome its few shortcomings, and some work is planned to improve the conditions spoken of. The work will be undertaken by both Frankford and Picatinny Arsenals and will cover the following:

1. Feasibility of diffraction testing without destructive preparation.

2. Investigation of causes of erratic diffraction readings.

3. Revise sampling procedure with possible cutdown in sample size.

4. Investigate performance degradation of ammunition caused by various methods or degrees of cone preparation.

BIBLIOGRAPHY

1. X-Ray Diffraction as a Functional Measurement Tool - by Warren W. Inglis, Frankford Arsenal, August 1961.

2. X-Ray Studies of Preferred Orientations and Stress-Strain Relations in Rapidly Deformed Copper - by M.K. Gainer and C.M. Glass, Ballistic Research Laboratories, Aberdeen Proving Ground, Maryland.

3. Elements of Physics - by A. W. Smith, Ohio State University, 1948.

4. Forming Alcoa Aluminum - Aluminum Co of America, Copyright 1962.

5. Ordnance Engineering Notes - by R. M. Schwartz.

6. FA-PD-M1-2423 Rev 4, Amendment #1, 5 Aug 1966.

7. Advances in X-Ray Analysis, Vol 5 - by William M. Mueller

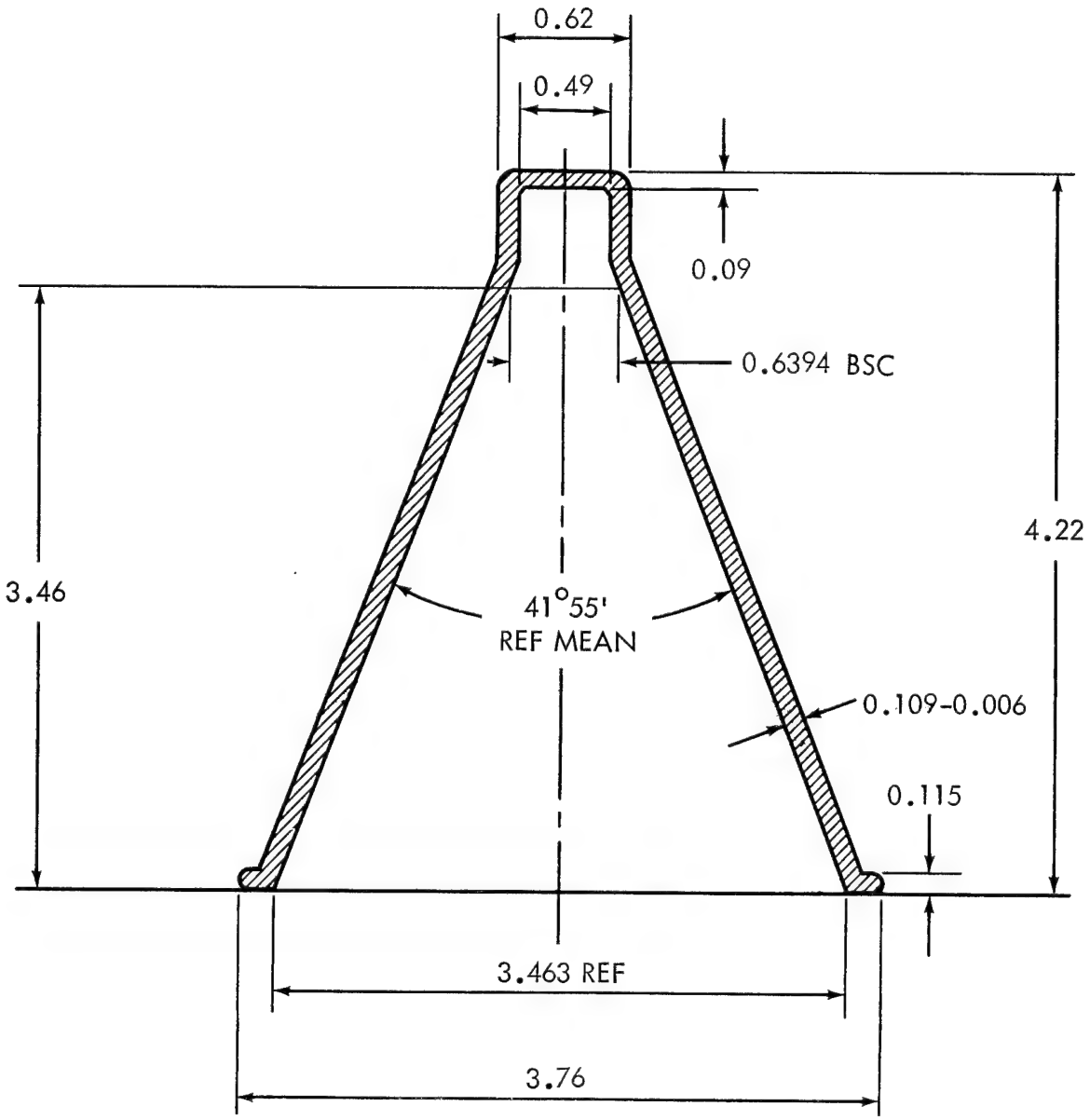

FIG.1 TYPICAL CONE DIMENSIONS

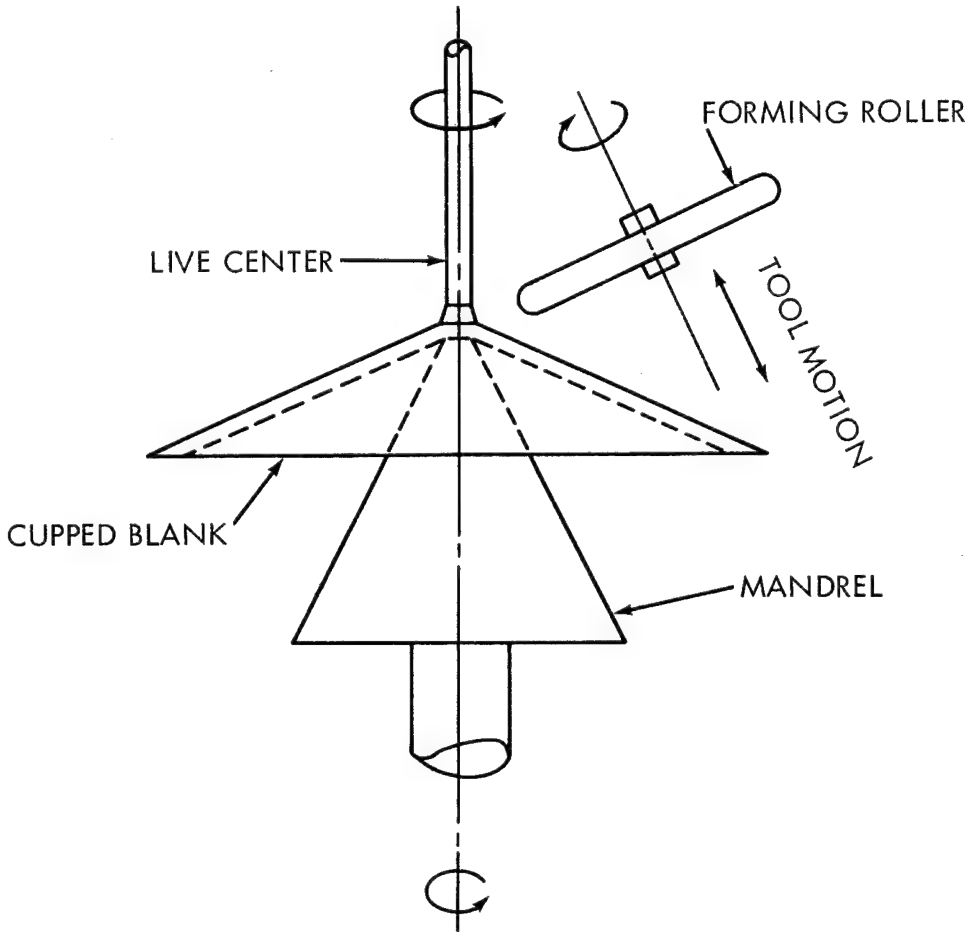

FIG.2 SCHEMATIC OF FLO-TURN PROCESS

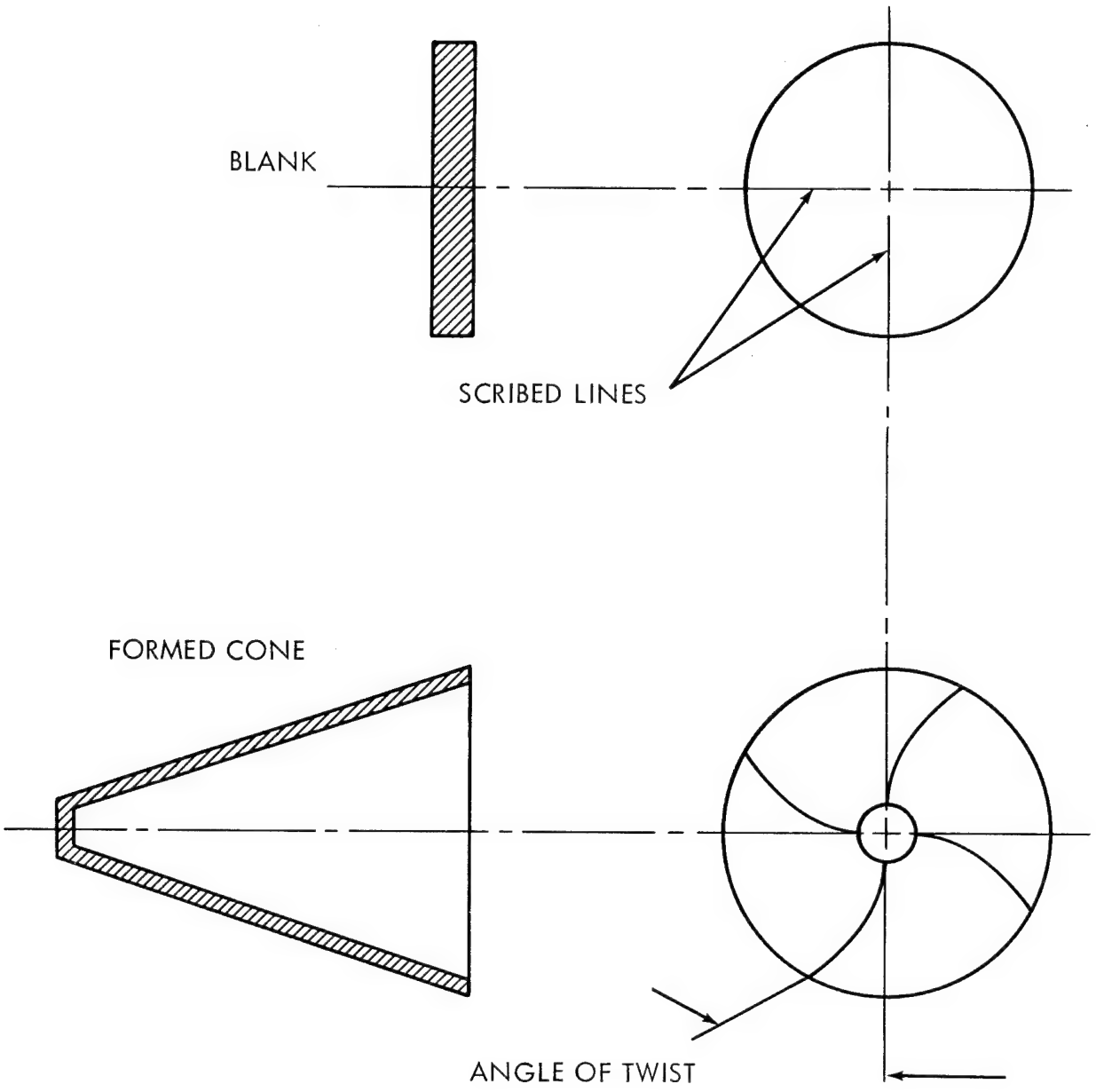

FIG. 3

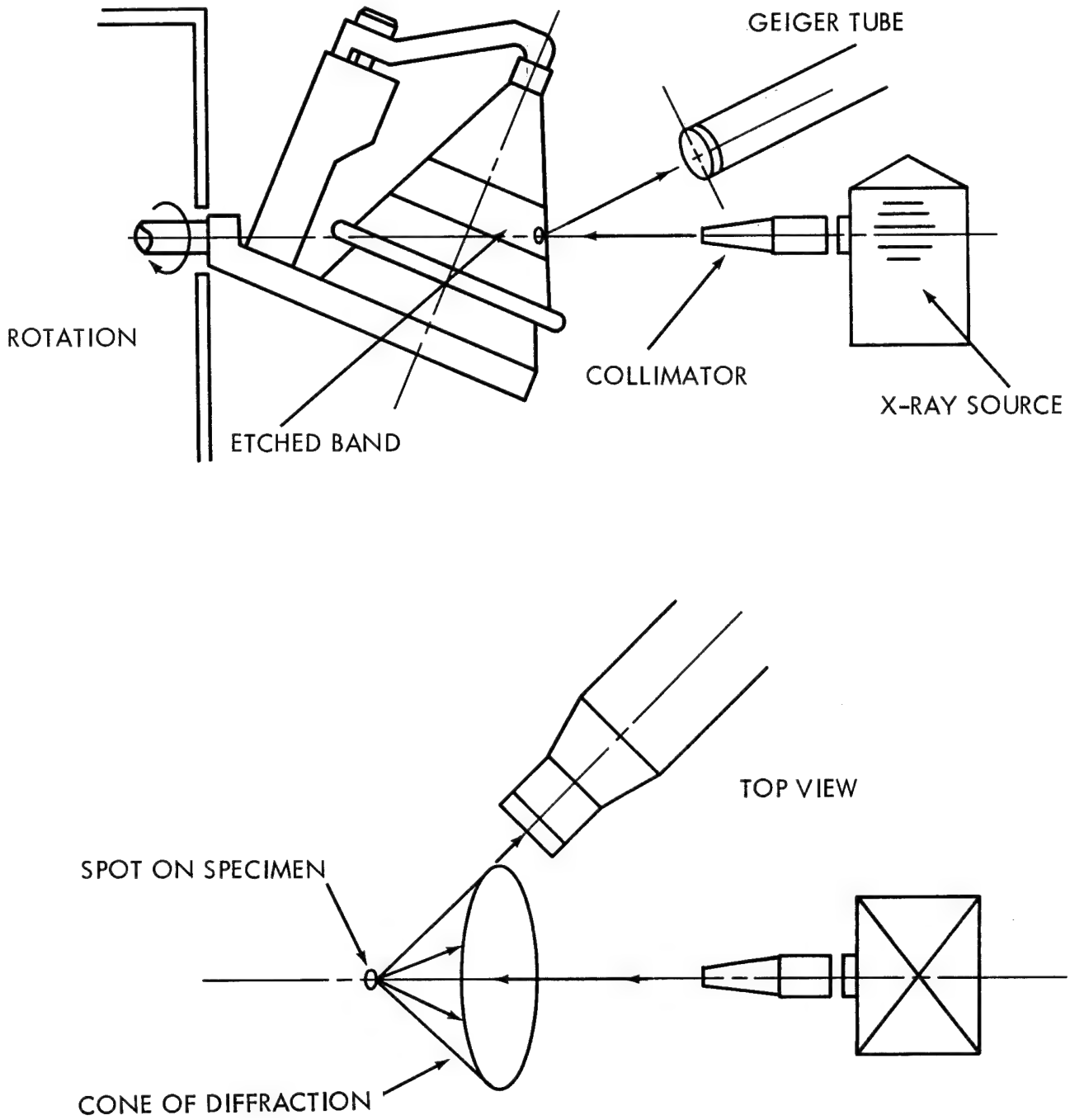

FIG.4 SCHEMATIC OF DIFFRACTION SET-UP

SUMMARY REPORT OF PROBLEM NO. 6

SHAPED CHARGE LINER FOR ARTILLERY AMMUNITION

William H. Baer
Problem Coordinator

This problem is concerned with a "Shaped Charge Liner for Artillery Ammunition". It was presented by S. Schiff, Mechanical Engineer, Picatinny Arsenal.

The liner is a flanged hollow cone used in anti-tank ammunition to shape and line the high explosive charge. The cone collapses upon detonation of the HE charge and forms a high velocity jet which penetrates the target.

The cone material is cold-rolled annealed copper, electrolytic quality. The material is purchased in strip and blanked into disks which are then lightly dished and cupped in a mechanical press. The blank is then formed into a hollow truncated cone by the rotary extrusion process, the flange trimmed by punch press, and the truncated end drawn to form a short cylindrical cup. The part is not stress relieved after forming.

During the rotary flo-turning process, the material grains are rotated and slip planes are brought into alignment at an angle with the cone axis. The proper degree and direction of grain orientation will provide the optimum penetrating capability when the charge is fired, by counteracting the tendency of the jet to break up when the round is spun during firing. The spin is imparted by the gun rifling.

Some factors which affect grain orientation during manufacture are:

1. Shape of forming tool edge.
2. Speed of rotation of blank during forming.
3. Feed rate of forming tool.
4. Hardness and type of copper blank.
5. Direction of machine speed and feed relations.

Present method of inspection is by X-ray diffraction measurements as determined by counts per second detected by a Geiger tube. Because the forming operation smears over some of the grains, a skin cut in a band is machined from

the outer periphery of the sidewall, and this area is acid etched. The average of four readings within this band must fall within the allowable limits established by a set of cones of known performance that are used as standards. Fifty cones are taken from each production lot and subjected to this test. Thirty-five cones made to these limits are detonated while suspended vertically above a target and spun about their longitudinal axis at various spin rates.

These samples must pass requirements for penetration at a specified spin rate before the limits set by the standard cones are adopted for subsequent production. The X-ray diffraction readings from cone to cone of the same lot may vary 50% or more of the established allowable range. The present method of inspection is destructive, expensive and time consuming.

A method of nondestructively determining the grain orientation in the sidewall of the cone so that preferred orientation, as determined by penetration test results, may be maintained, is desired. During the discussion period the following suggestions were proposed:

a. Use a more penetrating X-ray to minimize preparation of the cone for X-ray diffraction - J. G. Turbitt, Naval Torpedo Station, Keyport, Washington.

b. Use microradiography to determine grain orientation - R. L. Huddleston, Aberdeen Proving Ground, Maryland.

c. Change forming process by flo-turn, examine ends of cone by X-ray diffraction, draw flanges and trim off ends used for examination - E. J. Wheelahan, AMC, Redstone Arsenal.

d. Use ultrasonic attenuation to determine grain orientation, following the procedures used for steel by E. P. Papadakis and P. Sullivan - proposed by C. P. Merhib, AMMRC, Watertown.

e. Investigate the use of neutron scattering through the wall - Emmett Barnes, Picatinny Arsenal, New Jersey.

f. Use high resolution ultrasonics - M. Curtis, Naval Weapons Center, China Lake, California.

g. Establish strict controls on processing parameters so that grain orientation will be produced every time, within acceptable limits - W. H. Baer, U. S. Mobility Equipment Research and Development Center, Fort Belvoir, Virginia.

h. Investigate the use of through transmission - S. Goldspiel, NASL, Brooklyn, New York.

PROBLEM No. 7

ASSESSING INTERSTITIAL CONTAMINATION IN MULTIPASS WELDS IN THICK PLATE ALLOY TITANIUM

A. L. Chick
Naval Applied Science Laboratory
Brooklyn, New York

Name of Product to be Evaluated - Interstitial contamination (carbon, oxygen, hydrogen and nitrogen) in multipass welds in heavy section alloy titanium.

Kind of Material Involved - Welds are fabricated in alpha and alpha-beta type titanium alloys, such as Ti-721, Ti-621 (0.8 Mo), Ti-6-4 ELI. The sections considered at this time range from 1" to 4" thickness.

Type of Process Involved in Manafacture of Product - Welding is accomplished using the out-of-chamber, gas tungsten arc, gas metal arc, short-circuit, spray and pulsed arc welding processes. A typical out-of-chamber welding procedure is illustrated in Figure 1.

Design of Product - Joint design normally used in fabricating the welded assemblies is the double vee butt type having included angles between 60° and 90°, depending upon the welding process employed.

Quantity Involved in NDT Evaluation - The fabrications made are limited to laboratory scale samples intended for developing welding and nondestructive test technology. The Laboratory has formed 2-1/8" thick Ti-721 alloy plate into half cylinders, each 2-1/2' long by 7' diameter. These cylindrical sections were joined with four longitudinal welds and a girth weld to form a 5' long by 7' diameter cylindrical weldment weighing over 6000 pounds. A view of the completed cylinder is presented in Figure 2. In addition, heavy section welded assemblies up to 4" thick and up to 4 feet square have been fabricated. The large cylinder was welded under field operating conditions. Welds in these assemblies are subjected to 100% NDT inspection including visual, radiographic, ultrasonic, liquid penetrant and micro-hardness tests and subsequent to NDT, welds are subjected to destructive tests and stress corrosion studies. The method should be suitable for inspecting large structural weldments.

Kind of Quality Characteristic to be Evaluated - The specific quality characteristic which it is desired to measure, using a NDT method, is the relative level of interstitial contamination in multipass welds. It is necessary to develop a test method capable of detecting contamination within one or more weld passes in the total weld thickness.

Magnitude of Quality Characteristic Needed for Satisfactory Service - The levels of contamination normally acceptable in the type of titanium welds considered are as follows:

oxygen, ppm	800 to 1000
carbon, ppm	300
nitrogen, ppm	100
hydrogen, ppm	50

The method developed should be capable of detecting an increase of 50% over the tolerable limits in any pass of the multipass welds.

Basis of Judging Reliability - Contamination generally degrades weld toughness and ductility and may contribute to catastrophic failure of deep diving vehicles.

Urgency - The development of an NDT procedure for assessing contamination in welds is a top priority item in the NASL Titanium Program.

Feasibility of Redesign - Redesign has not been considered since the fabrication procedures used are standard for joining metals.

Present Inspection Method - A satisfactory NDT inspection method does not exist for assessing contamination in completed multipass titanium welds. Present method used to assure the quality of welds is to monitor each weld pass visually, to note apparent changes in weld bead color, luster and general appearance and to perform hardness tests at discrete intervals along the surface of each weld bead. In this method, any change in bead surface color and luster accompanied by an increase in surface hardness in excess of 3 points R_c is considered to be an indication of contamination. The method is time consuming and expensive, since the services of an NDT specialist is required during welding, and the test procedures tend to delay welding. In addition, the present method is of limited value for assessing completed, full length, multipass welds, especially for production welding.

Results obtained in an initial investigation conducted to develop an NDT method for continuously detecting contamination in multipass titanium welds indicated that, among four methods explored (neutron activation, ultrasonics, vacuum hot extraction and temperature coefficient of resistance) only neutron activation was capable of detecting carbon and oxygen contamination. The other methods were found to be unsatisfactory. Subsequent work using the neutron activation method indicated that this method was not sufficiently sensitive to detect carbon contamination. NASL has sponsored an investigation of the neutron activation method for continuously assessing oxygen contamination in completed full lengths or multipass welds. The work, to date,

has been conducted on three contaminated 12" long welded assemblies fabricated from 1" thick Ti-721 alloy plate. Different levels of oxygen contamination were incorporated in all the welded assemblies. Each assembly contained two contaminated weld bead segments at different locations in the weld and each assembly was fabricated with a total of 10 weld passes including the weld reinforcements which were left intact.

Each sample was subjected to neutron activation analysis using a mobile type neutron generator under simulated field operating conditions to detect and determine the levels of oxygen contamination. A simple transport frame was constructed to contain the sample so that the assemblies could be moved rapidly from the generator to the detector. The analyses were conducted by directing the neutron beam through the weld at discrete overlapping locations along the weld seams.

Results of the neutron activation analyses conducted on the samples revealed changes in oxygen levels along the lengths of the welds but these results did not correlate with known contaminated areas in the welded assemblies.

Limitations of Test Equipment - Any NDT method used to solve this problem shall not affect the physical or mechanical properties of the material and shall not leave residual radiation in the material.

Security Classification - Unclassified.

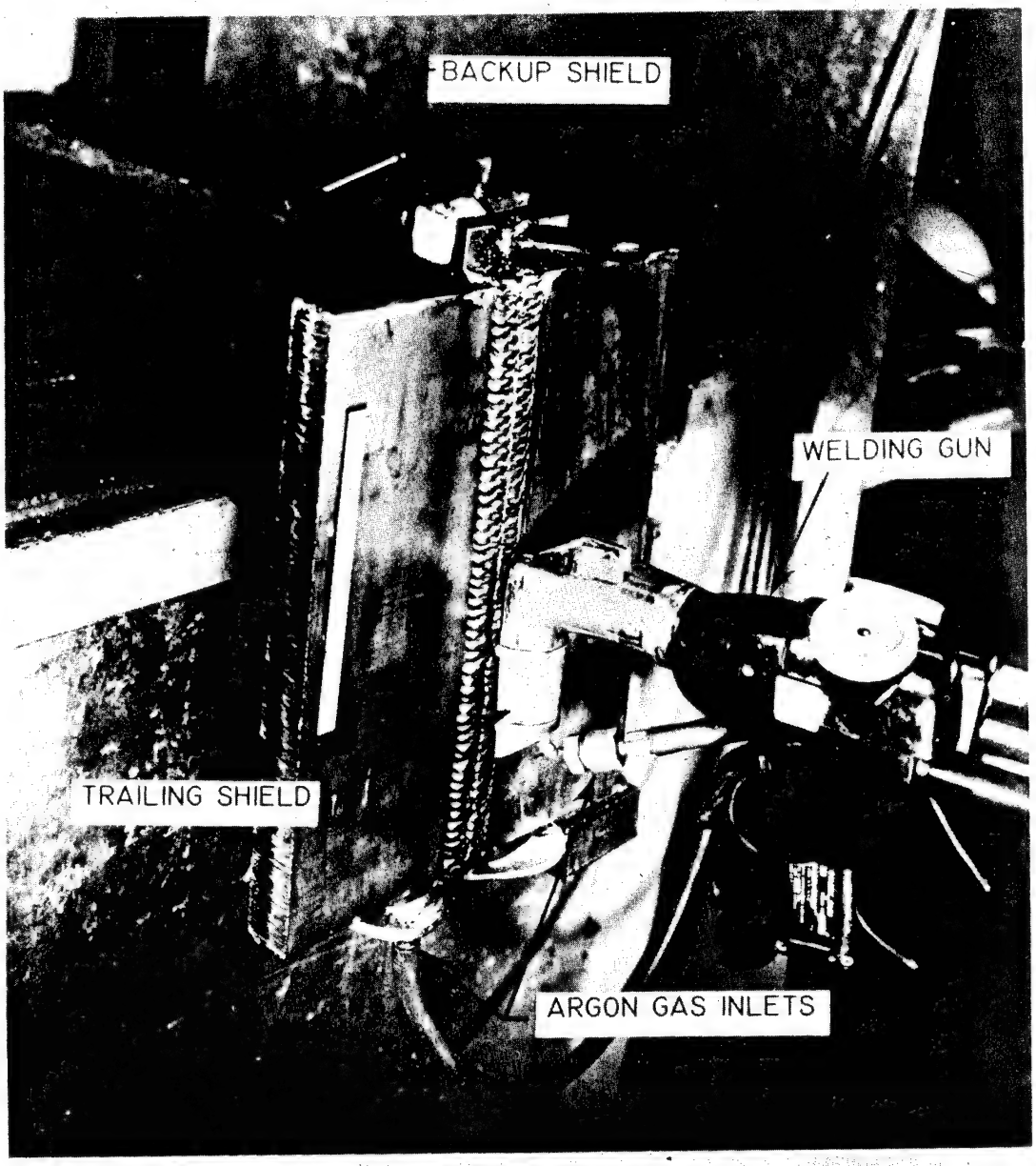

FIGURE 1 – OUT–OF–CHAMBER WELDING OF ALLOY TITANIUM

FIGURE 2 – VIEW OF $2\frac{1}{8}$" THICK X 7' DIAMETER X 5' LONG ALLOY TITANIUM CYLINDRICAL WELDMENT

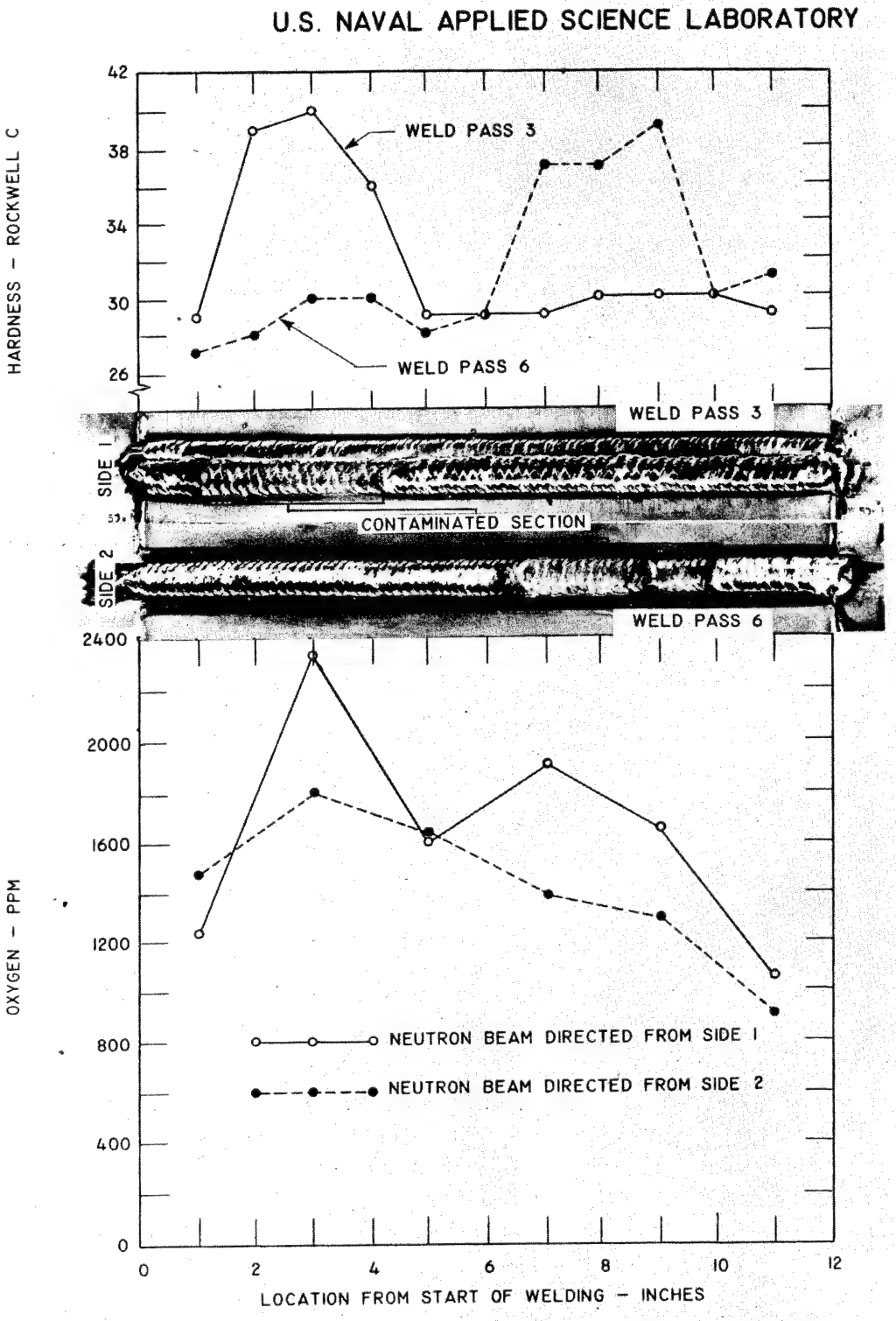

FIGURE 3 – COMPARISON OF HARDNESS AND NEUTRON ACTIVATION ANALYSIS OBTAINED IN ALLOY TITANIUM CONTAMINATED WELDED JOINT

SUMMARY REPORT OF PROBLEM NO. 7

ASSESSING INTERSTITIAL CONTAMINATION IN MULTIPASS WELDS IN THICK PLATE ALLOY TITANIUM

Bernard W. Boisvert
Problem Coordinator

A real problem with little or no help provided. Here are some of the comments:

1. Howard Heffan (NWS, Concord) suggested the possibility of an optical monitor with filters (active and passive modes) to view the weld pass during and immediately after the welding to detect discoloration indicative of a contaminated gas shield.

Mr. Chick's comment: Possible help, however, desire to examine completed weld rather than individual pass.

2. Emmett Barnes (Picatinny Arsenal) suggested photo activation with prompt detection of neutron emission. This is using high energy X-rays with analysis of resultant neutron output.

Comment: May be possible although some difficulties in adapting to field use.

3. B. Rosenbaum (NavShip Systems Command) - Considered the possibility of liquid crystals.

Comment: Have tried with no success.

4. Sol Goldspiel (Nav.Applied Science Lab). Possible to monitor the gas shield to alert for contamination. This is process control rather than inspection after the fact.

5. Doug Ballard (Sandia Corporation) mentioned that they provide additional shielding via portable hoods to reduce possible loss of or contamination of primary shield.

PAPER No. 1

DETECTION OF FATIGUE CRACKS IN THE M113, 175 MM GUN TUBE

K. A. Fowler

Army Materials and Mechanics Research Center
Watertown, Massachusetts

ABSTRACT

A method for determining the location and length of fatigue cracks in the M113, 175 MM gun tube is presented. This is accomplished by electronically detecting the magnetic leakage associated with cracks in a circumferentially magnetized tube. The history of this general technique dates back to 1944 when it was applied, as an in-process inspection aid, to the problem of finding cracks in smooth-bore tubes. However, serious attempts to apply the method to monitor service-induced fatigue damage have only recently been undertaken. A scanning mechanism employing a magnetic tape head as the detector has been developed. The scanner is inserted into the breach end of the tube and is capable of covering the area 54 to 86 inches from the breach which includes a portion of the chamber, the origin of rifling, and 23 inches of the rifled tube. The output of the detector is recorded either by means of a facsimile recorder to produce a map of the cracks in the tube surface, or by oscilloscope photographs which permit accurate signal amplitude measurements. Using this equipment, which has been designated the Magnetic Recording Borescope (MRB), tubes can be periodically inspected for progressive fatigue damage. At its present stage of development, the MRB is suitable for use at proving ground or depot level. There has been little opportunity to correlate the test indications with actual fatigue crack depth. Because crack depth is the most critical single parameter with respect to serviceability of the tube, the present inability to accurately deduce the approximate depth of the crack is the major limitation of the test. The results of a laboratory investigation conducted in support of the scanner design and a consideration of the complications introduced by the rifling and the compounding effects of erosion are also presented. The problems inherent in the present inspection procedure have stimulated an active search for auxiliary methods of indicating crack depth.

INTRODUCTION

Cracks are normally initiated in cannon bores as the first few rounds are fired and grow deeper with continued firing at a rate that is determined by numerous factors included in the design, type and condition of material, and service experience. If firing is continued indefinitely, the cracks reach some critical depth and the tube will fail.

The first attempt to detect and record bore cracks by nondestructive methods other than the optical borescope was undertaken by the Watertown Arsenal Laboratories in 1944. This program culminated in the development of the Magnetic Recording Borescope (MRB) models II and III which were "capable of accurately plotting the location and lateral extent of every bore surface crack in a smooth or nonrifled gun tube".[1] The MRB models II and III were primarily designed as in-process inspection aids. Cracks were identified in magnetized tubes by detecting the leakage field from the free magnetic poles created by the crack. Detectors were of the type commonly used in tape recorders which sense a time rate of change of magnetic flux.

The model IV, an outgrowth of the model III, was a calibrated unit designed expressly for the inspection of the smooth-bore powder chamber of the 155 mm howitzer. This sytem was capable of indicating approximate crack depth by reference to a calibration curve that was established by correlation of amplifier gain settings for threshold recording with actual crack depth observed in macroetched chamber sections. Although the resulting calibration curve showed a general decrease in amplifier gain with increasing crack depth, the scatter of individual data points was disappointing.

The relatively poor calibration curve led to a more detailed study by McElleney[2,3,4] of variables influencing the character of the leakage field associated with idealized artificial cracks. It was observed that the width of the crack, in addition to its depth, controls the magnitude of the leakage field. The leakage field and, in turn, the peak voltage induced in a tape head detector increase with both depth and width of simulated cracks.[3,4] Therefore, the peak voltage cannot be used as a unique measure of crack depth. As one might expect, the influence of crack width becomes more pronounced as the width decreases.[4] It was further found that the residual flux produced in different ring-shaped samples of similar properties varied even though magnetized at the same level of applied field.[2] Since magnitude of the leakage field is related to the flux density within the piece, this variable must also be considered when making comparison of voltage-crack depth relationships between different specimens.

Recently, there has been renewed interest in developing a nondestructive test system capable of monitoring progressive fatigue damage in the 175 mm M113. The area of interest is no longer restricted to the smooth-bore chamber, but extends some distance beyond the origin of rifling. In response, AMMRC undertook a limited preliminary investigation with the objective of reassessing the MRB approach to evaluate its potential in fulfilling the new requirements.

The existing MRB was then modified and a test program conducted at Yuma Proving Ground to determine the potential of the technique for monitoring progressive fatigue damage.

TEST PRINCIPLES

Magnetization

The most expedient way to achieve a magnetized condition in the bore surface of a 175 mm tube is by exposing the tube to a strong momentary magnetic field which magnetizes the tube to a sufficient intensity so that upon removal of the applied field, the tube retains a certain level of residual magnetization in accordance with the B-H characteristics of the steel. Because the cracks of primary concern run in a generally longitudinal direction, the residual magnetic flux must be circumferentially oriented in order to be intercepted by the crack at approximately 90 degrees. A flux of this orientation is produced when a direct current of roughly 2000 amperes is passed through a central conductor in the manner illustrated by Figure 1. The level of residual magnetization is controlled by maintaining a constant value of magnetizing current. Though small variations in the level of residual magnetization can occur as a result of differences in the B-H characteristics of the steel brought about by variations in composition, thermal and magnetic histories, and state of stress, the residual flux density is considered constant for practical purposes.

The resulting magnetic leakage flux associated with a crack-like defect is illustrated schematically in Figures 2 a and b. The tangential component of the leakage flux reaches a maximum value on the cracked surface at the center of the crack. The density of the leakage flux diminishes as one moves away from the crack, but at any given level above the surface, the maximum leakage flux density occurs directly above the center of the crack. The actual magnitude of the leakage flux density, at any level above the cracked surface, depends on the residual flux density within the tube, the depth of the crack, and the width of the crack. It should be understood that the idealized field shown in Figure 2 holds only for a smooth surface and is not representative of the distortions that occur when a rifled surface is considered.

Detection

In the more familiar magnetic particle method of inspection for surface cracks, ferromagnetic powders are used as the "detector", where the powder is collected by the leakage field emanating from the free magnetic poles associated with the crack. Although an electronic detector is substituted for the conventional ferromagnetic powder in the MRB crack detection system, magnetic leakage flux is detected in both cases. The reasons for utilizing an electronic detector are several: (1) increased speed of inspection; (2) more complete coverage of the cracked surface; (3) relative inaccessibility of the bore limits visual observation; (4) quantitative readout of a parameter related to magnetic leakage flux; and (5) permanent recording of the test data.

Two basic types of electronic detectors are available for sensing the existence and location of magnetic leakage fields. The first class of electronic detectors includes devices, such as magnetic tape heads, which generate an output voltage that is directly proportional to the time rate of change of the magnetic flux induced within the ferro-magnetic core of the head. The MRB system in its present form employs a magnetic field detector of this class. In order for this type of detector to function, either the magnetic field must vary with respect to time when the detector head remains stationary, or the detector head must be moved through a magnetic field when the field is static.

The second class of electronic detectors includes devices which utilize the Hall effect. A Hall probe is sensitive to a magnetic field, per se, rather than to the time rate of change of the magnetic field. These probes with appropriate readout instrumentation could, therefore, be used either to make static measurements of leakage fields or to scan a surface in the same manner as the MRB. Hall probes have not been utilized in the MRB because they generally are more fragile than tape detector heads and require more delicate readout instrumentation. However, this type of detector is being considered for future application to certain aspects of this testing problem.

Once the tube has been magnetized, the residual magnetic field strength on the surface remains static. Therefore, the tape head detector head is rotated around the inner circumference of the tube. Figure 2 illustrates the relation between the original magnetic leakage field and the output of the magnetic tape head detector. Although Figure 2b is labeled "Tangential Component of the Leakage Flux", this plot also represents, equally well, the magnetic flux induced in the core of the detector head as a function of position relative to the crack. Figure 2c shows the output of the detector which is proportional to dB/dt.

LABORATORY INVESTIGATION

Only a brief description of the laboratory phase of the investigation will be given here. The reader is referred to reference 5 for a complete account of this work. The primary purpose of this phase of the program was to determine if, in fact, relationships could be expected between the output of a tape head detector and crack depth and to evaluate the influence of rifling, level of magnetization, and crack width on such a relationship.

PROCEDURE

Test Fixture

Because response of a magnetic tape head is dependent on a rate of change of flux, relative motion must exist between the detector and the specimen. In

the MRB system, this motion is achieved by rotating the detector while the test piece remains stationary. For this laboratory investigation, it was more expedient to move the test piece relative to the detector, as shown in Figure 3 where a ring-shaped specimen is rotated by a variable speed motor.

Detector Head Assembly

The detector head holder is also shown in Figure 3. The holder provides for adjustment of the spacing between the detector and the specimen surface. The aluminum end plates are contoured to match the radius of curvature of the bore and serve as skids which maintain the fixed spacing between the detector and the moving surface.

Tape Head Detectors

Detectors are easily changed in the holder which permitted investigation of the influence of various tape head design parameters, such as gap width and coil inductance, on the detector performance in this application. The pertinent characteristics of the tape heads that were evaluated are listed in Table I. The head that is presently being used in the MRB system is head number 2. Tests indicate, however that other heads could be used equally well.

Table 1. TAPE HEAD CHARACTERISTICS

Head Number	D-C Resistance (ohms)	Inductance at 1Kc (henry)	Gap Width (inch)	Manufacturer
1	105	0.180	0.001	A
2	70	0.10	0.001	B
3	230	1.0	0.001	B
4	91	0.092	0.001	C
5	252	0.112	0.002	C
6	221	0.101	0.005	C
7	588	0.990	0.001	C

Test Specimens

The test pieces were in the form of 3-inch-long tube segments containing milled slots, 0.004 to 0.010 inch wide, cut longitudinally to simulate cracks with depths ranging from 0.010 to 0.250 inch. Although milled slots may not represent the best method of crack simulation, they were used because test pieces were immediately available and the procedure for making them was well established. These slots will subsequently be referred to as cracks. The smooth bore specimens consisted of an outside retaining ring of 2-3/8-inch wall thickness into which a second ring comprised of three equal segments was press-fitted. The wall thickness of the second ring, which contained the milled slots, was 0.5 inch and this ring was cut in thirds to facilitate the slot-cutting operation. The inside diameter of the finished ring was 6-1/16 inches. These test pieces were prepared for a previous investigation and a more complete description is found in Reference 2. Rifled tube sections were cut from 175 mm tubes. The OD was machined to fit the test fixture.

Electronic Setup

The signal from the tape head detector was amplified and applied to the input of an oscilloscope. Position synchronization was maintained by the voltage pulse generated as the small permanent magnet passes a coil wound on a ferrite rod (see Figure 3). The pulse was amplified and served as an external trigger for the oscilloscope trace. This procedure insures that each trace starts at exactly the same point on the specimen.

Rotational velocities of 30 and 60 rpm were used throughout the laboratory investigation. This permitted calibrated oscilloscope sweep rates of 0.2 and 0.1 sec/cm to be used with full utilization of the 10-cm trace length for one revolution of the test piece. With a knowledge of the crack location on the inside circumference of the segment, it is possible to locate them exactly on the oscilloscope trace.

RESULTS AND DISCUSSION

I. SMOOTH BORE TUBES

The first phase of the laboratory investigation was concerned with detecting simulated cracks in smooth bore tube segments after magnetization. To aid in the interpretation of Figure 4, Table II shows the location of each artificial crack on the inside circumference and its relative position based on ten linear units for a full revolution. Cracks 1, 6, and 9 are the joints between the three press-fit sections of the inner ring.

Table II. ARTIFICIAL CRACK LOCATIONS AND DIMENSIONS IN SMOOTH BORE SPECIMEN 5503

Crack No.	Location on I.D. Actual (inches)	Location on I.D. Relative (Based on 10 Units)	Dimensions (mils) Width	Dimensions (mils) Depth
1	0.00	0.00 units	1	500
2	0.75	0.36	8	75
3	1.50	0.72	10	250
4	5.25	2.50	8	150
5	6.25	2.98	8	100
6	6.95	3.30	1	500
7	8.30	3.95	6	40
8	12.65	6.03	8	60
9	13.95	6.65	1	500
10	15.30	7.30	6	30
11	19.60	9.35	4	10

After two successive magnetizations, a residual flux of 22 and 27 gauss was measured in a 1/4 inch diameter by 0.75 inch deep access hole for the first and second magnetizations, respectively. A tape head made by the manufacturer that supplied the heads for earlier models of the MRB was used (see head No. 1, Table I).

Characteristic defect indications obtained under these conditions are shown in the oscillograph of Figure 4. The crack indications are easily identified as a negative voltage followed by a sharp reversal to a positive voltage as the sign of the time derivative of flux in the core of the detector reverses. The form of the crack indication corresponds exactly with the theoretical model shown in Figure 2. Also shown in Figure 4 is the relation between peak-to-peak voltage amplitude and the depth of the corresponding crack. Note that two sets of data are shown representing the two levels of residual flux. The increase in induced voltage due to the higher residual flux appears to be greatest for the deepest cracks. The need for adequate control over residual flux in the test piece is quite apparent.

A reasonably good relationship between induced voltage amplitude and crack depth was obtained for the milled slots. Variations in crack width in the range of 4 to 10 mils did not appear to have a significant influence. However, the voltages induced by cracks 1, 6, and 9 are much lower than the relationship established by the milled slots would predict. These defects represent the joints between the 0.50-inch-thick insert and, because these were press-fitted into the outside retaining ring, the air gap is extremely thin. The reluctance of the crack is consequently reduced and the leakage field for a crack of any given depth is considerably diminished. This points up the drastic influence that crack width can have.

II. RIFLED TUBE

The first segment of rifled tube available for testing was taken from gun tube 550 which was finish machined but had never been fired and, therefore, contained no fatigue cracks. Three slots were milled in this specimen 0.010 inch wide by 0.135, 0.120, and 0.060 inch deep located at 12, 3, and 6 o'clock respectively.

The rifled tube segment was magnetized to produce a residual flux of 22 gauss as measured in a 1/4 inch diameter by 1-1/2 inch deep access hole. Figure 5 shows an oscillograph trace of the signal obtained for one revolution of this specimen. The indications from the three milled slots are the high-amplitude negative voltage spikes. Unlike the traces from smooth bore tubes, there is also a relatively high-level signal produced by leakage from the lands. The land signal varies both in amplitude and waveform around the circumference. It is quite apparent that the signal produced by the presence of small fatigue cracks at the base of the lands may be completely overshadowed by the land signal. These signals are quite characteristic of those observed while actually testing 175 mm tubes with the MRB in sections of the tube where a substantial portion of the rifling remain.

175 mm INSPECTION PROGRAM

In January 1967 an AMC program for 175 mm, M113 cannon was implemented with the objective of establishing criteria which could be used as an adequate basis for extending the useable life of the tube. Basically the test plan called for a total firing accumulation of 1000 zone-3 rounds on each of three gun tubes. MRB inspections of the tubes were made at intervals of 100 rounds or less. Upon completion of the 1000 rounds at ambient temperatures, the test plan required that 5 rounds be fired at -40°F with MRB tests before and after firing. The tubes were then to be fatigue cycled to failure in the laboratory and cut up for evaluation of metallurgical and mechanical properties, and crack depth.

THE MAGNETIC RECORDING BORESCOPE

As has been stated previously, the MRB is a nondestructive testing device which has been specifically designed to detect and locate both surface and near-surface discontinuities (such as fatigue cracks) within the bore of a previously magnetized cannon tube. The MRB employs a rotating, magnetic tape-recording head as a means of detecting the magnetic leakage emanating from the free magnetic poles associated with a discontinuity. The MRB readout is a recording which actually represents a three-dimensional map of the interrogated bore surface. The longitudinal and circumferential positions are indicated quantitatively, while the crack depth is indicated qualitatively. By augmenting this recording with an oscillographic readout, quantitative defect signal-amplitude data may be obtained which can then be used to obtain a correlation with crack geometry. The types of discontinuities capable of being detected include quench cracks induced by heat treatment, and fatigue cracks induced by firing. However, the depth of fatigue cracks cannot by accurately determined at this time from the induced detector-voltage amplitude due to the influence of interfering factors that will be discussed shortly.

The instrumentation for inspecting 175 mm cannon bores for defects is shown in Figure 6, and consists of three major units: a scanning mechanism containing a motor-driven, rotating detector-head; a console which contains a motor generator, control panel, and facsimile recorder; and finally, a signal monitoring oscilloscope. The Magnetic Recording Borescope, per se, is comprised of the first two major units.

To adapt the existing MRB equipment to the immediate 175 mm M113 cannon inspection requirements, it was necessary to completely design a new centrifugal-head scanning mechanism Details of the new centrifugal head MRB scanning assembly are shown in Figure 7. It should be noted that this new design provides three degrees of freedom for the magnetic tape-recording head: radial, tangential, and axial. The radial freedom assures maintenance of a constant relative air gap distance of approximately 0.006 inch between the recording head and bore surface. The tangential freedom assures perpendicularity of the recording head to the bore surface. The axial freedom assures constant alignment of the recording head with the bore surface during change-of-slope conditions within the chamber neck, forcing cone, and origin of rifling portions of the gun tube. The magnetic tape recording head rotates at 300 rpm and the axial traverse rate is 6 in/min.

The major components of the scanning system are shown in Figure 8. An outer positioning and fixturing tube (center left) is provided to locate the scanner along the axis of the gun tube. An inner tube (bottom) serves the multiple purposes of (1) providing support for the detector head and scanning motor; (2) functioning as an axial traversing mechanism; and (3), serving as a conduit for an electrical cable. The thrust tube, plate, and spring assembly for locking the scanner into position are shown at the center right position of

the figure. The axial-traverse motor appears in the upper position in the figure. The inner tube is gear-racked for traversing a distance of 32 inches, which includes a portion of the chamber, the forcing cone, the origin of rifling, and approximately 24 inches of the rifled portion of the tube. A close-up view of the scanning head is shown in Figure 9.

PROCEDURE

Selection of Tubes

Selection of three tubes (863, 1185, and 1382) for the test program was based primarily on a consideration of the manufacturers' reported mechanical property data. These tubes represent a range in mechanical properties and this is reflected in the variation in the life of the tubes. Table III summarizes the number of total rounds, zone-3 rounds, and fatigue cycles for each tube to failure.

TABLE III

		Zone-3 Rounds		
Tube No.	Total Rounds	Ambient	-40 F	Fatigue Cycles
863	1005	1000	5	6
1185	1021	1000	1	0
1382	1005	1000	5	406

*21 rounds fired in tube 1185 were zone 1 and 2.

Inspection Procedure

After each firing increment, the tube was magnetized with 1800 amps of direct current through a central conductor as illustrated in Figure 1. The MRB amplifier calibration was checked prior to each inspection. Facsimile recordings were then made at each of a number of amplifier gain settings and oscilloscope traces were recorded at those longitudinal positions where significant defect indications were observed. A timing mark occurring at 3 o'clock relative to the tube appears on the facsimile recordings at 63, 64-1/4, 67, 71, and 74-1/4 inches from the breech of the tube. The same timing mark was used to externally trigger the oscilloscope so that each trace starts at 3 o'clock. The detector scans the bore in a counter clockwise direction. Therefore, the o'clock position changes in the counter clockwise direction in going from right to left across the facsimile recording or oscilloscope trace. The width of the recording paper, or one scan line, represents the

circumference of the tube bore since the helix electrode and the detector head rotate at the same angular velocity. The length of the recording is linearly related to the scanning head axial-traverse distance by the ratio, 0.475 inch of paper per 1.0 inch of tube length. The third dimension provided on the recording is the marking intensity, which is directly proportional to the received signal level. Therefore, the recording provides a three-dimensional "map" of the bore surface where the position of a discontinuity is indicated both axially and circumferentially and the severity of the discontinuity is revealed by the marking intensity of the defect indication.

Tube 863

From the oscillograph records of crack indications in tube 863, 69 individual indications were selected and averaged to obtain an average indication amplitude at 925, 950, 975, 1000, and 1005 rounds. The average indication was used as a more reliable measure of rate of tube deterioration because the amplitude of individual indications does not increase uniformly with the number of rounds fired. This is the result of random cycle to cycle variations in signal amplitude originating from minor fluctuations in the way in which the head holder tracks the irregular eroded surface.

The amplitude of the crack indication at approximately 1130 o'clock was plotted against longitudinal position between 65 and 73 inches at 925, 1000, and 1005 rounds.

No detailed crack depth information is available at this time for correlation with defect amplitudes.

Tube 1185

Thirty-one defect indications were selected and averaged at 825, 875, 900, 925, 950, 975, 1000, and 1021 rounds. The amplitude as a function of length, between 62 and 72 inches, of the crack occurring at about 1100 o'clock was plotted at 700, 800, 900, and 1021 rounds. Preliminary crack depth measurements were also available from the fracture surface of a fragment of tube 1185.

Slices from a fragment of 1185 were cut and macroetched to reveal the crack pattern and photographed. Figure 10 shows an example of the crack patterns occurring in these slices. Because the cracks did not propagate in a radial direction, there is a question as to what portion of the crack should be measured for correlation with defect signal amplitudes; however, the maximum radial depth was measured for this purpose.

Tube 1382

No average crack indication amplitudes were calculated for tube 1382 because of the relatively low amplitudes and slow growth rates observed.

Tube 1382 failed after 406 laboratory fatigue cycles. The apparent origin of failure was a crack at 1000 o'clock extending from 62-1/16 to 64-7/16 inches from the breech of the tube. The crack depth at the completion of firing was measured on the fracture surfaces and then correlated with the amplitude of the indication.

RESULTS AND DISCUSSION

In Figures 11 through 17 several facsimile recordings of the three tubes are shown. It should be noted that the facsimile recordings have been reduced for reproduction. The recordings of 1185 were selected to illustrate the indication of progressive damage suffered by the tube as firing was continued to 1000 rounds. The recordings are arranged in order of increasing tube number and increasing number of rounds fired. All recordings were made at the same MRB settings.

The portion of the facsimile recording nearest the breech end of the tube is at the top of the page. In each case, the approximate position of the origin of rifling can be located, longitudinally, by finding the first dark timing mark. Reference to Figure 12 will illustrate the features common to all of the recordings. The portion of the recording from the top of the picture to the first timing mark represents the smooth-bore chamber area. This is followed by the rifled portion of the tube where magnetic leakage from the lands produces a pattern of the rifling. It will be noticed that the rifling pattern in tube 1185 prior to firing was quite uniform.

The progress of damage in tube 1185 can be followed in Figures 12 through 16. At 300 rounds a crack indication has developed to the right of the 3 o'clock mark in the vicinity of 12 o'clock. Also there is evidence of land erosion in a V-shaped area around the 12 o'clock position. Between 300 and 600 rounds rapid deterioriation occurs and continues to 1021 rounds with individual cracks joining to form long continuous cracks running longitudinally down the tube. At 12 o'clock the lands are completely removed by erosion.

Comparison of Figures 11, 16, and 17 show that both 863 and 1185 had suffered severe damage upon completion of 1000 rounds of zone-3 firing, while tube 1382 showed much less damage. It is also interesting to observe that the rifling pattern in Figure 17 is not at all uniform. This variation is thought to be due to variations in the residual stress, however, this has yet to be confirmed.

Although the recordings made on the three tubes used in this program would appear to allow one to determine the initiation and approximate rate of growth of fatigue damage, caution must be exercised in the significance attached to these indications. It is, for example, impossible at this time to predict the depth of the crack from the indication, especially early in the life of the tube when a substantial portion of the rifling remains. Because the sensitivity of the detector to cracks forming at the root of the land is greatly influenced by the distance above the cracked surface, the point at which one first observes a significant crack indication may be a function of the rate of land erosion. The reason that this is stressed is that under certain conditions, cracks of considerable depth can go undetected if they occur in a portion of the rifled tube that has experienced only minor erosion.

Figure 18 shows a plot of the average indication data against the number of rounds. The reason for the rather abrupt increase followed by the plateau between 875 and 950 rounds for tube 1185 is not known. It is equally difficult to say with any certainty that this increase in signal amplitude corresponds to a marked increase in crack depth in the tube. It is interesting to note that the slopes of the curves for tubes 1185 and 863 are about the same, indicating approximately the same rate of deterioration if the hump in the curve for tube 1185 is ignored. The most significant feature of these curves is the marked increase in the average amplitudes of selected defects in 863 caused by the five rounds fired at -40 F. Since the low-temperature firing would be expected to cause a significant increase in crack growth rate if other factors are held constant, this might be the best evidence that the rate of increase of the average-crack-amplitude parameter is a valid measure of the rate of accumulation of fatigue damage.

Longitudinal Crack Indication Profiles

Figures 19 and 20 show the variation of indication amplitudes with longitudinal position and number of rounds for the most severe crack indication in tubes 863 and 1185. It will be noticed that, although there is a general increase in the maximum amplitudes of the indication with increasing rounds, the increase is not uniform along its length. In fact, at some points the amplitude may actually decrease with increasing numbers of rounds. This seemingly peculiar occurrence may be brought about by the effects of erosion in the tube which can round off the corners of the cracks, thereby reducing the intensity of the leakage field. In some cases, formation of a groove at the crack has been observed which effectively increases the detector lift-off. Changes in the bore surface may cause the head to bounce in the vicinity of the crack again yielding a low or inconsistent voltage reading. In general, as the number of rounds is increased, the crack indication profiles retain the same shape and there seems to be some correspondence between the estimated depth of the crack in tube 1185 (Figure 20) and the variation of indication amplitudes.

Correlation with Crack Depth

Although a quantitative correlation between the indication and crack depth is the most important single objective of this phase of the program it is also the most elusive. Efforts to arrive at such a correlation are continually frustrated by the many uncontrollable factors that influence the defect signal in addition to depth. Among these are the effective lift-off of the detector from the cracked surface, the width of the crack, the smoothness of the surface at the crack, the angle at which the crack intersects the surface, and the manner in which it propagates through the wall. The relative contribution of each of the factors is unknown and the quantitative importance cannot begin to be assessed on the basis of present knowledge. As a result it has been necessary simply to correlate the peak-to-peak voltage amplitudes with the total estimated radial crack penetration knowing that this will produce a very wide scatter band and that with time, and more judicious measurement of crack and defect signal parameters, a better correlation may be obtained. The available crack depth information for correlation with defect signal amplitude is quite meager at this time. The type of crack patterns also varies considerably from the almost radial cracks found in tube 1382 to the curved cracks observed in tube 1185 (Figure 10). The information that is available is summarized by tube number.

Tube 863

No detailed crack depth information is available at the present time.

Tube 1185

Only one piece of 1185 in the critical origin of rifling area at 1200 o'clock was retrieved after failure. The location of this piece relative to the MRB facsimile recording is shown in Figure 16 by the outlined area. A transverse slice of this fragment is also shown in Figure 10.

An excellent correlation was found between the position, both longitudinally and o'clock, and the location of the crack indications on the facsimile recordings. Correlation of signal amplitudes with crack depth, however, is a different matter. With respect to the estimated crack depth in tube 1185, there is the added uncertainty of the amount of crack propagation produced as a result of the last round at -40 F that caused failure. The crack depths after failure had to be correlated with the defect signals obtained immediately prior to the last round. However, from the section cut between the 71-1/2- and 72-inch positions, the material next to the bore surface was removed and broken along the existing cracks. Examination of the crack surfaces revealed that they were very dark and, with the exception of a very short length at the crack tip, had apparently existed for several rounds. The crack depth, at least at this position, was not materially affected by the last round fired.

Figure 21 shows the oscillograph records at several locations. These records illustrate the range of crack signal waveforms that are obtained. Peak-to-peak voltage measurements were made in each case regardless of symmetry of the waveform.

Table 1382

The cracks in 1382 were quite shallow and generally radial. The depth was estimated from fracture surfaces on material taken from the failed tube.

A composite plot of all of the crack depth data is shown in Figure 22. Although the scatter band is very broad, there is a general trend toward increased signal voltage with increased depth of crack. It is possible that some of this scatter is the result of the non-radial nature of many of the cracks and the uncertainty that this created in measurement of crack depth. Nevertheless, there are many sources of error which have already been indicated that contribute to the scatter observed in Figure 22. Some of these sources of error are basic to the method and it is for this reason that an active search is in progress for auxiliary methods that offer a potential capability for more accurate crack depth evaluation.

CONCLUSIONS

1. From the laboratory investigation it was found that there can be relatively good relation between peak-to-peak defect signal amplitude and simulated crack depth. However, the results suggest that the signal amplitude for a given depth is reduced as the crack becomes thinner and the sides of the crack come in contact.

2. Rifling reduces the sensitivity of the method to small cracks, however, large defects can be readily detected. Smaller cracks may not be detected because of the combined effects of land noise and increased detector lift-off.

3. The MRB system is capable of detecting cracks in the chamber and origin of rifling areas of the 175 mm gun tube and producing an accurate map, in the form of a facsimile recording, of their longitudinal and o'clock position and length. The minimum depth of crack that can be detected is dependent on the surface condition of the bore; that is, the progress of land erosion. It is fortunate from the standpoint of this test that usually by the time cracks of significant depth have formed in the critical zone the rifling is nearly removed so that an essentially smooth bore condition prevails. Under most conditions it can be conservatively estimated that cracks as shallow as 1/4 inch can be readily detected.

4. The facsimile recordings are reproducible and with them one is able, in a qualitative way, to monitor progressive fatigue damage with increased firing. This is presently considered to be the most important result of the program.

5. An excellent correlation was found between the indications of cracks on the facsimile recordings and actual crack locations in the tubes after sectioning.

6. The correlation between crack signal amplitude and crack depth is influenced by a variety of factors which contribute to a wide scatter of the data. Nevertheless, a general trend does exist between the peak-to-peak signal amplitude and depth. The existing correlation between depth and signal amplitude, however, has not been refined to a point where it can be used to accurrately predict the depth of fatigue cracks.

PRESENT STATUS

Work on the MRB system is being expanded. The correlation between crack depth and signal parameters will be the object of intensive effort. The MRB system itself is undergoing several modifications. Present plans call for the MRB console containing the facsimile recorder to be replaced by a recording fiber-optic cathode ray oscillograph. Consideration is also being given to tape recording the detector output during the actual inspection of the tube. The tape would then be played back into the oscilloscope to produce C-scan recordings and single sweep recordings for voltage measurement. With these modifications the system will be capable of providing a greater amount of quantitative data more rapidly.

LITERATURE CITED

1. HASTINGS, C. H., DARCY, G. A., AND MC ELENEY, P. C. "Crack Depth Measurement in Powder Chambers of Cannon". Army Materials and Mechanics Research Center, WAL TR 732-123, 1 July 1953.

2. MC ELENEY, P. C. "Crack Depth Leakage Flux Characteristics in Ferromagnetic Materials". Army Materials and Mechanics Research Center, WAL TR 148.1/1, April, 1960.

3. MC ELENEY, P. C. "Influence of Crack Width and Depth on Magnetic Flux Leakage Fields". Army Materials and Mechanics Research Center, WAL TR 148.1/2, August 1960.

4. MC ELENEY, P. C., and BONANNO, J. W. "Electric Field Analogy of Crack Width and Depth Effect on Leakage Flux in Ferromagnetic Materials". Army Materials and Mechanics Research Center, WAL TR 148.1/3, December 1961.

5. FOWLER, K. A. "Magnetic Methods for Crack Detection in Cannon Bores". Army Materials and Mechanics Research Center, AMRA TR 67-06, February 1967.

Transverse cross-sectional view of the direction of the magnetic field induced within the walls of the gun tube

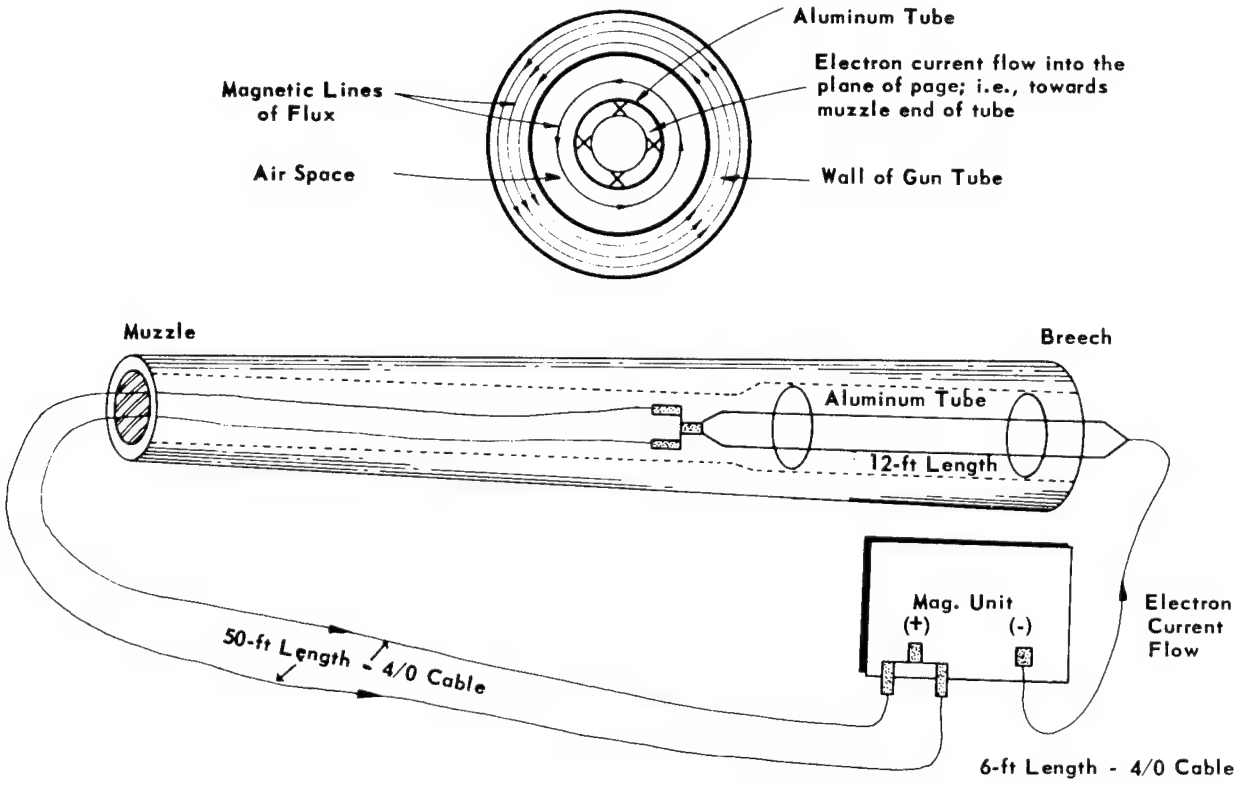

Figure 1. MAGNETIZATION SCHEMATIC

ARMY MATERIALS AND MECHANICS RESEARCH CENTER

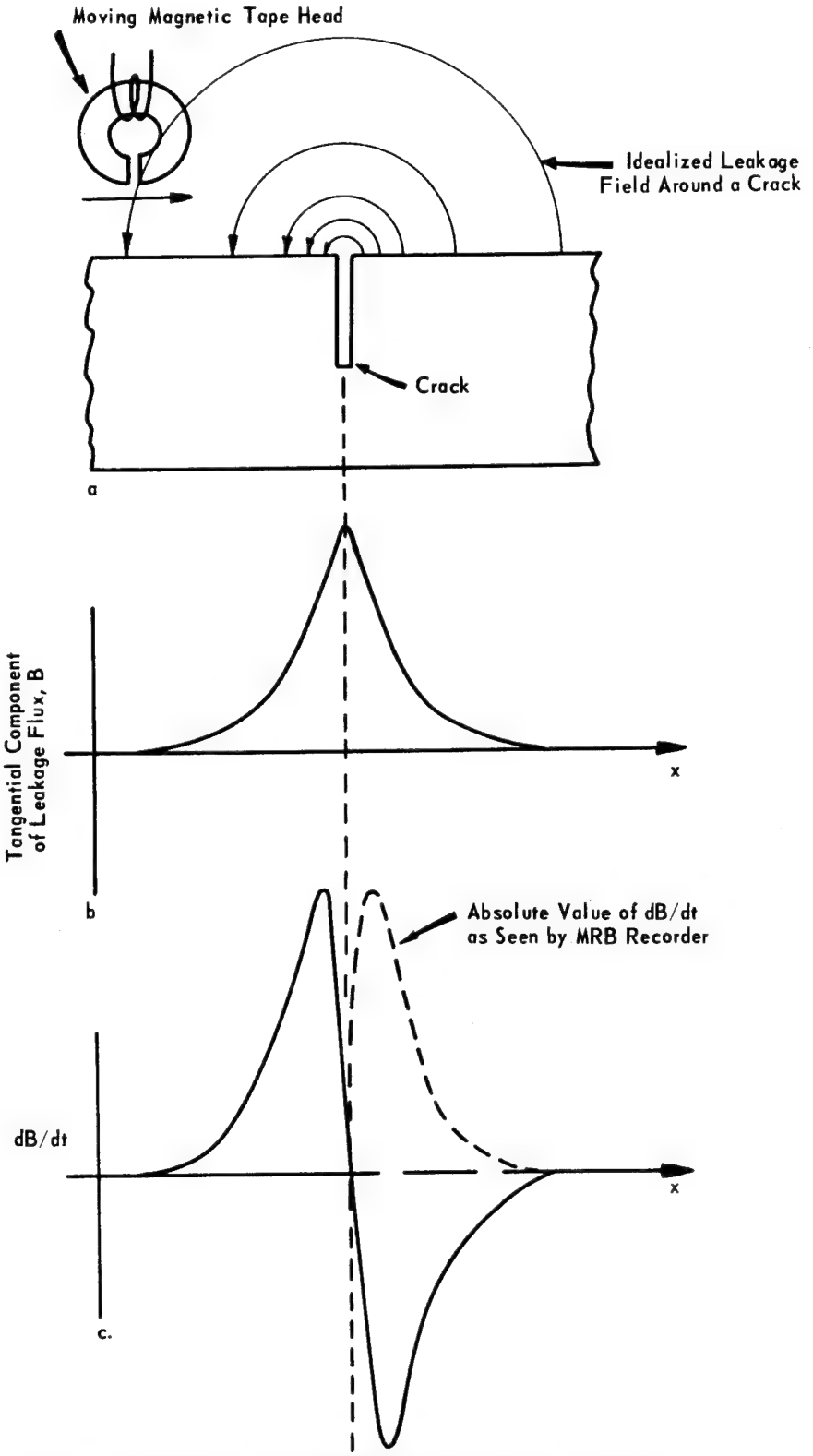

Figure 2. BASIS FOR ELECTRONIC DETECTION OF MAGNETIC LEAKAGE ASSOCIATED WITH CRACKS

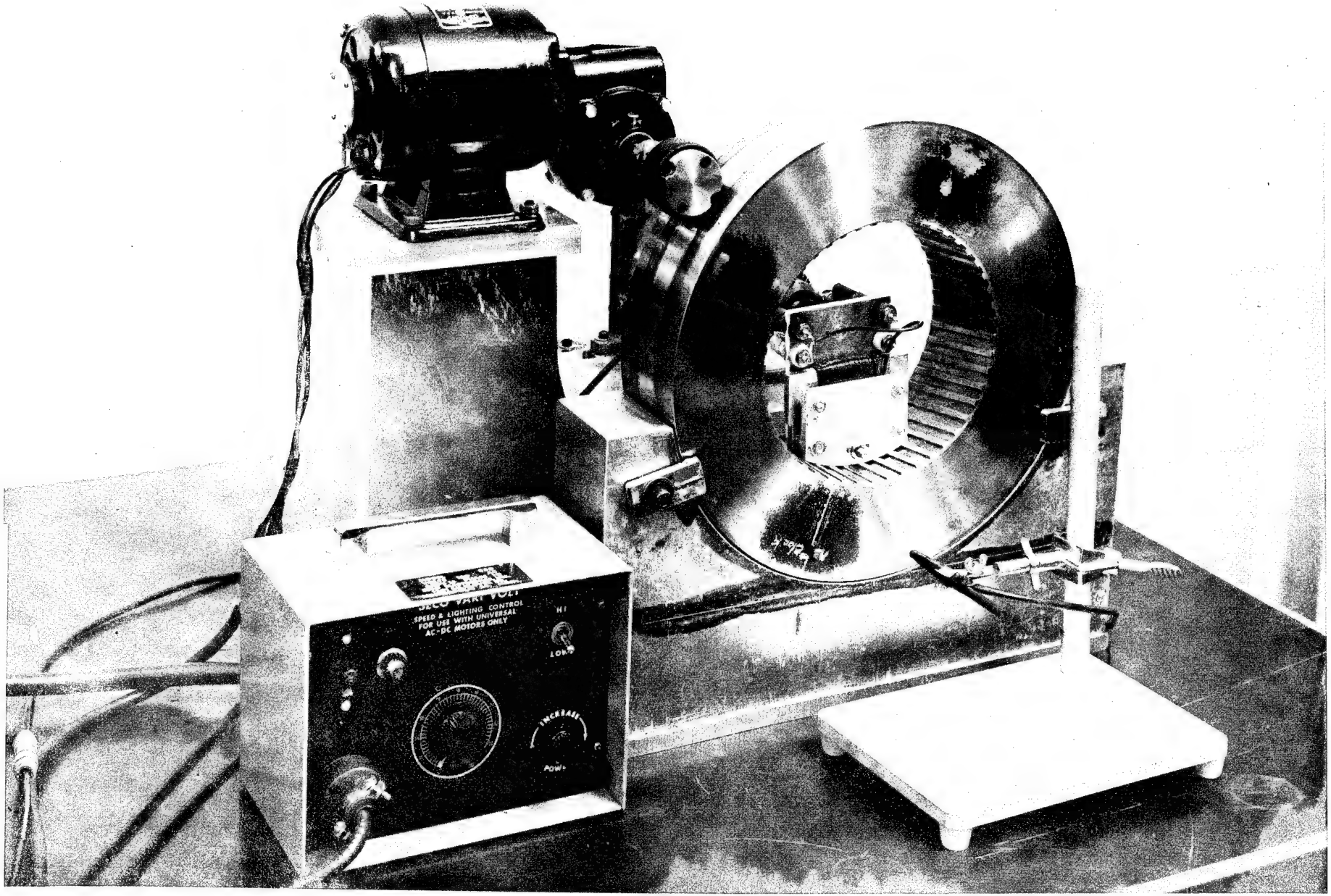

Figure 3. LABORATORY FIXTURE FOR INVESTIGATING MAGNETIC METHODS OF NONDESTRUCTIVE CRACK DETECTION IN THE BORE OF GUN TUBES

U. S. ARMY MATERIALS RESEARCH AGENCY

19-066-1568/AMC-66

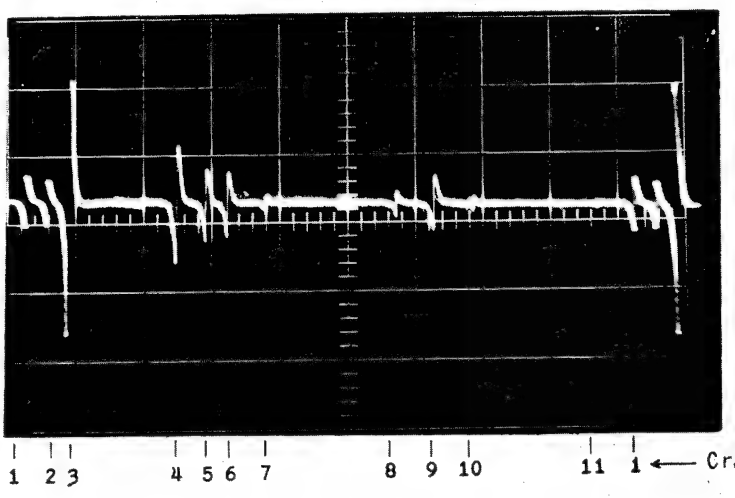

Specimen No. 5503
Rotational Speed - 60 rpm
Surface Speed - 1260 in/min
Vertical Sensitivity - 200 mv/cm
Sweep Speed - 0.1 sec/cm
Tape Head No. 1
Tape Head Lift-Off - 3 to 4 mils
Premagnetized - 27 gauss

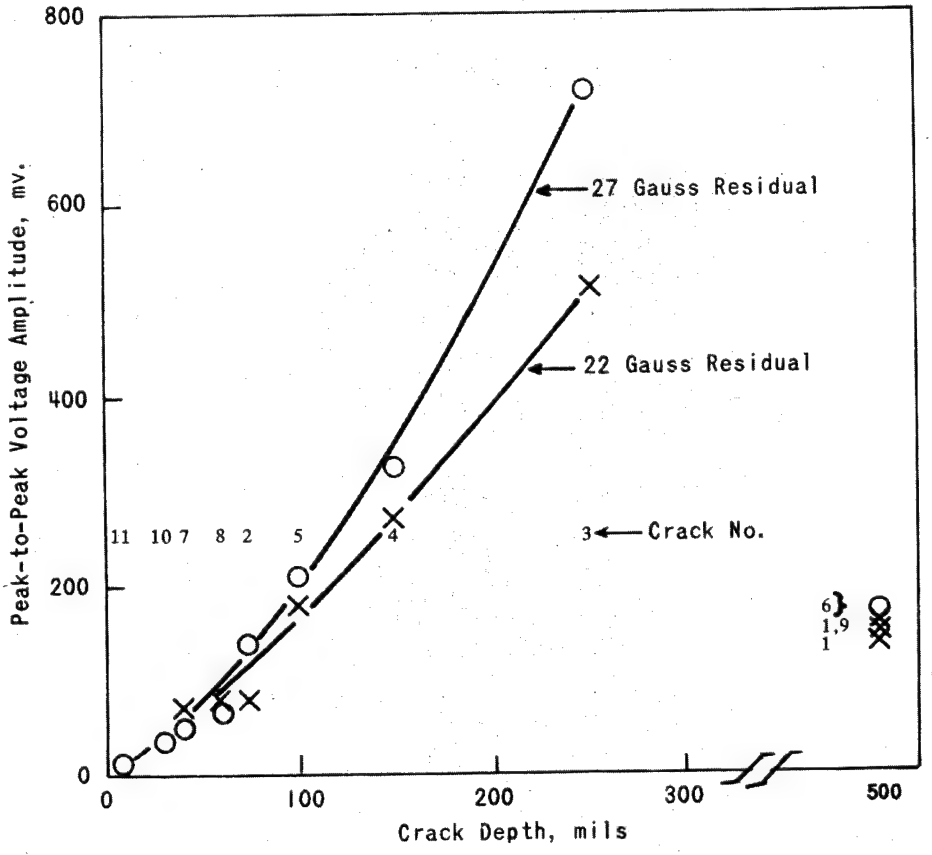

Figure 4. OSCILLOGRAPH OF CRACK INDICATIONS AND RELATION BETWEEN INDUCED VOLTAGE AND CRACK DEPTH USING RESIDUAL MAGNETIZATION

ARMY MATERIALS AND MECHANICS RESEARCH CENTER

19-066-1245/AMC-67

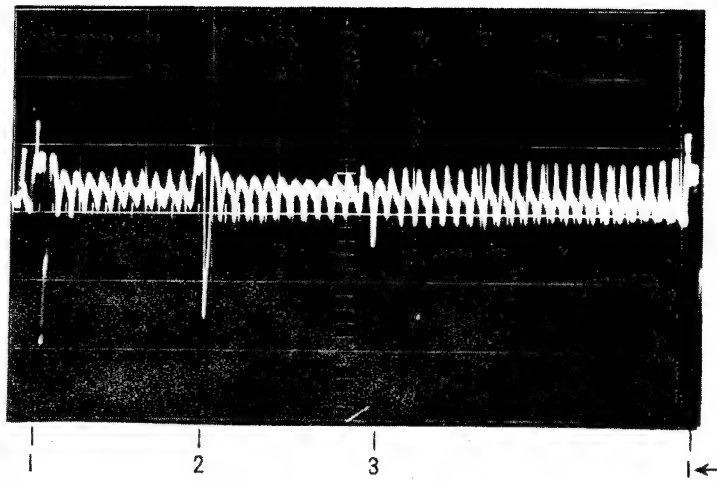

Specimen 550-B-2
Rotational Speed - 60 rpm
Surface Speed - 1300 in/min
Vertical Sensitivity - 50 mv/cm
Sweep Speed - 0.1 sec/cm
Tape Head No. 3
Tape Head Lift-Off - 4 mils
Premagnetized - 22 gauss

Figure 5. OSCILLOGRAPH OF SIGNAL FROM RIFLED TUBE SEGMENT

ARMY MATERIALS AND MECHANICS RESEARCH CENTER

19-066-1244/AMC-67

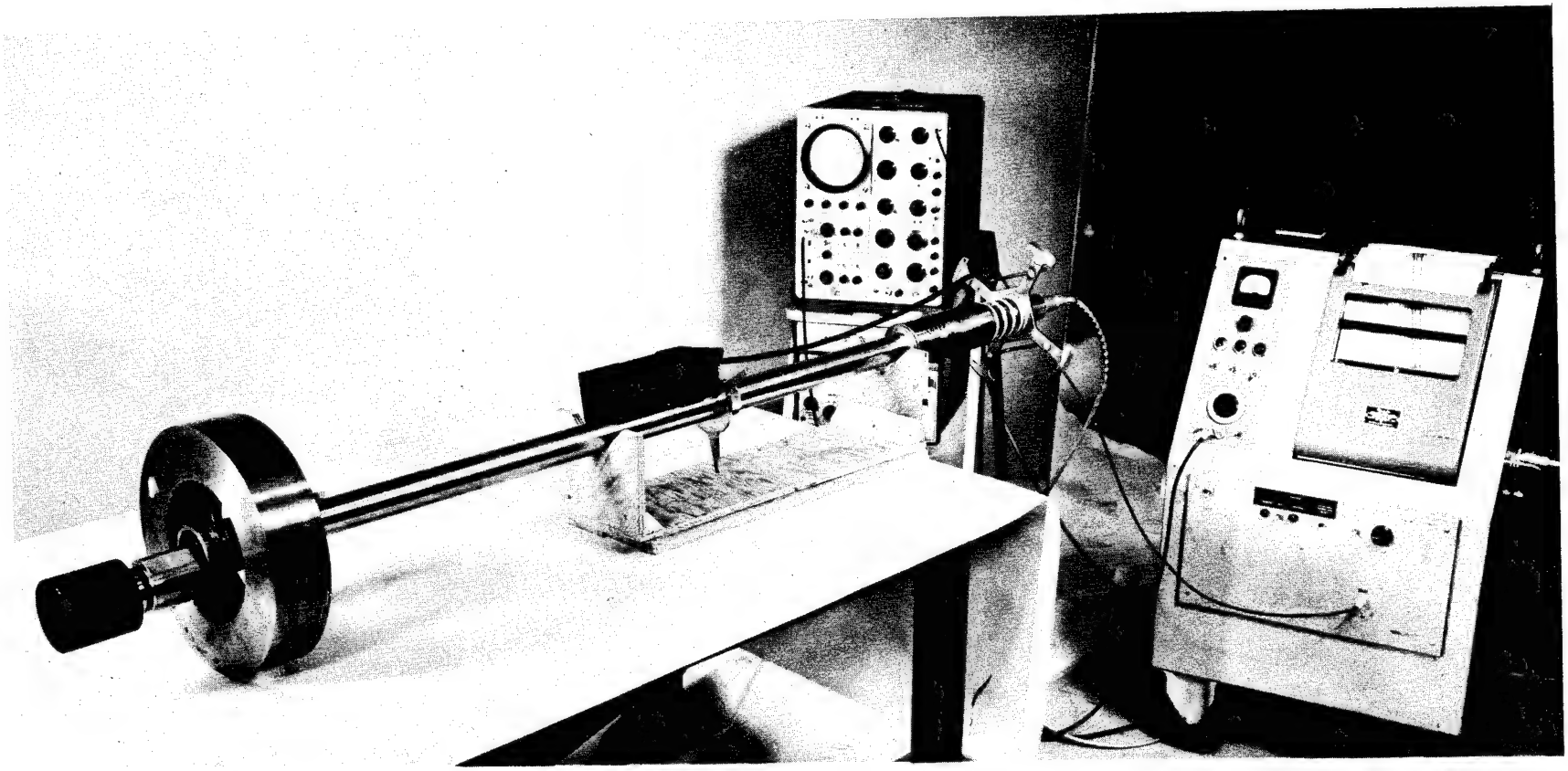

Figure 6. MAGNETIC RECORDING BORESCOPE ADAPTED TO 175-MM GUN TUBE SCANNING SYSTEM - AMPLIFIER-RECORDER AND OSCILLOSCOPE

ARMY MATERIALS AND MECHANICS RESEARCH CENTER
19-066-774/AMC-67

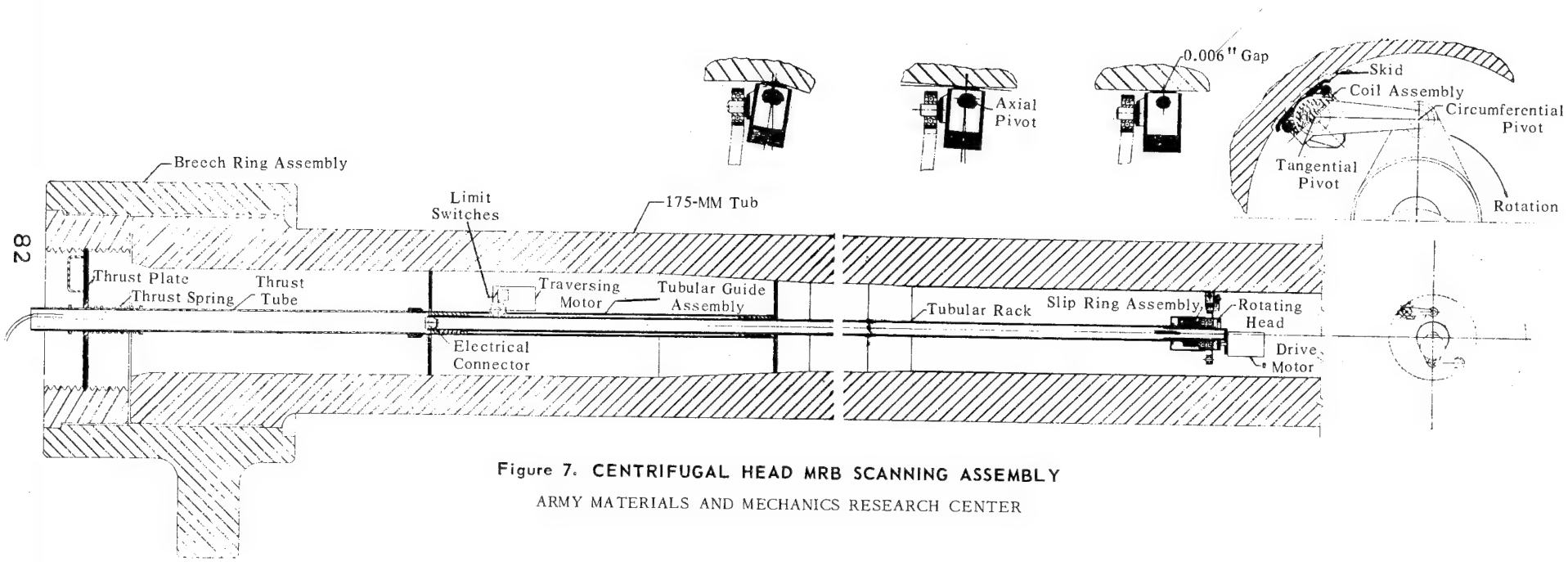

Figure 7. CENTRIFUGAL HEAD MRB SCANNING ASSEMBLY

ARMY MATERIALS AND MECHANICS RESEARCH CENTER

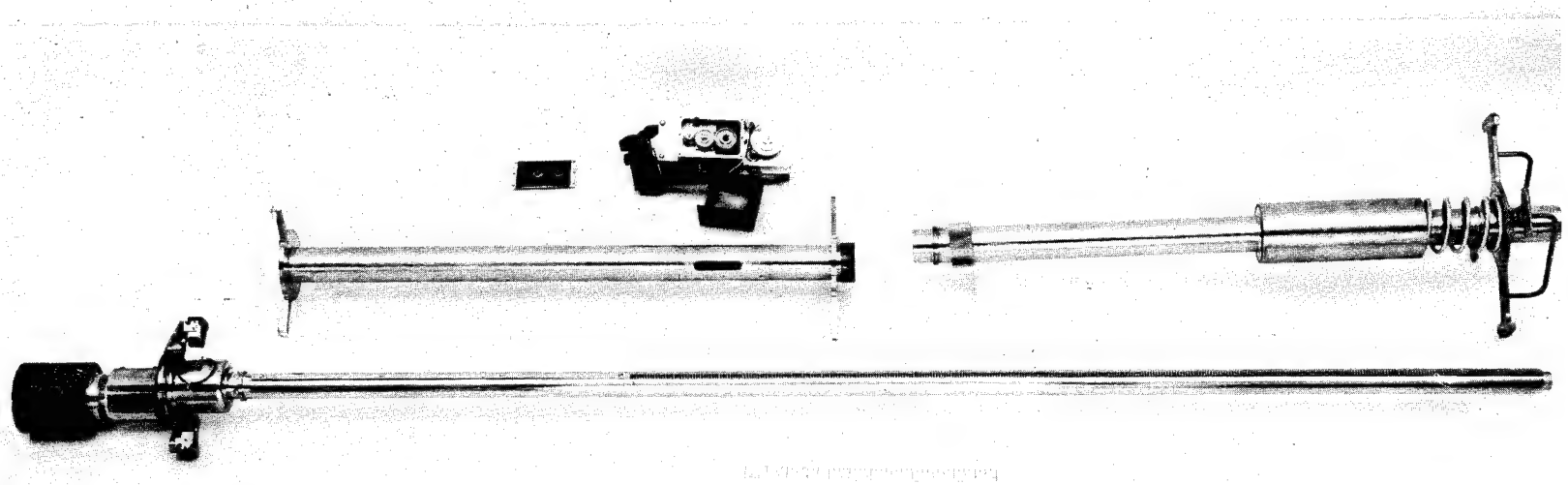

Figure 8. MAJOR COMPONENTS OF SCANNING SYSTEM

ARMY MATERIALS AND MECHANICS RESEARCH CENTER
19-066-776/AMC-67

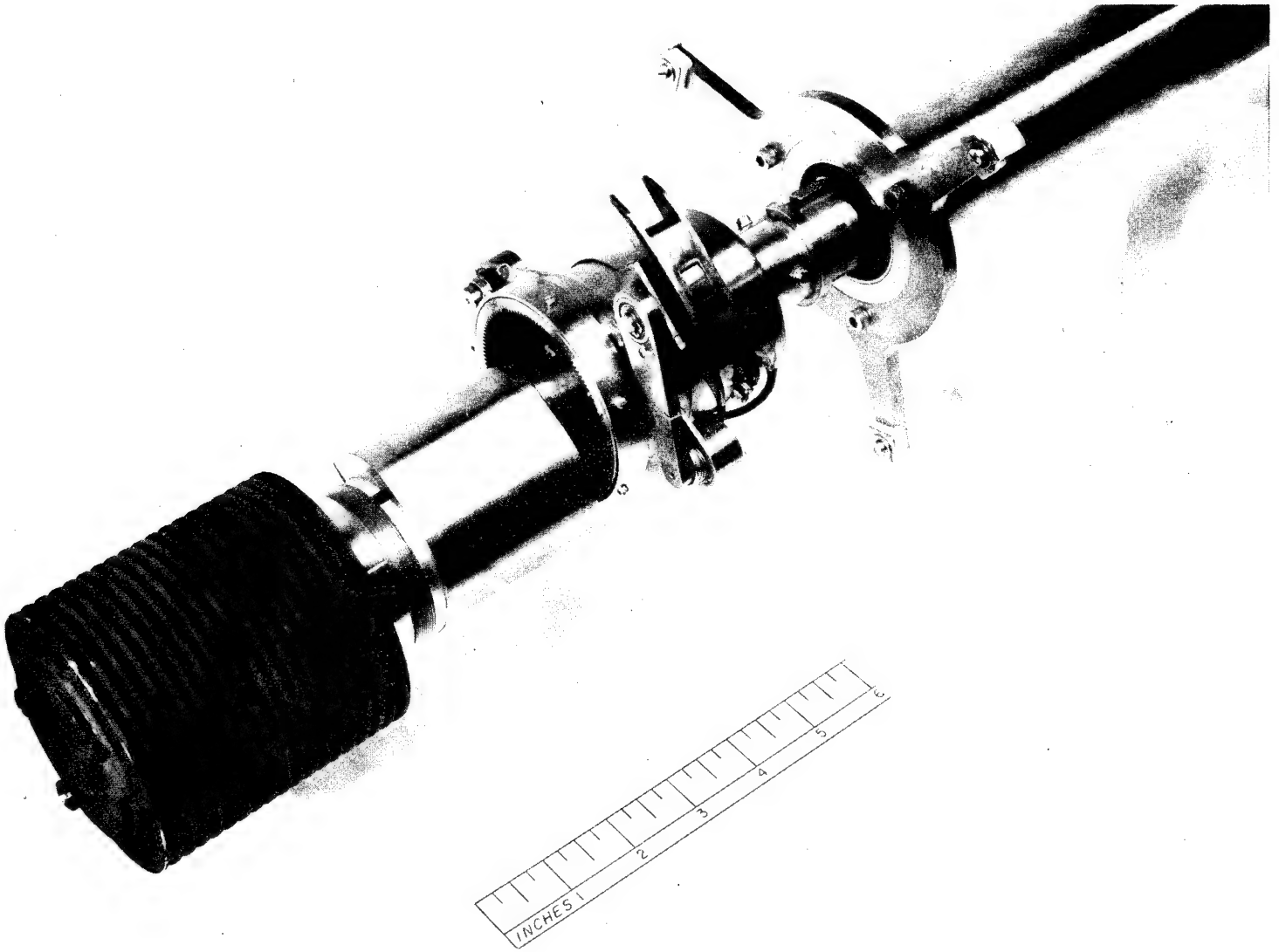

Figure 9. MRB SCANNER - 175-MM. FRONT VIEW OF CENTRIFUGAL SCANNING HEAD, WITH MOTOR DRIVE AND EXTENDED SKID ASSEMBLY.

ARMY MATERIALS AND MECHANICS RESEARCH CENTER

19-066-786/AMC-67

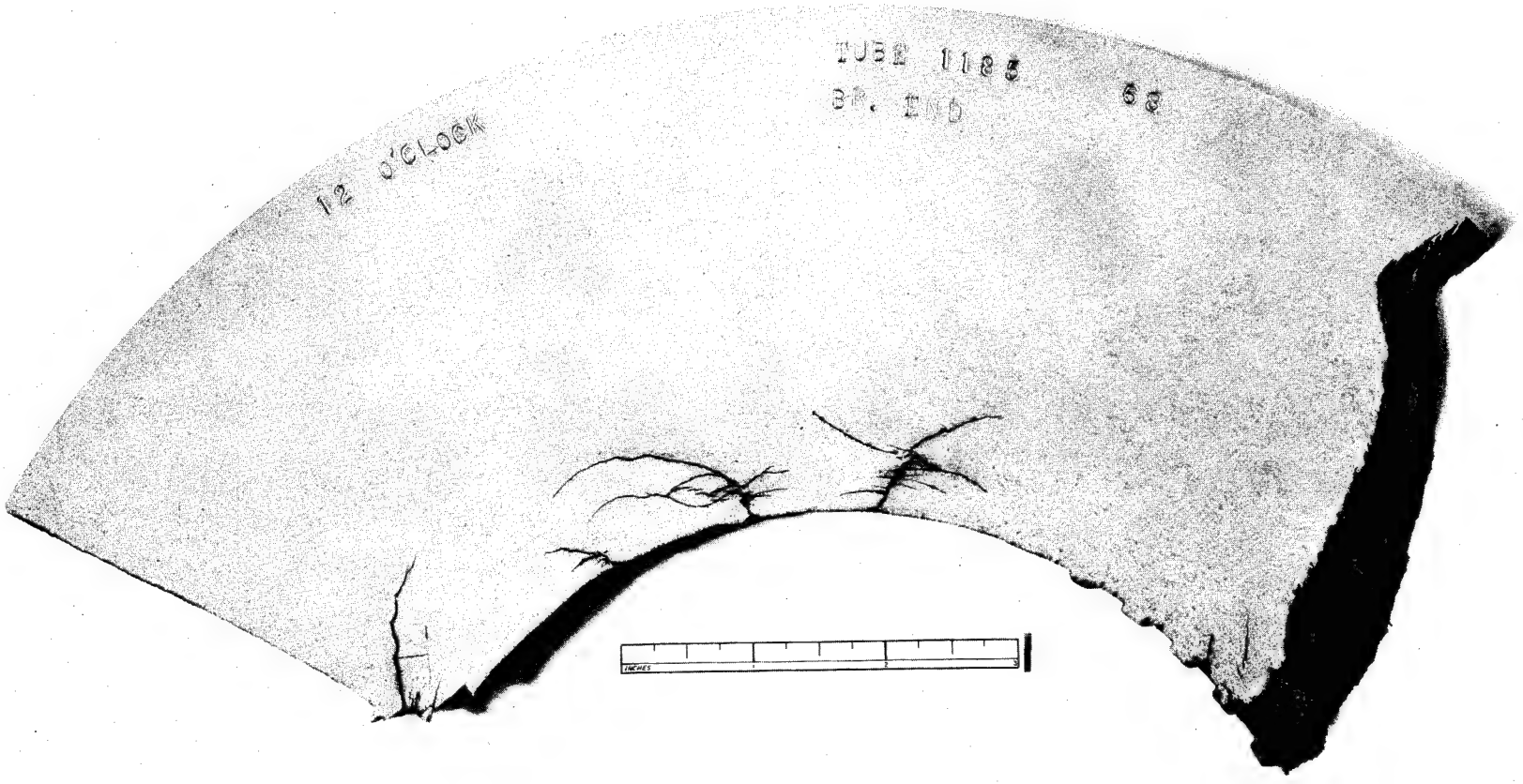

Figure 10. TRANSVERSE SLICE, CUT FROM FRAGMENT 16 OF TUBE 1185, WITH SURFACE AT 68 INCHES FROM THE BREECH.

ARMY MATERIALS AND MECHANICS RESEARCH CENTER

19-066-952/AMC-67

Figure 11. MRB FACSIMILE RECORDING NO. 178 OF TUBE 863 AT 1000 ROUNDS

ARMY MATERIALS AND MECHANICS RESEARCH CENTER

19-066-913/AMC-67

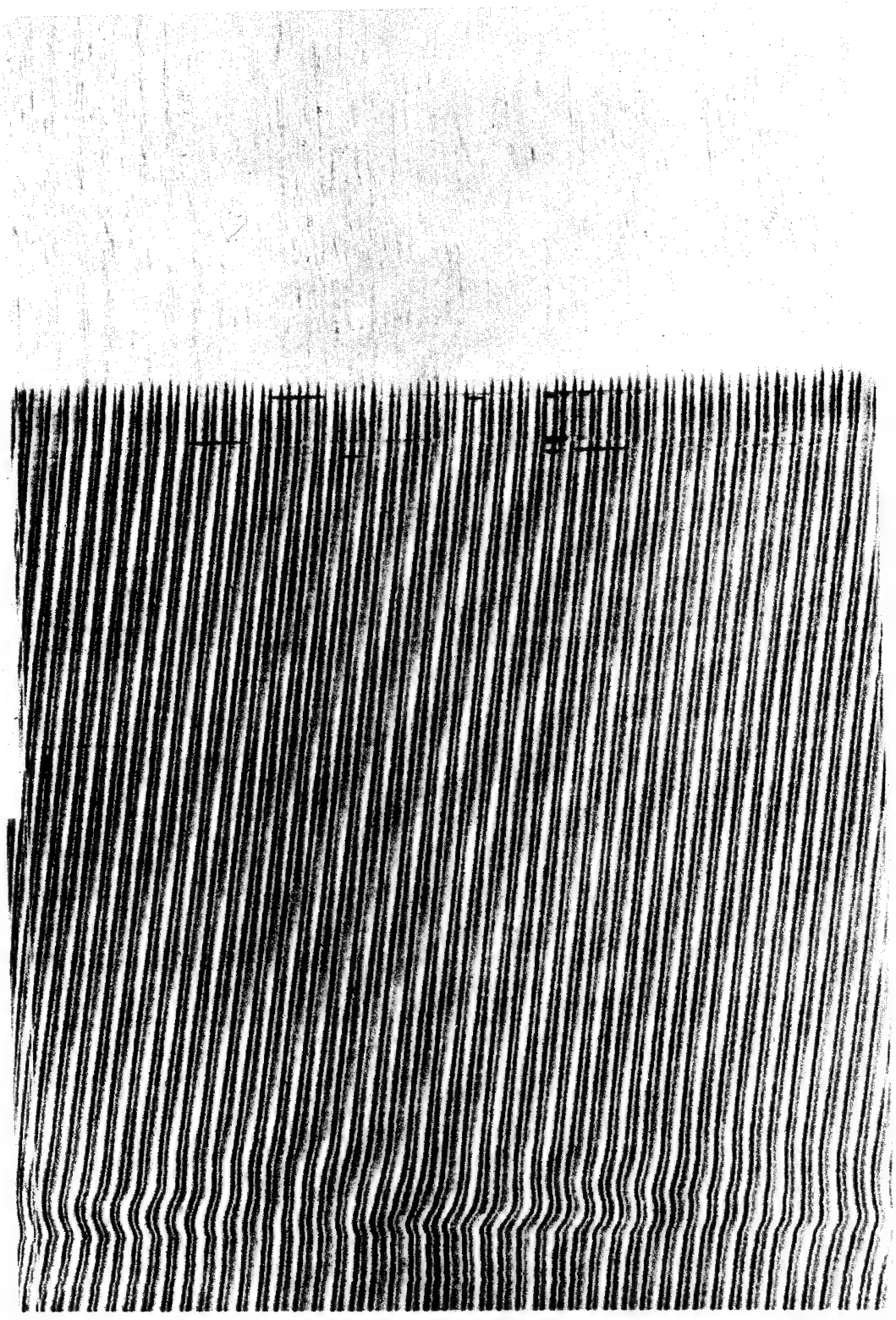

Figure 12. MRB FACSIMILE RECORDING NO. 69 OF TUBE 1185 AT 0 ROUNDS

Figure 13. MRB FACSIMILE RECORDING NO. 111 OF TUBE 1185 AT 300 ROUNDS

ARMY MATERIALS AND MECHANICS RESEARCH CENTER

19-066-918/AMC-67

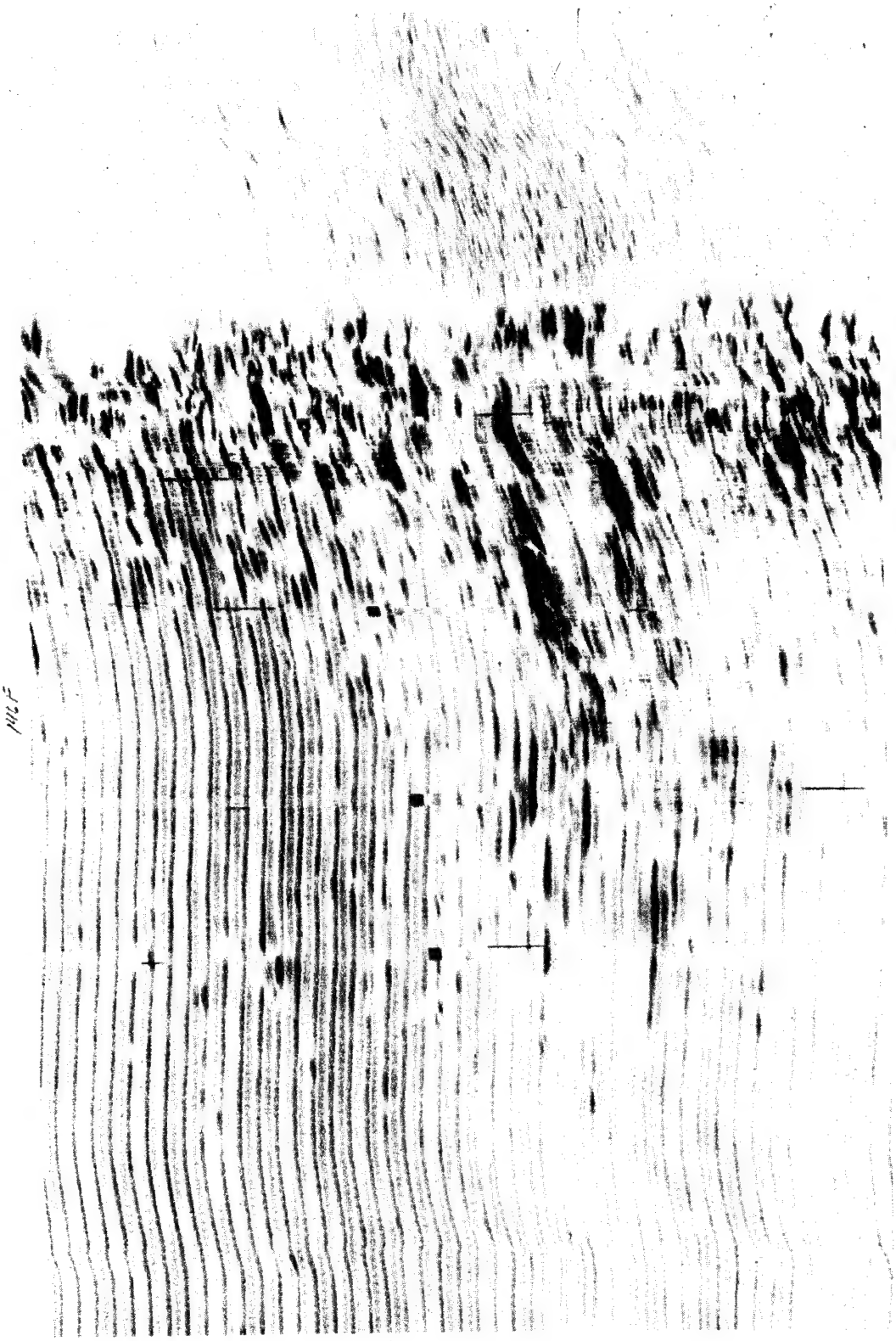

Figure 14. MRB FACSIMILE RECORDING NO. 146 OF TUBE 1185 AT 600 ROUNDS

ARMY MATERIALS AND MECHANICS RESEARCH CENTER

19-066-921/AMC-67

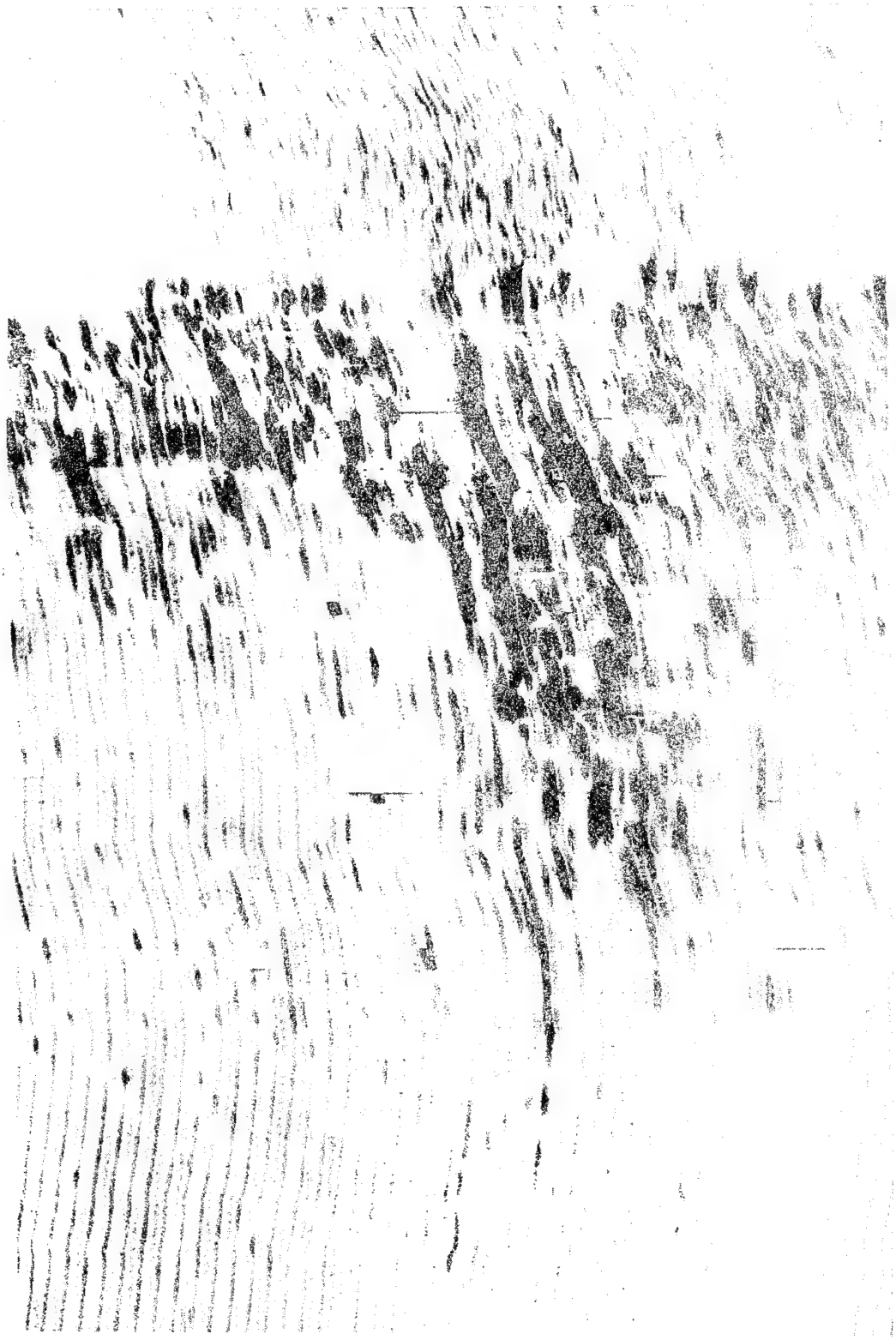

Figure 15. MRB FACSIMILE RECORDING NO. 188 OF TUBE 1185 AT 800 ROUNDS

ARMY MATERIALS AND MECHANICS RESEARCH CENTER

19-066-923/AMC-67

Figure 16. **MRB FACSIMILE RECORDING NO. 218 OF TUBE 1185 AT 1021 ROUNDS**

ARMY MATERIALS AND MECHANICS RESEARCH CENTER

19-066-928/AMC-67

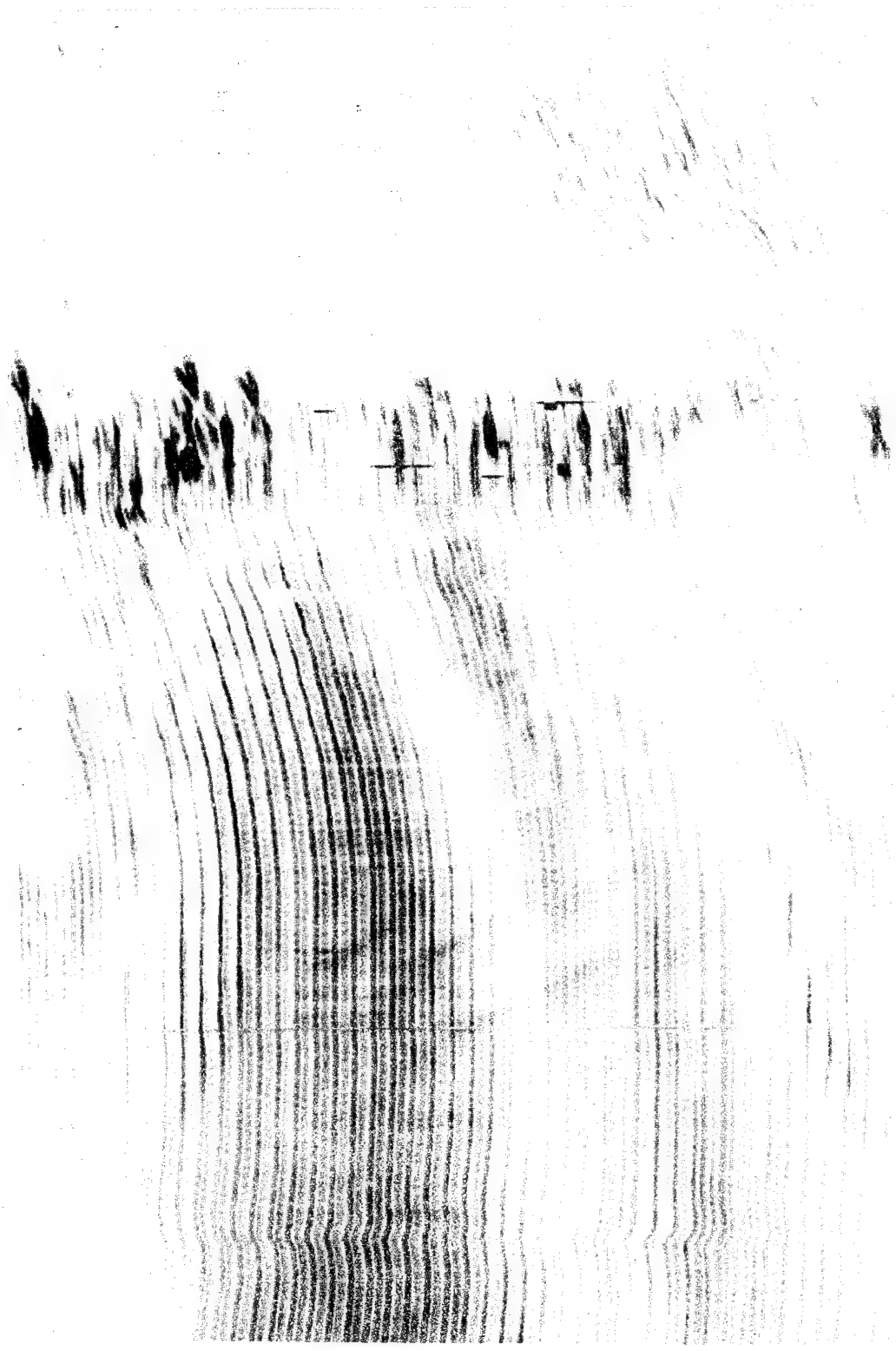

Figure 17. MRB FACSIMILE RECORDING NO. 141 OF TUBE 1382 AT 1000 ROUNDS

ARMY MATERIALS AND MECHANICS RESEARCH CENTER

19-066-937/AMC-67

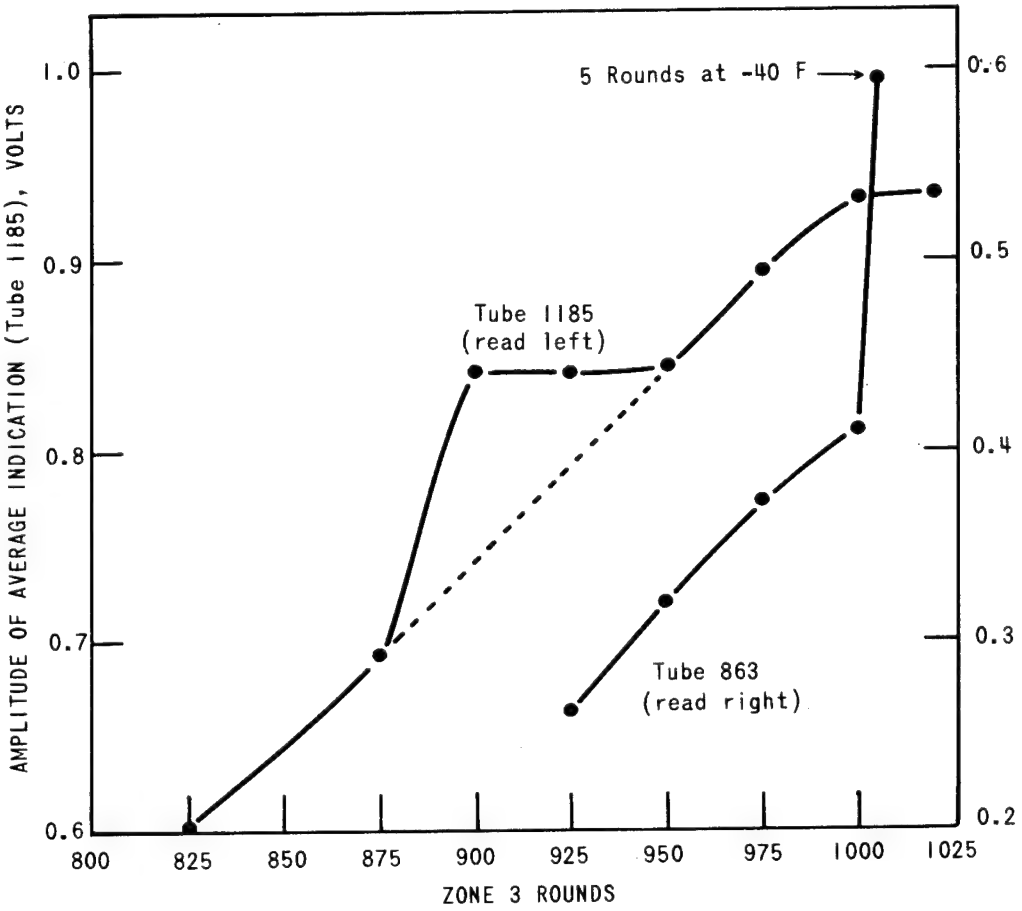

Figure 18. RELATION BETWEEN THE AMPLITUDE OF AN AVERAGE CRACK INDICATION AND NUMBER OF ROUNDS FIRED, TUBES 1185 AND 863

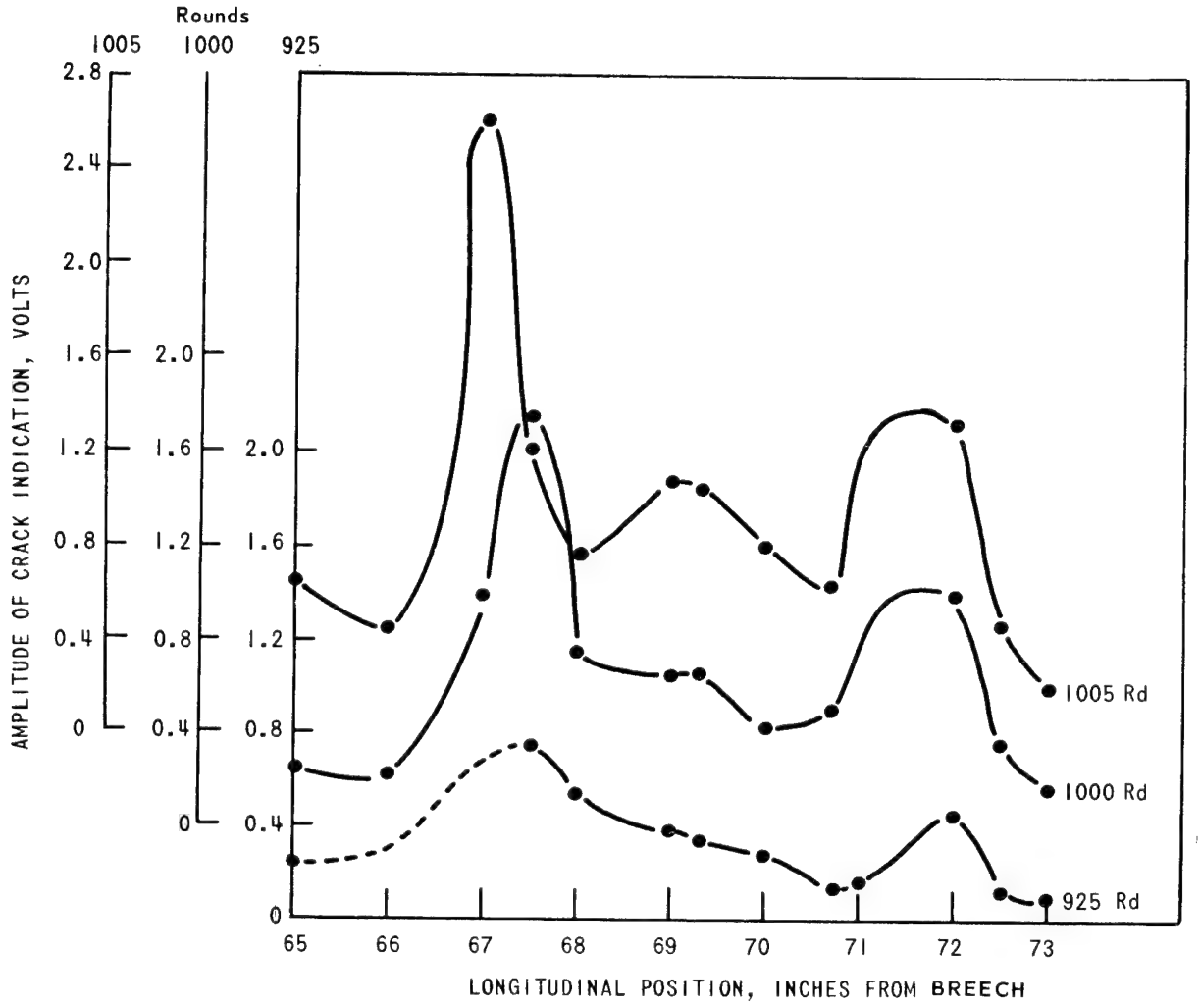

Figure 19. VARIATION OF CRACK INDICATION AMPLITUDE WITH LONGITUDINAL POSITION AND PROGRESSIVE FIRING FOR TUBE 863 AT 11:30 O'CLOCK

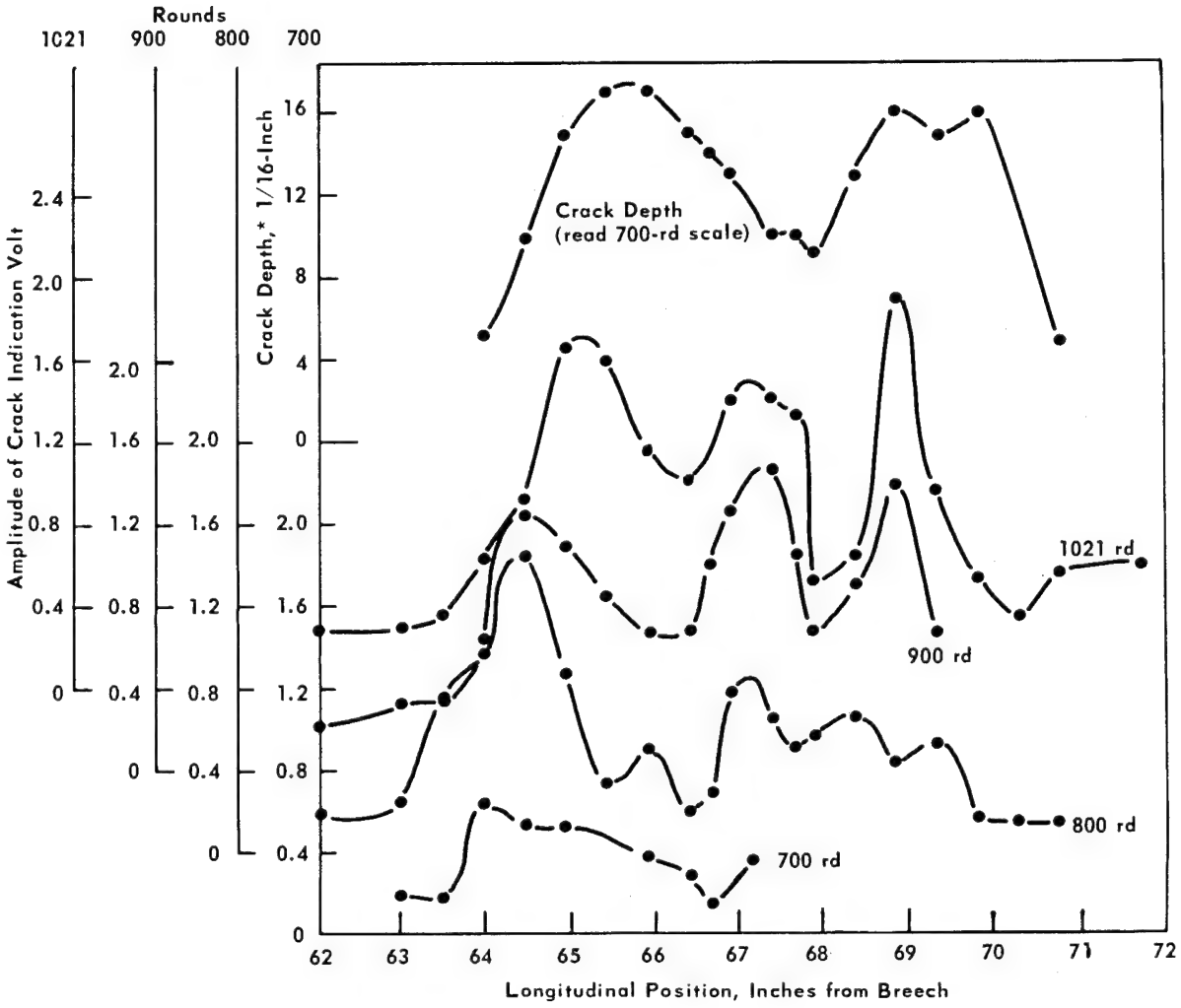

Figure 20. VARIATION OF CRACK INDICATION AMPLITUDE AND ESTIMATED CRACK DEPTH WITH LONGITUDINAL POSITION FOR TUBE 1185 AT 11:00 O'CLOCK

*Radial crack depth estimated from fracture surface of fragment No. 16.

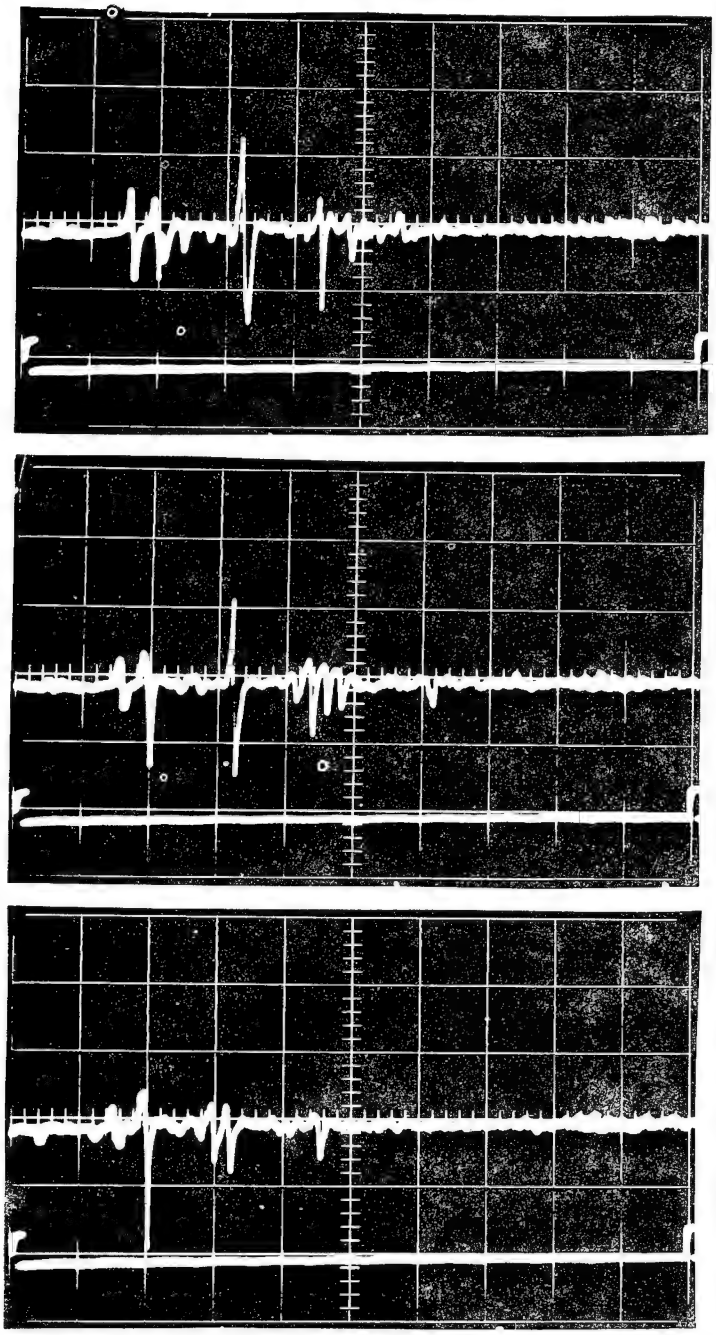

Longitudinal Position: 67 Inches

Vertical Sensitivity: 0.5v/cm

Longitudinal Position: 67½ Inches

Vertical Sensitivity: 0.5v/cm

Longitudinal Position: 68 Inches

Vertical Sensitivity: 0.5v/cm

Figure 21. OSCILLOSCOPE RECORDS SHOWING SIGNAL AMPLITUDE AT INDICATED LONGITUDINAL POSITIONS FROM THE BREECH END OF TUBE NUMBER 1185

ARMY MATERIALS AND MECHANICS RESEARCH CENTER

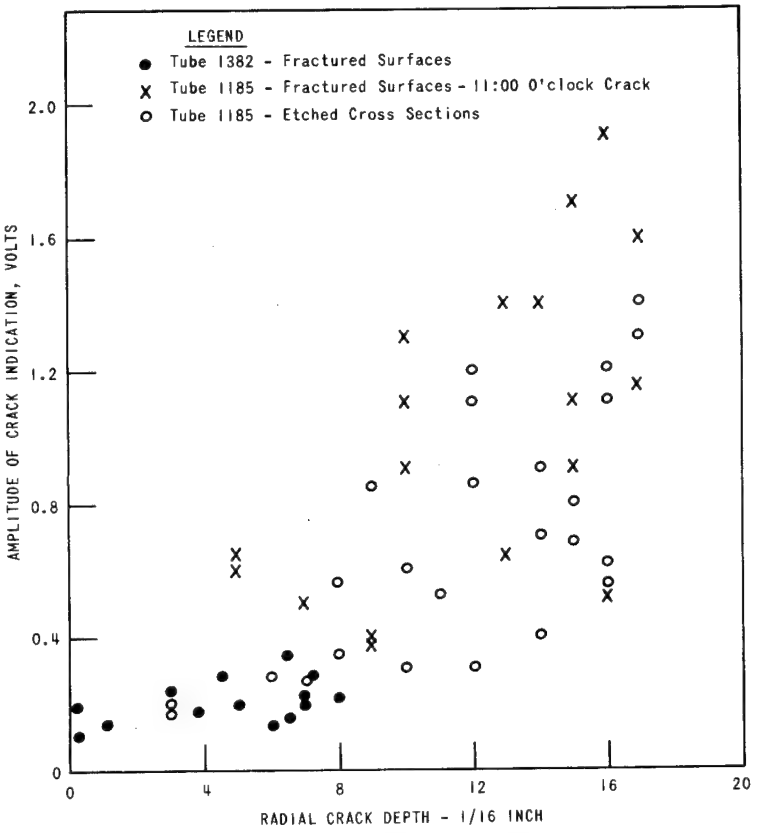

Figure 22. COMPOSITE PLOT OF ALL REPORTED CRACK DEPTH DETERMINATIONS VERSUS SIGNAL AMPLITUDE

PAPER No. 2

NONDESTRUCTIVE DETERMINATION OF CASE DEPTH OF CARBURIZED STEEL BY HARMONIC VOLTAGE ANALYSIS

H. P. Hatch
Army Materials and Mechanics Research Center
Watertown, Massachusetts

ABSTRACT

A method of nondestructively measuring the case depth of carburized steel parts based on analysis of a secondary voltage for its harmonic content is described. A first-generation test system has been built, which consists of a high-power, low-distortion oscillator, tuned amplifier, phase meters, and spectrum analyzer. This system permits rapid, accurate measurement of amplitude, phase, and inphase and quadrature components of harmonic frequencies generated as a result of the interaction of a sinusoidal applied field, with the test piece. The design of the instrument is such that a wide range of fundamental frequency, applied field strength, and harmonic frequency can be investigated. Comparative measurements on homogeneous plain carbon steels has shown that the results obtained by harmonic analysis are primarily produced by additional surface carbon content rather than such secondary factors as residual stress or retained austenite. Application has demonstrated that the method is effective in measuring case depth through 0.075 inch. Parts of various geometries have been investigated, and in all cases a correlation was obtained with case depth. The effects of variations in carburizing treatment, alloy or composition, and demagnetizing factors are considered. One of the major advantages of this method is that several voltage parameters are available for measurement. This, at times, makes it possible to effectively separate two simultaneously changing variables, for example, case depth and tempering temperature. The chief limitation, at the present time, is that there has not been enough applications experience to establish operating instructions.

NONDESTRUCTIVE DETERMINATION OF CASE DEPTH OF CARBURIZED STEEL BY HARMONIC VOLTAGE ANALYSIS

INTRODUCTION

This paper describes the results of a continuing investigation started in 1964 and supported by the Army's Materials Testing Technology Program to develop new and improved methods of nondestructively evaluating the properties of weapons systems components. Many weapons rely heavily on carburized steel parts for high-strength, wear-resistant applications and it is important that the case depth be within specified limits. If the case depth is too thin, resistance to wear and surface deformation will be inadequate; whereas, too thick a case reduces the cross-sectional area of core material and increases the tendency toward catastrophic impact failure.

Generally, carburized parts are checked for compliance with specifications by destructive examination of a number of finished parts from each heat-treated lot. Several relatively common electromagnetic nondestructive test methods could be applied to the determination of case depth (1)* if this were the only variable. However, when many simultaneously changing variables are present, as in production parts, inability to discriminate between variations in case depth and changes in other process variables make the results of these methods difficult to interpret.

This problem is illustrated in Figure 1 which shows the relation between the unbalance voltage of a comparator-type bridge circuit and case depth.(2) The standard curve represents samples of increasing case depth that were oil quenched and tempered. The relationship between unbalance voltage and case depth is completely changed by water quenching. Samples originating from a different heat of the same type of steel produce additional changes in the relationship. Variations in tempering treatment can also produce large deviations from the standard curve. Obviously, errors of this magnitude are unacceptable in a quantitative measurement, and any method of this type is subject to uncertainty.

This paper therefore deals with the development of a method which provides a measurement parameter that is predominately dependent on case depth for the conditions considered. The method is based on the relationship between the harmonic components present in an induced voltage and the amount and depth of additional carbon at the surface of carburized steel. (3)

*Numbers in parentheses refer to literature cited in the bibliography

ORIGIN OF HARMONIC DISTORTION

The basic test principle involves the measurement of variations in the non-linearity of magnetic response in terms of the distortion generated when a ferromagnetic material is under the influence of a sinusoidal-exciting field. The distortion is in the form of odd-order harmonics which can be filtered from the voltage wave developed in the secondary winding of a test coil. After the individual harmonic components have been extracted from the distorted secondary voltage wave form, the harmonic amplitude and phase, as well as the harmonic in-phase and quadrature components, are measured.

A generalized representation of the hysteresis characteristics of low alloy steels at low-to-moderate field strengths is shown in Figure 2 to illustrate the origin of harmonics. The distorted flux wave was constructed from a sinusoidal field wave using the hysteresis curve as a transfer function. The flux curve was then reduced to its fundamental and harmonic components by Fourier expansion (4). Therefore, the induced secondary coil voltage must also contain harmonics since it is proportional to the rate of change of flux with time.

There are four major factors which contribute to the harmonic distortion generated by the interaction between the test piece and an a.c. field of a given maximum strength. These are the normal magnetization curve, the magnetic hysteresis, eddy currents and demagnetizing factor.

First, consider a hypothetical ferromagnetic material of very high electrical resistivity that exhibits a magnetization curve as shown in Figure 3 and has no hysteresis. This can be thought of as an ideally soft or magnetically reversible material. If the applied field is low enough not to exceed the initial portion of the curve, the material would behave linearly, magnetically speaking, and no harmonics would be generated. Now, if the maximum applied field strength was increased to the value of H_o shown in the figure, the magnetization curve is no longer linear and therefore the flux wave will be distorted and an odd-order harmonic content is obtained. Only odd-order harmonics are generated because the waveform satisfies the condition that the amplitude of the waveform at any wt is equal, but opposite in sign to the amplitude at $(wt \pm \pi)$. A graphical analysis (4) of the distorted waveform yields the relative amplitude and phase angle of the individual harmonic components. This analysis was performed, and the results are shown in composite form in Figure 3.

The important thing to note is that all of the harmonic components of the distorted flux wave have only sine components

and therefore are either in phase or 180° out of phase with the original field wave. The shape of the magnetization curve determines the relative amplitude of any given harmonic and whether it will be in or 180° out of phase with the applied field. In addition, the induced flux is exactly in phase with the applied field. This would be the case for any shape of magnetization curve without hysteresis. In other words, if there is no hysteresis, there will be no cosine components to the harmonics generated in the flux wave, provided the zero-cross of the original field wave is taken as the reference point.

However, real ferromagnetic materials such as steel display magnetic hysteresis when under the influence of an alternating field. The character of the hysteresis can be drastically changed by variations in the composition or condition of the material. This is shown in Figure 4 by a comparison of the hysteresis curves of fully hardened and tempered 1020 and 1095 steel measured on thin toroidal specimens. The harmonic distortion generated by the two materials at a given field strength is completely different. Figure 5 illustrates the generalized case in composite form of a real ferromagnetic material reduced to its harmonic components by graphical methods (4).

Unlike the previous case, the harmonic components are comprised of both sine and cosine components. There is, in general, an angular lag other than 0° or 180° between the field wave and both the distorted flux wave and the harmonic components of the flux wave. The result is that the individual harmonics have an angular relationship to the applied field and can be characterized by in-phase and quadrature components with respect to the original field wave.

Because the normal magnetization curve generates only in-phase harmonics, the in-phase components of the flux wave can be said to be related to the normal magnetization curve or permeability, whereas the quadrature components may be referred to as being related to core losses (5).

The representation shown in Figure 5 is applicable only where eddy currents are negligible and demagnetizing factor is zero. Normally, production parts that are considered for nondestructive evaluation have cross sectional dimensions sufficient for the flow of eddy currents induced by a changing flux. Therefore, the effect of eddy currents on harmonic generation by a ferromagnetic material must at least be considered in a general way.

From Lenz's law, the direction of eddy current flow will be such that the flux they generate will be opposite in direction to the change in flux which produced them. Eddy currents, therefore, have a cancelling effect and shield the interior

of the material against magnetic induction. The instantaneous eddy current density is proportional to the instantaneous rate of change of flux which is, in turn, determined by the hysteresis characteristics of the material. Because of this, eddy currents can lead to either an increase or reduction of the harmonic distortion produced by the hysteresis characteristic alone. The effect of eddy currents on harmonic distortion is principally determined by the shape of the hysteresis loop at the operating field strength. (3) However, at the frequency (100 Hz) used throughout this investigation, the influence of eddy currents on test results has been found to be negligible when comparing measurements on samples of the same size and shape.

The three preceding factors, magnetization curve, hysteresis and eddy currents are each dependent on the characteristics of the material. There is, however, a fourth factor which can significantly influence the harmonics generated by a test piece which is related to the geometry of the piece. This is the demagnetizing factor.

In showing the harmonics generated in the flux wave in Figures 3 and 5, a sinusoidal field wave was assumed. A sinusoidal field can be achieved by passing a sinusoidal current through a field coil wound uniformly around a toroidal specimen. If however the specimen is in the form of a cylinder and the field coil is a solenoid, a demagnetization field is superimposed on the applied field wave. The actual field acting on the specimen is then given by the following equation: (6)

$$H_{actual} = \frac{H_{applied} - N/4\pi B}{1 - N/4\pi}$$

where B is the magnetic induction and N is the demagnetizing factor. The actual field is less than the applied field. Because the flux wave is distorted, the difference between the distorted demagnetizing field wave and the sinusoidal applied field wave will result in an actual field applied to the sample that is both out of phase and distorted with respect to the applied field wave. This effect, although present, is not readily measured, and for this reason a purely sinusoidal current has been maintained as a constant point of reference throughout the investigation.

Although the analysis presented in this section is an over-simplification, it is an approach which has been useful to qualitatively represent the various effects encountered in applying the harmonic analysis method.

EXPERIMENTAL PROCEDURE

A. Test Circuit and Instrumentation

In generating an electromagnetic field for use in the analysis of harmonics resulting from the nonlinear hysteresis characteristics of ferromagnetic materials, two important factors should be considered. First, the exciting current, or field, waveform should not be distorted by interaction with the ferromagnetic material being tested, and secondly, the applied field waveform should be sinusoidal with as little harmonic content as possible.

To satisfy the first consideration, the output impedance of the generator must be high in comparison to the impedance of the field coil. (7)(8) This is necessary to supply a constant current to the field coil which will not be distorted through interaction with the test piece. The second consideration requires a low distortion generator. However, even when generators having good harmonic distortion characteristics are used, the harmonic content in the field current is sufficient to cause minor variations in results when different generators are employed. In order to meet these requirements, a test coil circuit such as that shown in Figure 6 was used.

In this circuit, an apparent high generator impedance is obtained by the two air core inductors L_1 and L_2, where $L_{1,2}$ is $>> L_3$. By virtue of the reactance of capacitor C, the higher frequencies, or harmonics, contained in the driving current are attenuated and, by selecting C to resonate with $L_{2,3}$ at the fundamental frequency, optimum filtering is achieved. In addition, the resonant circuit supplies a current through the field coil, measured at I, which is several times greater than the generator current.

It will be noted that a differential secondary winding is shown. This configuration subtracts the air core induced voltage, and thereby provides a voltage at E_s which is due only to the rate of change of flux in the test specimen.

The associated instrumentation and test circuits for extracting harmonics from the secondary voltage for measuring harmonic in-phase and quadrature components are fully described in a previous report (3) and will not be repeated here. However, a block diagram of the test instrument developed during this investigation is shown in Figure 7 to illustrate how measurements of the various harmonic-voltage components were obtained. The generator shown in the block diagram has a maximum power output of 200 VA and, at a frequency of 100 Hz

has a total harmonic distortion of 0.42%. However, by using the L-C circuit described, the total harmonic distortion of the field current waveform is substantially reduced to a level of less than 0.02%. This reduced level of distortion was found adequate to meet requirements.

The procedure for obtaining the reported measurements was to tune both the harmonic filter-amplifier and the harmonic generator to the frequency under consideration and to record, at various field strength, the resultant harmonic amplitude (E_n), the phase angle ($\emptyset$), the in-phase component (b_n), and the quadrature component (a_n) The magnitude of the amplified field was continually monitored by the field current meter which had been calibrated by measuring the field strength at the center of the field coil. In all cases, the harmonic reference voltage was set to be exactly in phase with the exciting field current and, therefore, b_n and a_n are the n^{th} harmonic voltage components in phase and in quadrature with the applied field. Similarly, $\emptyset_n$ is the phase angle between the n^{th} harmonic and the applied field.

The measurements reported for E_n are actual values, but those for b_n and a_n are relative and include a proportionality factor which can be determined by knowing the amplitude of the reference voltage and the gain of the amplifier preceding the multiplier circuit. This proportionality or scale factor is a sensitivity adjustment for the zero center ± full scale meter. The actual values of b_n and a_n may also be calculated from the resultant harmonic amplitude and phase angle, where:

$$b_n = E_n \cos \emptyset_n = \text{In phase component}$$

$$a_n = E_n \sin \emptyset_n = \text{Quadrature component}$$

Even though a fundamental frequency of 100 Hz was selected as optimum for this investigation, the instrument provides the capability of selecting any desired harmonic voltage in the range between 150 to 4500 Hz and, by changing a few circuit components, it can easily be modified for measurements at both higher or lower frequencies.

B. Preparation of Test Samples

Test samples were prepared to evaluate the harmonic analysis method in terms of sensitivity to variations in case depth, quenching rate, tempering treatment, heat of steel,

test piece geometry, chemical analysis, and carburizing method. The test was first established using 0.75-inch diameter cylindrical test specimens taken from two heats of 8620-H steel to determine the influence on test results of small variations in chemistry and processing. Heat treatment schedules were arranged to produce case depths in the range of 0.005 to 0.025-inch. All carburizing was done in a salt bath at 1600 F, but quenching rates were varied on some samples to produce core microstructures. Following the heat treatment, a 1-inch section was cut from the end of each specimen leaving a cylinder test piece 3-inches long. The end sections were examined metallographically to determine the case depth and core microstructure. The case depths are reported as total case; that is, the estimated end point of carbon diffusion as evidenced by no further change in microstructure.

Additional samples used to show the effect of the other variables on test results were prepared in a similar manner throughout the investigation as required. However, some samples were not sectioned for metallographic examination in order to preserve dimensions. In these cases, it was necessary to correlate harmonic measurements with carburizing time rather than actual case depth.

RESULTS AND DISCUSSION

A. Measurement of Case Depth

Prior to the construction of the harmonic analysis instrument, early work in the program demonstrated the relation between the amplitude and phase of the third harmonic component of an induced secondary coil voltage and variations in surface carbon content of steel parts brought about by either carburization (2) or decarburization (9). The first observed correlation was between the phase of the third harmonic component and the case depth of the 0.75-inch diameter cylindrical test samples shown in Figure 8. The standard curve represents samples from heat 1, carburized for various times at 1600 F, oil quenched and tempered for 1hour at 400 F. Other points represent similarly carburized specimens containing controlled variations of quenching, tempering and heat of steel from which the sample originated. These samples are the same as shown in Figure 1 and a comparison of Figure 8 with Figure 1 illustrates the effective suppression of interfering variables that was achieved with harmonic phase measurements. This, and the importance of the in-phase and quadrature components, led to the decision to develop the necessary instrumentation to facilitate rapid measurement of the various harmonic voltage parameters for not only the third, but higher order harmonics as well.

In order to demonstrate that the observed correlations between harmonic voltage parameters and case depth are the result of increased surface carbon content, similar measurements were made using fully hardened and tempered plain carbon steels SAE numbers 1020, 1045, and 1095, of the same size and shape as the carburized 8620-H test samples. The plain carbon steel samples were copperplated and heated to an appropriate austenitizing temperature in a salt bath and then brine quenched to produce a fully hardened, martensitic structure. For the purpose of comparison, test specimens of 8620-H (heat 1) with case depths of 0, 0.009" and 0.020" were selected. Figures 9 and 10 show comparisons between the in-phase and quadrature components of the third and fifth harmonic voltages as a function of field strength for both the carburized and homogeneous carbon-steel samples. In each case, a very close similarity between the curves for the carburized and carbon steel samples was observed, indicating that the variations are predominantly a result of the influence of carbon content rather than residual stress or retained austenite. It should be pointed out that the curves in Figures 9 and 10 are valid only for the specimen-coil configuration, and fundamental frequency used. Demagnetizing factor and eddy current density variations would tend to modify these curves if test piece geometry or fundamental frequency were changed.

Construction of the type of curves shown in Figures 9 and 10 is of value in selecting an operating field strength and the most useful test parameter. A peak field strength of about 100 oersted has been found to be a generally satisfactory level for both third and fifth harmonic voltage measurements.

Figure 11 shows the effect of variations in the quenching rate and heat of steel on the correlation between case depth and the a_3 and b_5 harmonic voltage parameters using the same samples shown in Figures 1 and 8. This comparison illustrates the fact that better suppresion of interfering variables may be possible with one parameter than with the other. In this case, the b_5 component completely suppresses the effects of increased quenching rate and different heats of steel. It is important that small quenching rate variations not adversely affect the correlation since, if groups of components are quenched simultaneously, small variations in cooling rate will undoubtedly occur.

B. Effect of Tempering Temperature

The most severe interfering process variable introduced in this investigation was that of tempering temperature. Figure 12 illustrates the effect of variations in tempering

temperature on the third harmonic quadrature component and the fifth harmonic in-phase component for various carburizing times or case depths. As previously reported (2), the changes in magnetic permeability accompanying the various stages of tempering are the result of the nature of the tempering reactions on the microstructure and residual stresses occurring at various tempering temperatures. Figure 12b indicates that the in-phase component of the fifth harmonic is less affected by variations in tempering temperature in the range from room temperature to 400°F than is the quadrature component of the third harmonic (Figure 12a). However, in both cases, the largest change occurs in the range of 400°F to 450°F, which is also true of the variation of permeability with tempering temperature as reported by Bain (10). In any case, it is obvious from the curves that, in order to accurately determine case depth, tempering temperature must be known. Generally, tempering treatments can be accurately controlled, and if maintained within a 25°F range below 400°F, only minor errors will be introduced in the determination of case depth. However, an actual separation between the two independent variables (tempering temperature and case depth) is possible by use of the harmonic analysis method.

Figure 13 is a plot of the in-phase versus quadrature components of the fifth harmonic voltage generated by a set of test specimens containing controlled variations in both case depth and tempering temperature. It was found, in this case, that both variables could be effectively separated and determined simultaneously with reasonable accuracy. Accordingly, it appears that case depth can be determined in the presence of the independent tempering variable, providing suitable coordinates are established by a prepared group of selectively heat treated samples similar to those shown in Figure 13. This observed relationship demonstrates the advantage of the harmonic analysis method where both the in-phase and quadrature harmonic components can be measured simultaneously. It also suggests that other variables which affect the normal magnetization and hysteresis characteristics of steel could be effectively separated in a similar manner.

C. Effect of Sample Dimensions

To determine the effect of demagnetizing factor, or length-to-diameter ratio, a set of test samples was prepared from 1020 steel in the form of one-inch O.D. tubes with various lengths of 3/4 inch, 1-1/4 inch, two inches, and three inches. The samples were carburized for different lengths of time to produce variations in case depth for each l/d ratio. Figure 14 is a plot of both third and fifth harmonic phase angle versus case depth and illustrates that an increase in the demagnetizing factor only decreases the sensitivity of results. The curves shown in Figure 14 are similar to those obtained using the three-inch long 8620H test samples.

D. Effect of Chemical Analysis

To determine the effect of variations in chemical composition on harmonic measurements for the evaluation of case depth, samples were fabricated from three different grades of carburizing steels. The alloys selected were AISI 4620, 8617 and 9310. Table 1 shows the accepted range of the major alloying elements.

Table 1

AISI	C	Mn	Ni	Cr	Mo
8617	.15-.20	.70-.90	.40-.70	.40-.60	.15-.25
4620	.17-.22	.45-.65	1.65-2.0	--	.20-.30
9310	.08-.13	.45-.65	3.0-3.5	1.0-1.4	.08-.15

Prior to this portion of the investigation, only 8620 steel has been considered with case depths ranging from 0 to .025 inch. Therefore, it was decided to extend this part of the program to include a greater range of case depths in order to determine the limitations of the harmonic analysis method in evaluating deep cases produced by carburizing (11). The samples were in the form of cylinders, 5/8 inch in diameter and 2-1/2 inches long. They were gas carburized in production furnaces at a carbon potential of 1.10 percent for various lengths of time to produce case depths in the range of 0 to .075 inch, then quenched in oil at room temperature. After heat-treatment, a 3/4-inch section was cut from the end of each sample for the metallographic determination of case depth.

Harmonic measurements were taken at a fundamental frequency of 100 Hz on all samples of the three different alloys, using the harmonic analysis instrument. Figure 15 is a plot of the results of these measurements and illustrates the correlation obtained between third harmonic phase shift and case depth up through .075 inches for each of the three carburizing steels. Considering the relatively large differences in both the nickel and chromium-alloying elements, the substantial amounts of austenite retained in the deep-cased 9310 samples, and the fact that all previous work was limited to case depths up to .025 inch, the results illustrated in Figure 15 are most promising. The curves for each of the steels are not only similar, but fall within a relatively narrow scatterband. In addition, the slope of the curves from 0 to .025 inch is identical to that previously obtained using liquid-carburized 8620 test samples.

SUMMARY

The harmonic analysis method has been shown to be an effective means of nondestructively evaluating the case depth of carburized steel. It was found that harmonic phase shift not only correlated well with case depth, but could be made relatively insensitive to selected interfering variables intentionally introduced in a number of experimentally heat-treated test samples. It was also demonstrated by comparative measurements made on hardened and tempered plain carbon steels that the results of harmonic analysis measurements of case depth are primarily influenced by variations in the surface carbon content. In continuing the program with the prototype harmonic analysis instrument, this investigation has demonstrated that the method is effective for the measurement of deep cases through .075 inch, and that results are similar on samples heat-treated by either the liquid or gas-carburizing process. It was also found that substantial variations in alloying elements produced only minor differences in harmonic measurements and experiments established that the effect of demagnetizing factor only influenced the sensitivity of results.

These findings, therefore, demonstrate the advantage of the method where a relatively large number of voltage parameters provide the versatility sometimes required for the establishment of an unambiguous relationship between test results and the desired material variable. The data presented were obtained from laboratory test samples but are sufficient to serve as justification for application of this method to production testing.

In conclusion, it should be remembered that the case depths discussed in this paper are those produced by carburization and not by induction or flame hardening. Cox reported (12) the method was not applicable to the measurement of induction hardened surface layers. In addition, there are some process variables which have not yet been investigated; namely, variations in carbon potential, carburizing temperature and cycle. Nevertheless, it is the opinion of the author that the magnitude of the variables introduced in these test specimens is more severe than would be encountered in production parts and evaluation proceeded on the assumption that if the most drastic variations could be suppressed, the errors produced by normal production fluctuations would be minimal.

BIBLIOGRAPHY

1. Nondestructive Testing Handbook, edited by Robert C. McMaster, Vol. II, Section 42 (New York: Ronald Press 1959).

2. Hatch, H. P., and Fowler, K. A. - "Experimental Electromagnetic Test Methods for the Nondestructive Evaluation of Carburized Steel Parts", Springfield Armory Technical Report SA-TR19-1509, 1964.

3. Fowler, K. A., and Hatch, H. P. - "Harmonic Analysis Method for the Nondestructive Determination of Carburized Steel", Springfield Armory Report SA-TR19-1514, 1965.

4. Manley, R. G. - Waveform Analysis (New York: John Wiley & Sons, Inc., 1945) Chap. VII, pp 183-211.

5. Peterson, E. - "Harmonic Production in Ferromagnetic Materials at Low Frequencies and Low Flux Densities", Bell Systems Tech. Journal, 7, pp 772, 1928.

6. Bozorth, R. M. - Ferromagnetism, D. van Nostrand Company, Inc., New York, 1951, pg 846.

7. Peterson, E. pg 771.

8. Bean, C. P., and Becker, J. J. - "Permeability and Losses of Ferro- and Ferrimagnets", Ch 9.3 in Methods of Experimental Physics, Vol 6, Part B (New York: Academic Press 1959) pg 222.

9. Hatch, H. P. and Fowler, K. A. - "Electromagnetic Method of Nondestructively Examining Components for Excessive Decarburization", Springfield Armory Technical Report SA-TR19-1508, 1964.

10. Bain, E. C. and Paxton, H. W. - Alloying Elements in Steel, Second Edition, p. 229, American Society for Metals, Metals Park, Ohio, 1961.

11. Hatch, H. P., and Fowler, K. A. - "Developments in the Harmonic Analysis Method for the Nondestructive Determination of Case Depth of Carburized Steel", Technical Report SA-TR19-1520, 1966.

12. Cox, T. A. - "Electromagnetic Inspection of Hardened Steel", Frankford Arsenal Memorandum Report M67-24-1, 1967.

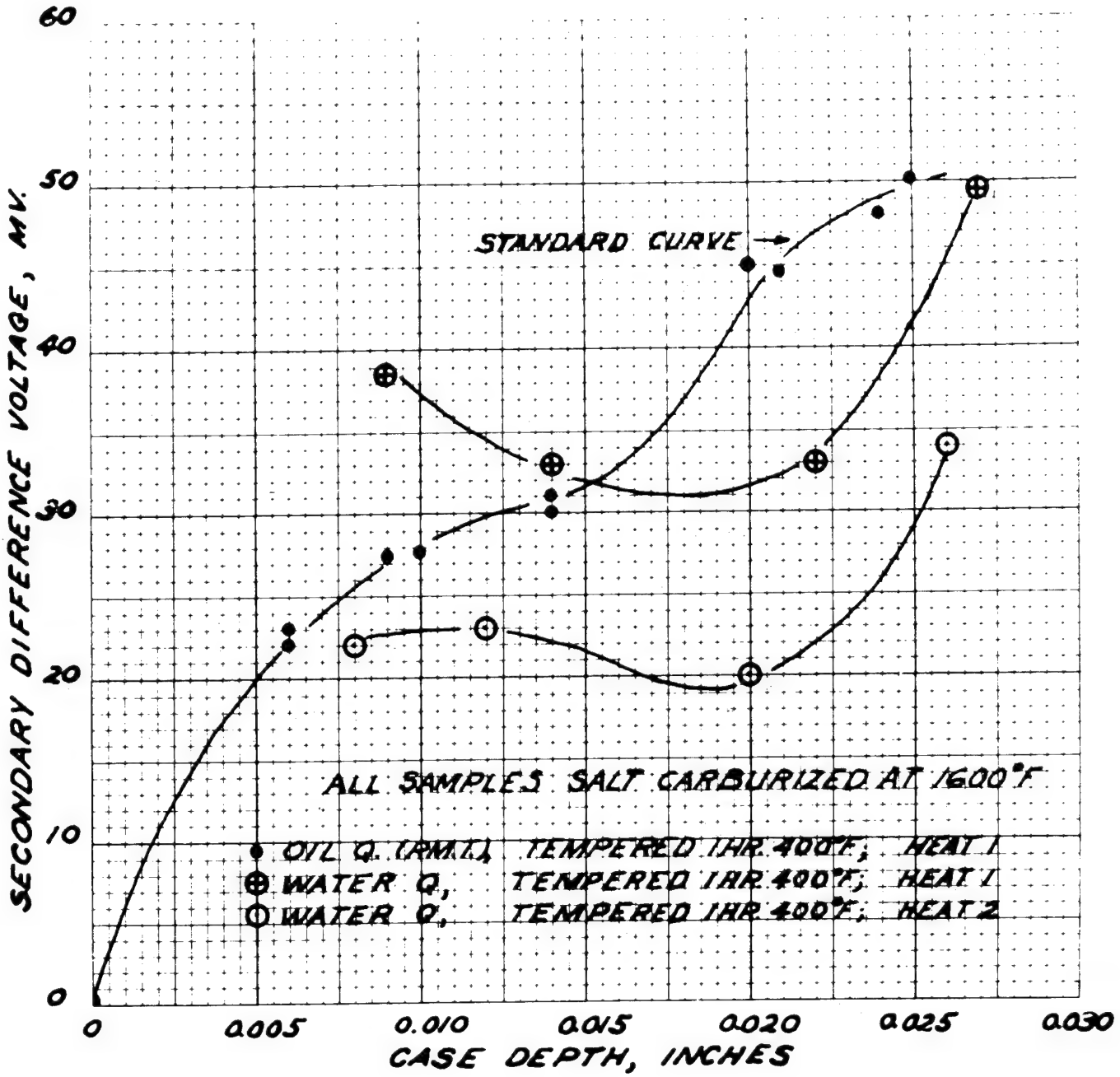

Figure 1. Relation Between Secondary Difference Voltage and Case Depth. Frequency - 1000 cps. Field Strength - 1 Oersted.

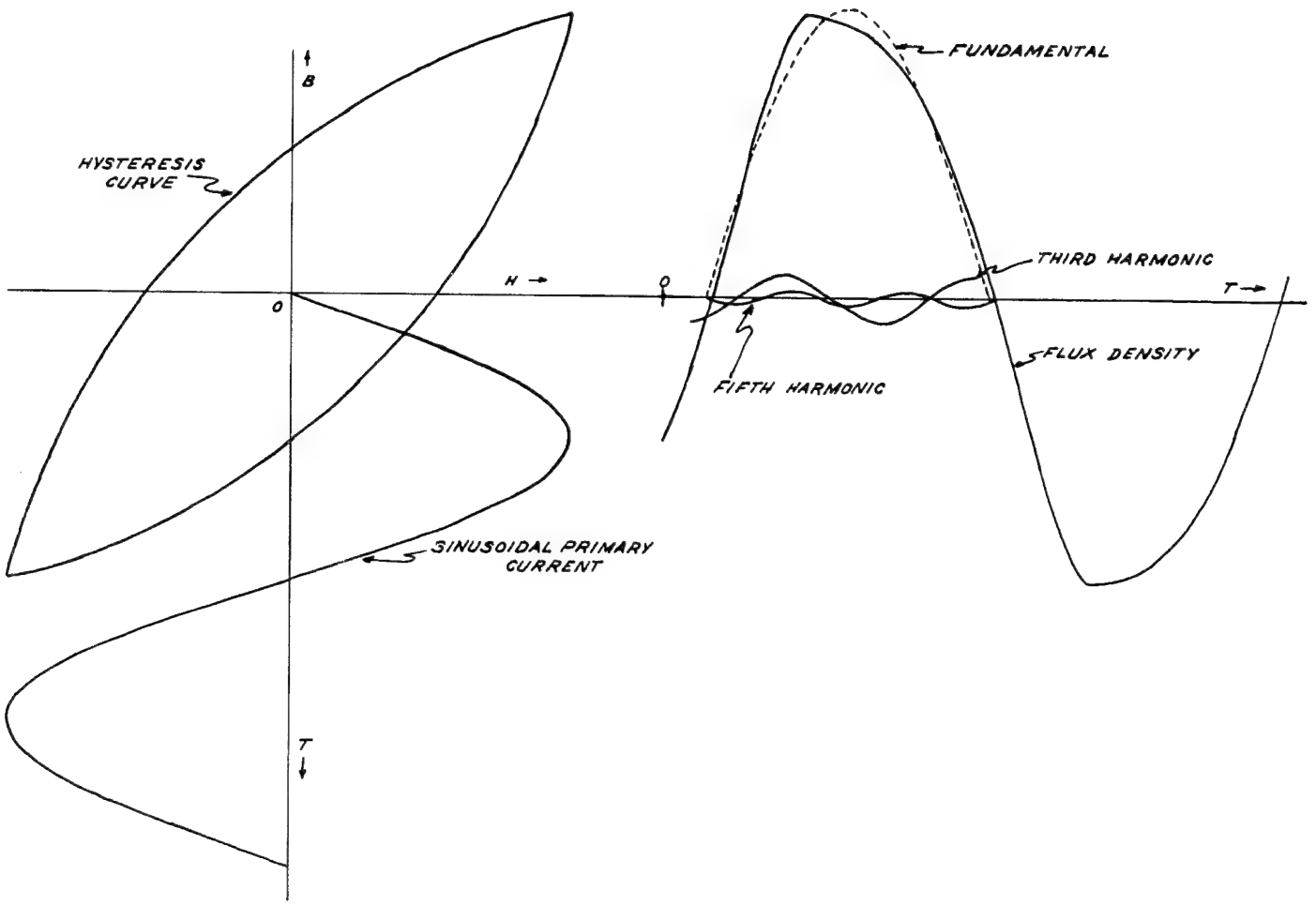

Figure 2. ORIGIN OF HARMONIC DISTORTION FROM A FERROMAGNETIC CORE

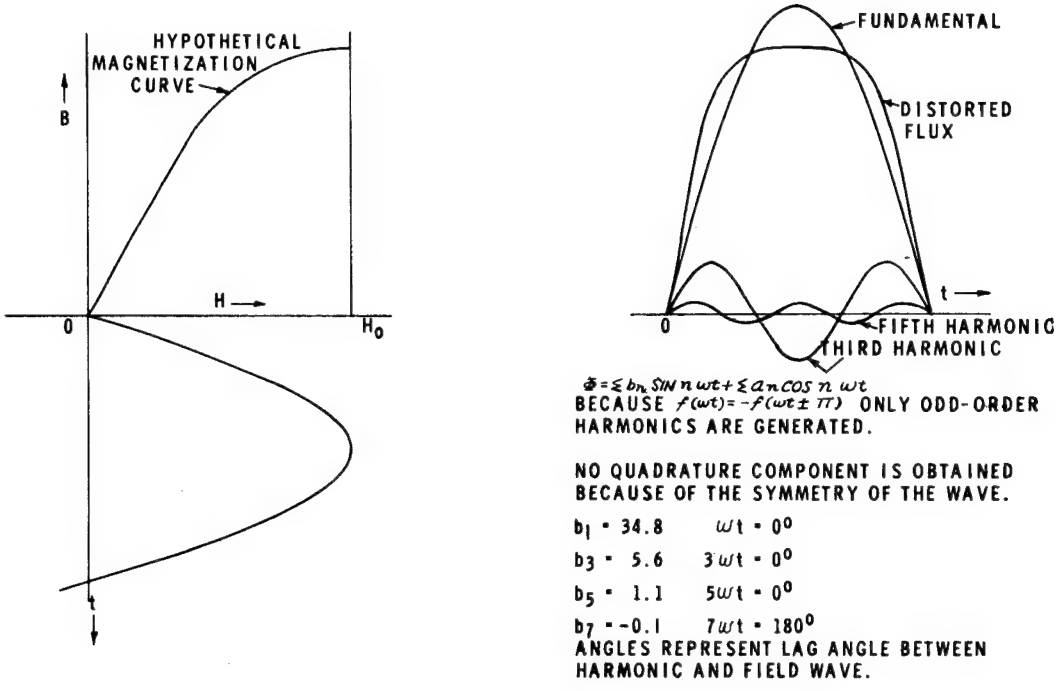

FIGURE 3. GENERATION OF HARMONIC DISTORTION BY INTERACTION OF A SINUSOIDAL FIELD WAVE WITH THE MAGNETIZATION CURVE OF AN IDEALLY SOFT MAGNETIC MATERIAL.

ARMY MATERIALS AND MECHANICS RESEARCH CENTER

19-066-1231/AMC-67

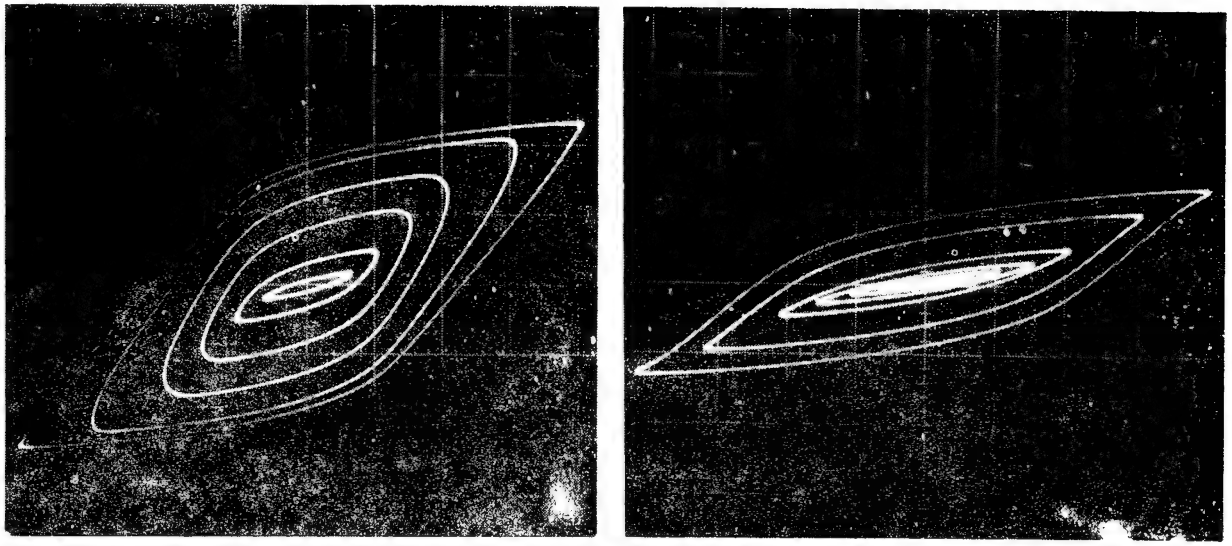

4a. 1020 Steel

4b. 1095 Steel

Figure 4. Comparison of the Hysteresis Curves of Hardened and Tempered SAE 1020 and 1095 Steel, Measured at 100 cps. Scale Factors of Band H are Equal for Both Oscillographs.

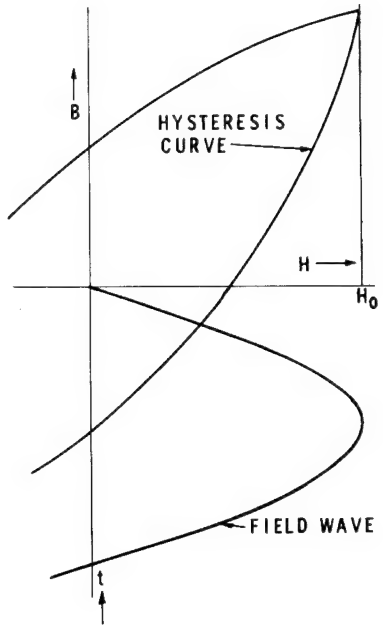

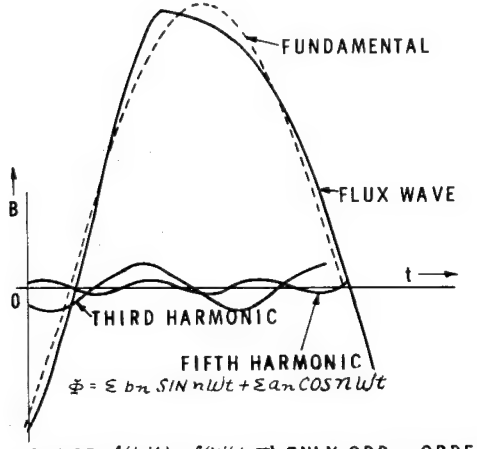

BECAUSE $f(\omega t) = -f(\omega t \pm \pi)$ ONLY ODD - ORDER HARMONICS ARE GENERATED.

HYSTERESIS PRODUCES FLUX WAVE THAT DISPLAYS ALTERNANCE RATHER THAN SYMMETRY AND CONTAINS BOTH IN-PHASE AND QUADRATURE COMPONENTS.

$b_1 = 26.6$	$a_1 = 15.1$	ANGLE OF LAG ωt	$= 29.5^0$
$b_3 = -1.99$	$a_3 = -1.24$	$3\omega t$	$= 148^0$
$b_5 = 0.43$	$a_5 = 0.49$	$5\omega t$	$= 319^0$

Figure 5. GENERATION OF HARMONIC DISTORTION BY INTERACTION OF A SINUSOIDAL FIELD WAVE WITH A HYSTERESIS CURVE CHARACTERISTIC OF THAT OF A LOW-ALLOY STEEL

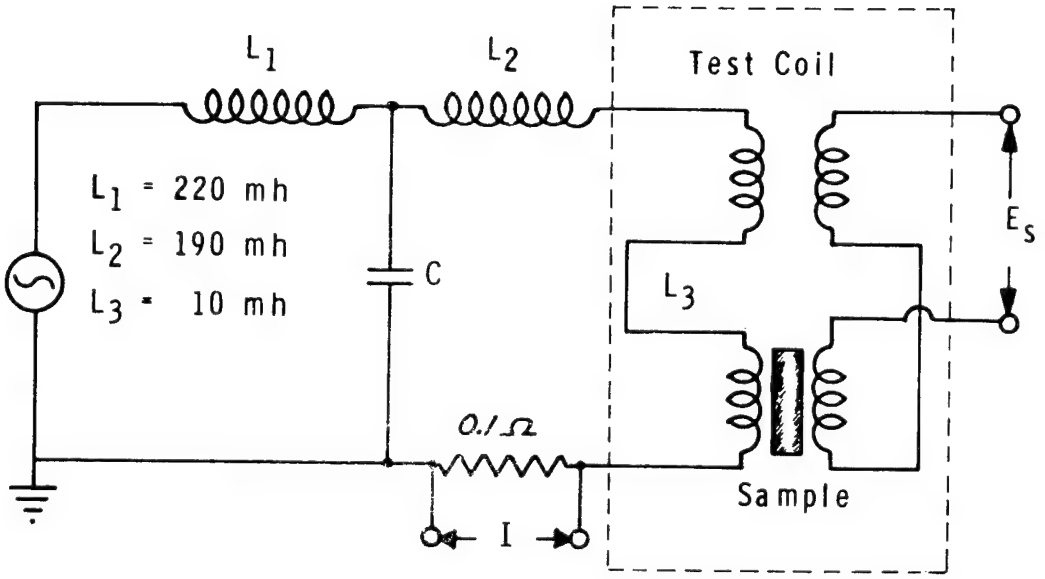

Figure 6. Generator-Test Coil Circuit for Generation of Low-Distortion, Constant-Level Exciting Fields

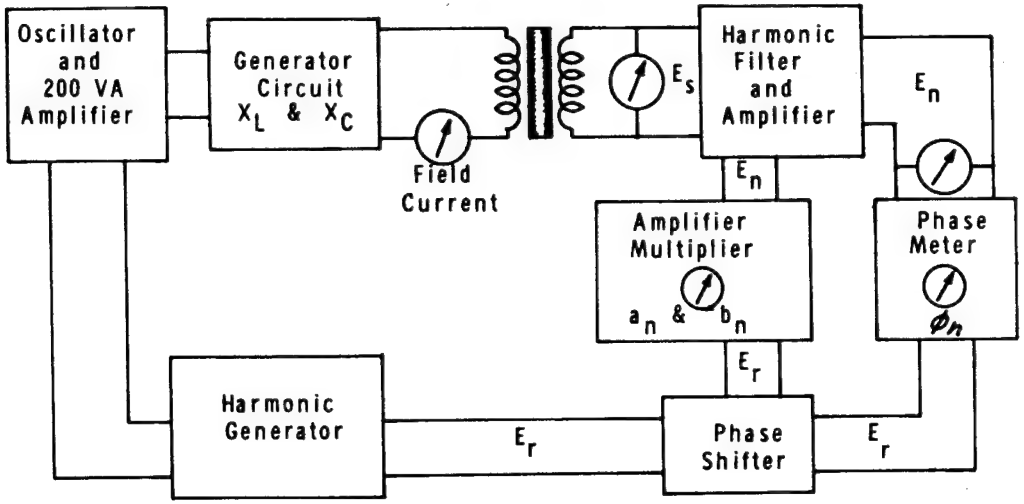

Figure 7. **Block Diagram of Harmonic Analysis Instrument.**

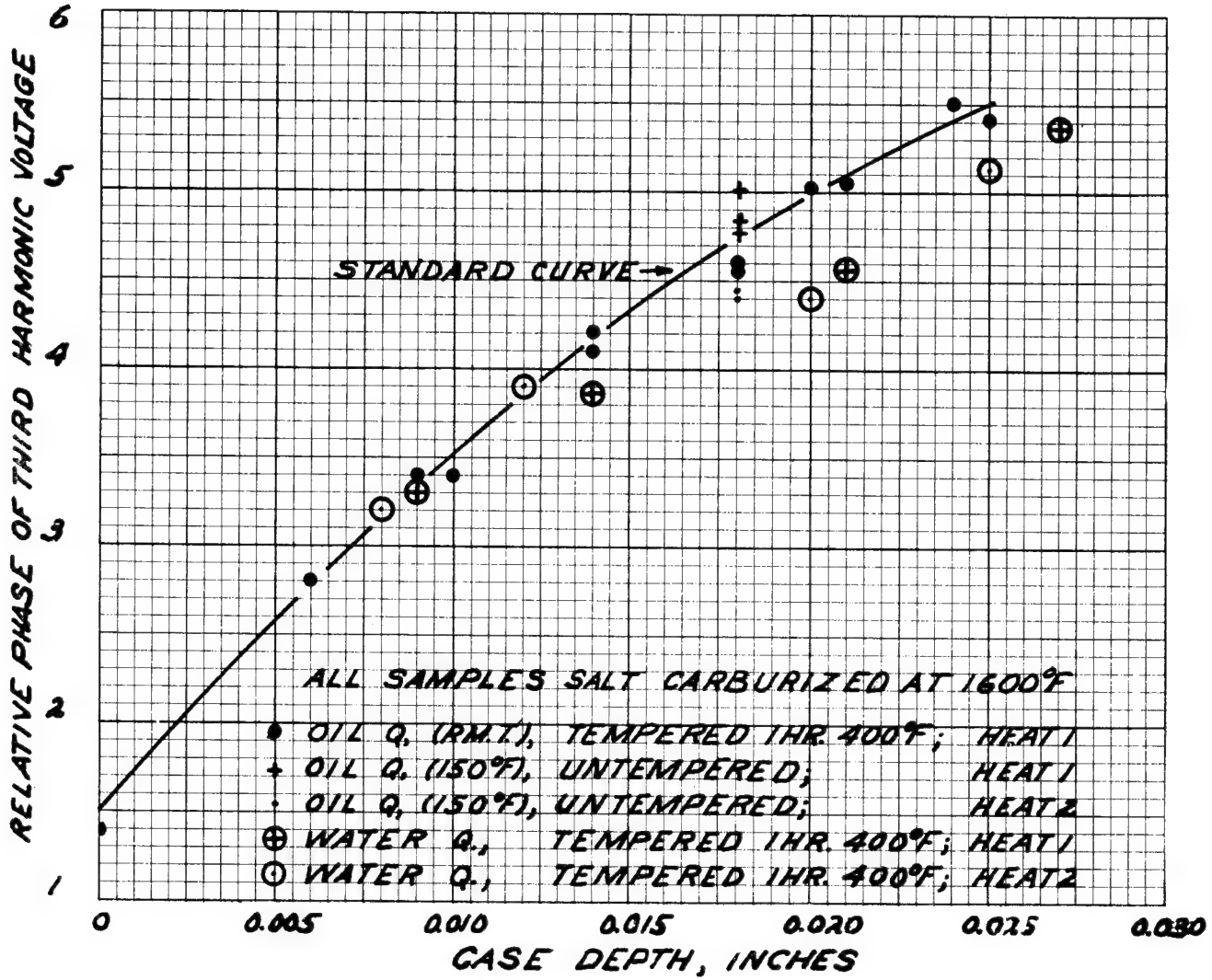

Figure 8. Relation Between Phase of Third Harmonic Voltage and Case Depth for 0.75-Inch Diameter Test Samples. Fundamental Frequency - 150 cps. Field Strength - 105 Oersteds.

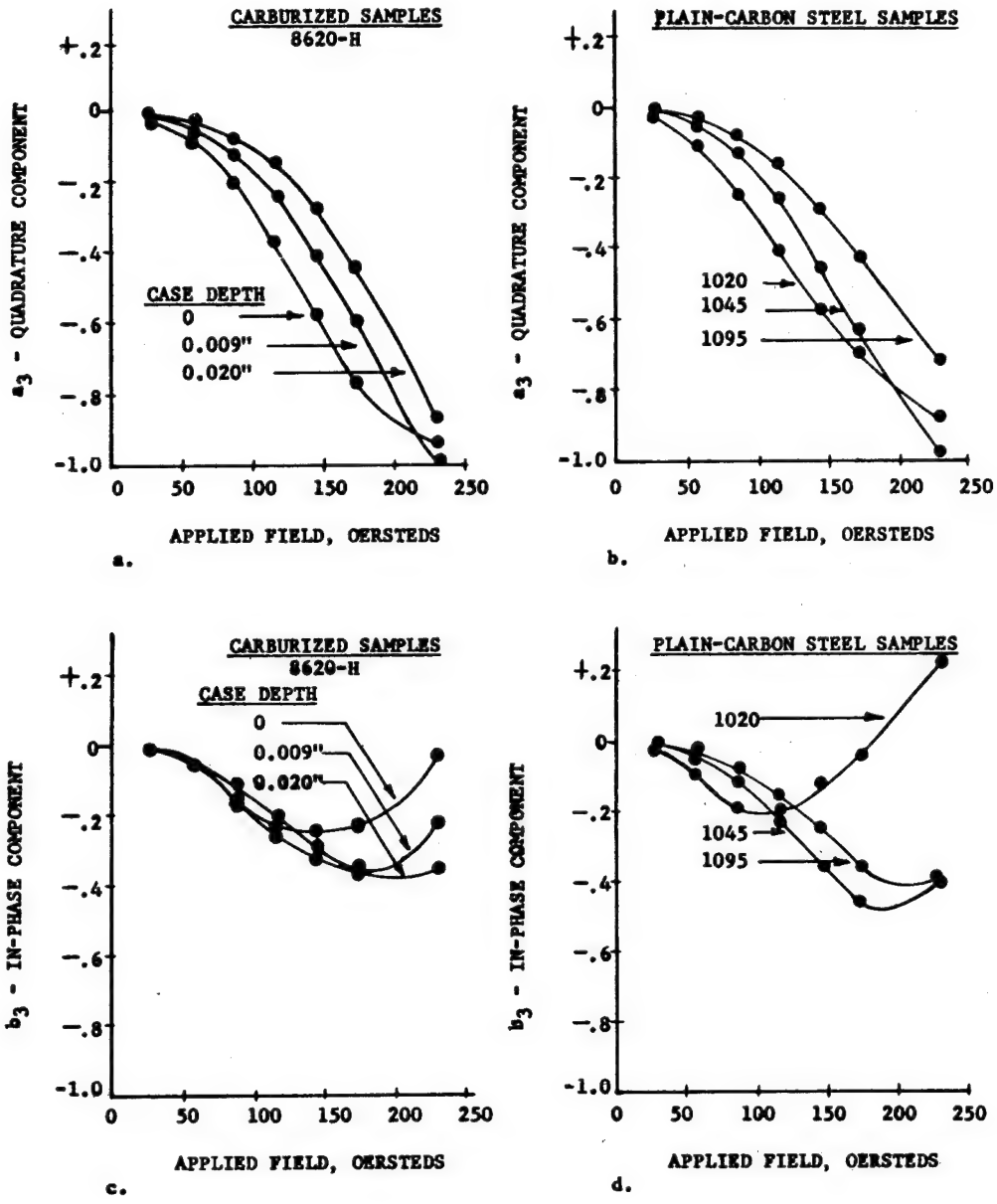

FIGURE 9. COMPARISON OF THIRD HARMONIC COMPONENTS VERSUS APPLIED FIELD STRENGTH. CARBURIZED 8620-H AND PLAIN CARBON STEEL SAMPLES.

ARMY MATERIALS AND MECHANICS RESEARCH CENTER

19-066-1232/AMC-67

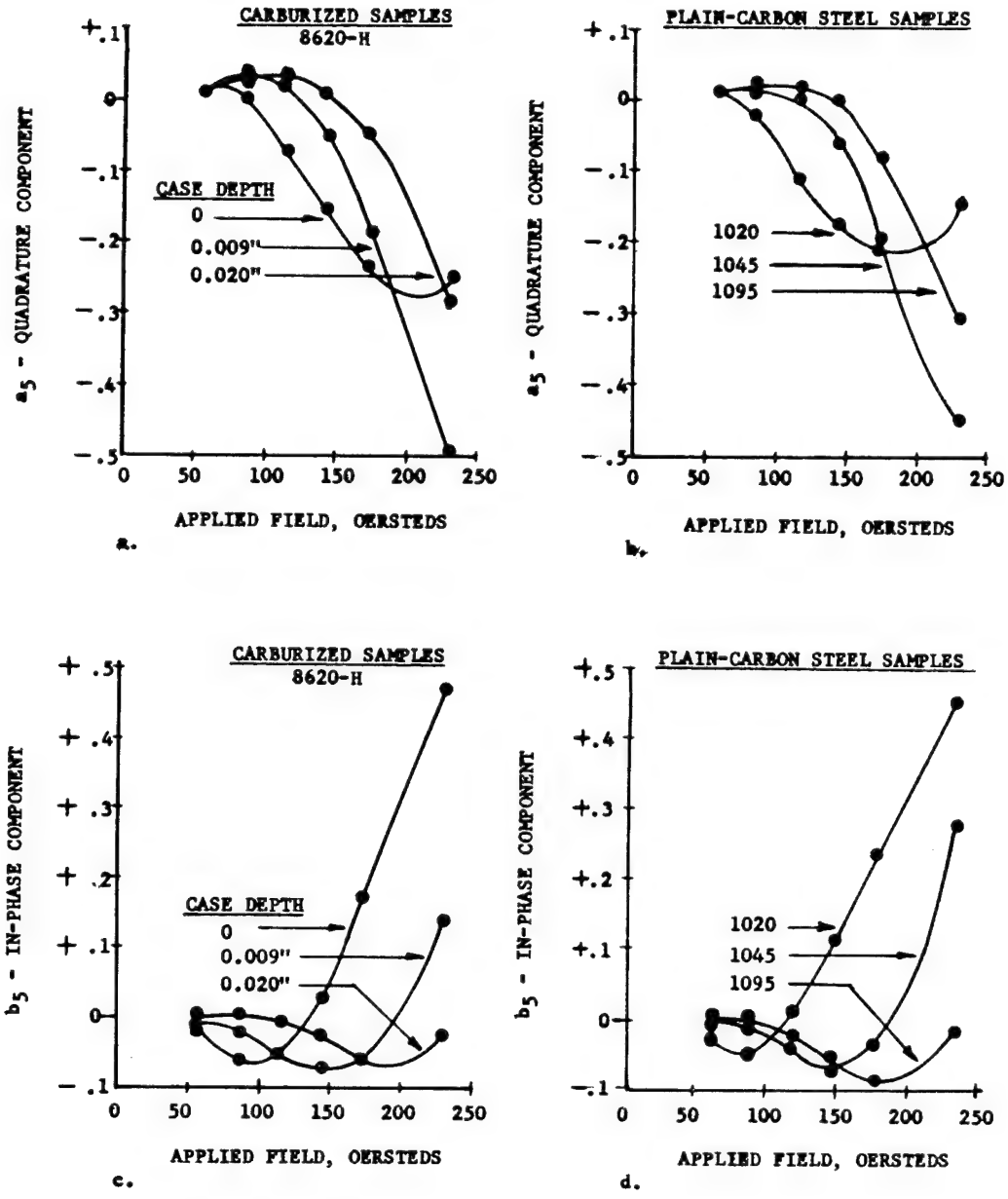

FIGURE 10. COMPARISON OF FIFTH HARMONIC COMPONENTS VERSUS APPLIED FIELD STRENGTH. CARBURIZED 8620-H AND PLAIN CARBON STEEL SAMPLES.

ARMY MATERIALS AND MECHANICS RESEARCH CENTER

19-066-1233/AMC-67

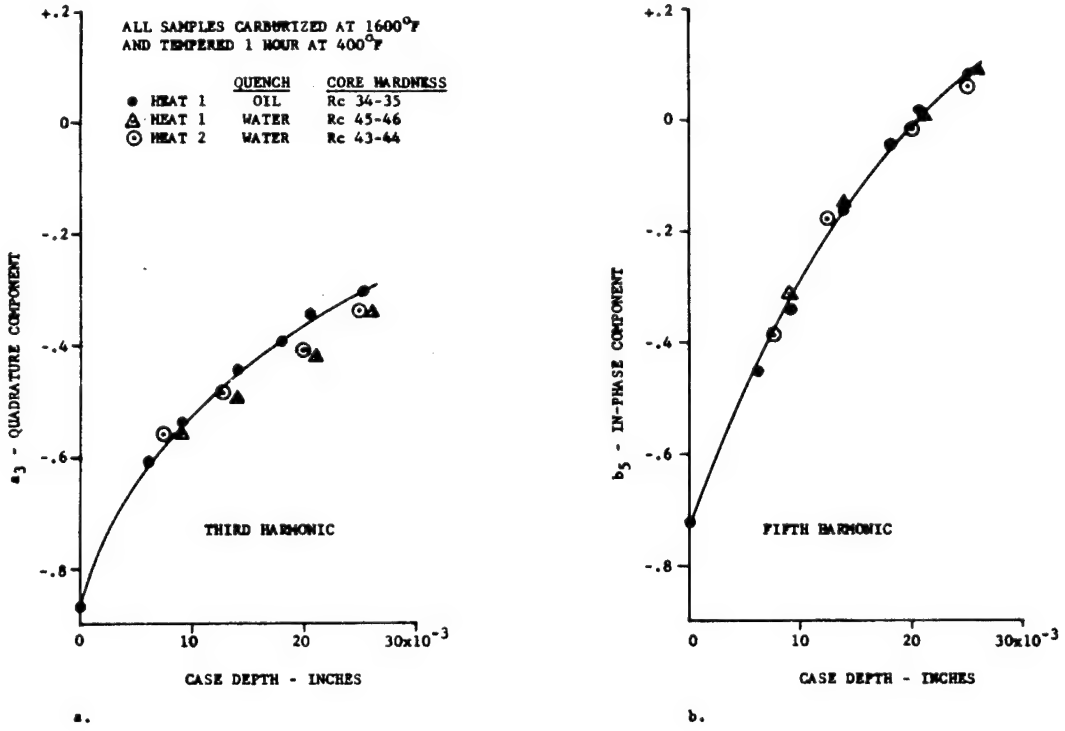

Figure 11. Influence of Quenching Rate Variations on the Correlation Between Harmonic Components (a_3, b_5) and Case Depth for Two Heats of 8620-H Steel. Fundamental Frequency 100 cps., Applied Field Strength - 100 Oersteds.

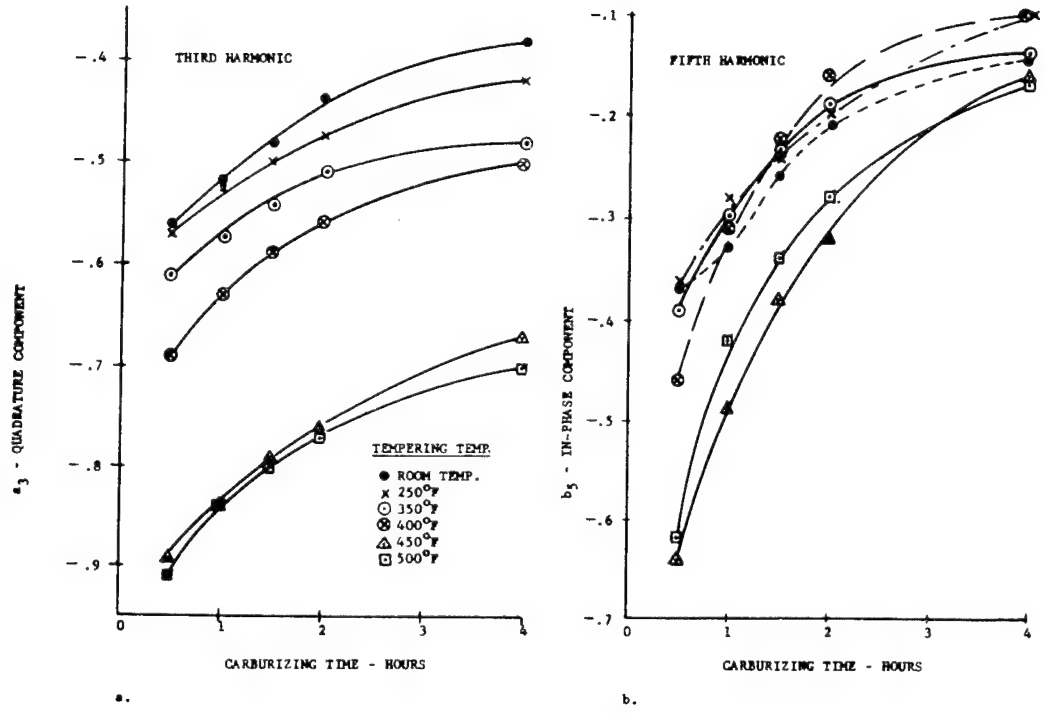

Figure 12. Influence of Tempering Temperature on the Correlation Between Harmonic Components (a_3, b_5) and Carburizing Time. Fundamental Frequency - 100 cps. Applied Field Strength - 115 Oersteds. All Samples Held 1 Hr. at Tempering Temperature.

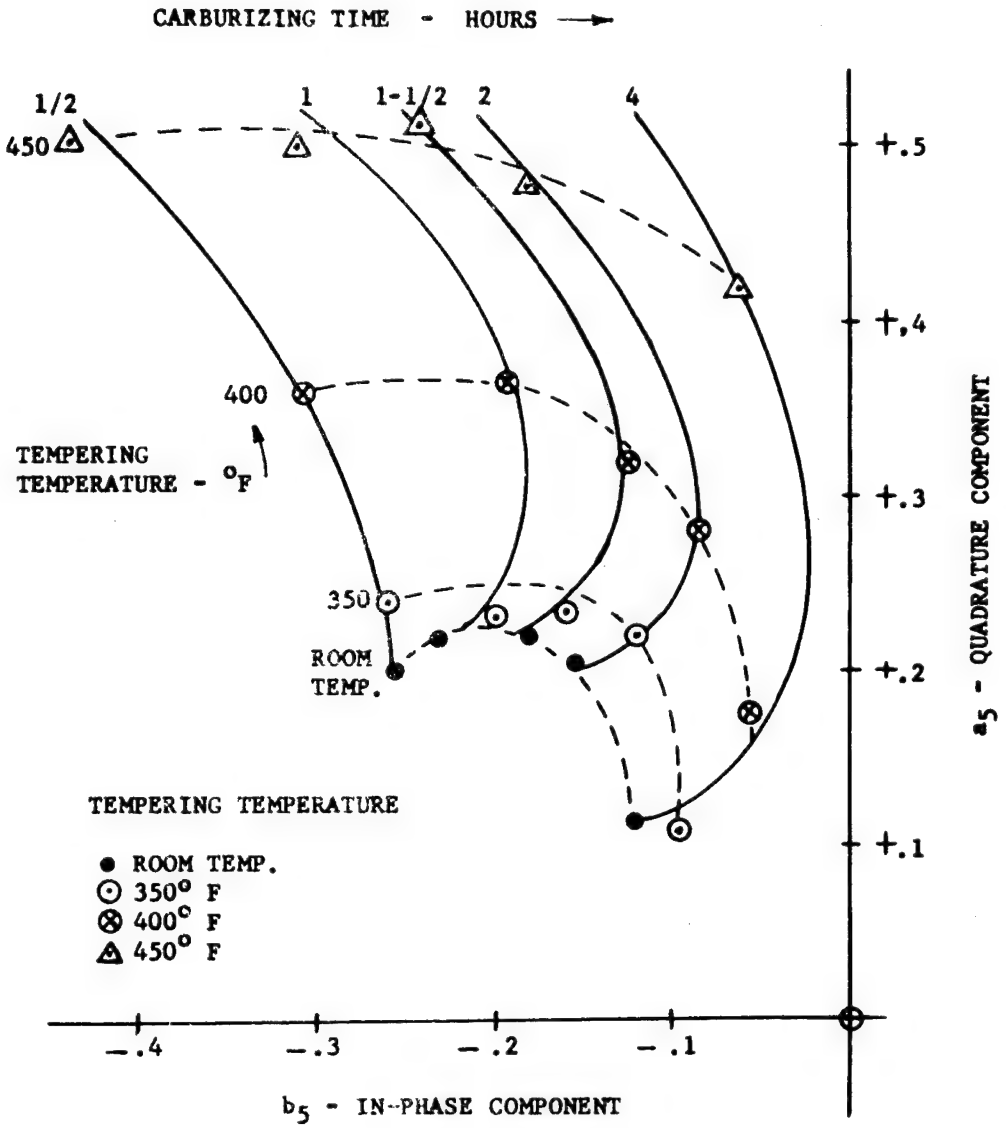

Figure 13. Plot of In-Phase and Quadrature Components of the Fifth Harmonic Showing Separation of Two Simultaneously Changing Variables; Case Depth and Tempering Temperature. All Samples Tempered 1 Hr. at Indicated Temperature. Fundamental Frequency - 100 cps., Applied Field Strength - 115 Oersteds.

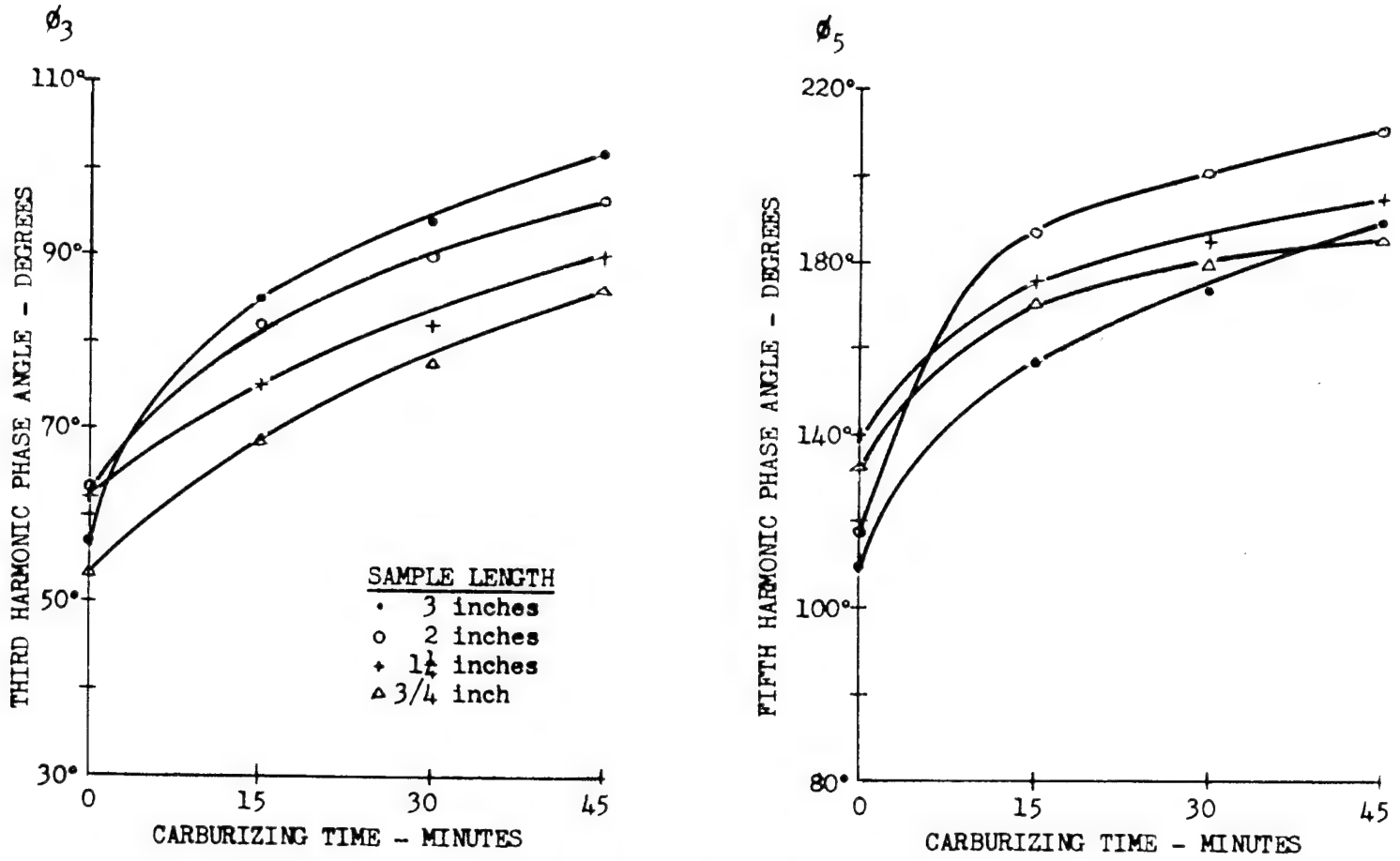

Figure 14. Effect of Demagnetizing Factor on the Relationship Between Harmonic Phase Shift and Case Depth. Samples .075-inch Wall Thickness, 1 inch O.D. Fundamental Frequency - 100 Hz.

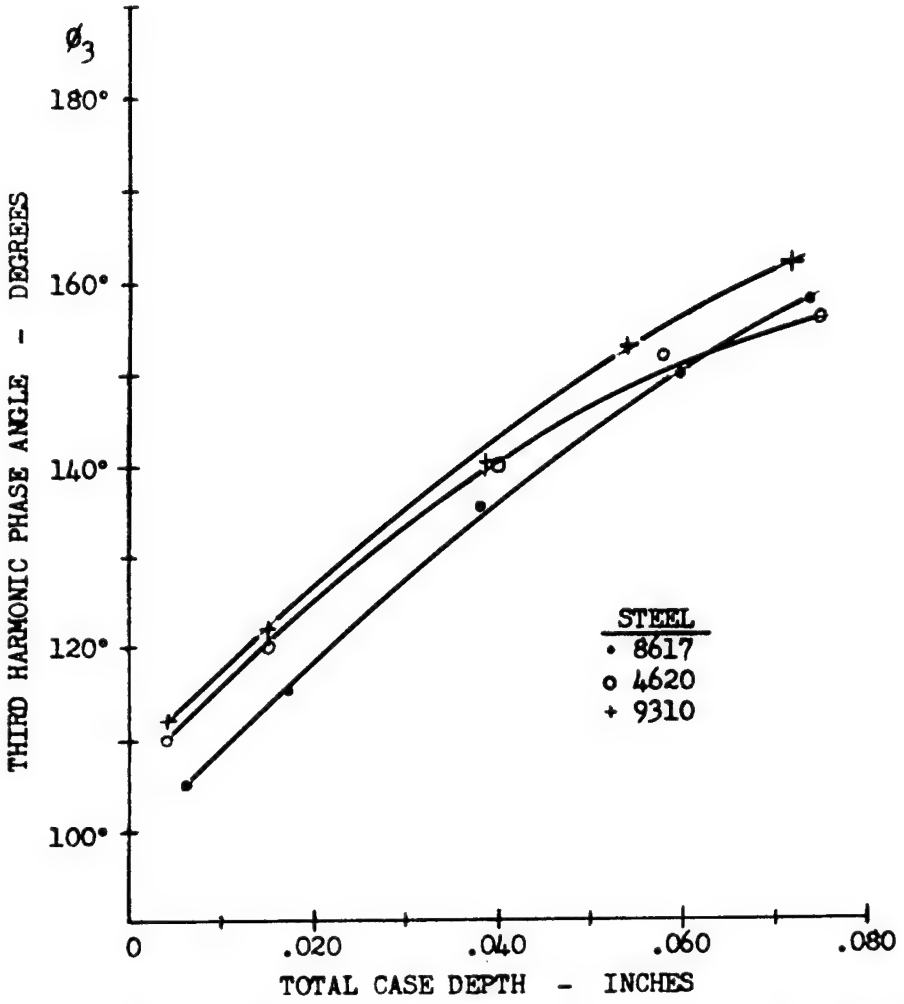

Figure 15. Plot of Third Harmonic Phase Angle Versus Case Depth Showing the Effect of Differences in Alloying Elements. Samples Were Gas Carburized and Oil Quenched. Fundamental Frequency - 100 Hz.

PAPER No. 3

NONDESTRUCTIVE TESTING TECHNIQUES ADAPTABLE TO ULTIMATE LOAD AND FATIGUE LIFE TESTING OF STRUCTURAL COMPONENTS

By

Dwight O. Fearnow
Air Force Flight Dynamics Laboratory
Wright-Patterson Air Force Base, Ohio

ABSTRACT

This presentation is treated as a technical paper even though it is, strictly speaking, a statement of a problem. It is a description of possible approaches to the problem of determining ultimate strength or fatigue life of structural components under both laboratory and field conditions.

General H.M. Estes, Jr. of the United States Air Force said in his keynote address to the 10th National Symposium on Reliability and Quality Control, "It is surprising how little we have applied the various non-destructive inspection techniques to reliability measurements...". He went on to say, "We cannot always afford to consume the product to prove its quality, and we must therefore adapt non-destructive testing know-how to the reliability task".

Implementation of this important concept has introduced many new problems to all segments of the Department of Defense. One of the more complex problems posed to the Air Force Materials and Structures Engineer is the ability to predict the ultimate static and fatigue strength characteristics of complex structures, such as aircraft wings or airframes, without loss of the complete test article; in other words, by laboratory non-destructive testing techniques. A logical progression in the implementation of this important concept is the ability to monitor fatigue damage as it accumulates on in-service aircraft where certainly we cannot "afford to consume the product" to prove its structural fatigue life. There is presently no methodology, no known tool for monitoring and accurately evaluating in-service accumulated fatigue damage on an individual component basis.

For many years the aircraft industry in general and the Air Force in particular have been plagued with this inability to accurately predict either the fatigue life or the fatigue strength of individual structural components. The accompanying catastrophic structural fatigue failures have resulted in the loss of lives and aircraft, but probably the major impact has been unscheduled "down-time" affecting combat readiness. Many methods have been devised to measure fatigue damage; for instance, the use of V-G and V-G-H recorders, loads and stress measuring resistance-wire strain gages, and fatigue sensors using the strain hardening principles of annealed foil gages. Despite the fact that all these methods give, in one form or another, a measure of the load history to which the structure has been subjected, they tell us nothing directly concerning the fatigue strength of each individual component. Consequently, a large measure of reliance must be placed on the statistical approach to the prediction of individual component as well as full-scale aircraft fatigue life. As you know however, the statistical approach has its limitations. One of the major factors contributing to these limitations is the small sample size which can be tested practically. Another major factor is the inability of any known statistical distribution function to predict fatigue life with a reasonable degree of confidence in the low probability of failure regime. Other factors which may be equally important are our inability to predict accurately the environment in which the aircraft will be operating and our inability to reproduce that environment accurately in the laboratory. Forgive me for wandering from the main point of this paper. It is not my intention to be caught between the Statistician and the Engineer, the pure and the practical. It is true however, that the limitations on today's fatigue life prediction techniques have resulted in not only the loss of aircraft and lives where fatigue cracks were not caught in time but also much "down-time" due to unscheduled inspections. In addition, there is costly rework or retirement of many structural components before their true fatigue life potential is exhausted.

In order to realize the full life and strength potential of individual components, it is almost a certainty that NDT methods must be devised which will advise us of the changes taking place within the structural material itself as damage occurs and progresses. In addition, it is almost equally certain that measurement of these changes must be made on an intergranular and microscopic scale. Hopefully by so doing we can greatly increase the accuracy and reliability of our static and fatigue strength predictions.

One of the biggest hurdles to be overcome in an NDT approach, or for that matter any approach to the solution of the material and structural strength prediction problem, is the widespread belief in and use of stress or strain as the only parameters indicative of that strength. This relationship seems to have become indelibly and irrevocably stamped into our every day life. Stress and strain however, although a function of material properties, are not even expressed in terms of those properties. Instead they are expressed in terms of loads and dimensions. Stress for instance, is P/A or MC/I in pounds per square inch, while strain is deflection, $\Delta\ell/\ell$ in inches/inch. Isn't it time we looked beyond the exclusive use of these parameters when there are basic material properties which can be used; properties which are sometimes called "uncommon" but appear to be common to most materials, including composites; properties which are dependent upon changes taking place within the material itself under applied load; properties which are perfectly willing to advise us of changes as they take place if we are willing to listen, to observe, to measure them?

One of these properties is that materials under load emit energy, acoustic energy. This emittance may be in either the audible or the inaudible regimes. John Hawley of the Mechanical Technology Laboratory of the General Electric Company has said that "in essence acoustic emission provides a Maxwellian Demon who sits everywhere within the material being tested, sending out information of significant events inside the material, to be detected by the observer with his instrumentation at any convenient spot on the material surface, the important qualification being that the material itself creates the signal which is then transmitted out through the material".

Alan B. Simpkins, Delcon Division of the Hewlett-Packard Company, has reported in the March 16, 1966 edition of Design News that when a material is subjected to load testing "it emits ultrasonic energy under forces that are only a fraction of the structure's design load". This emittance apparently changes in frequency and intensity as the load is increased, and specific characteristics of the emission vary with different materials and different metallurgical make-up of a given material. If one can learn to recognize the specific material signature curve, i.e., the sharp rise and fall of the acoustic emission just before rupture, one can predict failure. Moreover, Mr. Simpkins goes on to say that the Hewlett-Packard Company has developed ultrasonic translator detectors for measuring these ultrasonic emission, these "silent sounds".

Brad Schofield of Teledyne, formerly Lessells and Associates, Incorporated of Waltham, Massachusetts is another interested investigator of "Acoustic Emission Under Applied Stress". Some of his work has been done under Air Force contract and is reported in WADC-TR-58-194, Aeronautical Research Laboratory Report ARL-150, ASD-TDR-63-509 Part I and Part II, AFML-TR-65-106, and AFML-TDR-66-92. This work by Mr. Schofield strongly suggests a working relationship between structural strength and acoustic emission.

In a paper entitled "Sounds of Stress Warn of Failure About to Happen", in the June 6, 1966 edition of Product Engineering, Nicholas P. Chironis reported on the acoustic phenomenon as observed during the proof test of a large rocket-motor-case. Mr. Chironis' account may be a bit dramatic and perhaps a little controversial, but in effect he said that a number of acoustic transducers were placed at strategic points on the rocket-motor-case and that each of these transducers fed signals to its own amplifier, speaker, and tape recorder. While the test pressure built up slowly some of the speakers began emitting a sound like "bacon frying". Strain gages showed the case material was at a stress of about 40,000 psi, well below its yield stress of about 230,000 psi. The test pressure was only about half the required proof pressure. Suddenly however, as the test pressure slowly increased, the "frying sound" rose in intensity "as if the gas had been turned higher under the bacon". (There is some disagreement concerning the use of this particular terminology in that it is thought the "bacon frying" sound might more nearly represent the acoustic emission from a fibrous reinforced composite rather than from a metal). Nevertheless, according to Mr. Chironis, a few seconds after this dramatic change in the acoustic emission the rocket-motor-case exploded into dozens of pieces.

Lockheed Missiles and Space Company has demonstrated the feasibility of using ultrasonic emission to achieve quantitative and qualitative analysis of structural integrity during proof loading at levels reduced to 50% of normal practice on the materials tested. These materials include simple weldments, simple and complex fiber reinforced resin, and complex wood and metal structures. Mr. Parker, Senior Material and Process Engineer for Lockheed at the time, stated that "due to the complete absence of adverse results on the specimen tested it can be assumed that the method is useful as an inspection method on any structure that is proof loaded". Mr. Parker's work also shows acoustical evidence of progressive deterioration of the material tested with repeated applications of the proof load.

Aerojet-General Corporation under contract with the National Aeronautics and Space Administration has recently demonstrated the feasibility of an acoustic depressurization system designed to prevent accidental destruction of large rocket-motor-cases during proof pressure testing. The program was undertaken to establish an acoustic technique (nicknamed SWAT for Stress-Wave Analysis Technique) to detect and locate a growing flaw, monitor its growth, and at the opportune time arrest the flaw growth by depressurizing the system.

This method utilizes the stress wave emanating from the tip of a flaw, since it is believed that the most probable cause of premature failure in large rocket-motor-cases during proof testing is propagation of a flaw which has remained undetected despite normal inspection techniques.

The foregoing is of necessity, only a partial listing of the work being conducted in the area of material acoustic emission under applied stress. I believe however, it does ably demonstrate the potential advantages to be gained by "listening" to the material itself tell us of the significant events, the significant changes taking place therein. As a matter of fact, the Air Force has completed sufficient background study to justify additional effort in that direction. An in-house research package is now being documented to study the subject further. Hopefully, this brief presentation will inspire similar efforts by other Government Research Divisions.

Another "uncommon" material property which appears to be common to most materials is their ability to accept, to be impregnated with a wide variety of gases. Common examples are gases which contain carbon and are used in the carburizing process, and gases which contain nitrogen and are used in the nitriding process. The impregnation is generally accomplished under closely controlled elevated temperature and pressure conditions. Ion-bombardment is also used with some of the rare gases. This ability of materials to be impregnated with a gas has been recognized for some time. The potential advantages of using a material impregnated with the radioactive isotope of Krypton is of more recent vintage. Kr^{85} is especially inviting since it has a relatively long ten year half life, a low energy but easily detectable Beta emission and virtually no Gamma activity. This latter characteristic minimizes the health hazard usually associated with radioactive materials and facilitates handling problems. In addition, Krypton is an inert gas and as such its incorporation into the material intergranular structure does not affect the material physical or chemical properties. Mechanical or chemical disturbance of the impregnated material however, will cause the gas to be released, thus enhancing its application as a universal tracer for studying various parameters which affect the material lattice state. The release of the gas appears to be proportional to the extent of disturbance and is measurable by the loss in material residual radioactivity.

The technology of Krypton-Kr^{85} impregnated materials is still relatively new and I hesitate to expand on the subject because every time I open my mouth, I am accused of violating someone's "Proprietary data" rights. Besides, I have just about exhausted my knowledge in the area. Most of the published work to date makes use of Krypton-Kr^{85} impregnated materials to detect phase changes in solids, maximum surface temperatures, and surface alteration rates resulting from such phenomena as oxidation and wear. Maximum surface temperatures by an "after-the-fact" process are readily determinable since the Krypton impregnated material will release a fraction of its Kr^{85} upon being heated at a constant temperature. Further or repeated heating at or below this temperature apparently results in no additional loss in radioactivity.

As recently as 1962, it was postulated that actions within the material itself (such as dislocation pile-ups, intrusions, extrusions, perturbations, intergranular slip, or whatever it is that takes place while a material is being strained or during the phenomenon known as fatigue damage accumulation) might also cause a loss in the residual radioactivity of Kr^{85} impregnated materials, and further that this loss might be measurable and that these measurements might be correlated with material strength. As recently as this past spring, the Army, through its Aviation Materiel Laboratory at Fort Eustis, Virginia let a contract to determine if a correlation exists between metal stress levels and the capability of a metal to absorb or retain an inert gas. Concurrently, the Air Force is in the negotiating stages of a complementary contract to determine the feasibility of using the Krypton-Kr^{85} impregnated material technique as a measure of metal fatigue damage. Despite the fact that this technology is still in its infancy, its potential is such that it has attracted the attention of a number of industrial firms, many of whom are engaged in company-funded projects to further explore and exploit that potential. Related programs are also being conducted by investigators in foreign countries.

In summary I reiterate, "We cannot always afford to consume the product to prove its quality, and we must therefore adapt non-destructive testing know-how to the reliability task". The advent of the space and nuclear age brought this concept sharply into focus. No less important however, is the ever increasing cost of manned aircraft. For example, ten years ago the cost of the B-58 static test article (airframe) alone was about 3½ million dollars. Several airframes were consumed during laboratory tests. Today, the cost of the C-5A static test article (airframe) alone is about 25½ million dollars. At least two airframes will be consumed during laboratory tests. The cost of a laboratory test article is small however, compared with the loss in total resources resulting from catastrophic in-service failures. This loss of course, includes lives as well as complete aircraft and mission abortion. Certainly we cannot afford to exhaust the fatigue life of the product in-service, and non-destructive testing know-how must be adapted not only to laboratory tests of complex structures, but also to the problem of monitoring fatigue damage as it accumulates during service usage.

Two possible techniques which appear to have potential for accomplishing this are: (1) the use of material acoustic emissions in either the audible or the inaudible regimes, and (2) the use of Krypton-Kr^{85} impregnated materials as a measure of structural strength. Sufficient work has been done in both areas to warrant further investigations. Perhaps you already have perfected the methodology, the necessary tools for measuring changes in these so-called "uncommon" material properties as they react to applied loads. Perhaps even now the state-of-the-art in NDT is such that you can furnish the Structures Engineer with measurements he can correlate with structural strength. Perhaps you know of other "uncommon" material properties which will divulge significant events as they take place within the material. It is my sincere

belief that with the background and knowledge you have in the NDT technology, and possibly with only a very simple redirection of effort, you can furnish the Structures Engineer with the necessary information to enable him to solve this very important problem. A necessary prerequisite to the solution of any problem however, is the understanding by all concerned as to the nature of the problem. That is why I am here today!

01

PAPER No. 4

NUCLEAR QUADRUPOLE RESONANCE (NQR)

A NOVEL APPROACH TO NONDESTRUCTIVE INSPECTION OF REINFORCED PLASTICS STRUCTURES

JOHN J. GURTOWSKI
NAVAL AIR SYSTEMS COMMAND
WASHINGTON, D. C. 20360

ABSTRACT

The nuclear quadrupole resonance (NQR) tracer technique has been shown to be capable of detecting internal stress concentrations around defects and the internal stresses which develop during fabrication and cure or are the result of externally applied forces. In addition, it appears the NQR signal is proportional to the amount of "doped" resin in the structure and is capable of providing an accurate measure of resin distribution.

The NQR tracer technique has the potential for providing a direct measure of resin polymerization or the gradual degradation of the polymers under thermal and mechanical cyclic stressing. It can be used to determine the properties of reinforced plastic composites in service or when they are subjected to different storage and handling procedures.

From studies of failure mechanisms in tension and compression and the behavior of the reinforcement/matrix interface it is apparent the NQR tracer technique may contribute much useful design data and other information for improving the quality and extending the useful service life of reinforced plastic structures.

INTRODUCTION AND SUMMARY

Under Naval Air Systems Command Contracts NOw 66-0403-c and N00019-67-C-0415 Aerospace Research Associates, Incorporated, of West Covina, California have demonstrated a novel nondestructive test procedure which offers much potential for measuring stresses and temperatures within reinforced plastic structures. The concept is based on the principle of nuclear quadrupole resonance (NQR); that is, the interaction of an external radio frequency field with the internal electrostatic fields associated with the molecules of certain compounds incorporated in the structures; the interaction being sensitive to changes in temperature and stress.

The NQR method appears particularly attractive for investigating the parameters which influence the internal stress state of nonmetallic structures and resin castings. These parameters include fabrication variables, structure geometry, holes, surface defects, delaminations, voids and mechanical and thermal loadings.

1

The NQR concept appears to be an effective method for nondestructively assessing possible changes in structural characteristics during handling, storage and the in-service behavior of such primary structures as motor cases, radomes, pressure vessels, deep-submersible structures and many nonmetallic aircraft members.

The NQR tracer technique has the advantage over other nondestructive test methods in that it is capable of measuring internal stress distributions. It is also superior to the other procedures which use strain gauges, thermocouples, etc., for measuring stress and temperature within the nonmetallic composite in that no mechanical interaction takes place with the structure and there can be no effect on the physical properties being measured. Strain gauges, on the other hand are limited to measuring surface stresses. Further, attempts to measure internal stress distribution with strain gauges are complicated by the physical interference of the structure, the stress field introduced by the gauge, the attachment of the strain gauge, allowance for electrical leads and requirements for recalibration.

Current nondestructive inspection procedures are generally limited to identifying and locating relatively large density variations or macroscopic defects (radiography, ultrasonics, liquid penetrant technique, etc.) The NQR method, on the other hand, appears capable of directly measuring the structural quality of the body. An additional attractive feature is its flexibility, allowing the NQR method to make remote and continuous measurements and to inspect reinforced plastics structures continuously or intermittantly under varying service conditions.

BRIEF DESCRIPTION OF NUCLEAR QUADRUPOLE RESONANCE

The nuclear electric quadrupole is the axial distortion of the nuclear charge from that of a spherical distribution. If the distorted charge distribution is in the presence of an elctric field that is changing over the dimensions of the nucleus, there will be an energy associated with the orientation of the nucleus in this electric field gradient. This energy orientation is quantitized into a discrete set of energy levels; the orientation of each level is characterized by the quantum number m. The energy of these eigenstates, E_m for an axially symmetric field gradient is given by the following equation:

$$E_m = \frac{2e^2qQ}{4I(2I-1)} \left[3m^2 - I(I+1) \right]$$

where e is the electron charge, q is the electric field gradient, Q is the electric quadrupole moment of the nucleus, and I is the maximum value of m, that is the total spin of the nucleus.[1,2]

Nuclear quadrupole resonance (NQR) is produced by applying a radio-frequency (rf) magnetic field to the nucleus at a frequency such the E_m - E_m-1 = hf where h is Planck's constant and f is the frequency of the applied rf field. This induction of transitions between the adjacent eigenstates produces a net energy absorption from the applied rf field which is sensed as a power lors in the rf generator producing the field. This power absorption is sensed by the instrumentation as the nuclear quadrupole resonance.

The use of the phenomenon in this program is in the fact that the electric field gradient, q, is produced by the distribution of valence and ionic charges in a compound. There charge distributions change under pressure stress and/or temperature changes since the NQR frequency, f, is proportioned to, q, the change is stress or temperature experienced by the compound in a function of this resonance frequency, that is:

$$f_{NQR} = Gi\ (\sigma T)$$

A configuration of nuclear quadrupole resonance interactions is shown in Figure No. (1).

Under the program the Contractor is developing this stress and temperature sensitivity as an inert, homogeneous probe within a polymer. The inert material that gives the NQR response is distributed uniformly through the polymer as a dilute filter. Measurements of the NQR frequency, f_{NQR}, provide for stress and temperature profile throughout the polymer.

EXPERIMENTAL WORK PROGRAM

A. Test Specimens:

Cylindrical test specimens six (6) inches long and one-half (½) inches in diameter, with gripping threads at both ends, were selected for the exploratory feasibility investigation. The configuration is shown in Figure No. (2a). The resin system was based on 70% by weight of Epoxy 828 and 30% by weight of Versamid 140.

The first series of experiments consisted of resin castings with varying percentages (0 to 100%) of Cuprite (Cu20). The Cuprite was chosen for the initial experiments because of its strong NQR response, its dv/dp coefficient was constant over a wide temperature range, it is readily available, chemically inert and well characterized in literature 3,4,5,6,7.

After thorough mixing, the uncured castings were evacuated in a bell-jar vacuum system for 20 - 25 minutes to remove any trapped air. The first samples were curred in an air circulating oven at 250°F - 10°F for forty minutes, removed from the oven and quenched in water. The remaining samples were cured using different curing cycles and cooling procedures to learn whether

STABLE CONFIGURATIONS OF NUCLEAR QUADRUPOLE INTERACTIONS

(a) HIGH ENERGY ORIENTATION

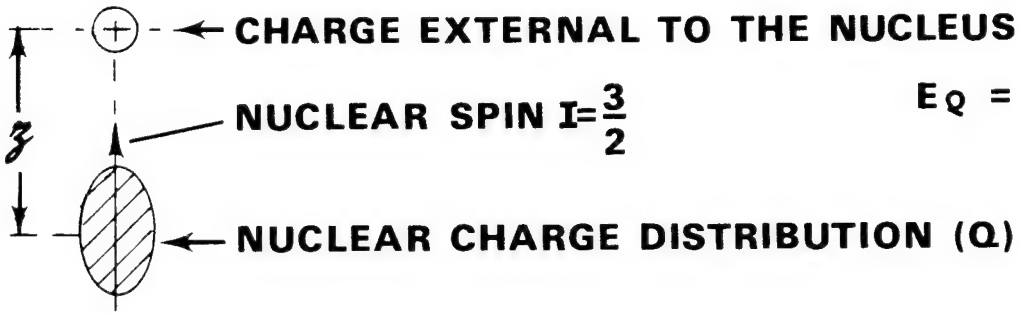

$$E_Q = \frac{6A}{z^3}$$

where $A = e^2 \frac{Q}{4I(2I-1)}$

(b) LOW ENERGY ORIENTATION

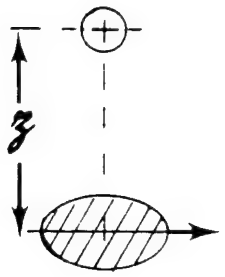

$$E_Q = -\frac{6A}{z^3}$$

FIGURE 1

SPECIFICATIONS OF SPECIMENS

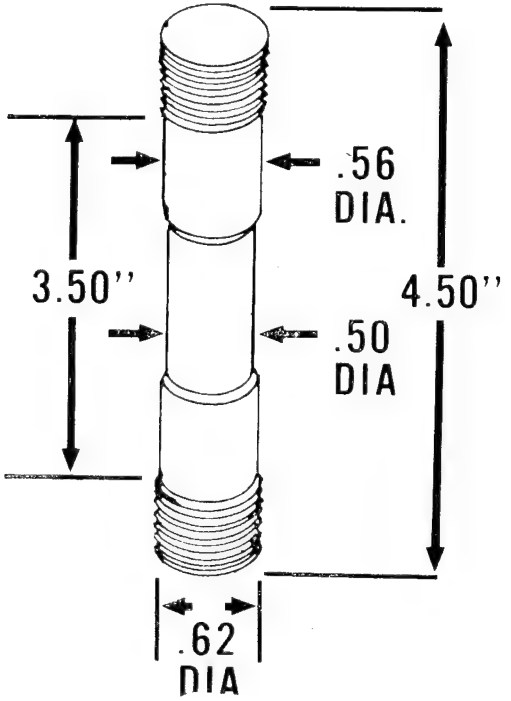

A GENERAL DESCRIPTION

RESIN: "EPON 828" 70% BY WEIGHT OF RESIN
"VERSAMID 140" 30% BY WEIGHT OF RESIN

GLASS LAMINATE: .50 x .010 EC11A FIBERGLASS RIBBON TWENTY LAYERS

TRACER: Cu_2O: 13.2% BY WEIGHT OF SPECIMEN

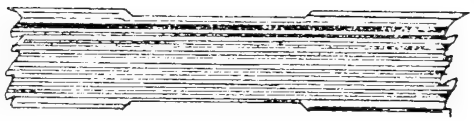

B GLASS LAMINATE

C GLASS LAMINATE WITH FLAW

FIGURE 2

the changes in curing and cooling procedures had any effect on the filler.

The above procedures were repeated with glass laminate samples without and with built-up defects as shown in Figure No. (2b).

Finally, to simulate a poor bond between the glass reinforcement and resin matrix, test specimens were prepared with the reinforcement coated with fluorocarbon in the neck-down section of the samples prior to its incorporation into the resin. The samples were then cured for forty minutes at 250°F - 10°F and allowed to cool slowly to room temperature.

The above experiments were repeated with several other inert fillers with strong nuclear quadrupole resonance responses. The samples tested are listed in Table I. Potential candidates scheduled for evaluation testing are listed in Table II.

B. Instrumentation:

The spectrometer consisted of an Rf oscillator with the coil of its tank around the test sample. The Rf magnetic field produced in the coil provided the energy absorbed by the nuclei. The energy absorption was smaller than the noise generated by the oscillator. To enhance the signal-to-noise ratio the energy absorption was modulated by turning it off and on with a square wave; on-off magnetic field. Modulation was set at a frequency of 100 cycles per second. Narrow-band sensitive detection was then used to maximize the signal to noise ratio. A block diagram of the apparatus is shown in Figure No. (3).

The circuit diagram for the superregenerative oscillator and detectors is shown in Figure No. (4). The theory of superregenerative oscillators is discussed by Whitehead[8]. Figure No. (5) shows the circuit for the latching SCR circuit for magnetic modulation. The Hewlett Packhard Model 202C instrument was used as the frequency generator and the strip chart recorder used was the Bristol Model 1PH560-51 recorder.

C. Test Apparatus and Test

The rod specimens were placed under axial loads of compression and tension as shown in Figure No. (6) and Figure No. (7). The loads for compression or tension were applied in discrete steps by weighing a lever arm with an 8:1 mechanical advantage of weight load to sample load. The extension or compression of the sample was monitored with a sensitive level-arm dial gage. Uniform temperature was maintained by immersing the sample in a constant temperature oil bath. Mechanical guide holes for the vertical rod connected to the sample kept the tension and compression force in alignment. The connection of the sample to the base of the test fixture was given enough play to avoid transverse forces being applied to the sample when stressed.

TESTING COMPOUNDS FOR NQR COMPATIBILITY

THE FOLLOWING GROUP OF COMPOUNDS HAVE BEEN TESTED FOR COMPATIBILITY WITH EPON 828 AND VERSAMID 140 FOR USE WITH NQR SPECTROMETER.

Compatible Mixtures	Melting Temp	Resonant Frequer in MH_z
1. KIO_3 (Potassium Iodate)	560° C	144.37 144.91 145.38
2. Sb_2O_3 (Antimony Trioxide)	656° C	165.49
3. $Ca(IO_3)_2$ (Calcium Iodate)	540° C	Unknown
4. CuI (Marshite)	605° C	Unknown

Uncompatible Mixtures	Melting Temp	Resonant Frequency In MH_z
1. $AsBr_3$ (Arsenic Tribromide)	32.8° C	171.480 172.728 173.143
2. I_2O_5 (Iodine Pentoxide)	300° C	178.01 307.80 316.10 318.05
3. HIO_3 (Iodic Acid)	d110° C	202.871

TABLE 1

SOME IODIC TRACER MATERIALS WITH HIGH MELTING POINTS AND UNKNOWN NUCLEAR QUADRUPOLE RESONANCE RESPONSE

Tracer	Melting Point
CaI_2	740°C
ScI_2	945°C
YI_3	1000°C
LaI_3	761°C
CeI_3	752°C
PrI_3	733°C
NdI_3	775°C
DyI_3	955°C
HoI_3	1010°C
ErI_3	1020°C
NiI_2	797°C

TABLE 2

BLOCK DIAGRAM OF THE SPECTROMETER

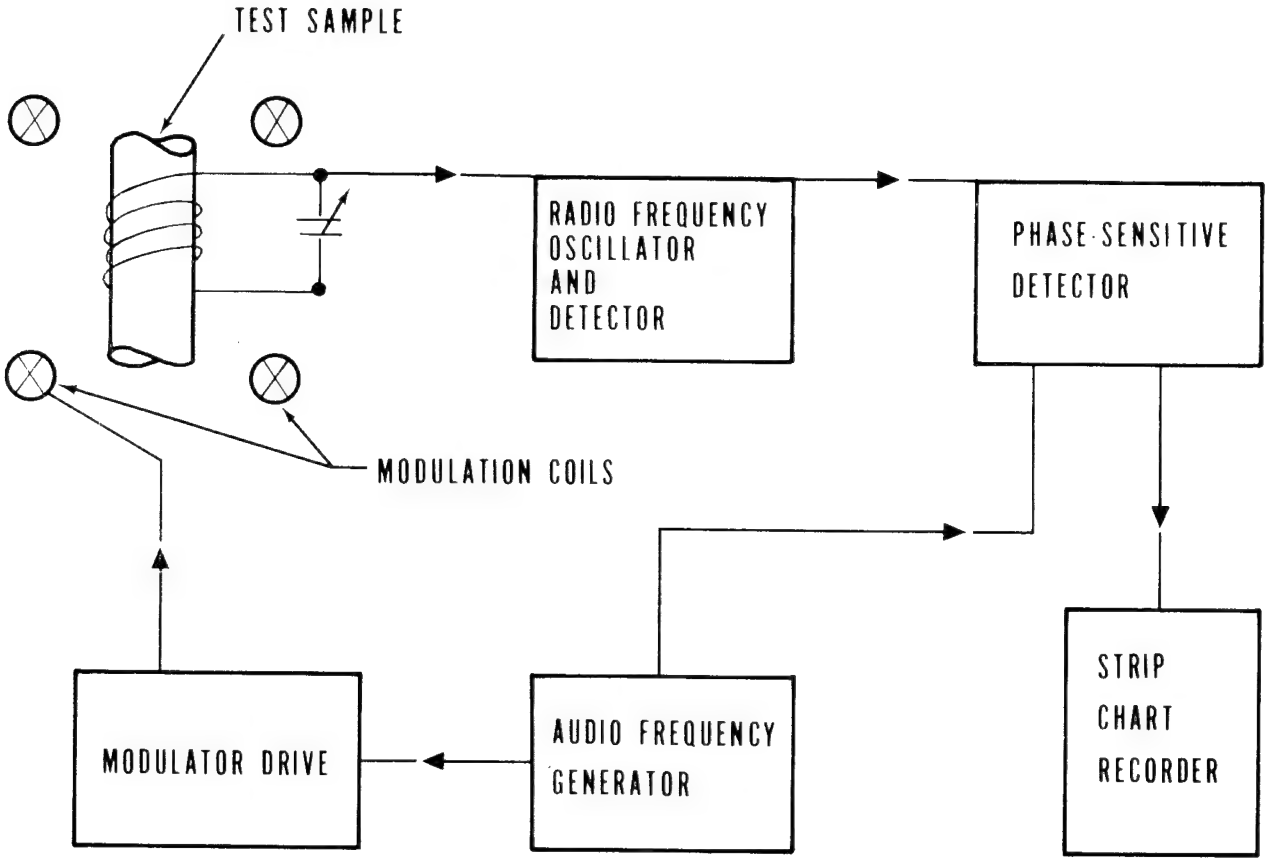

FIGURE 3

NQR MODULATOR

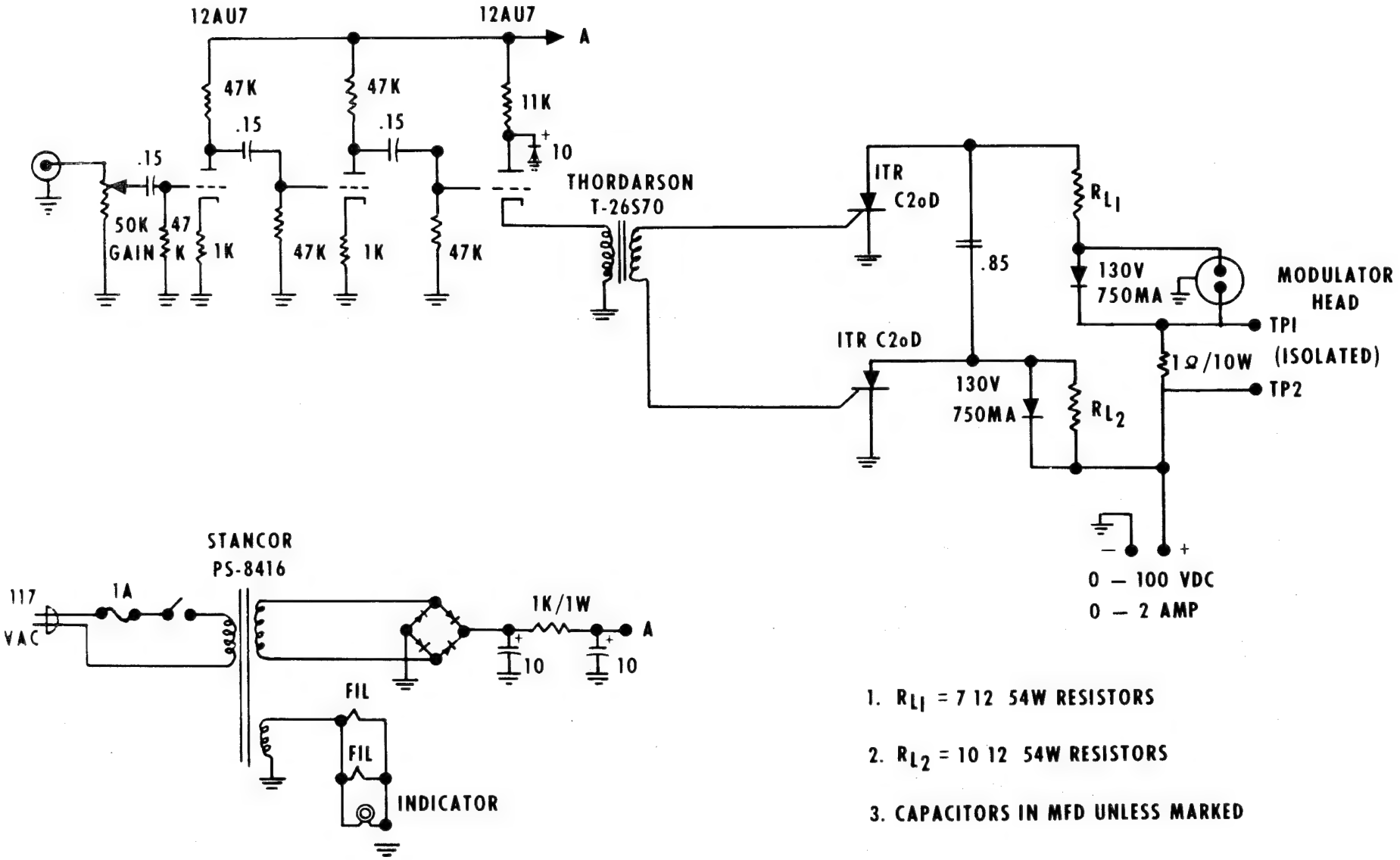

1. R_{L_1} = 7 12 54W RESISTORS

2. R_{L_2} = 10 12 54W RESISTORS

3. CAPACITORS IN MFD UNLESS MARKED

FIGURE 5

TEST SET-UP FOR COMPRESSION

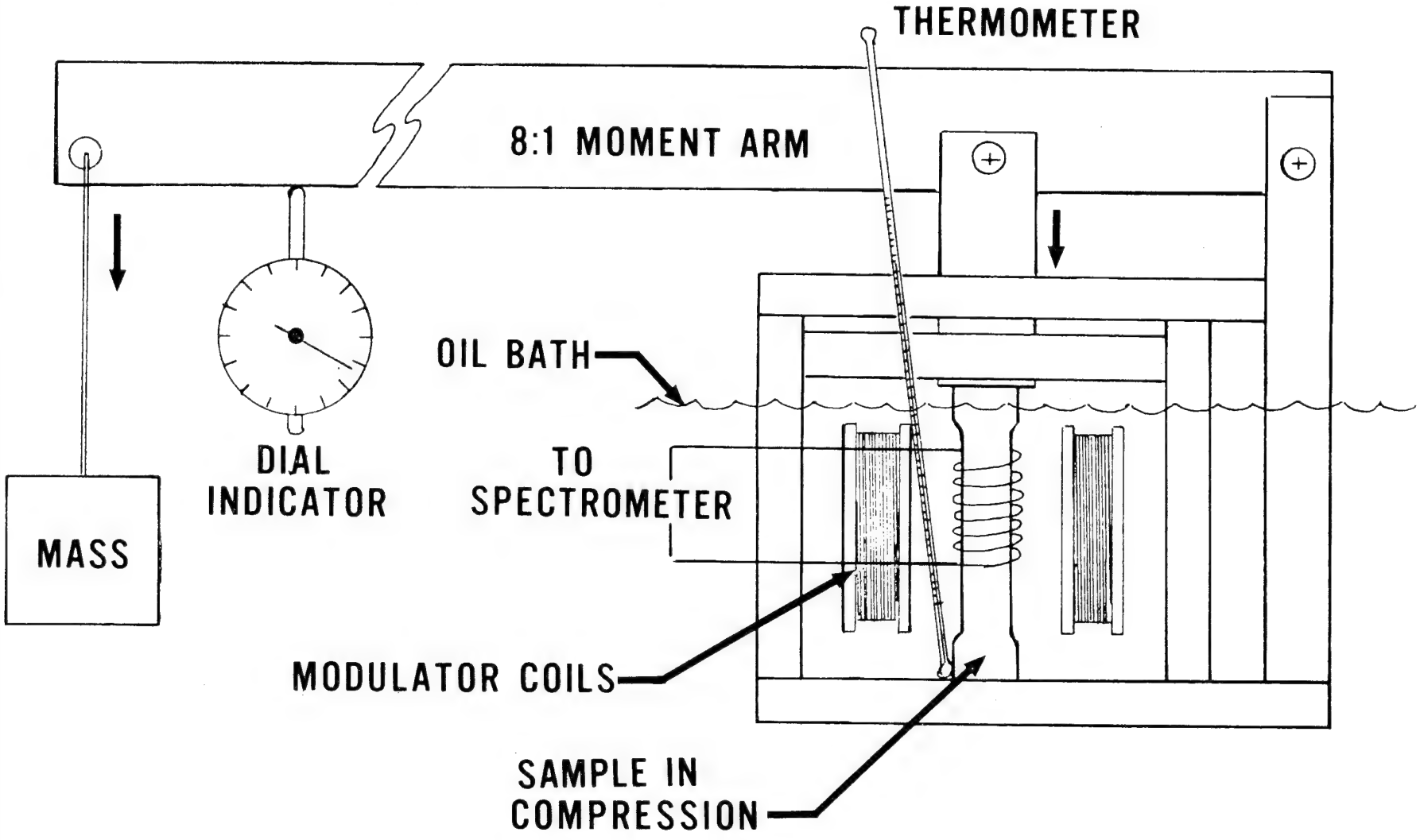

FIGURE 6

TEST SET-UP FOR TENSION

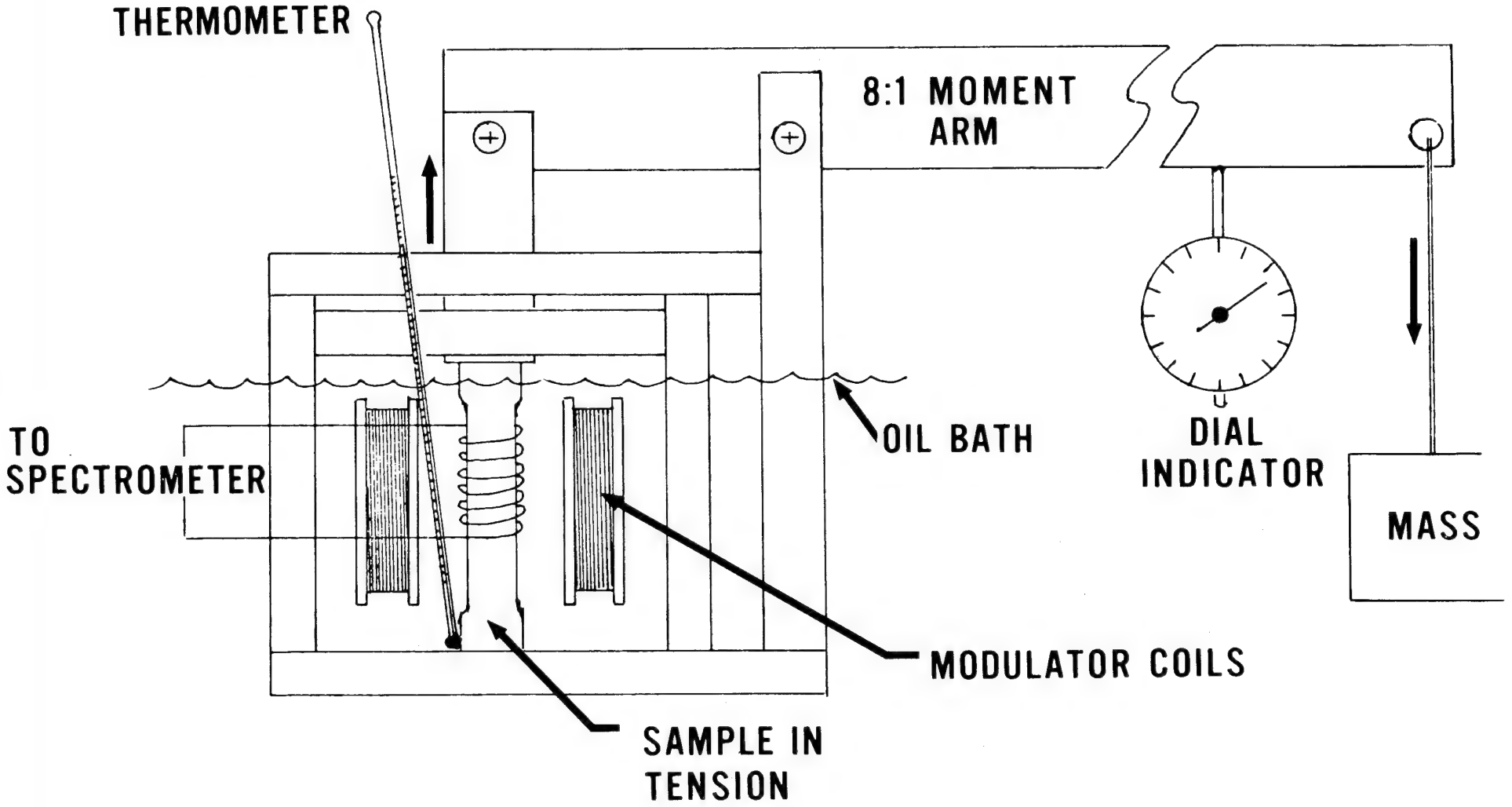

FIGURE 7

TEST RESULTS AND DISCUSSION

A. Cu_2o Tracer Material:

The results of axial compression and tension tests on cast resin and glass laminate resin samples to obtain stress-strain curves by both mechanical and NQR measurement techniques are shown in Figure No. (8) and Figure No. (9) and Figure No. (10). Examination of the figures reveals some very interesting results:

In Figure No. (8), the mechanical and NQR stress-strain curves clearly illustrate the hysteresis characteristics of the resin casting and that the change in resonant frequency with stress $\frac{\Delta f_o}{\Delta \sigma}$ is approximately 2.6 x 10 - $\frac{3Kc.}{PSI}$

The value is almost identical with the value found in the open literature for the pressure dependence of Cu_2O in its pure state as determined by a "pressure bomb" test. It is also apparent, from the curves, that the change in stress direction can be detected by the NQR measurements.

The fact that Cu_2O in the resin reacts to stress like Cu_2O in its pure state when under pressure is significant for it indicates that the tracer was evenly distributed in the resin and its nuclei simulated a nearly-infinite number of strain gages. The figure also reveals that NQR can be used to measure the polymer density profile. One of the most serious problems in quality control of reinforced plastics structures facing fabricators is monitoring the quality and uniformity of the polymer in the finished product.

Figure No. (9) shows that the hysteresis loop in the glass laminate-resin specimens are determined mechanically is considerably smaller than that found for resin castings and that the slope of the stress-strain curve $\frac{AF}{AE}$ for them is greater than for the resin castings. The stress-strain curve based on NQR measurements is also quite different and there was no evidence of resonant frequency change with applied stress, indicating that the applied stress was carried by the glass laminate rather than by the resin.

A gradual degradation of the specimens was noted when the samples were subjected to repeated high stress loading. This degradation was verified by the eratic NQR response. Additional specimens with known severe flaws were prepared and tested to exploit the eratic nature of the NQR curves. It is evident that the effects of flaws can best be shown by comparing the NQR curves at zero-applied stress and at different stress levels.

Figure No. (10) shows the effect of different flaws in the specimens when part or all of the load is carried by the resin. The curve also reveals that the flaw portions of the "doped" resin appear to carry some of the stress. Further, the NQR curve in the figure appears as a superposition of resonances corresponding to each flaw. This superposition results in a broadening of the NQR curve as more stress is applied to the specimen. It can be assumed therefore, that an evaluation of flaw severity can be made by measuring the broadness of the NQR curve.

NQR DUPLICATES STRESS-STRAIN CURVE FOR RESIN CASTING

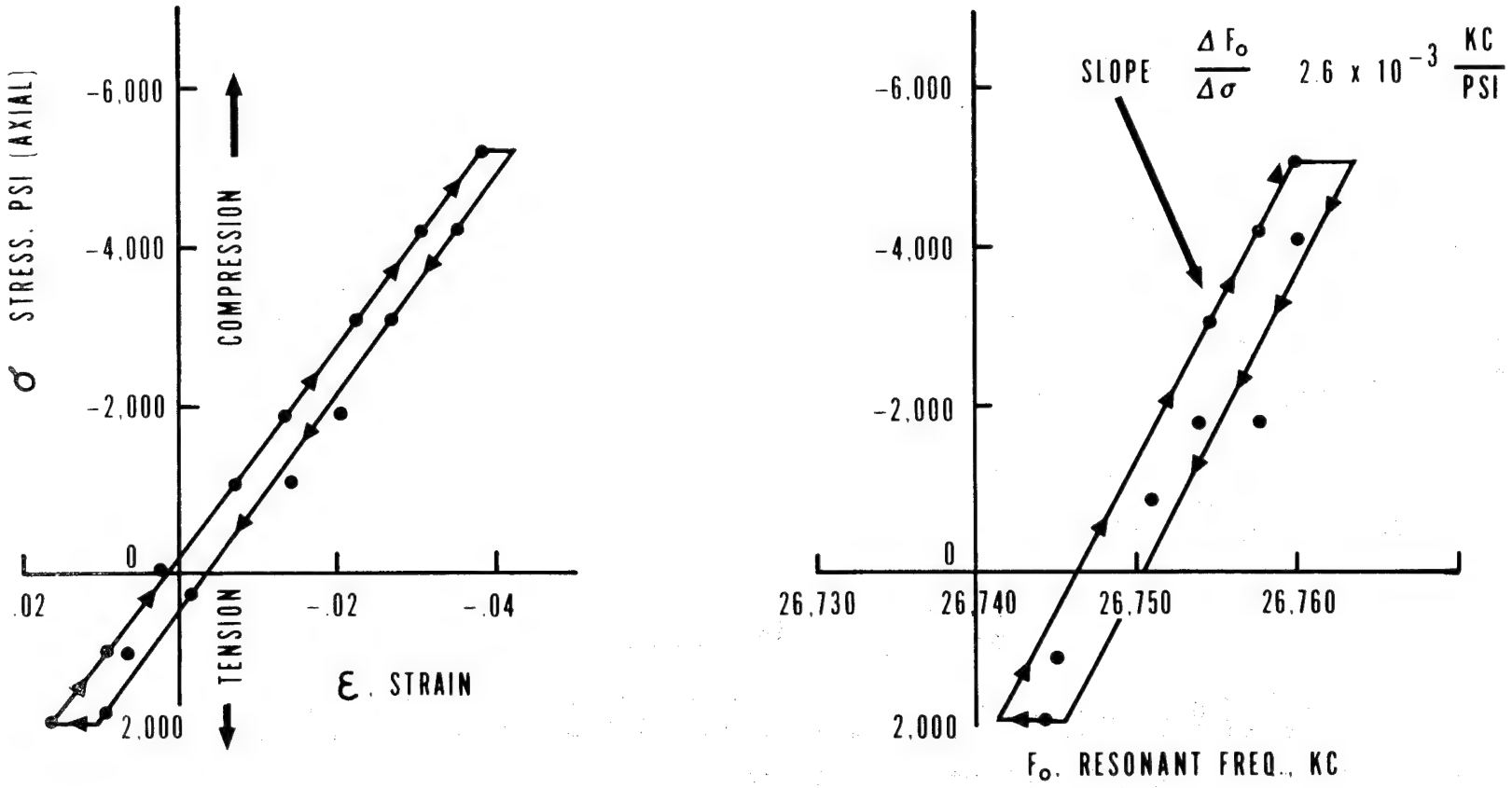

FIGURE 8

COMPARISON OF STRESS-NQR AND STRESS-STRAIN CHARACTERISTICS FOR GLASS-RESIN LAMINATE WITH NO FLAWS

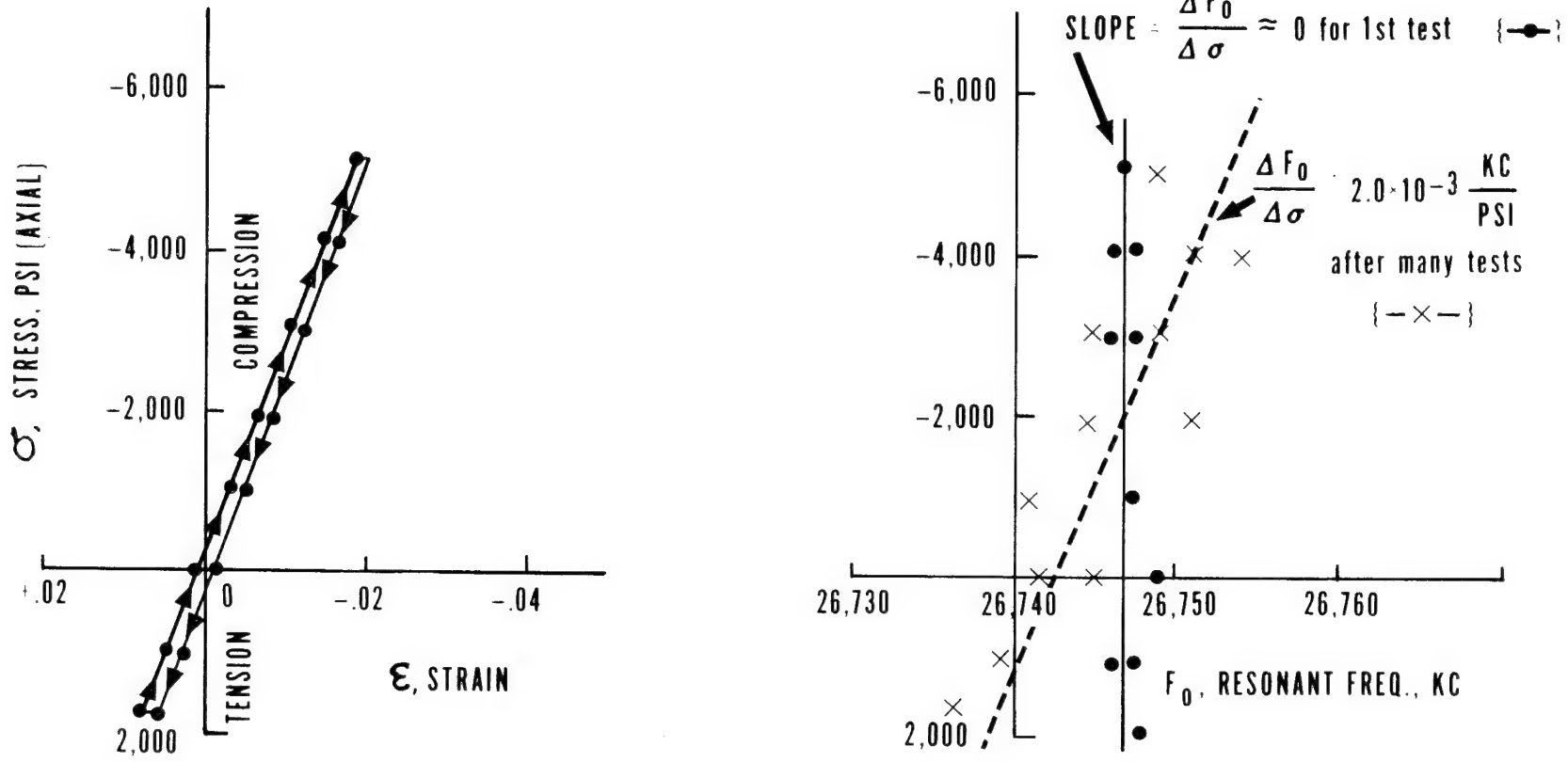

FIGURE 9

COMPARISON OF NQR CURVES WITH STRESS FOR

GLASS LAMINATE COMPOSITE WITH FLAW (SEVERED GLASS)

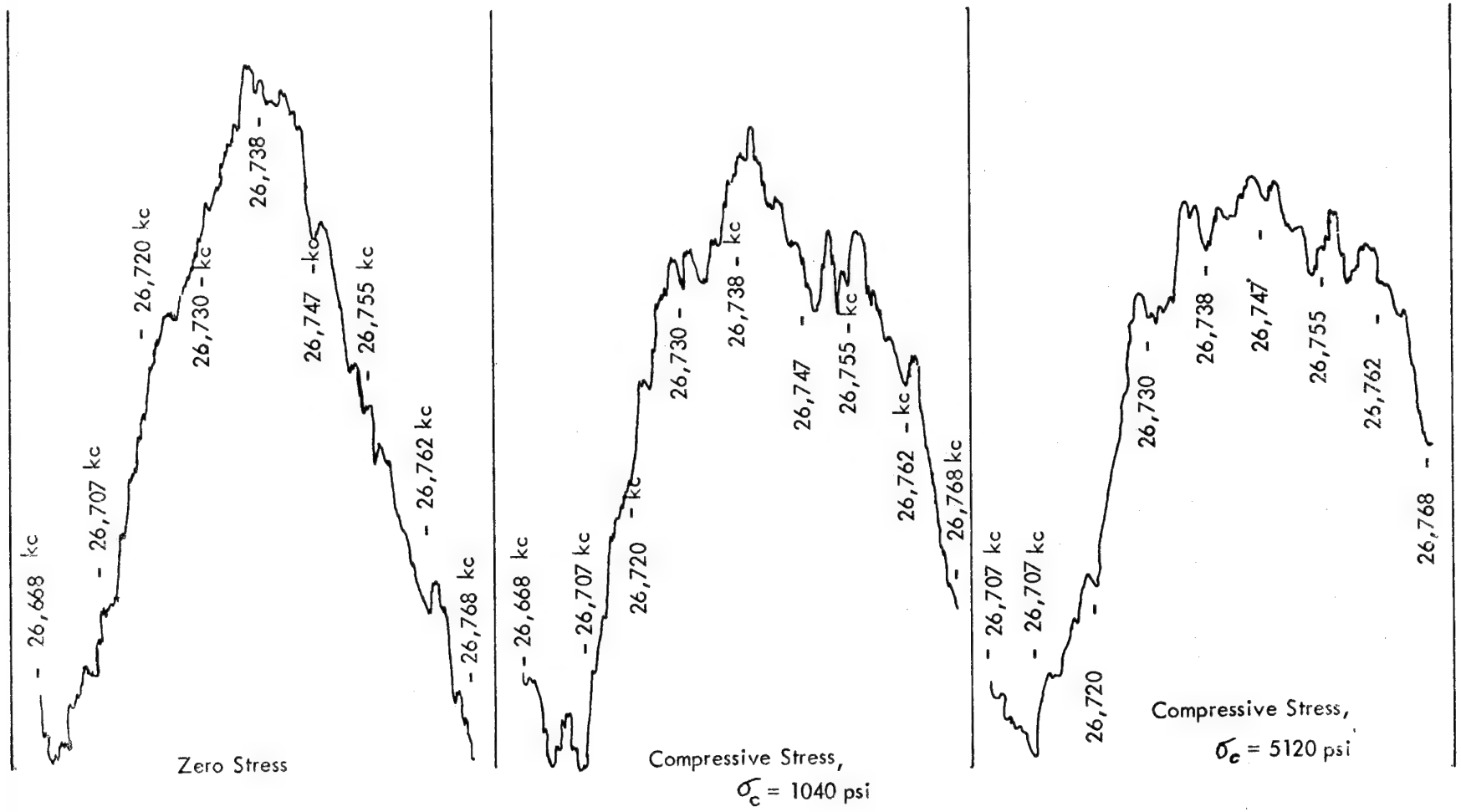

Figure 10

The instrumentation used in the initial test program was not very sensitive. Because of this poor sensitivity a minimum of thirteen (13) per cent of Cuprite (Cu_2O) was required to obtain a satisfactory signal. Repeated tests with more sensitive instrumentation[9] helped reduce the minimum required concentration of Cuprite (Cu_2O) from thirteen (13) percent to three (3) percent. The wiring diagram for a more sensitive superregenerative oscillator is shown in Figure No. (11).

B. Other NQR Tracer Materials:

This portion of the program is directed toward finding tracer materials which have sufficiently strong signals to allow doping the polymer with a maximum of one percent (1%) by weight of the compound. This stringent requirement on signal to noise for the tracer material limits the investigation to materials with resonances in the range of 150 megacycles and higher.

Antimony trioxide (Sb_2O_3), potassium iodate (KIO_3), arsenic tribromide ($AsBr_3$), iodine pentoxide (I_2O_5) and a number of other compounds were tested as potential candidate materials. Some of the compounds like arsenic tribromide and iodine pentoxide reacted violently with the resin and were dropped from further consideration. The best candidate materials appeared to be KIO_3 and Sb_2O_3. The compounds mixed well with the resin and did not react with the plastic on curing.

Most of the effort was directed toward evaluating Sb_2O_3 as a potential tracer material because it is an excellent fire-retardant and its NQR measurements are available [10,11]. Tests on KIO_3 were discontinued because of the very poor signal to noise in the NQR response.

The intensity of the nuclear quadrupole resonance in antimony trioxide in concentrations ranging from 0.3% to 100% are shown in Figure No. (12). The straight line shown is the theoretical value wherein it is assumed that all the tracer nuclei are participating in the resonance and its resonance intensity if proportional to the number of tracer nuclei present. Its stress dependence in the Epoxy 828 - Versamid 140 resin system is shown in Figure No. (13). The pressure dependence shown is opposite to that of the Cuprite (Cu_2O) tracer and it is a factor of ten smaller in relative sensitivity to stress.

Results of tests on Sb_2O_3 indicate it is not possible to use this one tracer to separate temperature and strain effects simultaneously. A second tracer material strongly sensitive to temperature and relatively insensitive to strain would have to be used making it a component of a two component tracer system.

The results also indicate the material's relatively small stress dependence and broad (100 KH3) resonance line make Sb_2O_3 less than ideal as a stess sensor.

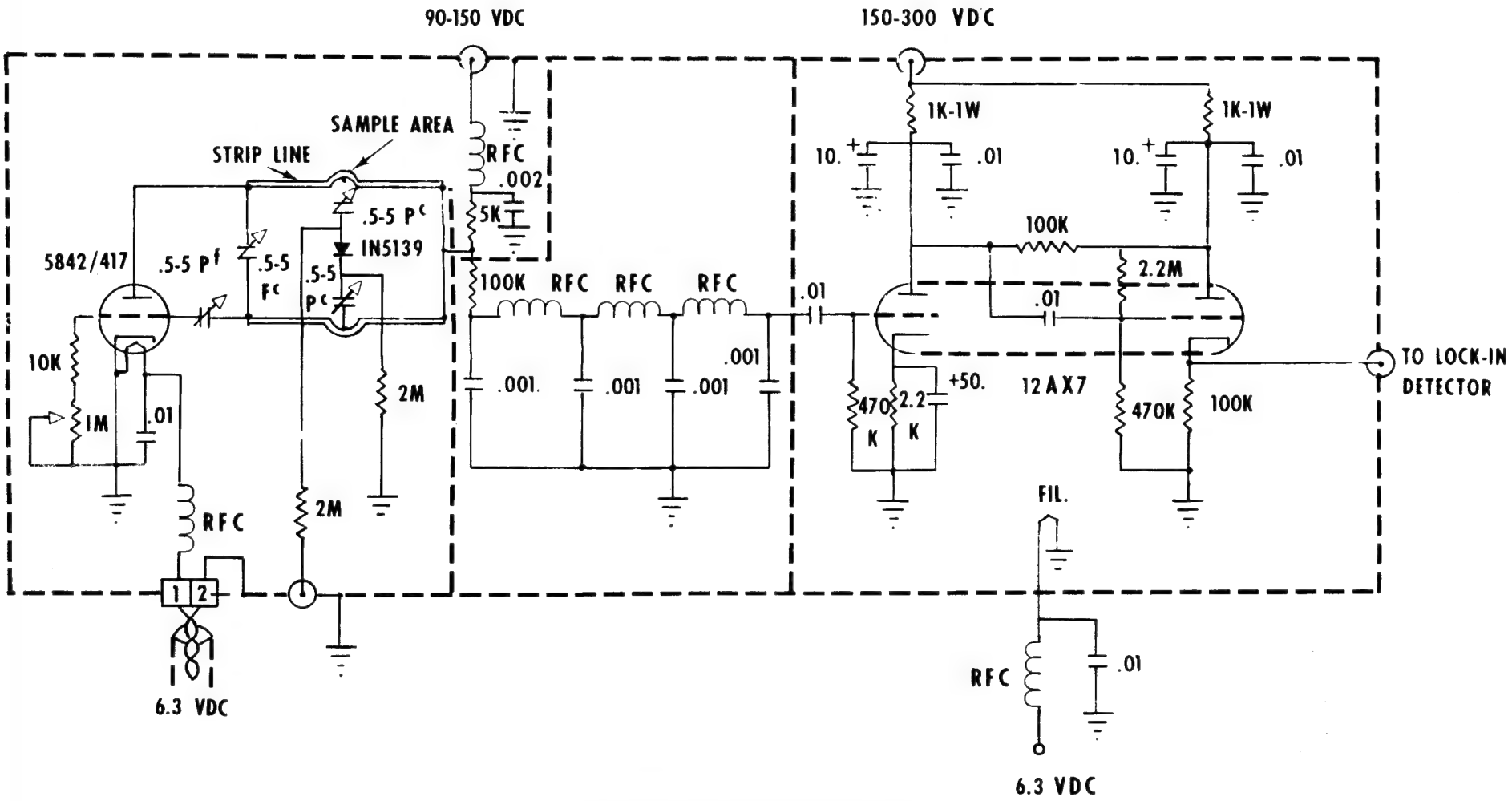

1. CAPACITORS IN MFD UNLESS MARKED
2. RESISTORS ½W UNLESS MARKED

FIGURE 11

SUPERREGENERATIVE OSCILLATOR

INTENSITY OF RESONANCE RESPONSE
VS. PERCENT Sb_2O_3 BY WEIGHT

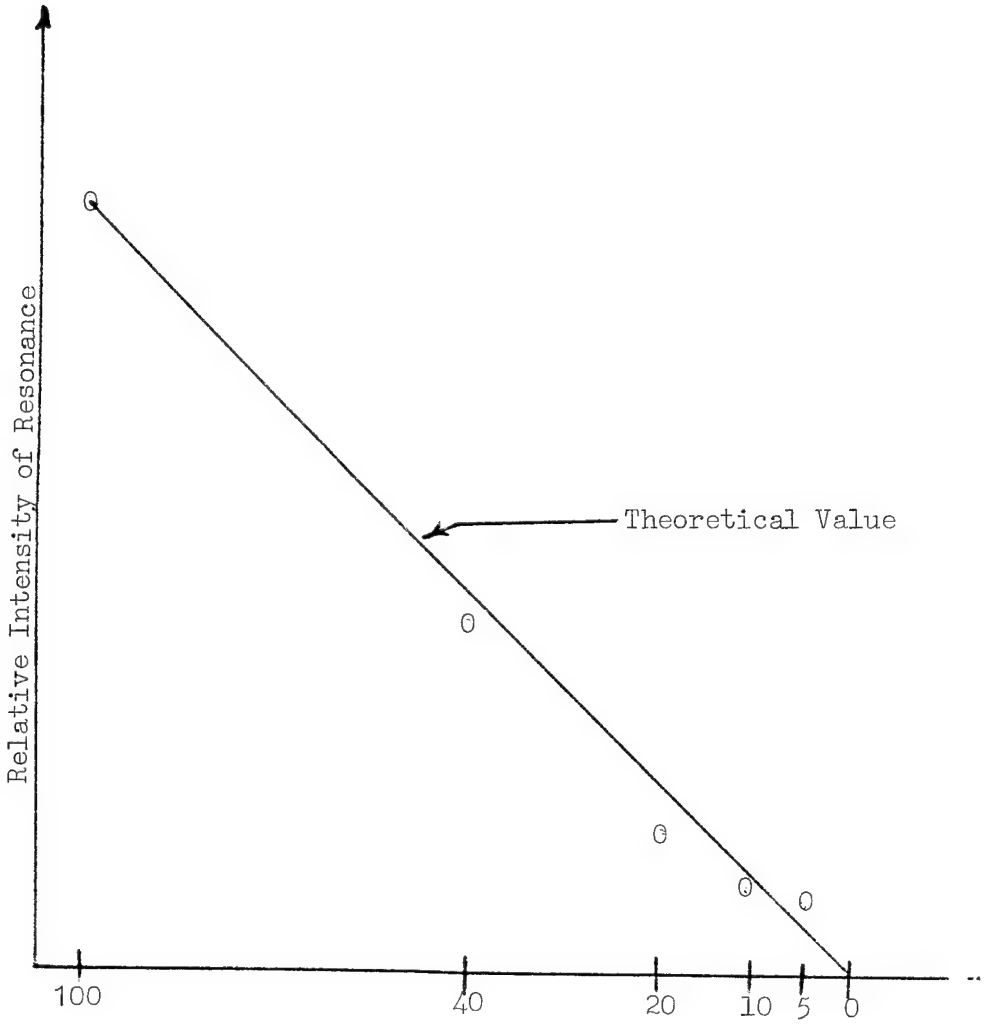

FIGURE 12

STRESS DEPENDENCE OF Sb_2O_3 IN 70% EPON 828 WITH 30% VERSAMID RESIN SYSTEM

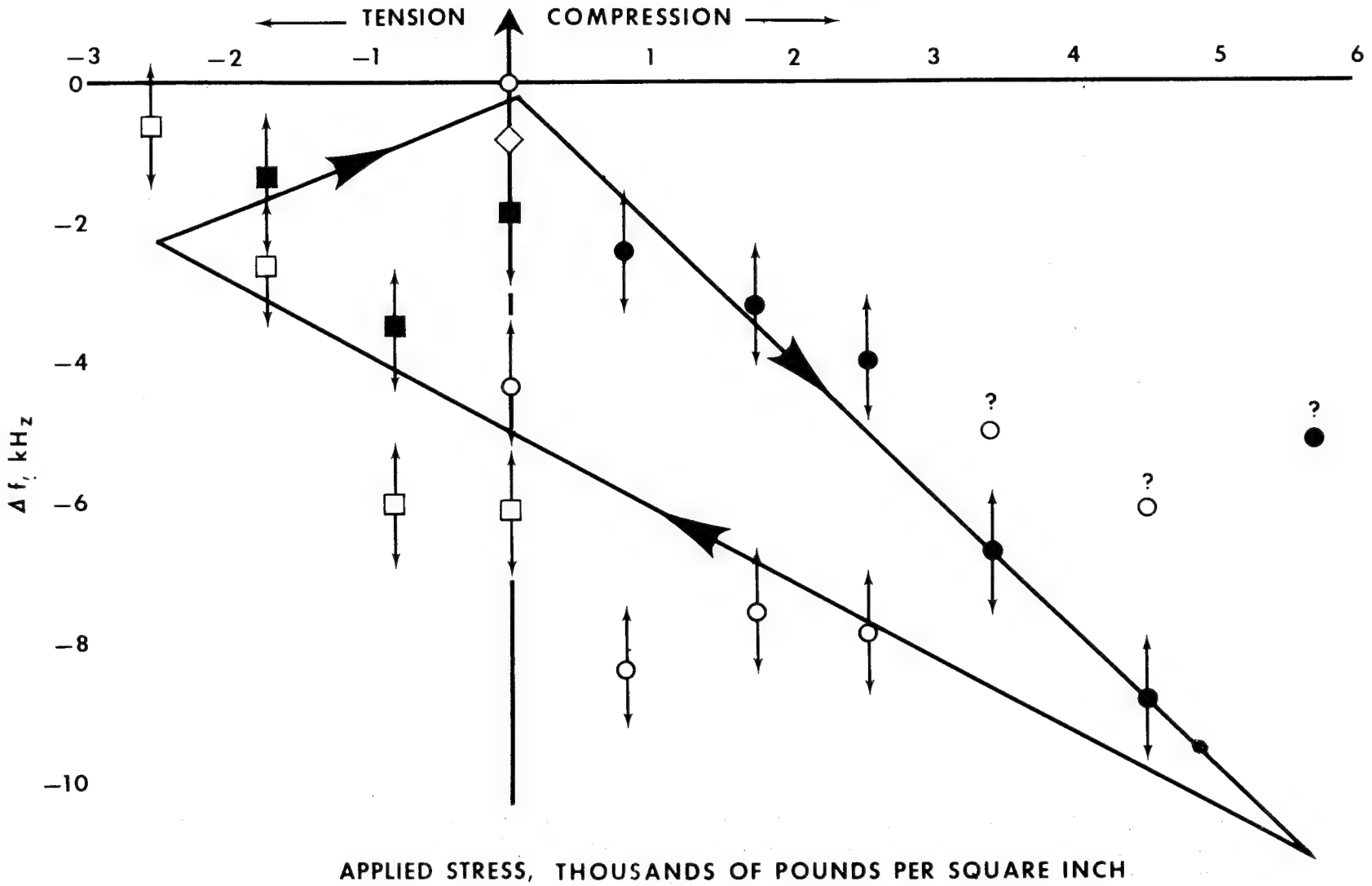

FIGURE 13

CORRELATION OF NQR AMPLITUDE WITH TRACER TO DETERMINE QUANTITY AND UNIFORMITY OF POLYMER

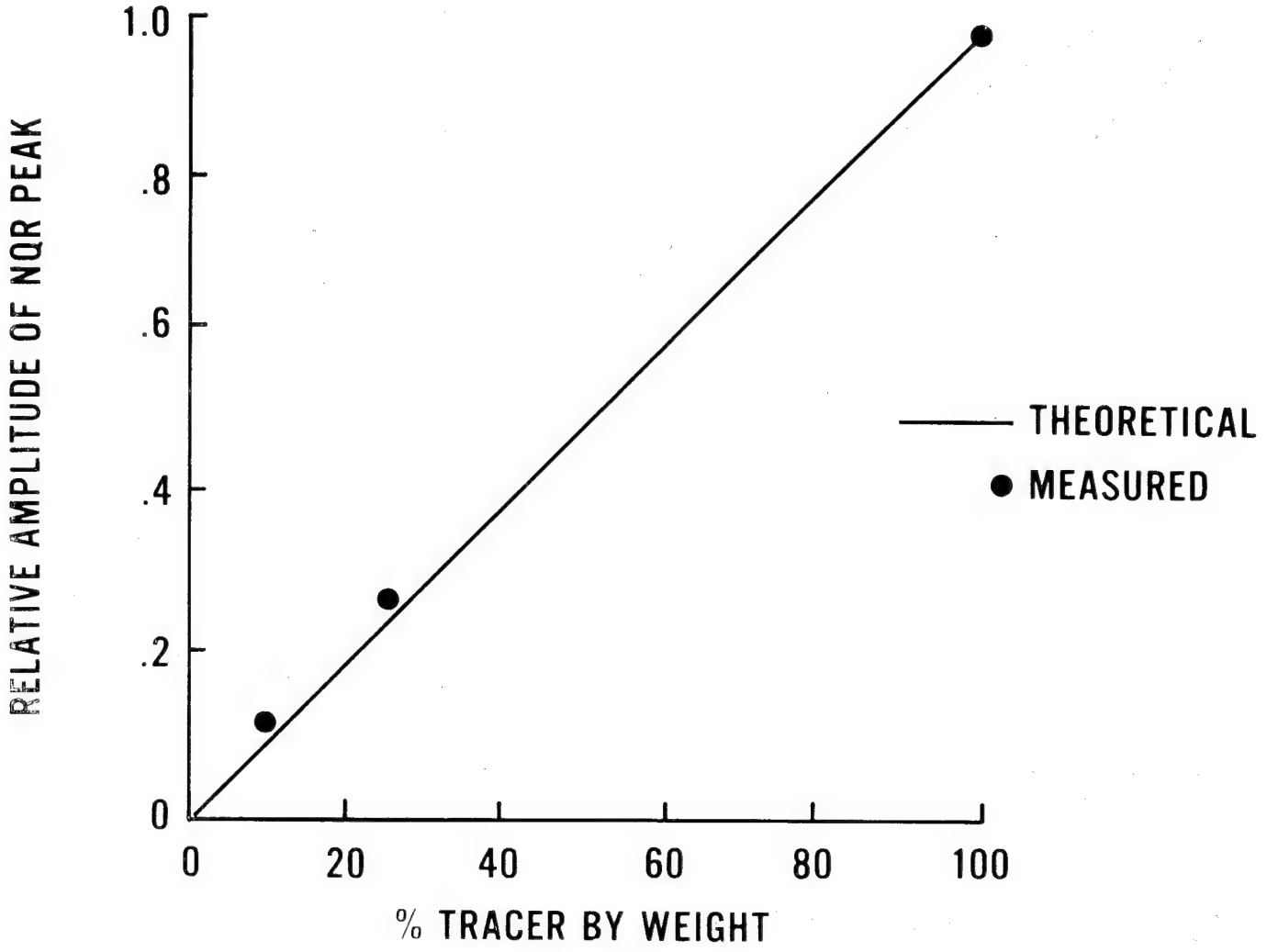

FIGURE 14

CONCLUSIONS

Results of completed exploratory feasibility tests indicate the NQR tracer technique is capable of detecting internal stresses and various defects in a reinforced plastic structure, the weaknesses which are produced in the composite during fabrication and curing operations, or are the result of externally applied forces. The results confirm the published conclusions of Epstein and Weinberg[12].

The data further indicates that of all materials tested to date, Cuprite (Cu_2O) with its strong NQR response is the most promising candidate tracer material. Sensitive instrumentation has helped reduce the minimum quantity of Cuprite (Cu_2O) required in the matrix (from thirteen percent of approximately three percent) to obtain an acceptable NQR signal. More sensitive instrumentation should further reduce the amount.

The three percent by weight of Cuprite (Cu_2O) in the matrix should not impair seriously the mechanical and electrical properties of most nonmetallic plastic structures. For structures which cannot tolerate this small quantity of Cuprite (Cu_2O) tracer, other more inert fillers with strong NQR responses when used in concentrations of one percent, or less by weight in the matrix must be found.

A more intensive investigation of the NQR tracer technique as a potential nondestructive test procedure for evaluating the properties of reinforced plastics structures is warranted.

REFERENCES

1. Nuclear Quadrupole Spectra in Solids - M. H. Cohen, Physics Review 96. 1278 (1964)

2. Table of Eigenvalues for Pure Quadrupole Spectra - R. Livingston and H. Zeldes - Oak Ridge - National Laboratory Department ONRL-1913 (1955)

3. I. A. Safin, Soviet Physics - Solid State 3, 2098 (1962)

4. T. Kushida, G. B. Benedek and N. Bloembergen Physics Review 104 1364 (1956)

5. O. T. Molyuchkov, B. N. Finkel'shtein and Ch'ih l - yang, Soviet Physics, Solid State 3, 2565 (1960)

6. H. S. Gutowsky, R. A. Bernheim, and T. Tarkow - J. Polymer Science 44, 143 (1960)

7. H. DeWijn and J. L. DeWitt - Physics Review 150, 200 (1966)

8. J. R. Whitehead - Superregenerative Receivers, Cambridge University Press (1950)

9. P. M. Bridenbaugh and G. E. Peterson - Review of Scientific Instruments

10. R. G. Barnes and P. J. Bray - Physical Review - Page 1177

11. S. Ogawa - Journal of the Physical Society of Japan - Page 1105 (1957)

12. G. Epstein and I. Weinberg - Proceedings - 22nd Annual Technical Conference S. P. I. Reinforced Plastics Division (1967)

ACKNOWLEDGEMENT

The exploratory work described herein is under the direction of Dr. Bernard Mazelsky, President, A. R. A. Inc. with Dr. R. R. Hewitt, University of California, Riverside, acting as technical consultant.

PAPER No. 5

A PROPOSAL FOR UNIFORM NDT PERSONNEL QUALIFICATION AND CERTIFICATION PROCEDURES

Harold S. Kean
Philadelphia Naval Shipyard

ABSTRACT

The weakest, most confused and bewildering aspect of nondestructive testing in this country, as elsewhere, is a uniform policy and procedure for qualification and certification of personnel performing nondestructive testing. The genesis of this churning indecisiveness has an economic base; that base is the often necessary search for competitive advantage.

Regardless of its origin, it has become apparent that it is absolutely imperative that industry and Government work together to provide clear, uniform, workable procedures in this area.

The mechanism which could operate to produce a uniform code of practice would require the following steps:

1. A uniform standard for performance of NDT for all military (DOD) activities and their application to all contracts and procurement actions.

2. A uniform code for qualification and certification of personnel performing nondestructive testing to the requirements of the above standard.

The results achieved by the combination actions proposed would be of benefit to DOD, other branches of Government and to industry by placing all activities on an equal competitive footing. It would also benefit NDT personnel to the extent that their security would be increased.

In the final analysis it is DOD which has the power and the ability to generate and enforce these requirements.

Personnel Qualification

The purpose of this paper is primarily to bring to this Conference, broadly based as it is, a point of view, an opinion if you will. It is firmly believed that this point of view, concerning personnel qualification, is important to the extent that it relates to every Government employee who performs, supervises, directs or calls out nondestructive testing.

This point of view is that there should be a uniform requirement for NDT personnel qualification. This requirement should be applied to private industry and Government. It should require that personnel performing NDT be capable of qualification and certification by an impartial and objective nongovernmental body with clearly recognized authority.

This is quite an order! It's a big lump for any activity to swallow, even one as big as the United States Government.

But the alternatives are easily apparent; they are all around us. These alternatives are the confusion, indecisiveness and personal insecurity which exist today. And, in case you didn't already know it, the situation abroad is no different than it is here.

I have said previously that a uniform requirement for NDT personnel qualification is necessary and desirable. To that I think it is essential to add that the procedure for determining qualification should also be uniform. For comparison, we can examine qualification procedures such as those which determine the awarding of other certification documents: high school diplomas, nursing school diplomas and degrees as doctors of medicine.

First: The high school diploma is awarded after successful completion of the four-year curriculum at the high school level of difficulty. Entrance to high school has, as a prerequisite, completion of eight years in the primary grades.

To obtain a diploma in the field of nursing, a general prerequisite is a high school diploma. After three years of combined formal classroom training and bedside nursing (on-the-job), a nursing diploma is awarded. If registration is sought, state boards are administered.

To obtain a license to practice medicine, the following program is generally followed:

1. High school diploma

2. Four-year college degree - premedical curriculum in the humanities, sciences and biology

3. Four years in a medical school (graduate professional school) leading to a doctorate in medicine

4. State Boards

5. One or two years of internship.

Now I'm not proposing any highly organized and difficult training periods for NDT personnel, such as those required for doctors and nurses; however, it is clear that for a recognized vocational area, including and <u>especially</u> nondestructive testing, there should be the following:

1. Prerequisites in terms of education and experience. Alternatives must be clearly stated, i.e., substitution of experience for education and vice versa.

2. Information areas to be covered in written and practical examinations for each level of qualification.

3. Grading requirements. A composite grade necessary for qualification should be established,weights assigned to each factor, i.e., education and experience, written test and practical test and method of computation given for determining composite grade.

4. Safeguards need to be established by obtaining documentation of education and experience claimed.

5. Selection of the organization which is to perform the qualification and certification functions.

All of the steps in this sequence are attainable without difficulty or delay, except the last. In fact, the entire program is contained in SNT's SNT-TC-1A. However, there is a strong difference in what is being proposed here as the qualifying and certifying authority, and what is SNT's program.

The Society for Nondestructive Testing's Technical Council document provides that qualified and certified Level III personnel, either employed by the same company as the applicant or from some other activity, shall perform qualification for Level I and II applicants.

This sharp point of difference in what has been proposed here and SNT's-TC-1A is vitally important. It is my belief that some organized group must undertake the task of training, qualification and certification, other than a Level III, privately employed by the same or other local company. The task is onerous and requires the energy, dedication and objectivity which is not likely to be found in profit-dependent private industry.

Further, I believe that either the Department of Defense, the biggest user of nondestructive testing, or the Society for Nondestructive Testing must fill the role.

In closing, let me give you an account, taken from Materials Evaluation, of a historic first cooperative effort by private industry and SNT to certify operators to Supplement A of SNT-TC-1A - Radiography.

"Recent graduation ceremonies climaxed seven months of Saturday classes for NDT students enrolled in a precedent-setting class in industrial radiography offered jointly by the Lockheed Missile and Space Company, Sunnyvale, California and SNT's Golden Gate Section.

"The course will be written into SNT annals as the first to implement requirements of the Society's new personnel qualification and certification code, as set forth in SNT-TC-1A, Supplement A, and facts available from the West Coast would seem to indicate that it wasn't an easy one.

"Out of 44 initial enrollees, 23 completed the course which met every Saturday from October 15 to May 27. Fourteen received LMSC certificates of completion, indicating grade averages of 70% or better for the course, and twelve of this group qualified for certification under SNT-TC-1A, Supplement A, including two to Level III, two to Level II and eight to Level I."

PAPER No. 6

AN INVESTIGATION OF THE FEASIBILITY OF INFRARED SCANNING TO DETECT POORLY SEATED ROTATING BANDS ON ARTILLERY PROJECTILES

Jay S. Pasman
Picatinny Arsenal

ABSTRACT

Infrared scanning has reached a state of sensitivity and hardware refinement which opens new areas to nondestructive testing. This paper describes the first in a series of feasibility experiments being conducted at Picatinny Arsenal with equipment of the most recent design. One of the first areas showing promise of useful application is the detection of improperly seated rotating bands. Six projectile bodies were examined covering a range of band seating from perfect to .025" air gap. The thermal profiles of each could be graded in a descending order of merit which matched the findings of the gaps observed after cross-sectioning. The display console contains circuitry, which preset at a temperature level of acceptance, has been used to trigger an electrical pulse indicating a reject. A more extensive series of tests will be carried out to confirm the validity of these preliminary results.

Introduction

With the advent of more sophisticated infrared instrumentation, the Quality Assurance Directorate of Picatinny Arsenal decided, in early 1966, to explore these techniques as a means of solving some of our more persistent inspection problems. For years no entirely satisfactory method has been found for detecting poorly seated rotating bands on artillery projectiles. Debate has continued over the importance of areas of poorly bonded ablative material on missile warheads, mainly because there has been no accurate, inexpensive method of nondestructive testing. The use of microminiature electronic circuits in missiles, with the inherent difficulty of applying conventional inspection methods also indicates a more pressing future need for expertise in the infrared field.

Because the above items are only representative of the many potential areas of applications, it was desirable to select the most versatile equipment available. Interest centered on camera-type units capable of sensing radiation over a field of view wide enough for conventionally sized components.

Description of Test Equipment

The system selected for the initial phase of our testing was a Model 710B Infrared Scanner manufactured by the Sierra Division of Philco-Ford. It consists of the two units shown in Figure 1: a camera unit, on the right, which senses the radiation by means of a cooled indium antimonide photovoltaic detector, and a display console containing a cathode ray tube (CRT) with an option of two modes of presentation. The television-type option scans the full subject each 5 seconds and displays an image whose brightness is proportional to the temperature pattern observed. The vertical scanning may be stopped at a point of interest to obtain an oscilloscope-type trace with a horizontal sweep across the subject each 33 milliseconds. The vertical displacement of the trace indicates the level of temperature as the focal point scans across the object. A dual CRT in the console permits viewing the image on a long-persistence screen while the image is being photographed, enabling a continuous observation of transient thermal patterns. A quantizer in the display console may be used with the video presentation to superimpose isothermal contour lines on the image; this unit will be discussed in more detail later.

The system covers a range from room temperature to 1200°C with a temperature resolution of approximately 1°F at 86°F. The optical system may be focused from 3 inches to infinity with a resolution of .029 inches at 3-1/2 inches.

Description of Test Material

The projectile bodies used in these experiments are steel, nominally 4" in diameter and 4" long. The cross-section view in Figure 2 shows the annular groove, 0.10" deep x 0.87" wide, into which the rotating band is pressed. The band is a pre-formed ring of sintered iron of a specified density. When the band is coined into position with the proper force it will be seated with metal-to-metal contact, as in Figure 2a, rather than the improperly seated band with the air gap, shown in Figure 2b. However, the force used must be limited so that the finished band does not exceed the density limitation. The various factors involved preclude a simple force measurement to assure adequate seating.

The present inspection method employed is cross-sectioning samples from each lot. In addition to the cost of preparing the specimen and the destruction of production samples, this method is not entirely satisfactory in that defective bands can escape detection. Ultrasonic inspection cannot be used because the complex contour on the inner surface of the body scatters the reflected signal. X-rays have been made, but the indication is not as positive as is desirable, nor does it lend itself to 100% inspection on a large production basis for this type item, since it is a slow costly process.

Test Method

The initial effort to determine basic feasibility was made on the laboratory bench set-up illustrated in Figure 3. One of the bodies is shown held in a horizontal position on a simple chem lab stand. Clamped to the inner diameter of the body, with an extended-throat C-clamp, is a 125 watt surface heater. A variable transformer was used to control the heat input, with a value of 62 watts proving to be most desirable. A 24-cfm centrifugal blower directed across the outer surface was used to increase the heat flow through the body. Thus, where the thermal conductivity was reduced by an air gap behind the rotating band a lower surface temperature would result. Temperature differences in the order of 1° to 5°F were determined to exist. Iron-constant thermocouples peened into the surface were used during one set of experiments to confirm the readings.

Six projectile bodies, or segments therefrom, with various degrees of band seating were made available. They could be graded from macrophotographs of their cross-section to range from perfect seating to a maximum of 0.025" separation. Experience has demonstrated that the gaps tend to be concentric with the body.

In order to remove the decision of acceptability from relative values to absolute levels, an improved method of determining and presenting the temperature levels has been developed. Temperature calibration of the IR Scanner is performed with a special 1"x15" long hexagonal bar designed by the supplier of the equipment. It contains a resistance heater, controlled by a variable transformer, on one end and a fan-cooled heat sink at the other end. In between, the highly polished bar contains 11 equally spaced black body cavities with a thermocouple embedded at the apex of each. A single horizontal scan across the bar from the hot end to the cold end produces 11 pips whose vertical displacement is proportional to the temperature indicated by each thermocouple. The five ranges of the scanner used in these tests (omitting the 5 higher ranges available with optical attenuation) were calibrated by repeating the process with a different heater setting for each attenuation range. The innovation developed for these experiments consisted of an ambient temperature plate placed alongside of the scanned object in all work, both with calibration bar and with the projectile bodies. The plate consists of 2 reflective sheets insulated and spaced apart to minimize radiation, with a black spray of known emissivity on the front face. By this means a family of curves with a common base temperature can be plotted, as shown in Figure 6. Similarly, the ambient temperature level adjacent to the projectile, clearly depicted in Figure 7, provides a known base-line from which all displacements can be measured accurately. This method compensates for the changing slope of the calibration curve. Changes in ambient temperature and emissivity of projectiles can be easily corrected for in using the curve.

More experimentation is now needed to identify the exact emissivities encountered in tested objects. During the early experiments described above, relative displacements were used as an indication, assuming that painted bodies and the bare metal bands had a constant ratio from one body to the next. Removing the paint from the bodies did not affect the relative grading of the 6 sample projectiles. However, more recent tests have shown a sensitivity to the variation in surface finishes of the bands as permitted by the drawing tolerance, as well as to any oxidation occurring on this surface. Until these factors are fully clarified, experimentation is continuing on the assumption that manufactured lots will be similar enough to permit comparisons with the lot. An interim method is being investigated, wherein the heater input and the scanner gain is adjusted to compensate for minor variations encountered.

A development of major potential value has been demonstrated with the Quantizer in the display console. In the normal display mode, the scanner displays a TV-type image with the variation

in brightness proportional to the temperatures across the target. The operator judges the range of temperatures by observing the degree of shading or, more accurately, by switching to the X-Y plot oscilloscope trace described earlier. The Quantizer is designed so that the incoming video signal could be modified to superimpose isothermal contour lines directly on the thermal image, or modified so that the image appears in a series of plateau levels or bands of uniform brightness. This is accomplished by the use of 6 independent circuits each triggered at an adjustable threshold level as the input signal increases in amplitude. By using the latter option in the X-Y plot display mode, the oscilloscope trace appears as a series of steps rather than a constantly varying analog signal. In this manner the signal from the projectile body was altered by two preset threshold levels. One level was at the higher body temperature level. The second was adjusted to a lower temperature commensurate with that of a rotating band which would be a reject due to an air gap. The pulsed output for a good assembly is shown on the lower trace of Figure 8. On the similar trace of Figure 9, the signal level exhibits an obvious drop as it passes over a poorly seated rotating band. Thus, we have the means of converting judgment of the inspector into a simple "go - no go" decision, with the ability to quickly document each reject with a Polaroid thermograph. It is easily seen how the output of this circuit could be used to trigger a reject action in an automated production process.

While it is not the immediate purpose of this program to develop a production set-up, it is desirable to refine handling so as to minimize variations between units. A tubular heater was coiled to fit the inner diameter of the projectile. The bodies are now mounted on a rotary table, the heater coil inserted, and a larger fan employed. The present equipment is shown in Figure 10. Thus, the body can be easily rotated to survey the entire circumference. More important, positioning variations of the heater and fan in the initial set-up have been eliminated. The thermograph in Figure 7 is representative of the improved quality of output, as compared to the other figures of this report.

Summary

In conclusion, much remains to be accomplished. Improvement in hardware techniques were a relatively simple but necessary step, in order to proceed with a much larger test sample. The

difficult problem of variations in surface finish and emissivity must be thoroughly analyzed and compensated for. There is no absolute assurance of success; certainly it will not come overnight. Implementation of any completely new method can only come as the result of an extensive, carefully controlled test program. But the results of these feasibility experiments indicate that it is a goal worth pursuing.

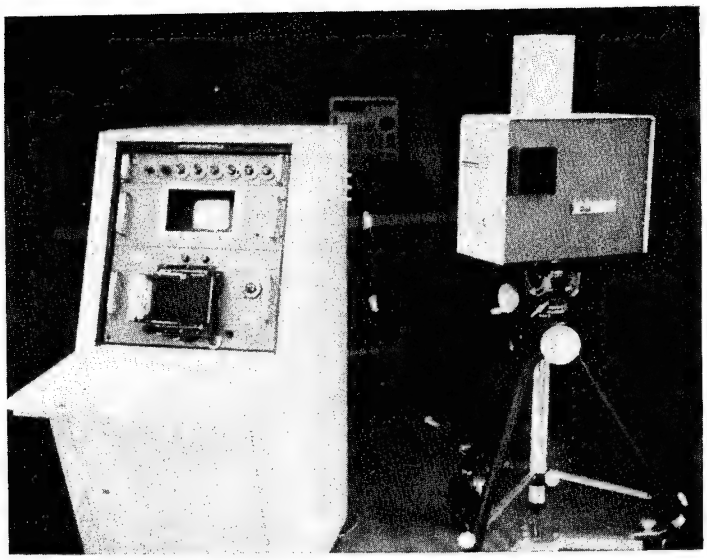

Fig. 1 - Infrared Scanner & Display Console

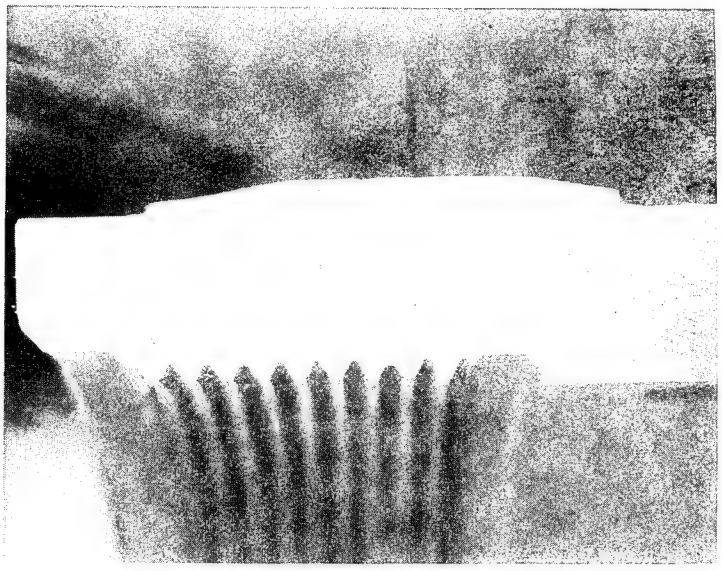

X3

a - Properly Seated Band, Ser. No. 187

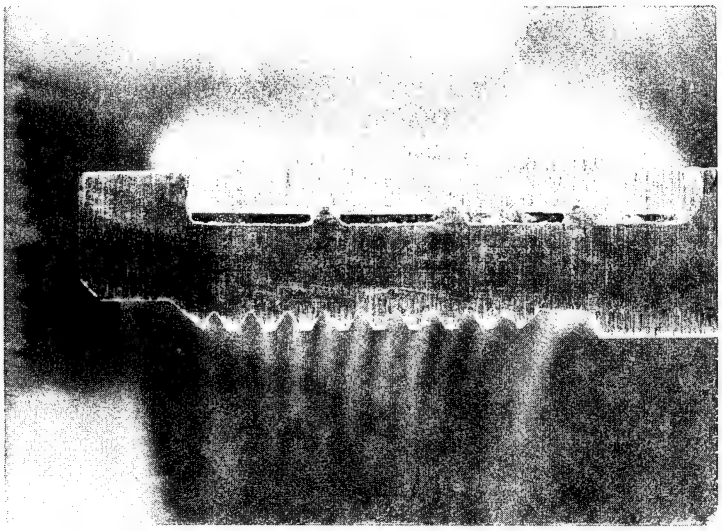

X3

b - Band with Air Gap (.025"), Ser. No. 160

Fig. 2 - Cross-sections of Projectile Body

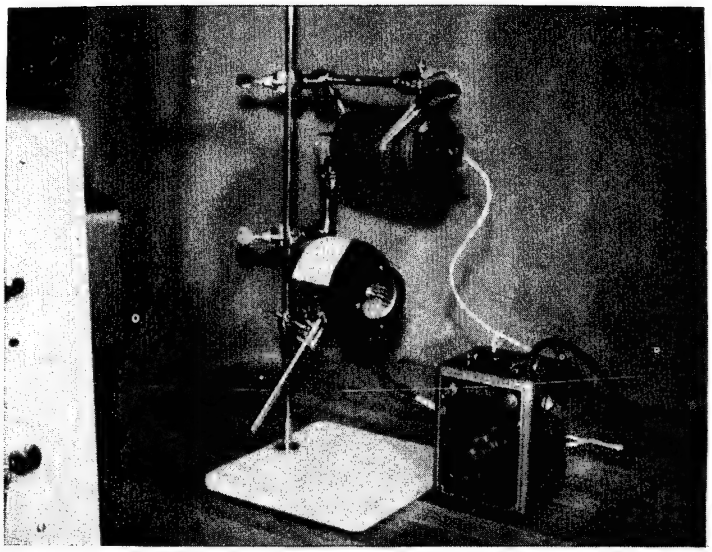

Fig. 3 - Initial Experimental Set-up

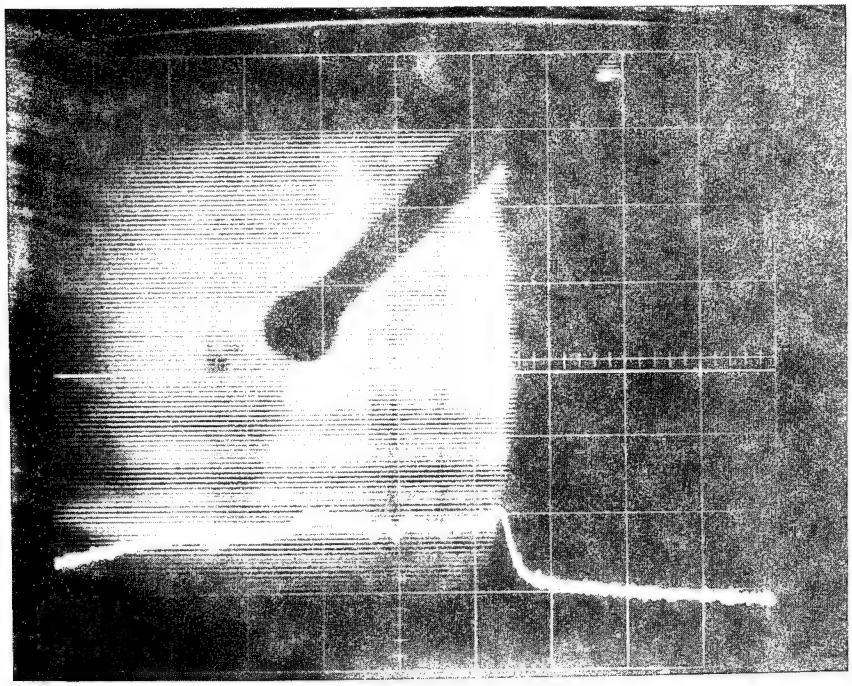

a - Good Projectile, Ser. No. 16

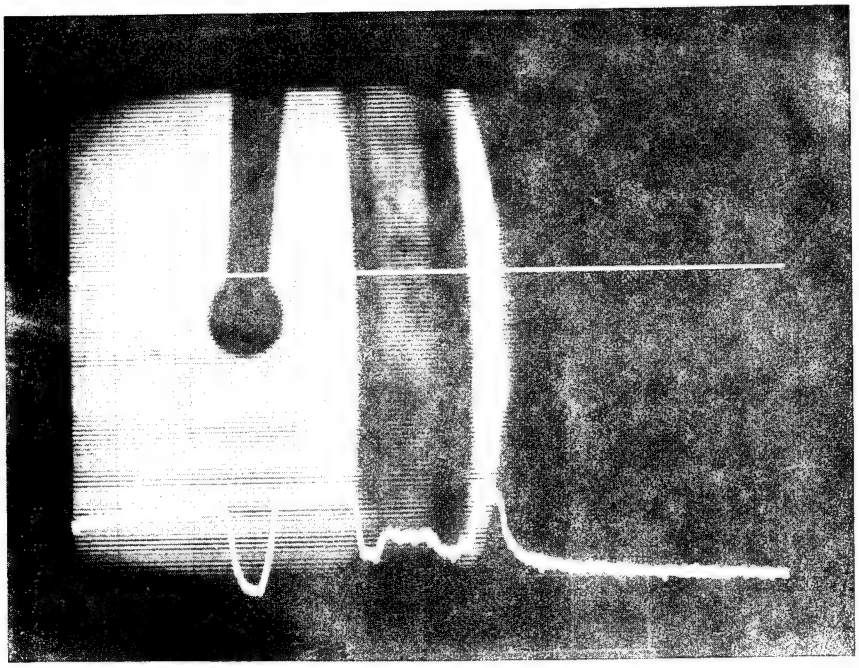

b - Poorly seated band, Ser. No. 160

Fig. 4 - Thermographs of Good (a) & Bad (b) Specimens

Projectile Body, Ser. No.	Air Gap Directly Observed	Displacement of IR Trace in descending order	Acceptability of Band
187	None	2	Good
16	Not sectioned	1	Good
185	Approx. 10% *	3	Good
15	Approx. 30% *	4	Good
135	Tapered from .005" to .020"	5	Reject
160	0.025"	6	Reject

* Percentage of mating surface not in direct contact.

Fig. 5 - Table of Findings

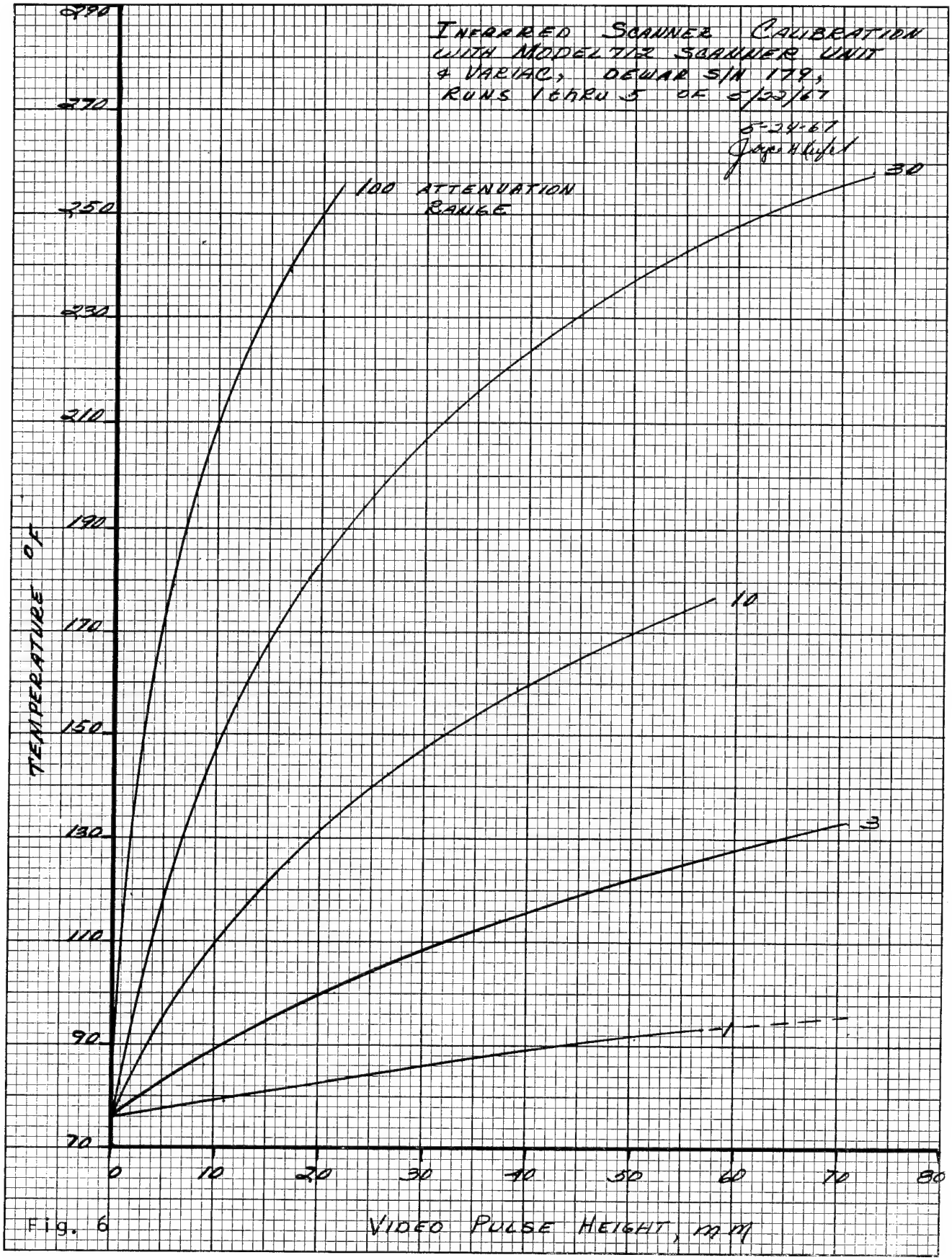
INFRARED SCANNER CALIBRATION
WITH MODEL 7112 SCANNER UNIT
& VARIAC, DEWAR S/N 179,
RUNS 1 THRU 5 OF 5/22/67
5-24-67
Jaye Hight
100 ATTENUATION RANGE
30
10
3
1
TEMPERATURE °F
290
270
250
230
210
190
170
150
130
110
90
70
0
10
20
30
40
50
60
70
80
VIDEO PULSE HEIGHT, MM

Fig. 6

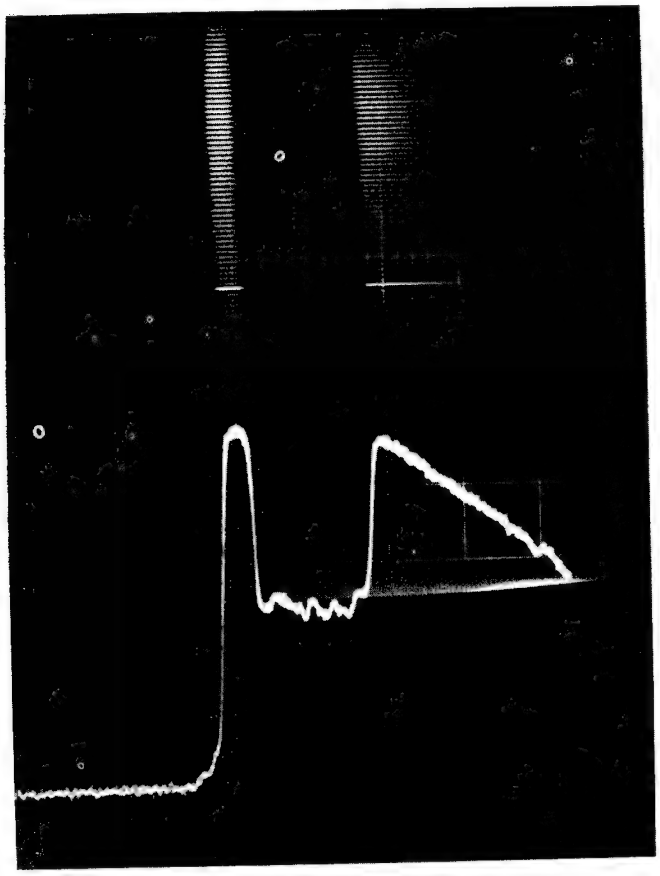

Fig. 7 - Use of Ambient Temperature Base Line

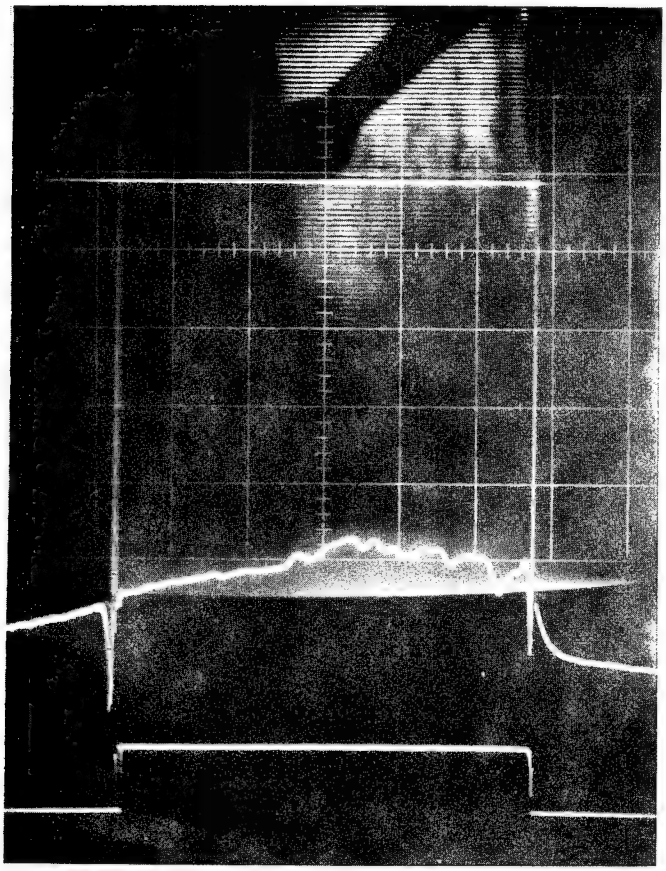

Fig. 8 - Use of Pulsed Output For Acceptable Band Seating

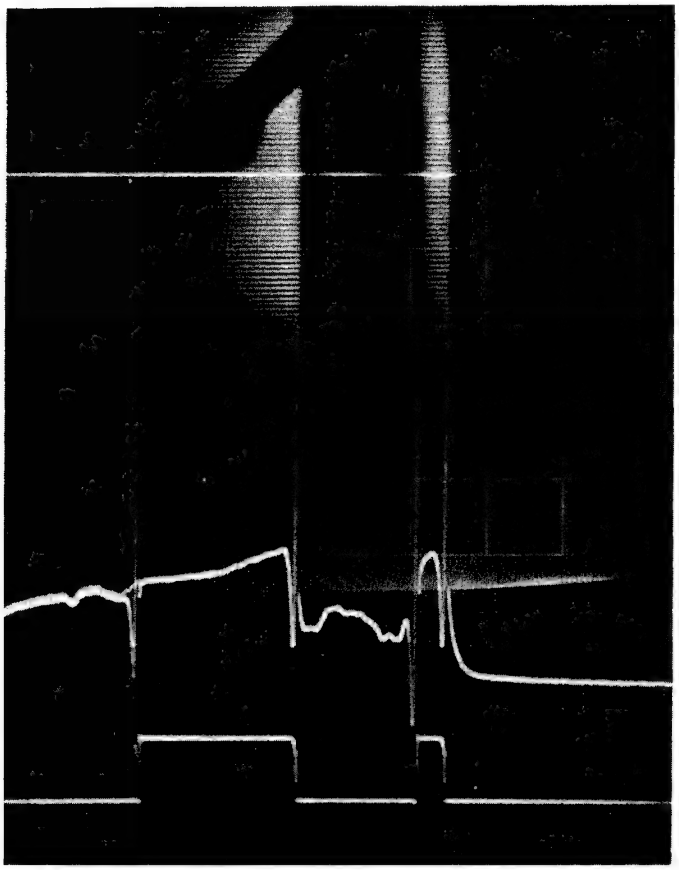

Fig. 9 - Use of Pulsed Output For Reject Band Seating

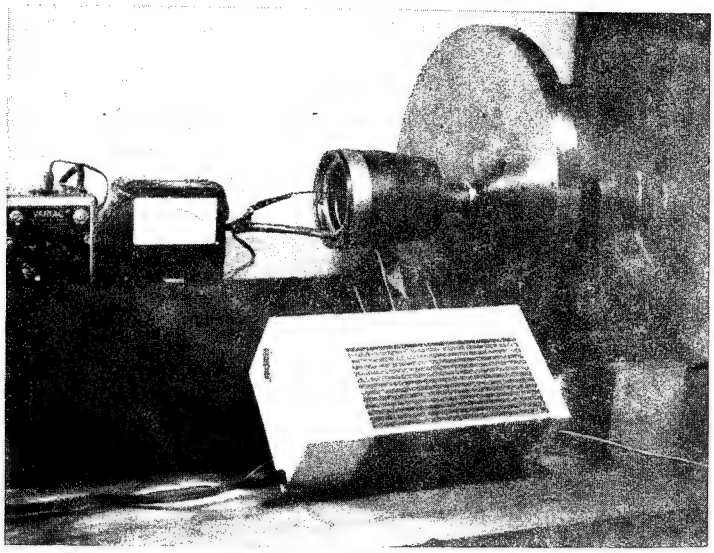

Fig. 10 - New Test Set-up

PAPER No. 7

DETECTION OF FLAWS IN METAL HONEYCOMB STRUCTURES BY MEANS OF LIQUID CRYSTALS

Presented by

Edmund J. Wheelahan
U. S. Army Missile Command
Redstone Arsenal, Alabama

ABSTRACT

Chloesteric liquid crystals are compounds that go through a transition phase where they possess the flow characteristics of a liquid while retaining much of the molecular order of the crystalline solid. Since liquid crystals have the ability to reflect iridescent colors, dependent upon the temperature of their environment, they may be used to project a visual color picture of minute thermal gradients associated with material discontinuities. This paper examines the nature of cholesteric liquid crystals and their utilization in nondestructive bond inspection.

The minimum defect definable in structures with skin thicknesses of 60 mils was one crushed honeycomb cell (3/16 inch), and in composition with 190 mil skins the minimum detectable defect was one square inch.

Present indications are that this technique can be adapted to full-scale honeycomb or similar composite structures for production quality assurance or for investigations of deployed components.

PAPER No. 7

DETECTION OF FLAWS IN HONEYCOMB STRUCTURES BY MEANS OF LIQUID CRYSTALS

by

Edmund J. Wheelahan, Chief, and Shelba P. Brown, Chemist
Materials Engineering and Development Branch
Structures and Mechanics Laboratory
U.S. Army Missile Command
Redstone Arsenal, Alabama

This work has been directed toward the development of liquid crystals capable of detecting defects in adhesively bonded composite structures. Visual techniques based upon color responses of liquid crystal materials to thermal stress have the advantage of being relatively simple in application. Highly instrumented techniques such as ultrasonics are frequently complex, time consuming, and difficult to use with irregularly shaped components. Our work has been specifically aimed at establishing this nondestructive technique for adhesively bonded honeycomb composite structures. See Figures 1 and 1a.

Let us first examine the nature of liquid crystal systems and their responses to temperature changes. We will then demonstrate how they can be used.

Without attempting a formal definition of the liquid crystal state, we have shown in Figure 2 the relationship between the liquid crystal state and the more familiar crystalline solid. A crystalline solid possesses definite volume and definite shape, and the structural units--the molecules themselves--are arranged in definite geometrical configurations. At a given temperature, crystalline solids may melt sharply to the liquid state which is characterized by molecular mobility in three directions and by a total lack of the rigid molecular orientation of the pre-solid state.

There are, however, some crystalline organic substances which, over clearly defined temperature ranges, appear to possess the flow characteristics of a liquid while retaining much of the molecular order of the crystalline solid. It is this mesomorphic state which has been given the name "liquid crystal." These phase changes are, of course, reversible. As the true liquid cools, it passes once again through the liquid crystal state before crystallizing into a true solid. This behavior is not so extraordinary as might be supposed, for it is estimated that one out of every 200 organic compounds is subject to liquid crystalline behavior.

Figure 3 lists the commonly designated classes of liquid crystals, with some indication of the kind of molecular order peculiar for each class. In the smectic configuration, molecules are oriented parallel to each other in well-defined planes, something like successive layers of honeycomb. In the nematic configuration, the molecules are still parallel to each other, but do not exhibit planar cohesion. The cholesteric state is similar to the nematic in that the molecules are almost parallel to each other but they are subject to a slight helical displacement. A simple model which has been suggested is that of a pile of library cards, each with one corner bent up. The cards will lie with flat surfaces parallel, but the bent-up corners will cause a slight displacement, or a slight twist, in the overall configuration. Since the derivatives of cholesterol, principally the esters, are important representatives of this configuration, the designation "cholesteric" has been given to the entire class.

Figure 4 shows the structure of cholesterol itself. This is the same steroid whose derivatives are blamed for so many of our circulatory illnesses today. Cholesterol itself does not behave as a liquid crystal.

Cholesteric esters, however, as represented in Figure 5, exhibit the behavior which lends their name to this entire class of liquid crystals. It is this cholesteric crystalline state which possesses the unique optical properties that we are now finding applicable in the field of nondestructive bond inspection.

Figure 6 shows some of the optical consequences of the molecular order of cholesteric crystals. (1) Birefringence is the property of transmitting light waves at different velocities in different directions through the material. All liquid crystals, including the nematic and smectic states, have this facility. (2) Optical rotation of polarized light is a property of the cholesteric state only. Cholesteric crystals are, in this respect, the most optically active substances known, since they rotate light through an angle several hundred times that of the usual optically active materials. (3) The third property listed here is responsible for the utilization of cholesteric crystals in visual inspection techniques. This is their ability to scatter white light, reflecting different wave lengths to give iridescent colors dependent upon the cholesteric substance, the angle of the reflected and incident beams, and the temperature. These crystals are generally colorless on each side of the liquid crystal state--colorless, that is, in the true solid and in the ultimate true liquid phase. Each cholesteric liquid crystal responds in its own way to changes in temperature. The change may be only from red to green, or from red through the entire color spectrum, or from green to blue. The important thing to remember is that each color corresponds to an exact temperature of the material being tested.

Since liquid crystals have the ability to reflect colors dependent upon the temperature of their environment, they may be used to project a visual, color picture of the transient temperature anomalies, or minute thermal gradients associated with material discontinuities. These discontinuities, which may be debonds, cracks, or other defect areas, may impede a flow of heat sufficiently to distort the normal temperature patterns of a material being tested. The defects will then show up as distinct color patterns, because of their impaired thermal transmission characteristics. This is illustrated in Figure 7.

As stated previously, these iridescent colors of liquid crystals arise from light reflectance. For most effective observation it is necessary to paint or spray liquid crystals on a dark background, prepared by use of any water-soluble black paint.

We began our development of liquid crystal systems for debond detection with evaluation of the commercial materials available to us. These cholesteric compounds and mixtures of compounds exhibit color sensitivities over ranges as small as one degree centigrade, or as large as 30 degrees. A sensitivity range of one degree is sufficient to define defects in composite materials with aluminum skin thicknesses of 20 mils or less. Our specific requirements, however, are for nondestructive inspection of composite structures with aluminum skins as thick as 60 mils. For this purpose, liquid crystal mixtures with sensitivity ranges of much less than one degree are required. Our approach was to blend available cholesteric esters to achieve increased temperature sensitivities.

Figure 8 illustrates the light reflectance of individual cholesteric esters as a function of their structure. The ranges of colors observed during a heating or cooling cycle are plotted against the number of carbon atoms in the acid group of cholesteric esters. Starting with the first position on the graph, neither the formic nor the acetic esters showed any color when heated through the liquid crystal state, whereas the propionic ester goes through the entire color spectrum. Evaluation of esters through the 18 carbon acid revealed no pattern to the color changes.

Figure 9 shows the observed color change range as a function of cholesteric ester structure. The color change amplitude of the ester of the three carbon acid is 35 degrees, and that for the 18 carbon acid is approximately three degrees. Obviously, blended mixtures are required to achieve the sensivities desired.

Figure 10 shows the color behavior of blends of cholesteryl pelargonate with cholesteryl butyrate. The compositions of the individual blends are plotted against the color change range. Pure cholesteryl pelargonate, on the left, has a color change diversity of 15 degrees. When 5 percent cholesteryl butyrate is added, the range

becomes one degree centigrade. Likewise, cholesteryl butyrate, on the right, shows a decreased range when blended with 5 percent cholesteryl pelargonate. From this chart it is evident that one material blended with a relatively small amount of a second material produces the most pronounced decrease in color change range.

Figure 11 shows the effect of blending pure materials with even smaller amounts of a second material. On the left, cholesteryl pelargonate blended with 3 percent cholesteryl butyrate gives a color change range of only 0.4 degree centigrade. Using this same approach on other materials, we have developed blends which go through the entire spectrum of colors in 0.1 degree centigrade or less.

Most blends with color change ranges of 0.5 degree centigrade or less were evaluated on aluminum honeycomb composite structures with simulated debond areas. Figure 12 shows a blend applied to panels with three types of debond simulations. In the first picture, a teflon insert was incorporated between the skin and the adhesive. This is a fair simulation of such common bonding errors as oil on the inner surface of the skin. Of synthetic debonds that we have tried, we have found the teflon insert to be the most difficult to detect. For this reason, all promising systems were first evaluated on panels with teflon inserts. Figure 13 shows the effect of crushed core which gives the most sharply defined outline of the defect. Figure 14 shows the effect of cured adhesive. This gives an equally well-defined defect outline.

The best blends work equally well on composite structures with skin thicknesses of 20, 60, or 190 mils. (Figures 15, 16, and 17.)

The minimum defect definable in structures with skin thicknesses of 60 mils is one crushed honeycomb cell, a hexagon (1/16 inch) and in composites with 190 mil skins, the minimum detectable defect is one square inch.

The following composite structures have been investigated with equal success: (1) aluminum skins with HRP honeycomb cone. (HRP is high temperature phenolic.); (2) glass cloth skins with glass fiber honeycomb core; (3) titanium skins with aluminum honeycomb core; (4) titanium skins with HRP honeycomb core; and (5) glass cloth laminates.

Figures 18 and 19 compare the effect observed when the teflon insert is included between the skin and the adhesive (Figure 18), or the adhesive and the core (Figure 19). As expected, the void nearer the surface is more clearly defined.

In the course of this work, we have found that incandescent lighting is best suited for these observations, although fluorescent lighting is adequate. We have also found that temperature control

is best achieved with simultaneous heating and cooling. For example, a test panel is heated on one side and cooled on the other.

Figures 20, 21, 22, and 23 show the color sequences observed during the heating of one crystal system through its liquid crystal state. Notice that the defect pattern remains unaltered except for color changes.

Other applications of cholesteric crystals, as shown in Figure 24, are detection of hot spots in electronic circuits, checking the special insulation required to prevent contact of dissimilar materials, and determining temperature variations over an area of human skin. This medical application is currently in use and has recently been widely publicized.

In conclusion, we believe that the cholesteric crystal systems, as presently developed, will be adequate for evaluating bond defects in aluminum honeycomb composite structures.

The next step in our program is to evaluate these systems on actual flight hardware, establishing tooling, techniques, and limitations for specific applications.

Figure 1

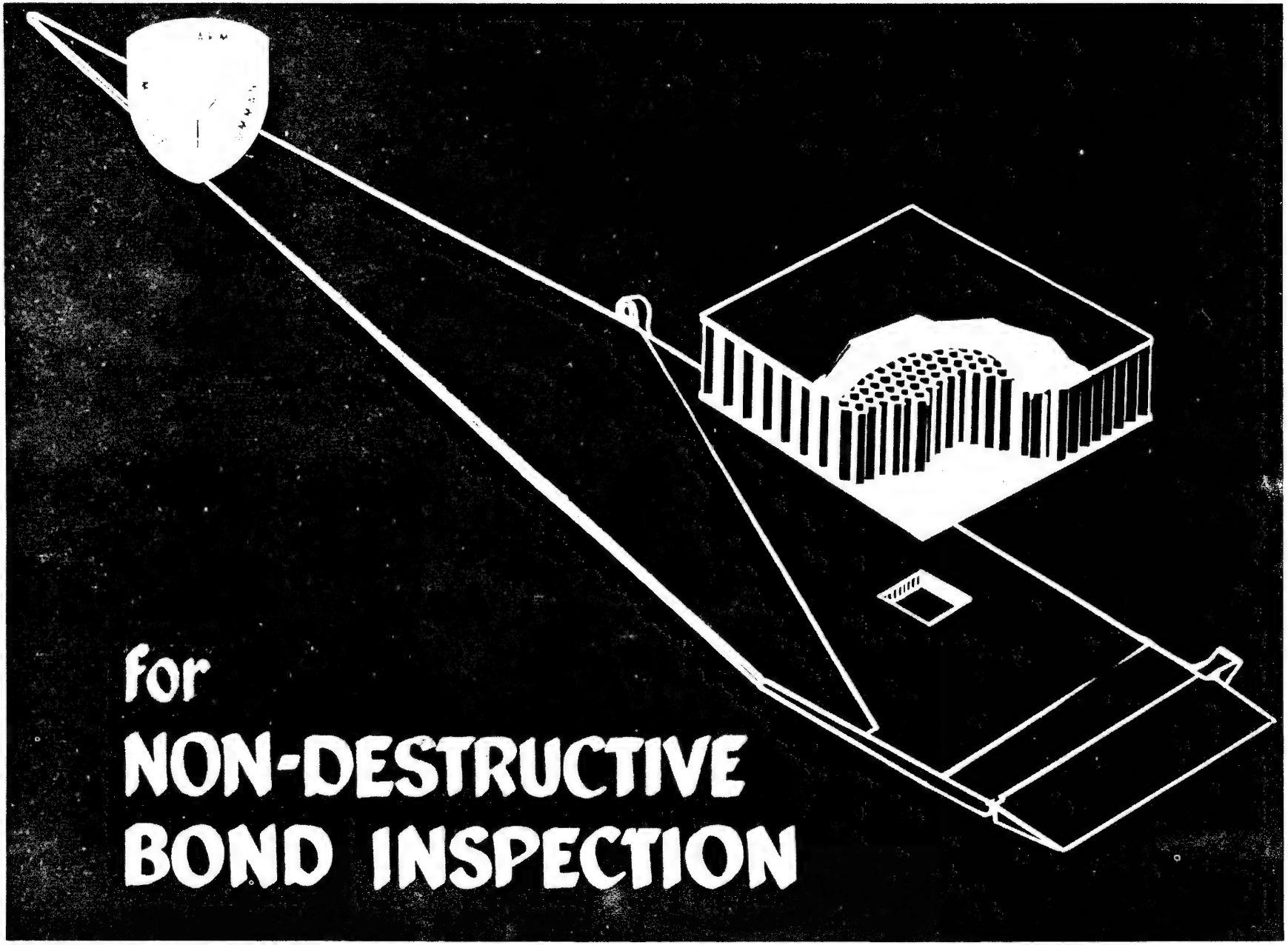

Figure 1a

TEMPERATURE DEPENDENCE OF LIQUID CRYSTAL STATE

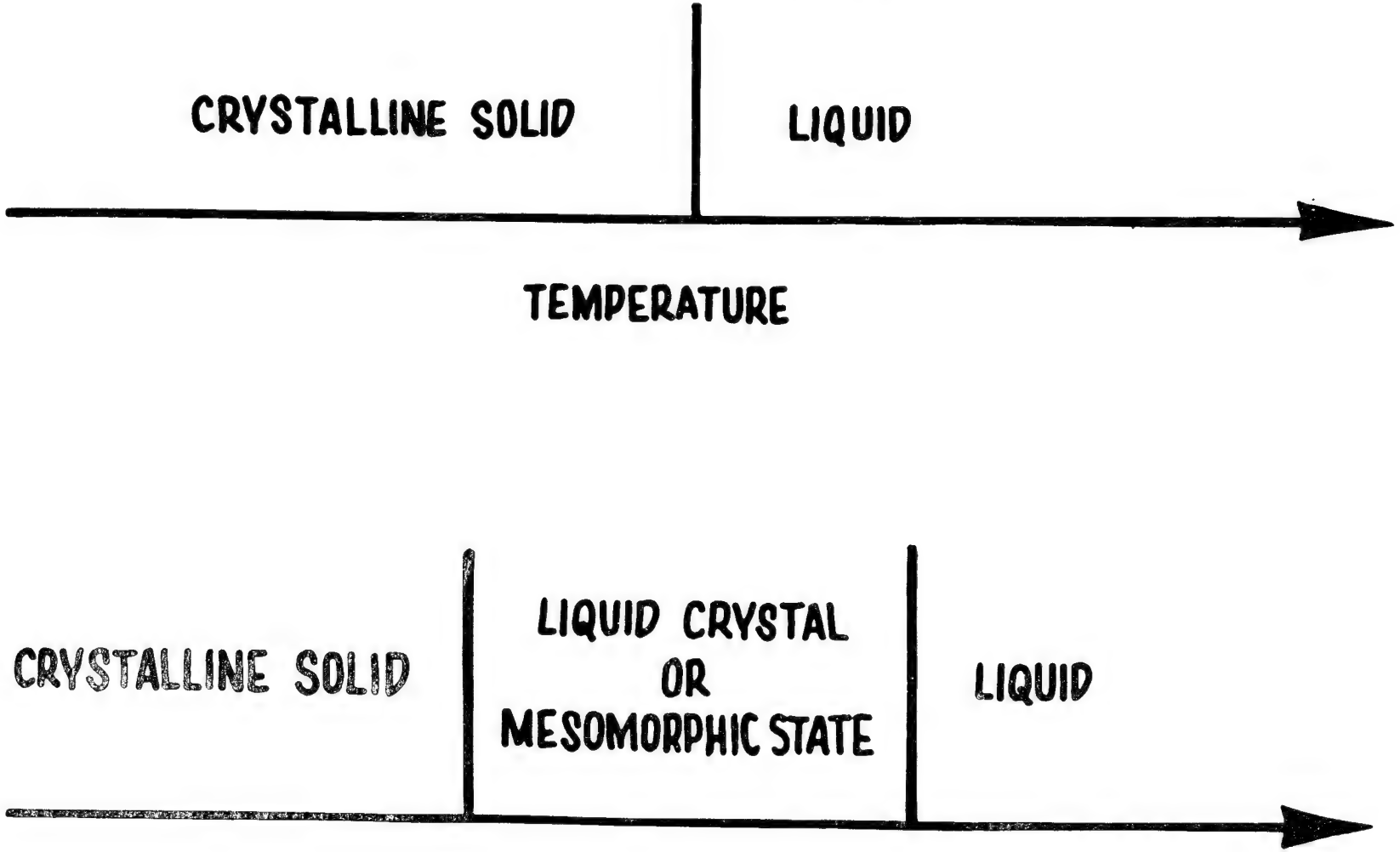

Figure 2

CLASSES OF LIQUID CRYSTALS

A. SMECTIC - PARALLEL ORIENTATION OF MOLECULES IN WELL DEFINED PLANES

B. NEMATIC - PARALLEL ORIENTATION OF MOLECULES BUT WITHOUT PLANAR COHESION

C. CHOLESTERIC - PARALLEL ORIENTATION WITH HELICAL DISPLACEMENT

Figure 3

U.S. ARMY MISSILE COMMAND

CHOLESTEROL

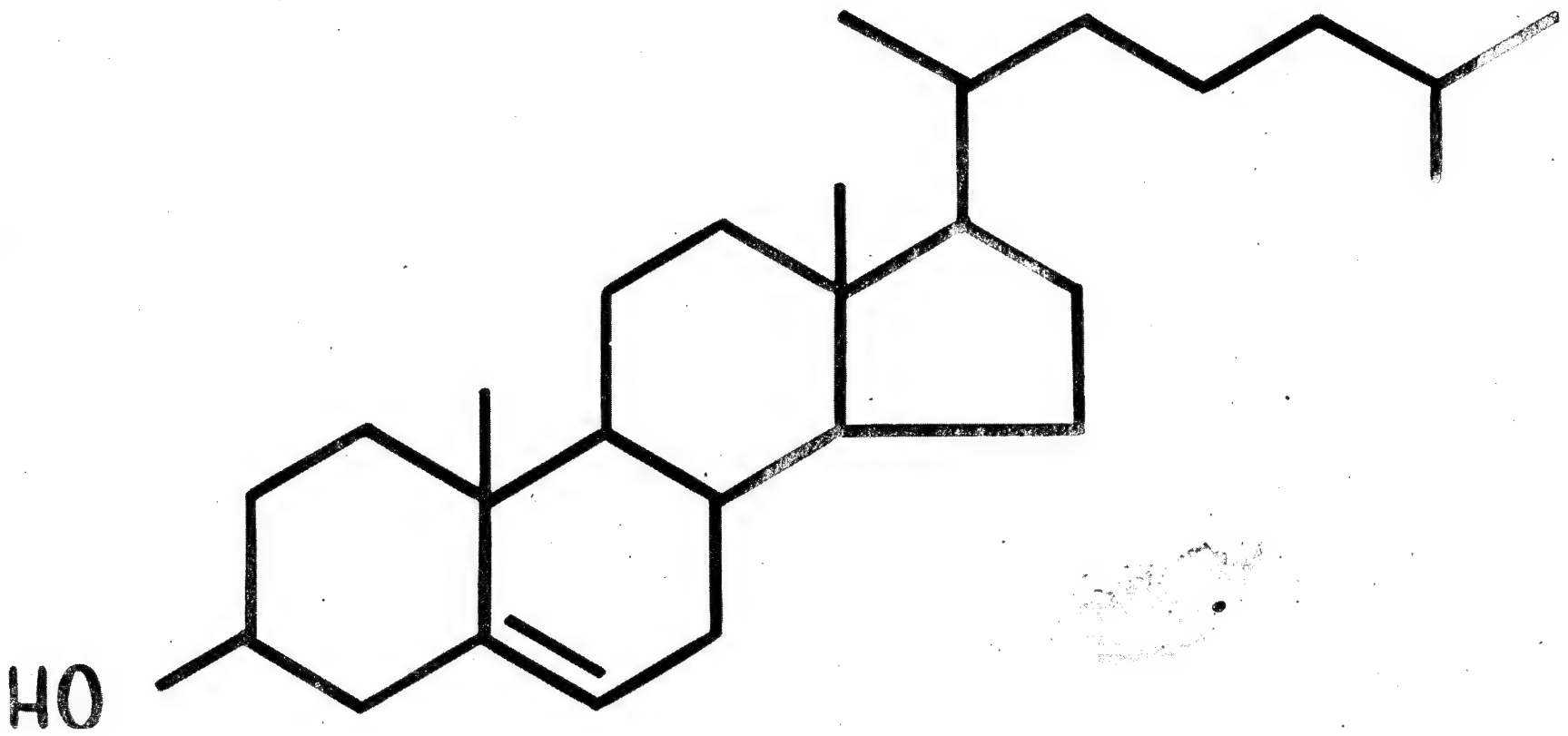

ESTER OF CHOLESTEROL

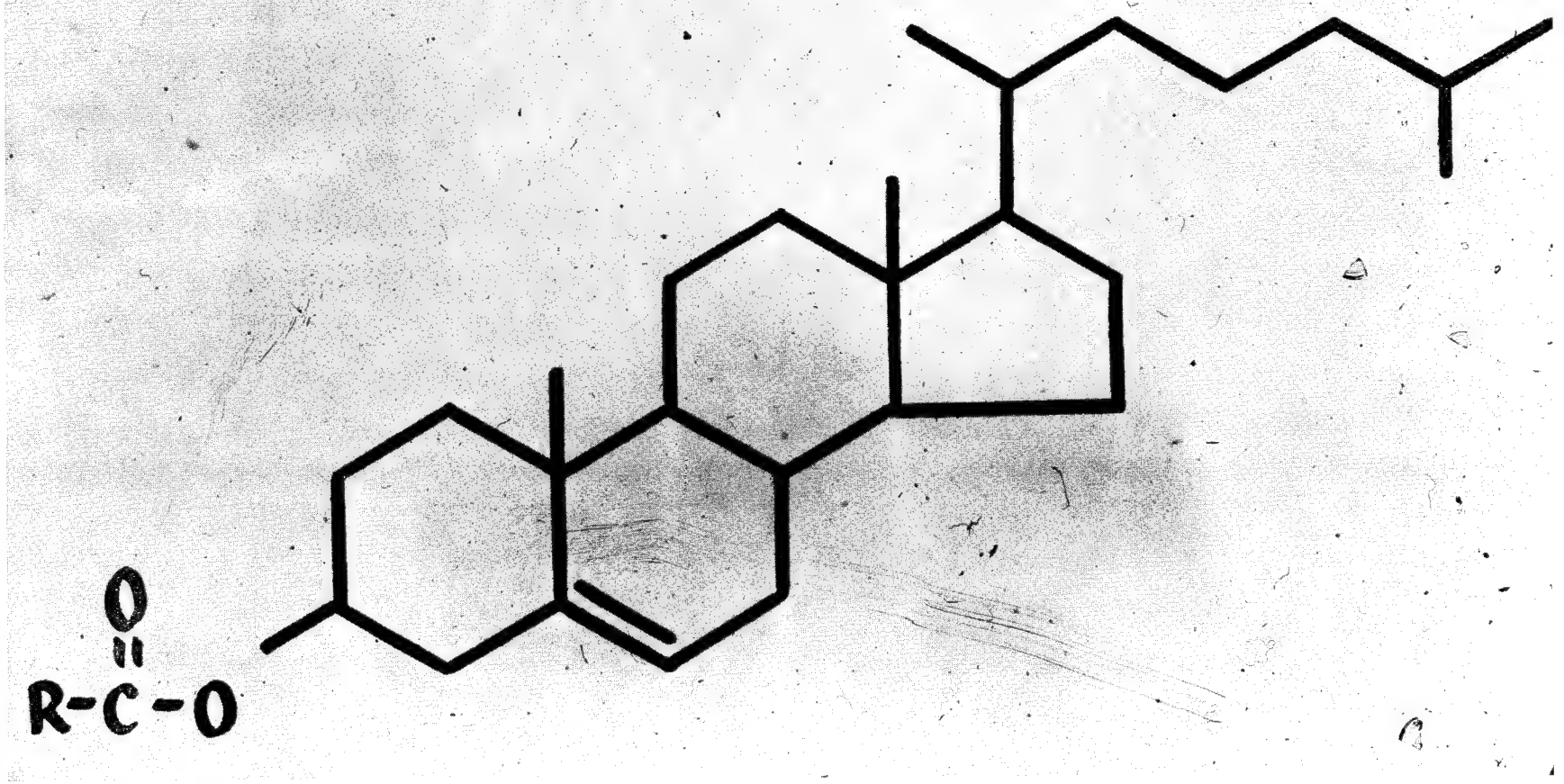

OPTICAL CONSEQUENCES OF MOLECULAR ORDER IN CHOLESTERIC CRYSTALS

1. BIREFRINGENCE
2. OPTICAL ROTATION
3. SCATTERING OF WHITE LIGHT TO REFLECT DIFFERENT WAVELENGTHS GIVING IRIDESCENT COLORS
   COLORS OBSERVED ARE FUNCTIONS OF:
   - (A) THE CHOLESTERIC SUBSTANCE
   - (B) ANGLE OF REFLECTED AND INCIDENT RADIATION
   - (C) TEMPERATURE

Figure 6

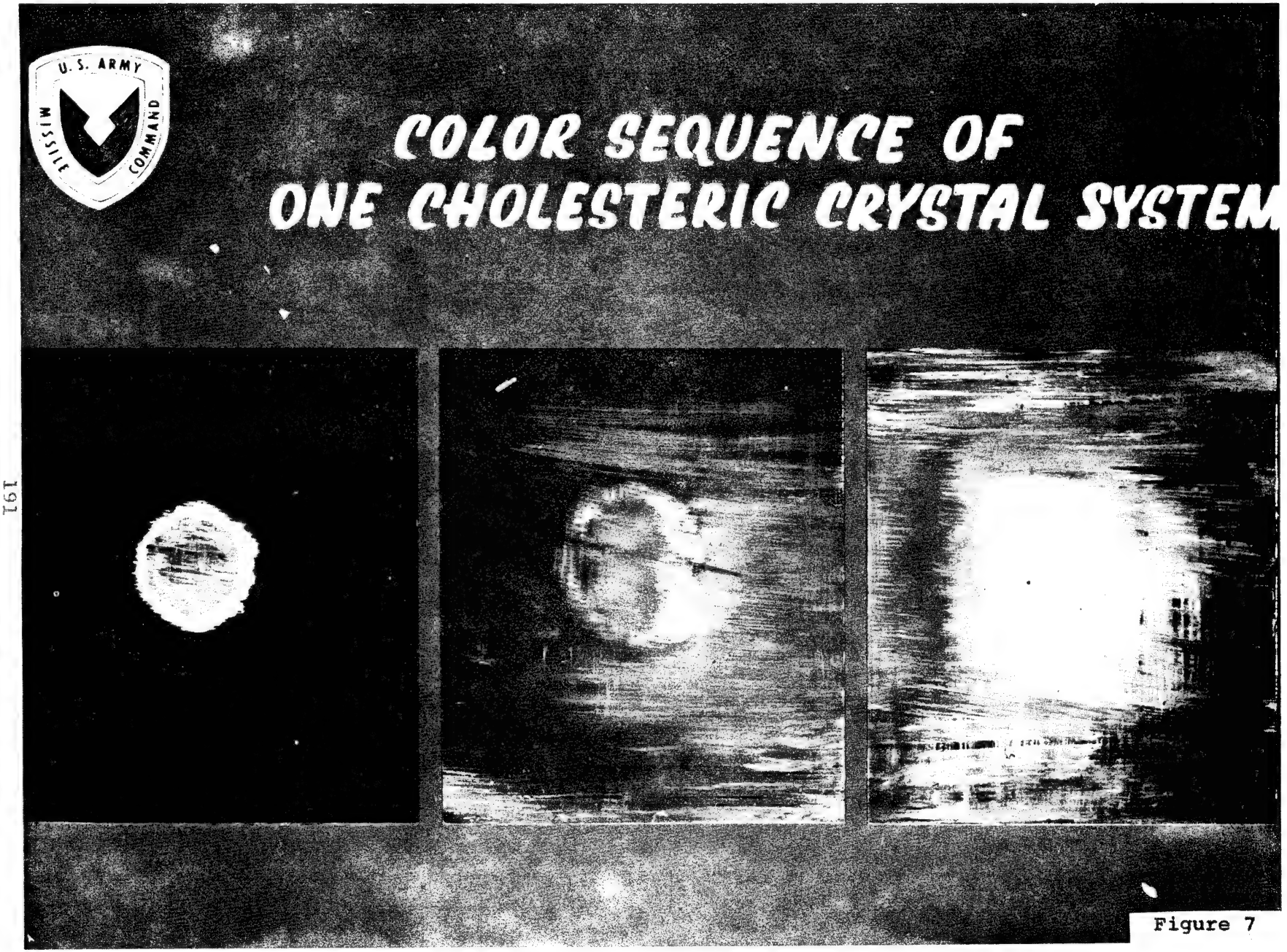
U.S. ARMY
MISSILE COMMAND
COLOR SEQUENCE OF
ONE CHOLESTERIC CRYSTAL SYSTEM

Figure 7

OBSERVED LIGHT REFLECTANCE AS A FUNCTION OF CHOLESTERIC ESTER STRUCTURE

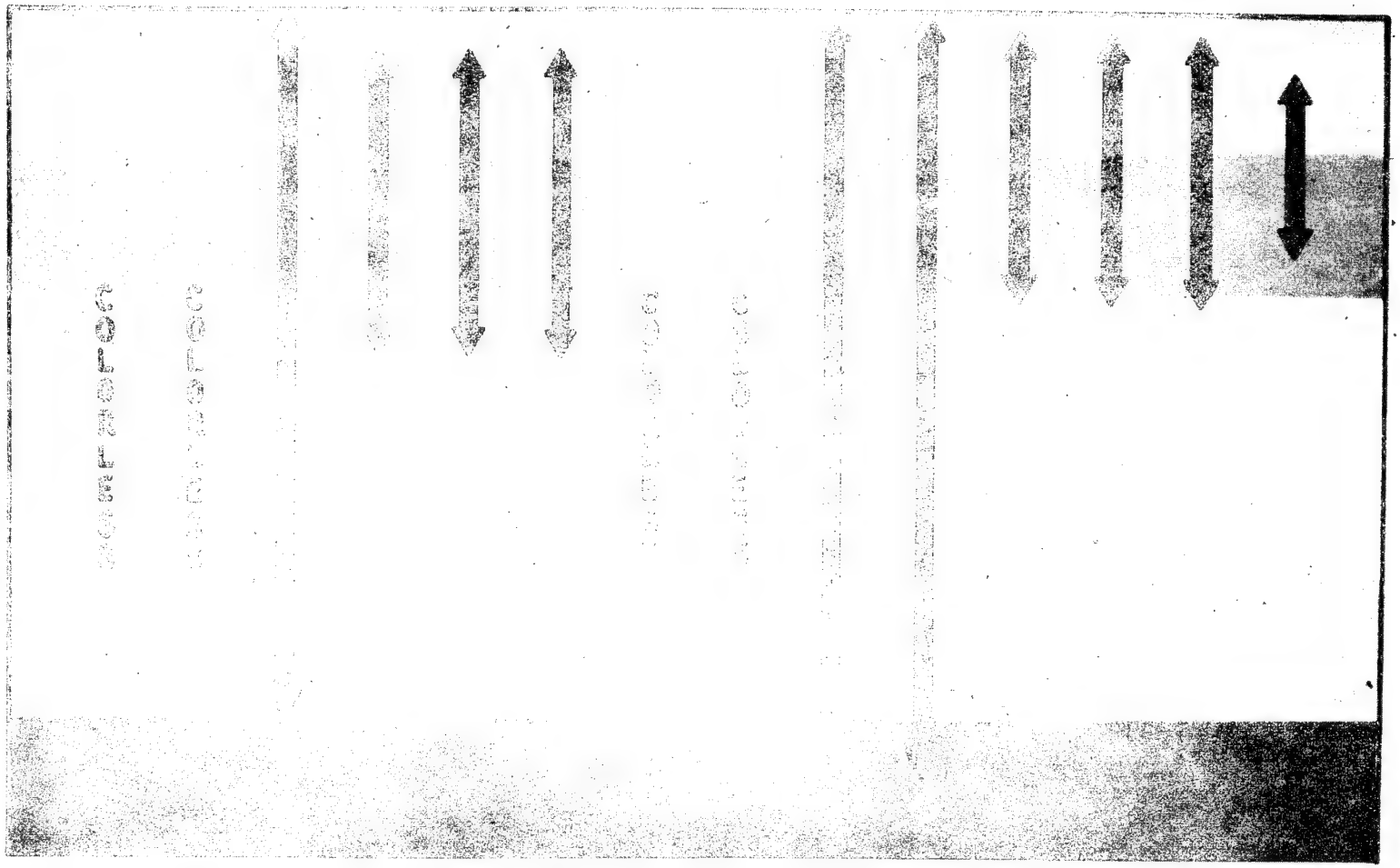

Figure 8

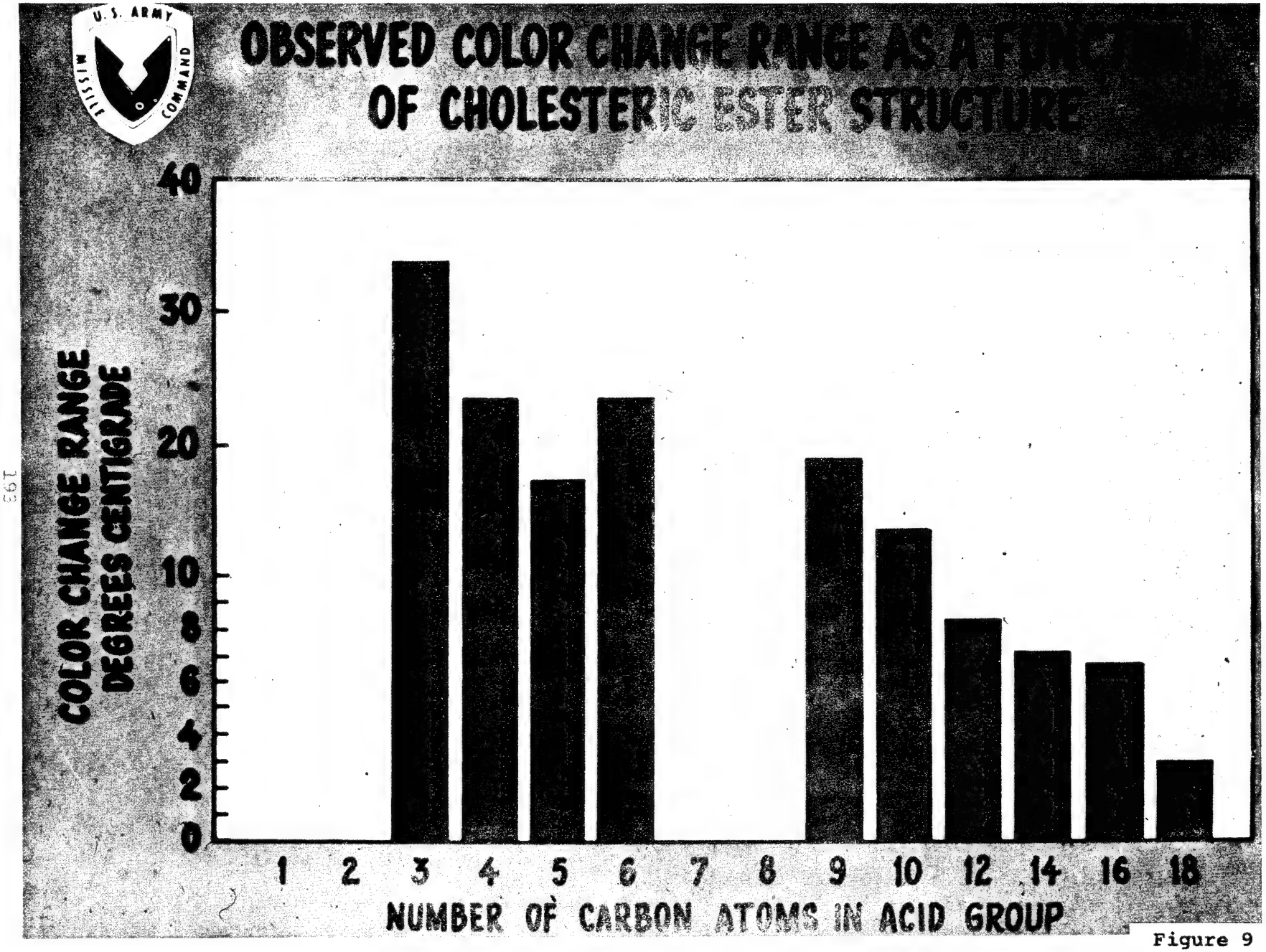
U.S. ARMY
MISSILE COMMAND
OBSERVED COLOR CHANGE RANGE AS A FUNCTION
OF CHOLESTERIC ESTER STRUCTURE
COLOR CHANGE RANGE
DEGREES CENTIGRADE
0
2
4
6
8
10
20
30
40
1 2 3 4 5 6 7 8 9 10 12 14 16 18
NUMBER OF CARBON ATOMS IN ACID GROUP

Figure 9

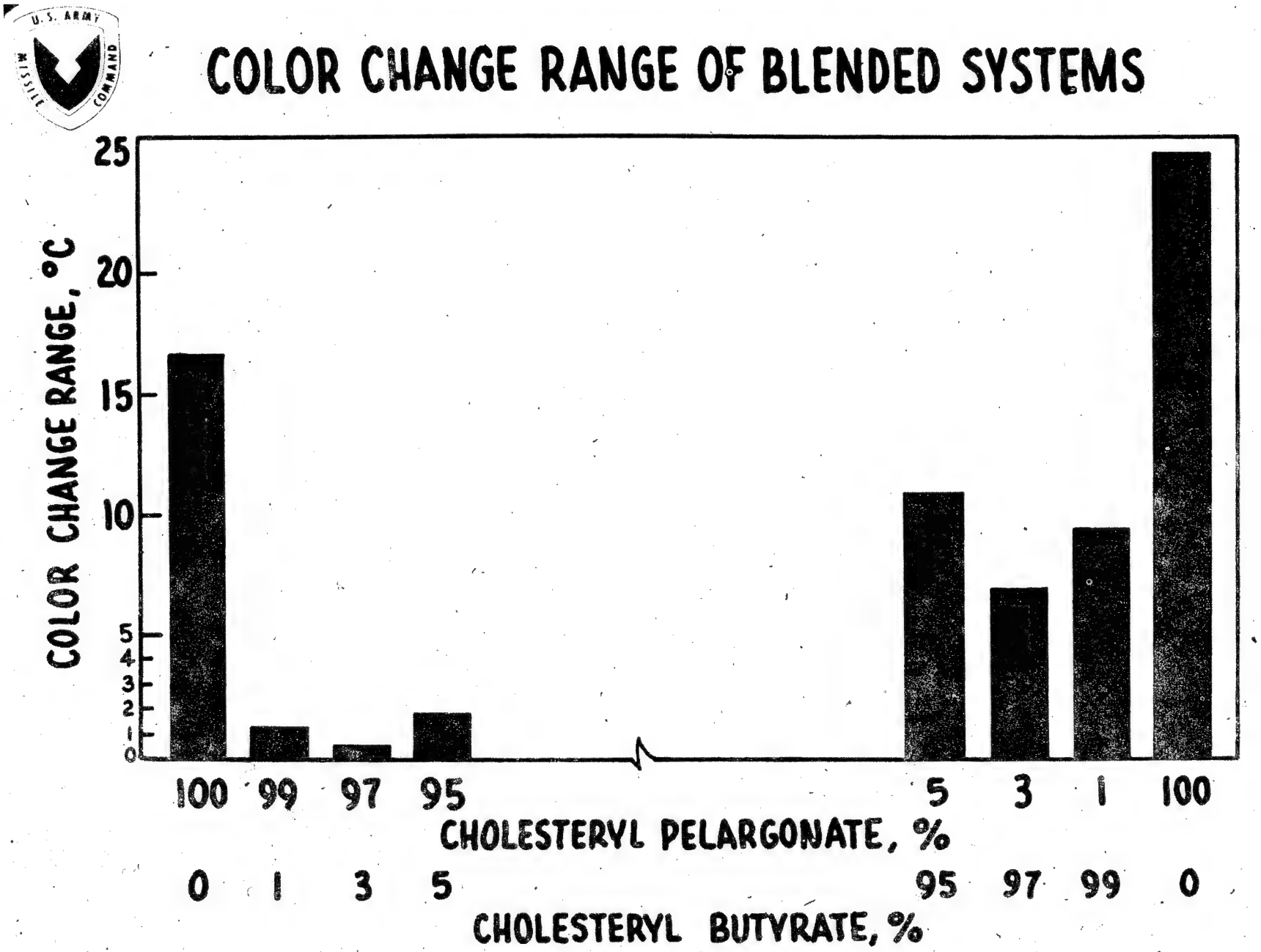
COLOR CHANGE RANGE OF BLENDED SYSTEMS
COLOR CHANGE RANGE, °C
25
20
15
10
5
4
3
2
0
100 99 97 95 5 3 1 100
CHOLESTERYL PELARGONATE, %
0 1 3 5 95 97 99 0
CHOLESTERYL BUTYRATE, %

Figure 10

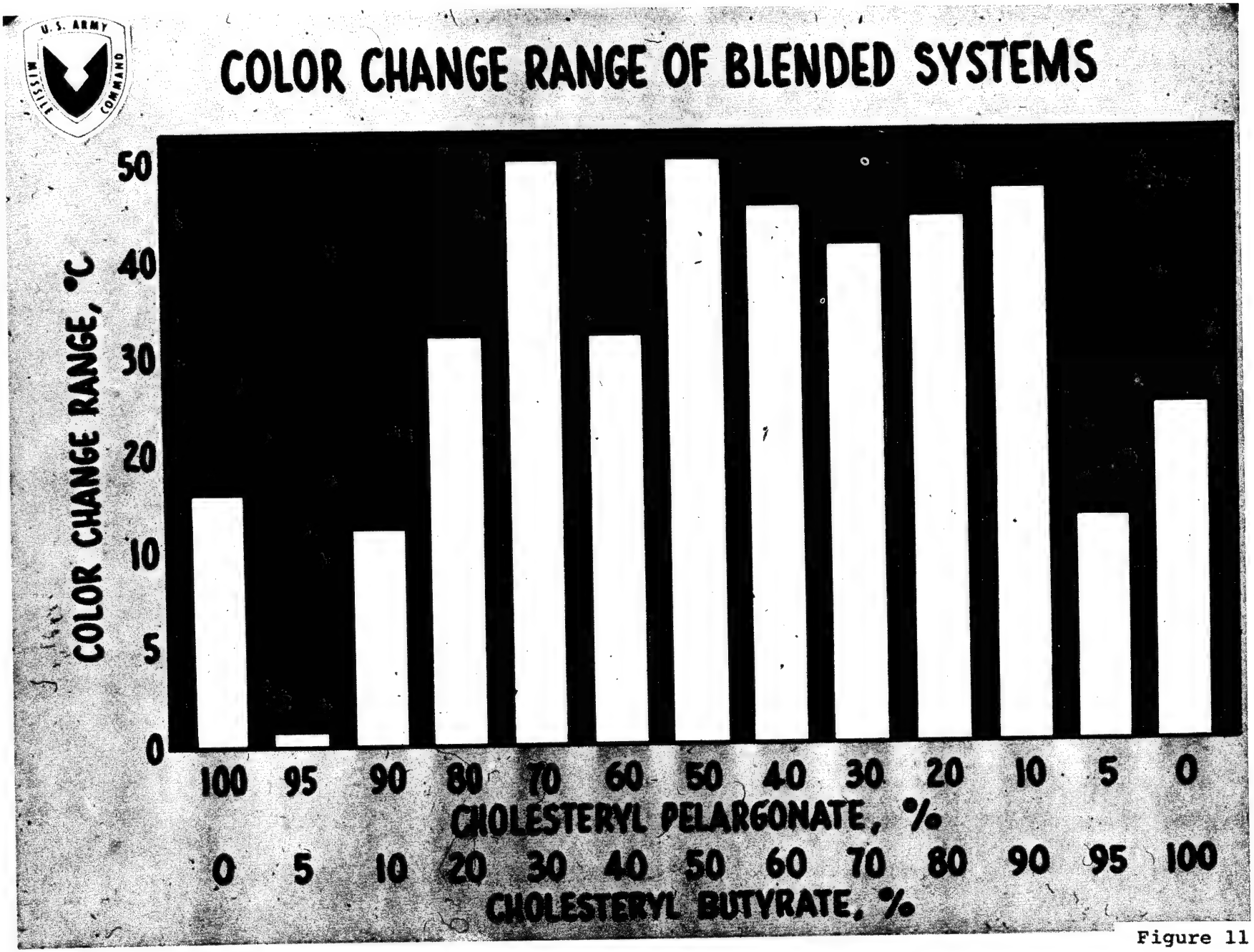
U.S. ARMY MISSILE COMMAND
COLOR CHANGE RANGE OF BLENDED SYSTEMS
COLOR CHANGE RANGE, °C
0
5
10
20
30
40
50
100 95 90 80 70 60 50 40 30 20 10 5 0
CHOLESTERYL PELARGONATE, %
0 5 10 20 30 40 50 60 70 80 90 95 100
CHOLESTERYL BUTYRATE, %

Figure 11

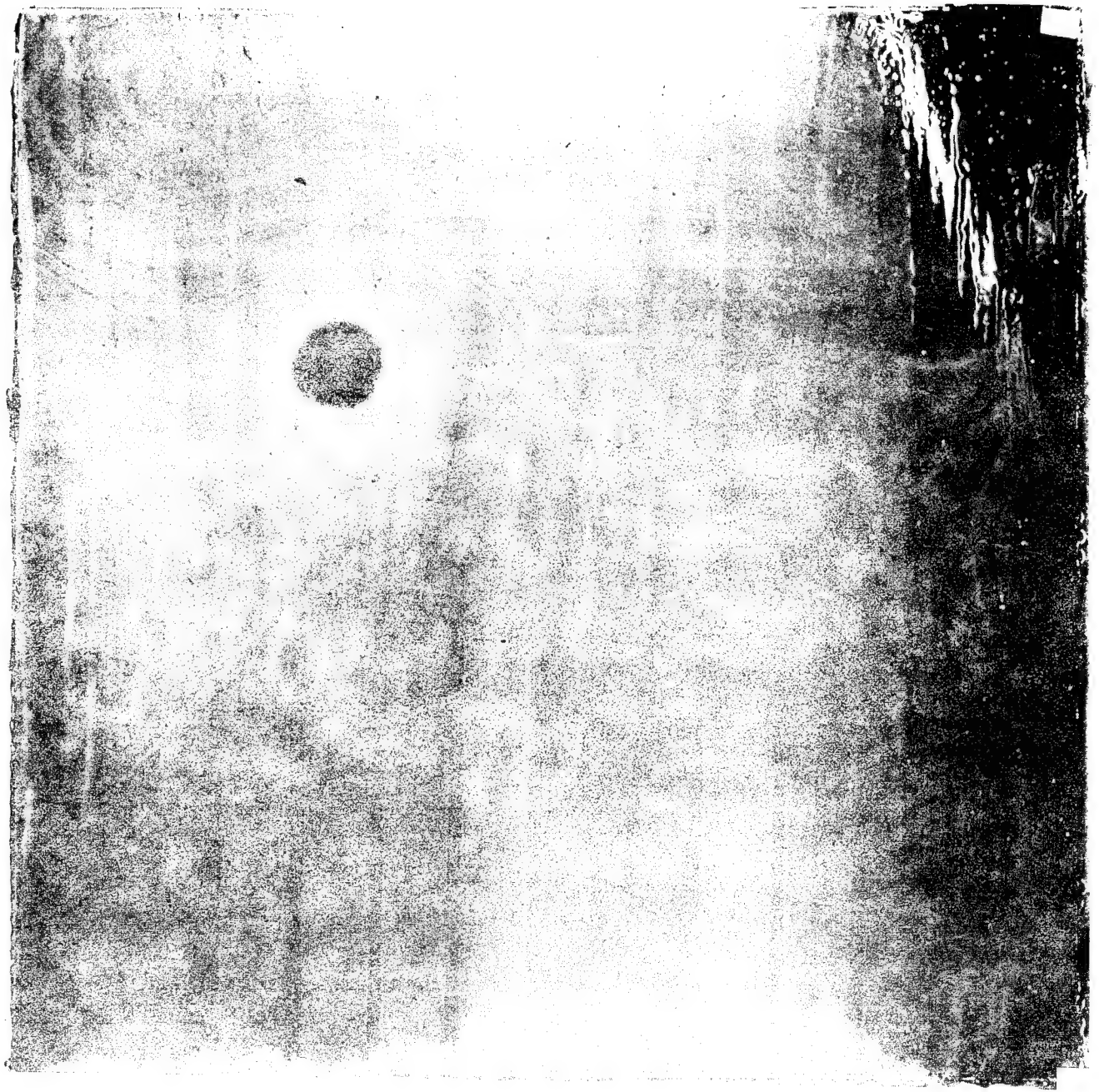

Figure 12

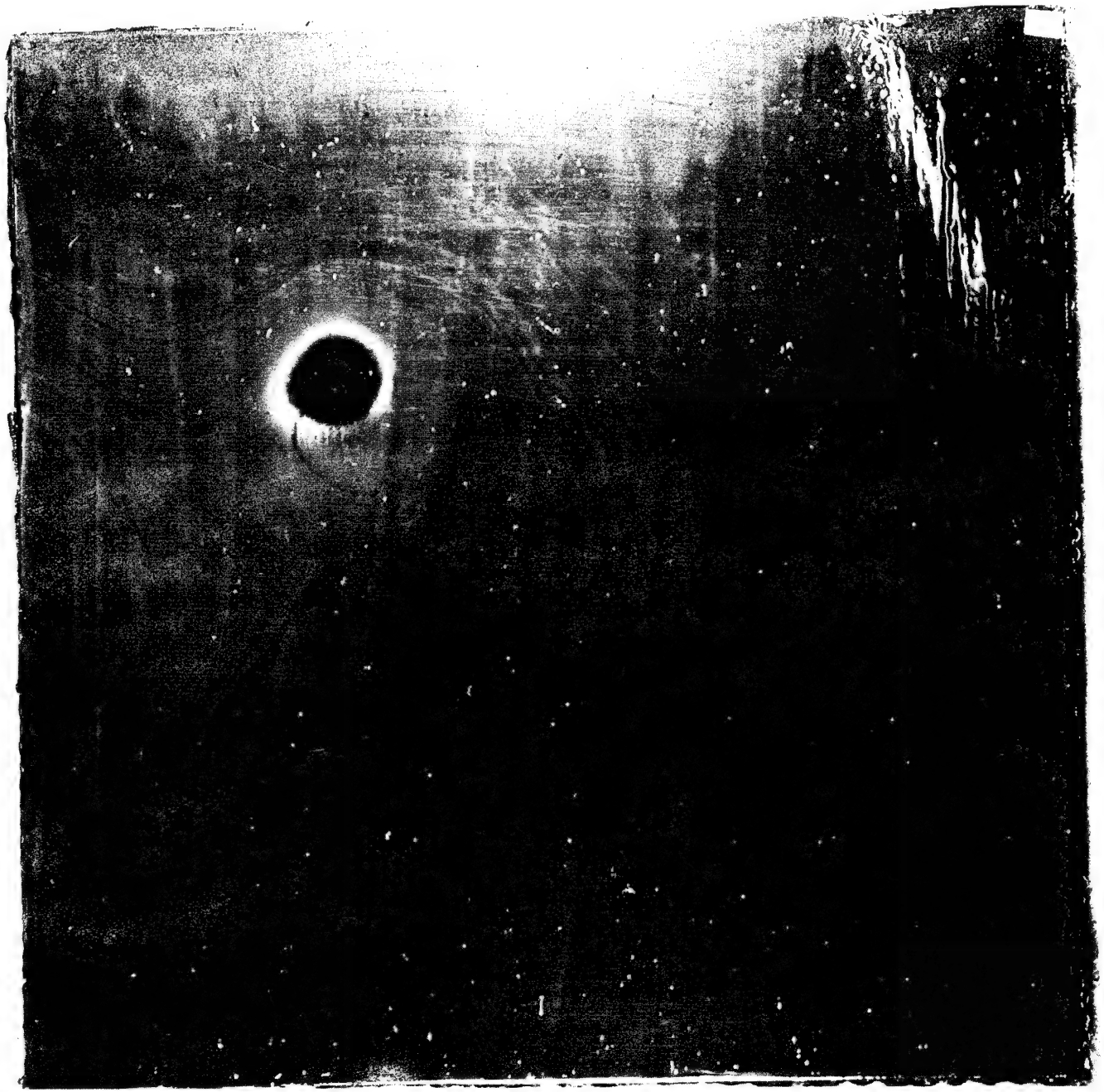

Figure 13

Figure 14

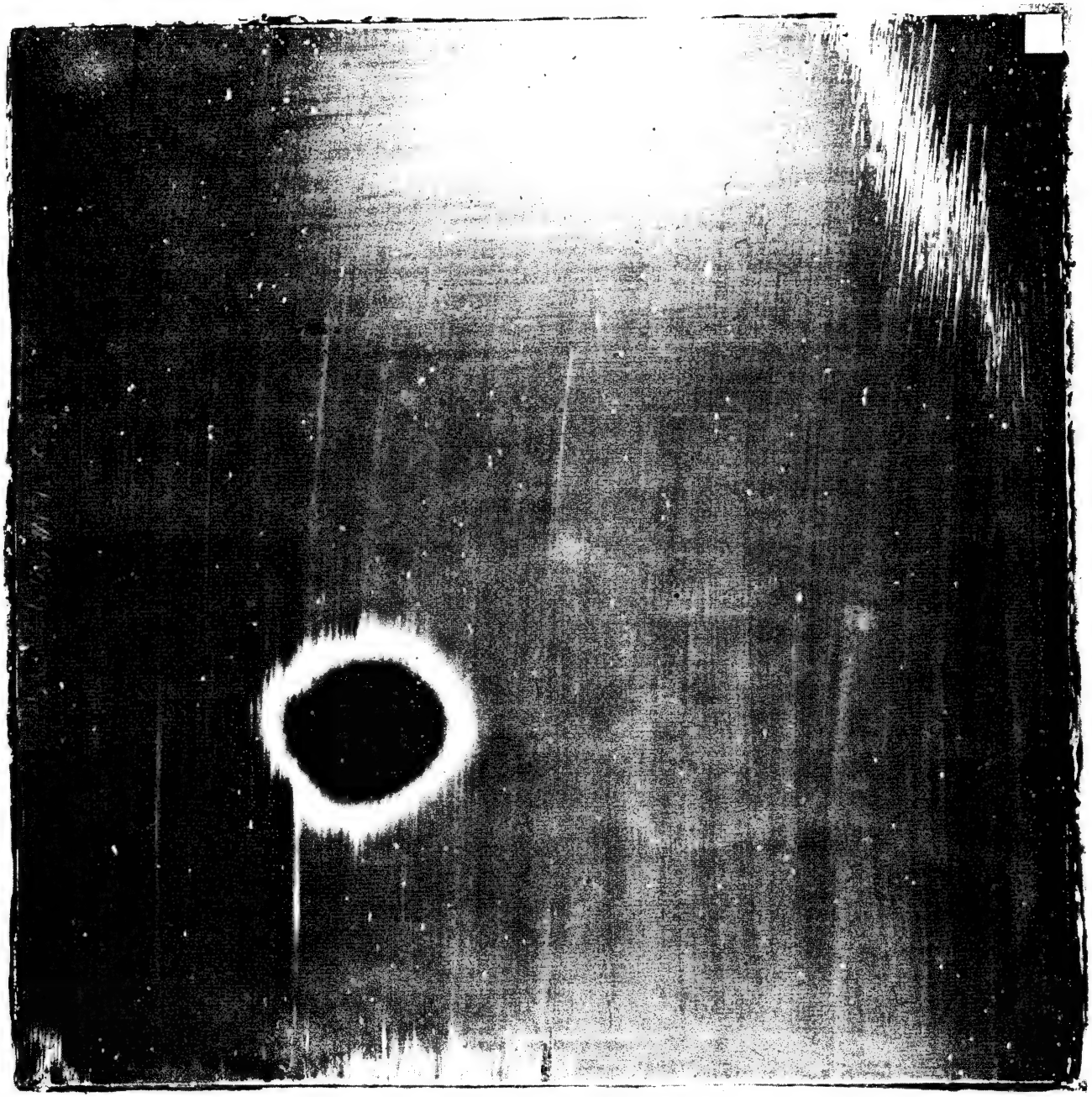

Figure 15

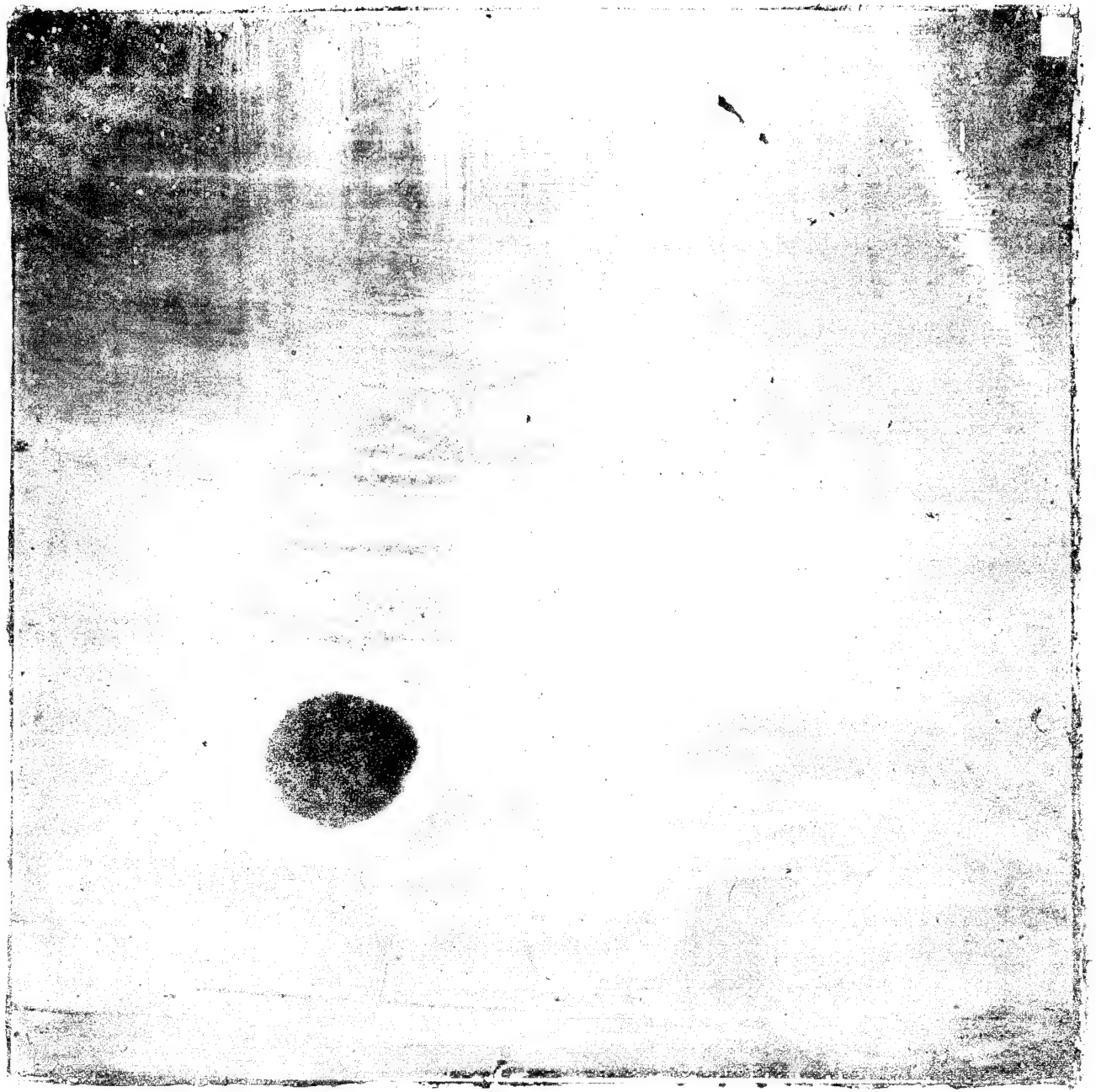

Figure 16

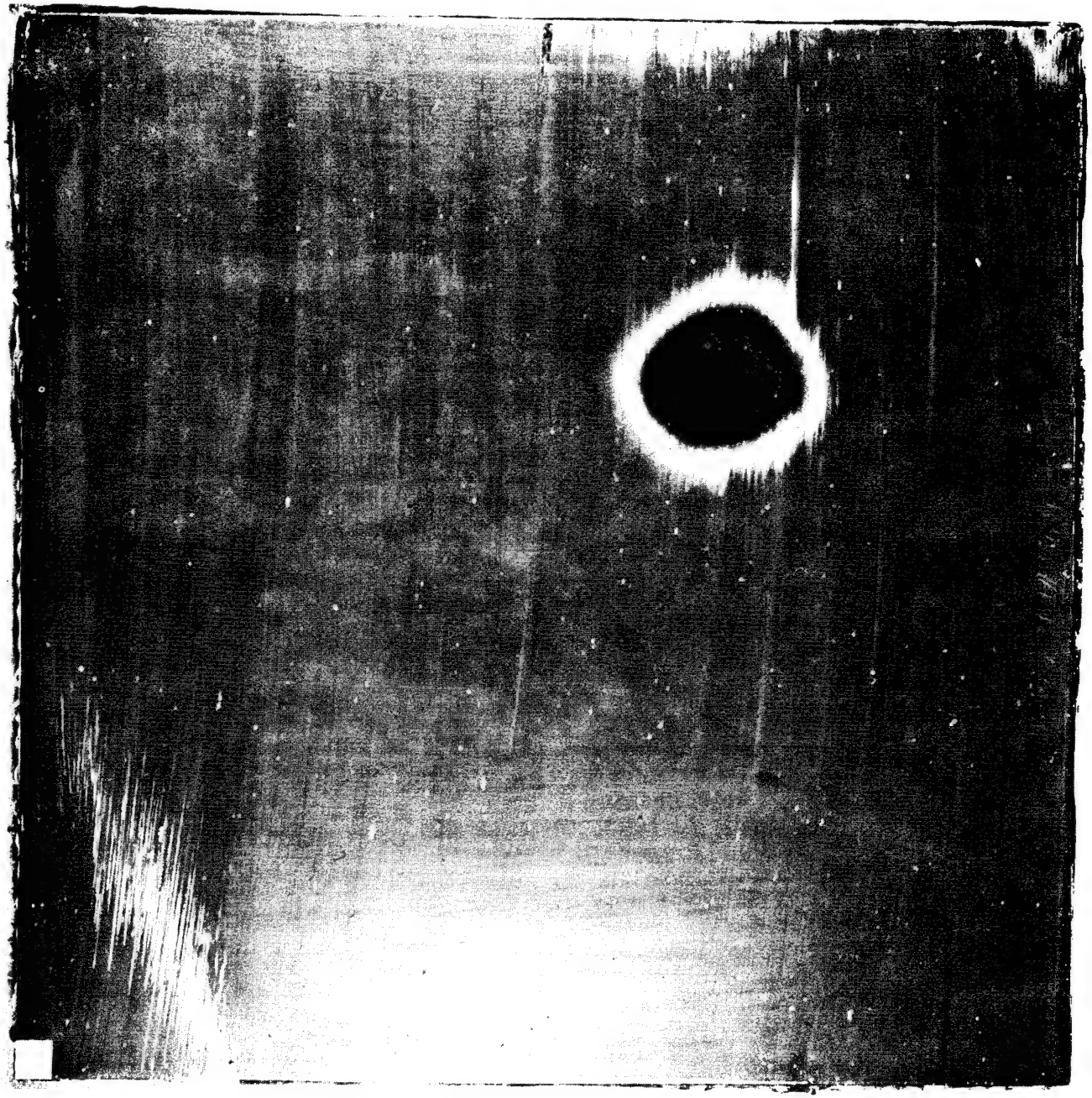

Figure 17

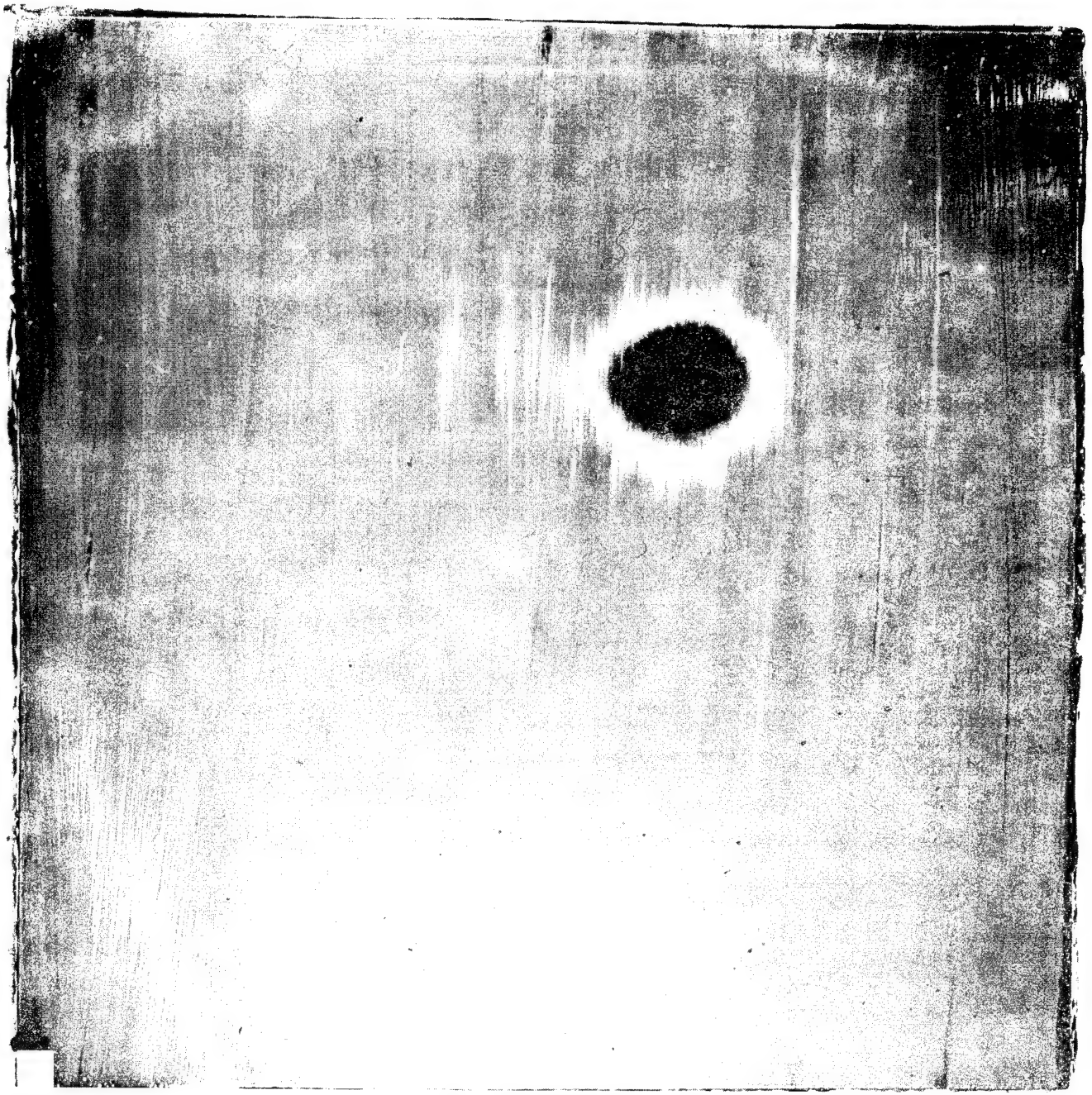

Figure 18

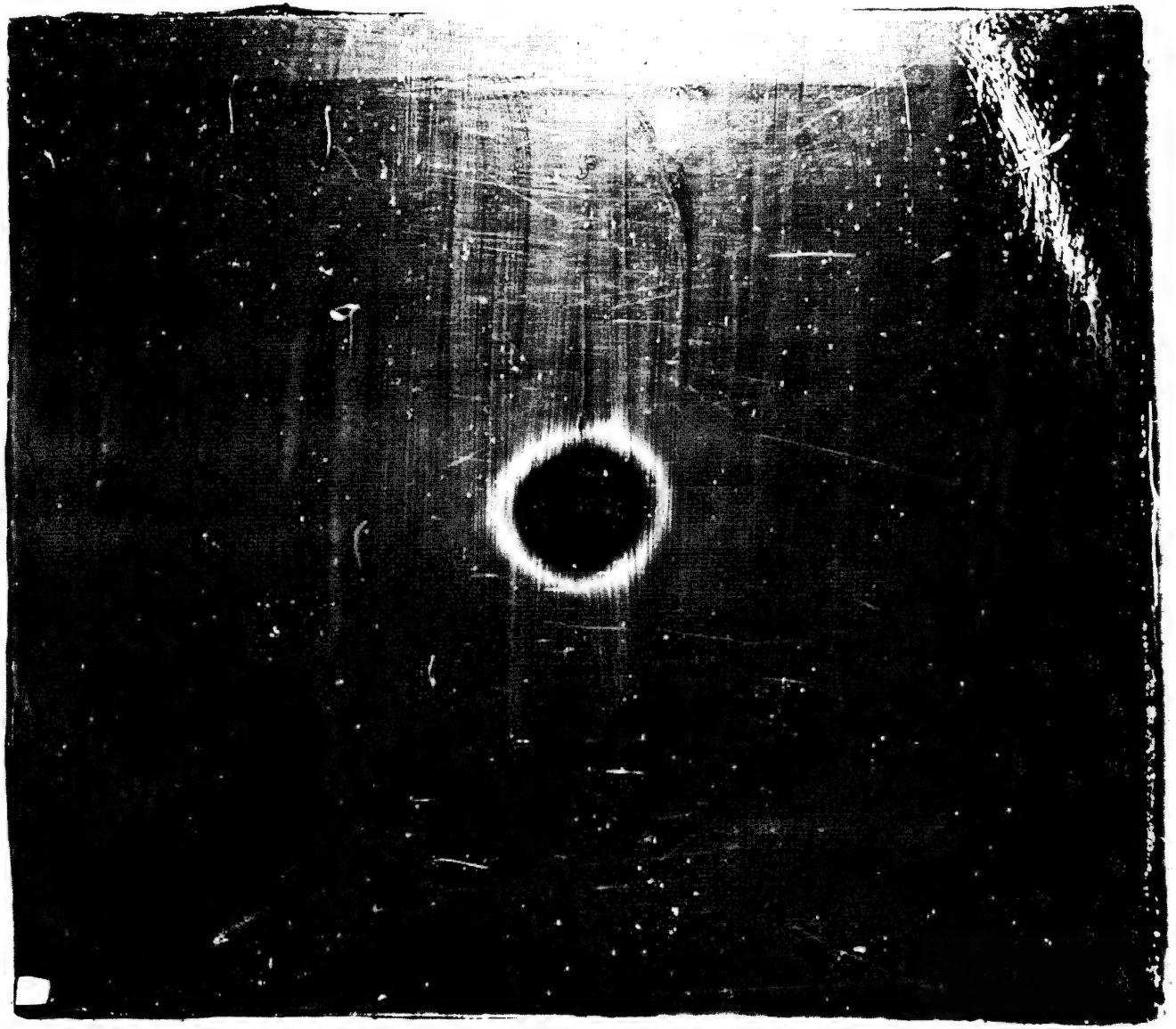

Figure 19

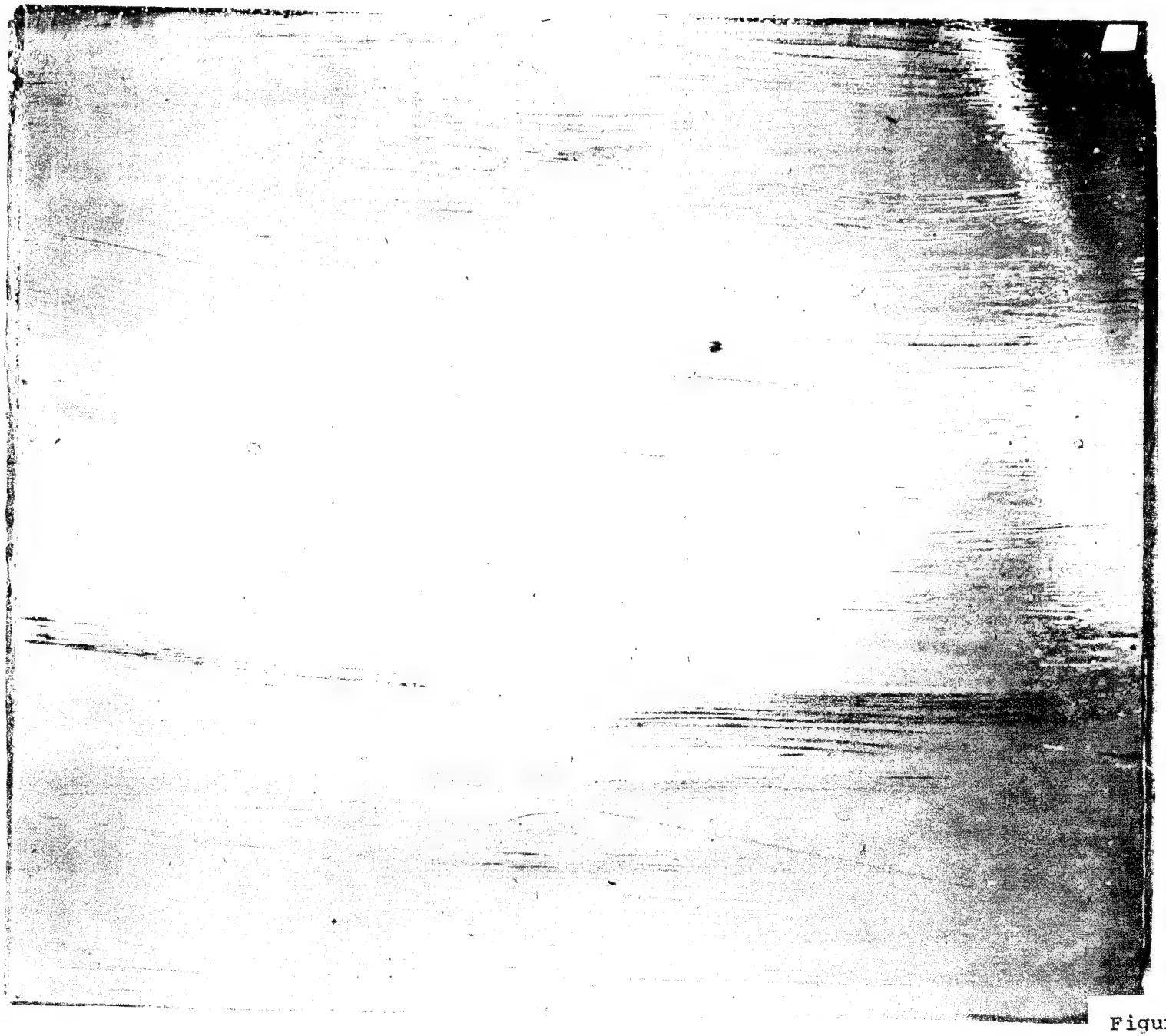

Figure 20

Figure 21

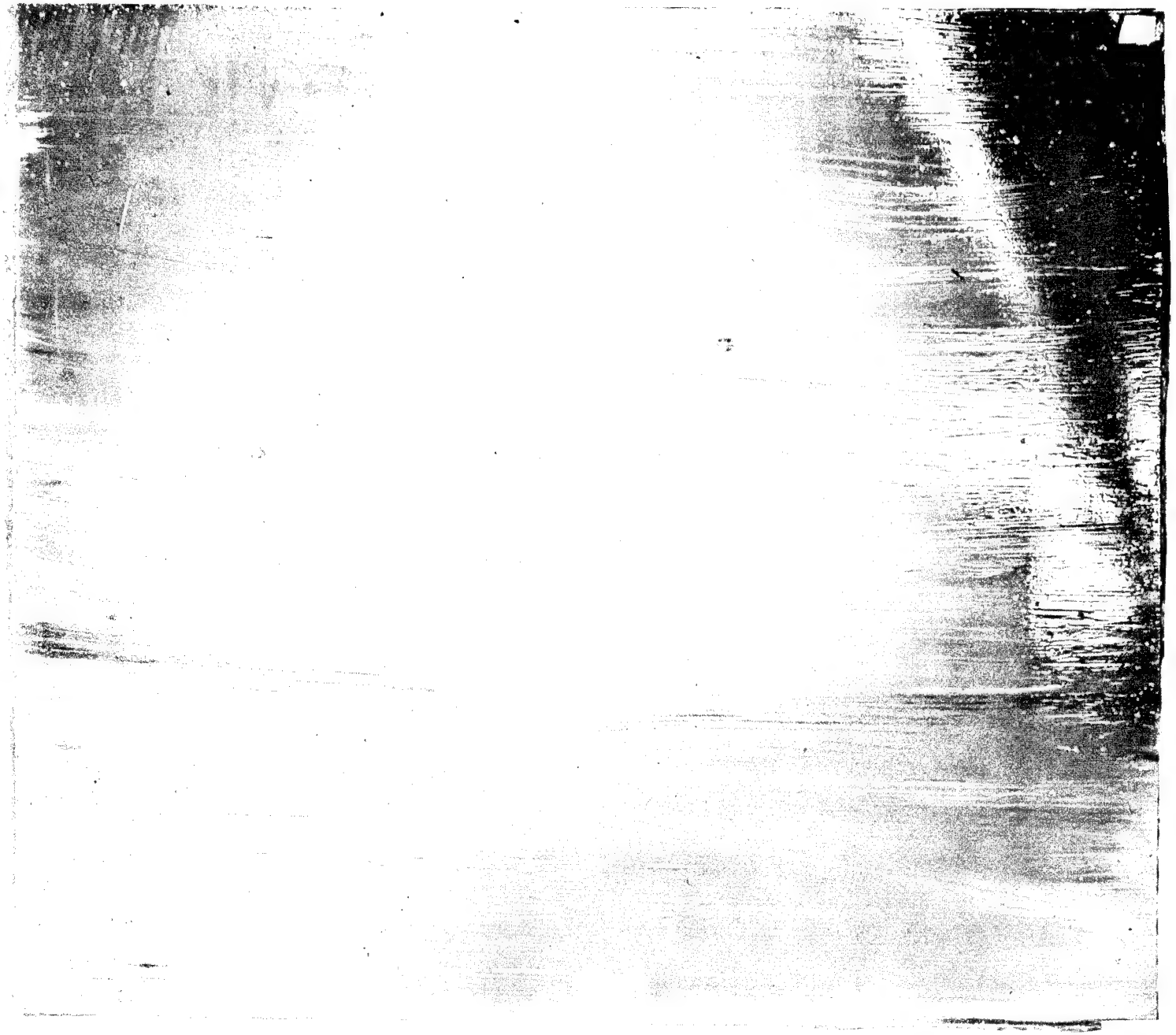

Figure 22

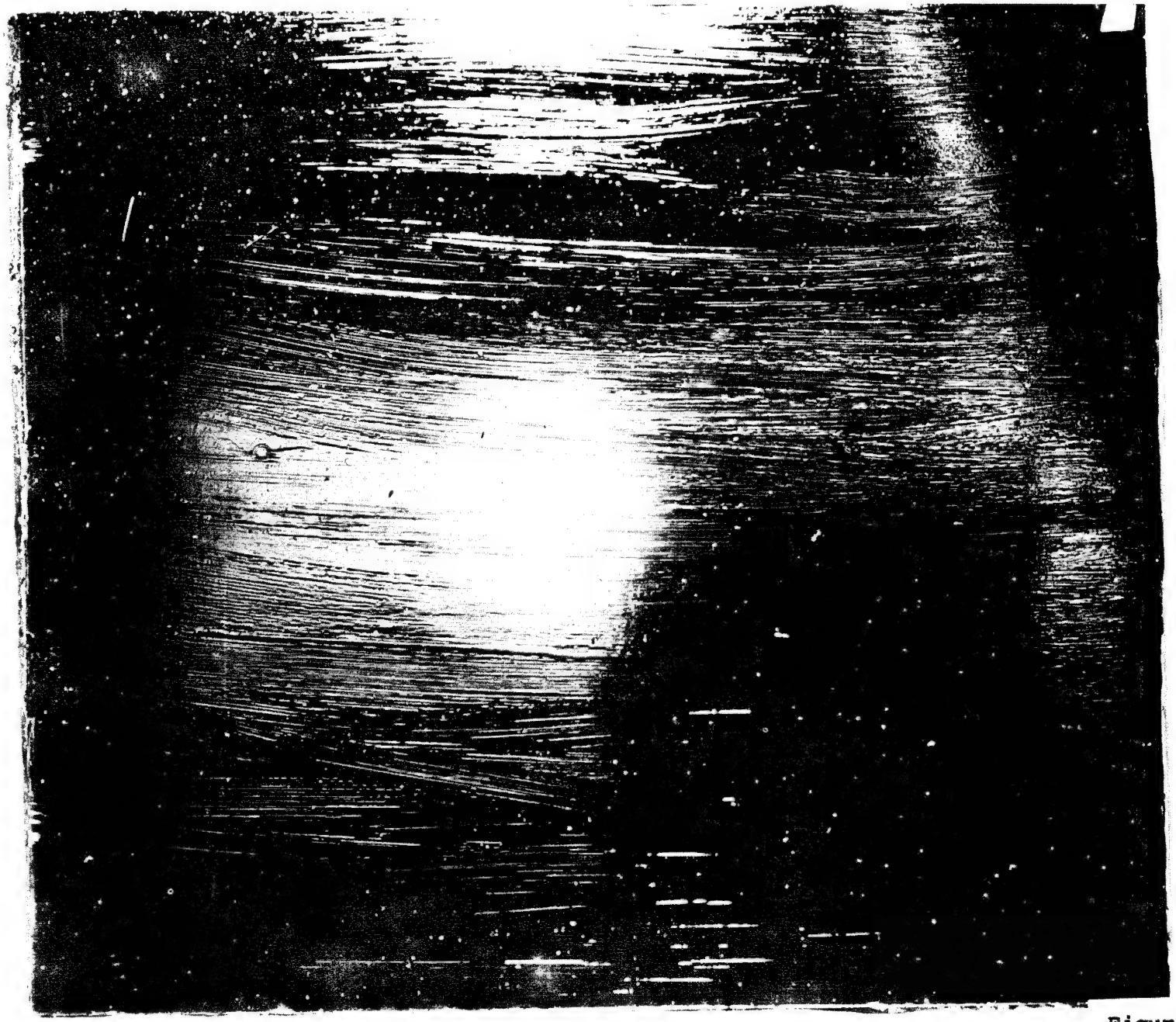

Figure 23

OTHER APPLICATIONS OF CHOLESTERIC CRYSTALS

I ELECTRONIC CIRCUITS

II INSULATION OF DISSIMILAR MATERIALS

III MEDICAL APPLICATIONS

Figure 24

PAPER No. 8

NONDESTRUCTIVE INSPECTION BY REMOTE CONTROL

J. Peale

Warner Robins Air Force Base

ABSTRACT

A method of managing a nondestructive inspection program to achieve a routine type inspection of aircraft using standard Air Force stock nondestructive inspection equipment and Air Force trained personnel.

NOTE - Due to special assignment the author was unable to have this paper available for presentation to the Conference or insertion in the Proceedings.

SPECIAL PRESENTATIONS

REPORT ON PROBLEMS PRESENTED TO THE 15th DOD CONFERENCE

by

David M. Moses

PROBLEM - Ductility Determination of Sintered Iron Rotating Bands for Artillery Shells

PROBLEM - Nondestructive Testing of 400-Gallon Water Tank M 149

PROBLEM - X-ray Examination of Torpedo Parts

REVIEW OF TYPICAL NDT PROGRAMS SUPPORTED BY THE AIR FORCE MATERIALS LABORATORY

by

James A. Holloway

Problem: Ductility Determination of Sintered Iron Rotating Bands for Artillary Shells

1. The following summarizes actions taken to determine NDT methods of determining ductility of rotating bands:

a. Non-impregnated bands were submitted to Mr. C. H. Dyer, Naval Ordnance Laboratory for determination of density, utilizing radiographic methods. It was determined that the density of the bands was not uniform and varied along the circumference.

b. By utilizing resonant frequency methods both the ductility and tensile strength can be determined by measuring the sonic and ultrasonic velocity. Mr. L. Cardinal Naval Research Laboratory, volunteered to test the bands; however, the heterogeneous density of the bands precluded the utilization of resonant frequency methods.

c. The recommended improved mandrel design utilizing a hydraulic ring expansion method for determination of ductility and tensile strength is being considered.

Problem: Nondestructive Testing of 400 Gallon Water Tank M 149

1. To briefly review: the object of our investigations is to determine a nondestructive method for locating voids in the tank insulating foam and disbond between the foam and plastic tank shells.

2. Four areas of NDT were investigated or are under investigation since the 15th Defense Conference, they are:

a. Microwave

b. Audiosonics

c. Infrared

d. Ultrasonics

3. Recently a small section of the water tank was given to Miss T. Lavelle of the Frankford Arsenal to examine with microwave equipment. A report is expected in the near future.

4. In the field of audiosonics, two approaches were attempted. One was tapping on the outer wall with a metal object and listening for a hollow sound, and the second was use of the sonic resonator by North American Aviation. The tapping was, at best, vague, and no distinction could be made between voids and disbond if found at all. The results of tests conducted by North American Aviation with their sonic resonator were reported as difficult to interpret. Both of these methods were regarded as unacceptable.

5. Infrared methods have shown a great deal of success in the location of voids and some success in the location of disbond. The technique used is to fill the tank with hot water and scan the outside with an infrared camera for variations in temperature. A Barnes T-5 camera has been purchased for acceptance inspection use in an upcoming contract. Work is being conducted to refine the test procedure to allow use of hot air instead of hot water.

6. A contract has been negotiated with General American Research in Chicago, to develop the low frequency ultrasonic method mentioned at the last conference. The contract, for six months, is near the end of the second month.

Problem: X-ray Examination of Torpedo Parts

1. The problem of radiographic examination of welds in torpedo parts was presented and discussed at 15th NDT Conference. Suggestions were:

Use of radiographic pellet.
Use secondary radiation.
Change geometry of source, specimen and film.
Use of ultrasonic methods.

2. Action by Naval Torpedo Station.

No suitable radioisotope has been available to us. Ir 192 is too penetrating.

Secondary radiation was tested using Co 60 gamma as the exciting energy and stainless steel, platinum and copper as sources for secondary radiation. In all cases, the secondary radiation was so weak that excessive exposure times are required. Also the set-up to shield the film from the primary radiation and unwanted scatter is very complicated.

By shooting the transducer weld as shown in the attached sketch, a better radiograph is obtained. Five X-rays are made instead of one but only a little more time is required as exposures are shorter.

We experimented a little with ultrasonic and it showed possibilities. Branson Instrument Co. also tried ultrasonics and felt it would be satisfactory. Preliminary tests at Naval Research Laboratory indicates the method would be feasible. However, this method would require new acceptance standards.

03

REVIEW OF TYPICAL NONDESTRUCTIVE TESTING PROGRAMS SUPPORTED BY THE AIR FORCE MATERIALS LABORATORY

Presented by

James A. Holloway
Wright-Patterson AFB, Ohio

ABSTRACT: A description is given of three programs typical of those in the area of nondestructive testing (NDT) technique development presently being supported by the Air Force. The NDT methods being evaluated under these programs are: an acoustic technique for detecting cracks, magnetoabsorption for measuring stress (either applied or residual), and electron radiography for characterizing refractory coatings. These programs reflect both contractual and in-house efforts with application to both advanced aerospace systems and in-service aircraft.

INTRODUCTION

Exploratory development of nondestructive testing techniques is an interdisciplinary field which requires a working knowledge of physics, metallurgy, electronics, and mechanical testing. It also requires a close liaison with the materials engineer: those involved in developing new materials and those serving in the field maintenance groups. The former, working in the area of research and development, has an understanding of materials which show promise for future aerospace application. The latter is certainly aware of current problem areas of in-service aircraft. The approach for developing NDT techniques to meet the needs of material engineers in these two categories is somewhat different. In the material development area, information concerning those discontinuities and variations in properties which adversely affects material performance is not well defined. Mechanical property measurements have generally not accumulated to permit a clear definition of the causes for failure of the material. It has also been asserted that NDT measurements during the early stages of material development have either been insignificant or relegated to a role of selecting the "good" material from the "bad", with little emphasis on destructively testing "bad" material. Nevertheless, development of new and utilization of existing NDT techniques for characterizing new materials is more difficult simply because the NDT measurement may or may not be related to the principal modes of material failure. Unless an empirical approach defines failure modes which are verified experimentally, the only alternative for obtaining a meaningful correlation between property variability, performance, and the NDT measurement(s) is destructive testing. However, utilization of well chosen NDT methods during these early stages of material development and testing will establish the applicability and validity of the techniques for predicting some of the primary modes of failure. More important, it may reveal factors which influence performance for which NDT measurements are inadequate or nonexistent. This is important because it establishes a "lead time" for the development of adequate NDT techniques, and hopefully, insures that they will be available when the material becomes part of an operational system. Unfortunately, this has not been the case in the past, as the materials engineer in the field will testify. Failure may occur on a specific aircraft structure, and NDT techniques may be

available which will solve the problem immediately. In many instances however they are not, and a lengthy delay results before adequate techniques can be developed and evaluated in the field. Consequently, the Air Force is supporting, not only NDT development for in-service application on operational systems, but development of NDT techniques for future systems. Programs which fall in the former category (present or near future Air Force Systems) include exploratory development of NDT techniques for non-metallic materials such as plastic honeycomb, etc., graphite, and titanium billets. A technique called magnetoabsorption is being developed to measure stress in ferromagnetic materials. An ultrasonic technique using Lamb waves is being evaluated for detecting delaminations in thin sheet material. An acoustic technique looks very promising as a method for detecting fatigue cracks in compressor disks and beneath aircraft fasteners. Exploratory development of NDT techniques is also being conducted for inspecting future aerospace materials including refractory coatings, diffusion bonded materials and fiber reinforced metal and resin matrix composites. A basic study of crack propagation in high strength steels is being pursued using acoustic emission. A more detailed description of three of these programs will be given. They reflect both contractual and in-house efforts with application to both advanced aerospace systems and in-service aircraft.

ACOUSTIC TECHNIQUE FOR DETECTING CRACKS

The detection of fatigue cracks hidden beneath aircraft fasteners is presently accomplished by drilling out the fastener and inspecting with eddy currents using a special bolt hole probe. It was felt that a technique could be developed which would detect the presence of a crack without fastener removal. The tap test has been used for many years to distinguish between sound material and material containing delaminations and lack of bond. Realizing that such a test could not be objective nor ultra-sensitive, a program was initiated with Arvin Systems, Inc., Dayton, Ohio to provide the necessary replacement for the coin, the accelerometer pick-up, amplifier, and readout system. A repetitive shock generator was constructed by modifying an electro-mechanical vibrator similar to that described in a report from the Federal Aviation Agency (1).

The vibrator is a standard 6 volt unit which produces a frequency of 60 Hz or pulses 12.5 milliseconds apart. The shock pulse detector is a Model 2220 Accelerometer manufactured by the Endevco Corporation with a resonant frequency of 35KHz and amplitude linearity of ± 2% up to 1000g. The mounting fixture, shock generator and accelerometer are shown in Figure 1. Analysis of the wave signatures of cracked and uncracked samples was undertaken using flat plate samples provided by the AF Materials Laboratory in a range of thicknesses and hole diameters. Also some of the plates contained corrosion around the fastener holes. Simulated cracks were incorporated in a duplicate set of samples. The simulated cracks were placed at the bottom of the fastener hole and ranged in length from 0.050 inches to 0.10 inches. Both cracked and uncracked samples were used to establish system response to such variables as fastener torque, stress, and corrosion. The signal difference between a cracked and the uncracked sample is shown in Figure 2. It can be seen that the damping time of the signal from the cracked sample is significantly increased. A band pass filter was employed after it was determined that the most significant crack indications occur above 4KHz. Tests on all of the samples indicate that all simulated cracks were detectable at frequencies between 4 and 10KHz. In addition a simple meter readout was incorporated as part of the instrumentation after it was found that a significant meter deflection was obtained for the cracked sample when the filtered signal was integrated over a suitable time period. The effect of torque variations on the signal was evaluated over a range from 1 to 19 inch pounds. Very little change in damping time was noted, but spectrum analysis revealed changes in the amplitude of the lower frequencies. The panels were stressed up to 41,500 psi. Spectrum analysis revealed a shift in frequency at the lower frequencies and no significant shift occurred above 5KHz. However, corrosion produces a significant change in the amplitude of the integrated signal. The meter reading is even higher for a cracked sample which also contains corrosion around the fastener hole.

A test was performed on a section of an F-102 wing which had undergone fatigue testing. A simulated crack which produced a significant meter indication was incorporated in one section of the wing containing a series of 5/16 - 24 fasteners. High instrument readings were also obtained from several other holes. The fasteners were removed and the presence of actual cracks was confirmed

with Zyglo penetrants. Tests were also conducted on several J-75 turbine discs in order to evaluate the capability of the system for detecting fatigue cracks at the bottom of the "fir tree" and in the tangs. One type of fixture designed to hold the accelerometer together with the impact generator is shown in position on the turbine disc in Figure 3. This particular disc contained a known crack across one of the tangs which had been detected by "wink" Zyglo - a penetrant test where the crack is detected only by applying stress to the part. With the acoustic technique, the crack was easily identified by the increase in the damping time of the signal at a frequency of 6KHz. In addition, other areas gave significant readings different from that corresponding to noncracked material at a frequency of 11KHz. Optical examination at 38X revealed fatigue cracks at the root of the "fir tree" in all of these areas. One of the cracked areas is shown in Figure 4. The areas were later examined with Zyglo without results. It can be seen from Figure 3 that these cracks were located with the blades in place. Future work will be directed toward obtaining a correlation between the fatigue crack size and the damping time. Also the vibrator/accelerometer assembly will be improved to provide more uniform repetitive results in all orientations. A complete documentation of the program is available in AFML-TR-67-167 (2).

MAGNETOABSORPTION

Magnetoabsorption is a magnetic method for measuring stress in ferromagnetic materials which is being developed by Southwest Research Institute, San Antonio, Texas. Basically whenever a ferromagnetic material is placed in the vicinity of a slowly changing magnetic field, the magnetic domains within the material attempt to align themselves parallel to the magnetic field, but not without well known hystersis effects. Figure 5 shows a plot of the external magnetic field intensity (H_B) versus the magnetic flux density B. If an r-f field is now impressed on the material, there is a certain amount of energy absorbed from the r-f field. This is known as magnetoabsorption. The smaller loop labeled H_Δ and $B\Delta$ in Figure 5 depicts this small cyclic r-f field superimposed on the larger bias field. As the size of the small cyclic field change approaches zero, the

ratio B/H approaches a limiting value of $\mu_o \mu_r = \mu$, where μ_o is the permeability in free space, μ_r is the relative reversible permeability, and μ is the reversible permeability. The reversible permeability is dependent on the reversible boundary displacement and the reversible rotation of the domains in the ferromagnetic material. This is a function of the type of material and its magnetic and stress history. The change in the energy absorbed is reflected as a change in the impedance of the r-f coil generating the r-f magnetic field, which is not only a function of the reversible permeability but also is related to the resistivity of the material. Early in the program, it was verified, both theoretically and experimentally, that the effect of changes in the resistivity of the material on impedance was small compared to the effect of the reversible permeability. Actually the change in impedance is proportional to the square root of the reversible permeability.

The change in impedance of the r-f coil is measured by making the coil part of a marginal oscillator circuit operating at 500KC. Any change in impedance is reflected as a change in voltage across the resonant circuit of the marginal oscillator which is connected to the Y-axis of an oscilloscope. The biasing voltage is tapped and connected to the X-axis of the scope so that the display is similar to a "butterfly". The biasing coil, with the r-f coil, sample, and typical oscilloscope display are shown in Figure 6. A change in stress produces a change in amplitude of the signal. Actually, there is not only a change in amplitude but a shift in phase of the signal harmonics. To illustrate the application of the technique, a description will be given of measurements made on a maraging steel plate which contained nine EDM slots, several of which had been ground or honed in order to close the slot. Figure 7 is a photograph of the sample with the positions of six EDM slots indicated. Each of the slots is 20 mils wide and 375 mils long. The three slots on the left side are believed to have been untouched and are approximately 30 mils deep. The three centrally located slots have been roughed to various degrees, while the right-handed slots have been ground and honed until the slots are hardly visible. Measurements were made along numbered scan paths using a double-D r-f coil shown in Figure 8. This coil develops fields normal to its symmetrical plane and also rejects induction by the external field. Using a wave analyzer, the changes in the amplitude of the signal harmonics could be measured

as the probe traversed each scan line. The data for the fundamental and the first six harmonics are shown in Figure 9. The very slight change in the amplitude of the 120 cps component across the surface of the plate indicates that the amplitude of the magnetic bias is relatively constant along the length of the sample and that the first harmonic is relatively insensitive to surface irregularities such as scratches or slots. The cold work caused by the honing process used to seal the rim of the center slot produces the decrease in amplitude shown in the figure. The amplitude of the harmonics show a much greater variation, not only in the areas which are cold worked, but to the unworked slots and surface scratches.

The technique can also be applied for measuring stress in nonferromagnetic materials if a thin nickel coating is first applied to the material. Figure 10 shows the magneto-absorption signal amplitude plotted against stress and elongation for a nickel plated aluminum rod 1/8 inch in diameter.

Present effort is directed toward obtaining stress profiles along the surface of J-75 compressor blades. Indications are that the initial stresses in the root of the blades change from compression to tension as a crack develops. If this can be verified, utilization of the technique will insure the quality of used blades prior to and after rework during engine overhaul. A complete documentation of the results has been published during the last several years of this investigation (3).

ELECTRON RADIOGRAPHY

The last investigation to be discussed concerns an in-house effort to develop a technique for inspecting refractory coatings. These coatings are applied to substrates, such as columbium, to protect them from oxidation at elevated temperatures. Materials of this nature will be used on future aerospace vehicles where multiple re-entry missions are required. Characterization of the quality of the coating using NDT methods is essential to assure mission success. One of the methods considered applicable was electron radiography (4) and an in-house program was initiated to investigate and establish the optimum technique.

Electron radiography utilizes an ultra-fine grain x-ray insensitive film to record electrons emitted from the surface (or near surface) of a material when irradiated by a beam of x-rays. In the energy range of interest, radiation is absorbed by the photoelectric and the Compton process. Each process ejects electrons from the material. The photoelectric effect predominates for the higher atomic numbered materials. Two techniques can be employed to obtain electron radiographs: the back emission technique and the forward emission technique. These are shown in Figure 11 and 12. When the back emission technique (Figure 11) is employed, the samples are placed next to the film in a vacuum cassette and positioned so that the x-rays pass through the film. The electrons are ejected in a direction opposite to that of the x-rays. With the forward emission technique (Figure 12), the x-rays pass through the sample, ejecting electrons in a direction parallel to the x-ray beam. The back emission technique can be applied to inspect coated surfaces whose substrate is too thick for adequate x-ray penetration. The forward emission technique, capable of higher resolution than the back emission technique, was thought to be only useful for inspecting very thin, low density materials which would permit the electrons to be transmitted through the sample. During the course of the in-house investigation, the forward emission technique was utilized to obtain an electron radiograph of the coated samples. As with the back emission technique, the x-ray tube kilovoltage employed is between 150 KVCP and 200 KVCP. With Eastman Kodak Fine Grain Positive Film (FGP) film exposure time is less than 5 minutes. Attenuation by the columbium substrate, which is approximately 0.010 inches thick, is not significant enough to reduce electron emission appreciably. The resulting radiograph, shown in Figure 13 has a greater resolution than that obtained with the back emission technique.

At the present time, the in-house program is being directed toward determining the dose required to produce a given density for Kodak FGP film at various x-ray kilovoltages. Data have been obtained relating density and atomic number at several kilovoltages. A typical example is shown in Figure 14 which is plotted for the back emission technique only. Planned in the near future is an investigation of the forward emission technique.

The back emission technique is being used in an Air Force Materials Laboratory program conducted by the AVCO Corporation. Program objectives (5) are to develop and

apply NDT techniques for inspecting refractory coatings. Figure 15 is an electron radiograph of a Cr-Ti-Si base coating on a columbium substrate. The radiograph revealed high and low density areas in the coating. Failure occurred in the low density areas after 38 hours of furnace exposure at 2600°F. Results of electron beam probe analysis indicate that the low density areas are low in chromium content. This condition results in reduced oxidation resistance.

The limitation of the technique is that intimate contact must be maintained between the surface to be inspected and the fine grain emulsion. At present, the technique can only be utilized to inspect large refractory coated surfaces or curved leading edges. By taking advantage of the rapid advances in particle encapsulation and strippable films, it may be possible to obtain an electron sensitive, x-ray insensitive, film emulsion which can be sprayed or painted on the surface to be inspected. After exposure to x-rays, the emulsion can then be stripped and developed by conventional methods. This would assure availability of an NDT method for inspecting refractory coatings on future aerospace vehicles.

CONCLUSIONS

Three programs have been described which are typical of programs being supported by the Air Force in the field of nondestructive testing. The investigation of the impact method is being conducted in order to develop an NDT technique for inspecting operational aircraft for fatigue cracks in turbine discs and beneath fasteners. As such, the program represents a developmental effort directed toward solving a current problem on in-service aircraft. This is in contrast to electron radiography and other NDT techniques presently being investigated for inspecting refractory coatings. Refractory coatings are developmental materials which will be utilized on future aerospace vehicles to protect leading edge structures from oxidation. Magnetoabsorption, a method for measuring residual and applied stress in ferromagnetic materials, would be applicable for both operational and future Air Force systems. At the present time the method would be useful for determining the stress distribution (and possibly, incipient fatigue failure) in critical aircraft structures such as landing gears and engines.

Thus an effort is being made by the Air Force not only to develop and apply NDT techniques to in-service aircraft, but also to developmental materials which may become part of future aerospace vehicles. Application of conventional NDT methods and exploratory development of new NDT techniques for materials in this latter category is more difficult because the principal causes for failure have not been determined. This requires an extensive program to correlate mechanical properties, property variability, and performance with the NDT measurement(s). Such an effort is justified because it establishes the limits of sensitivity of conventional techniques, and more important, points out areas where these techniques may be inadequate. In this manner new techniques may be developed which will be available to permit a complete inspection of the material when it becomes part of an operational system.

REFERENCES

1. "Device for Inspecting Helicopter Blade Bonding," Development of General Specifications for FAA Test and Experiment Division, Atlanta, N.J., Nov., 1959.

2. Schrocer, R. and Garmhausen, T., "Research on Exploratory Development of Nondestructive Methods for Crack Detection," AFML-TR-67-167, June, 1967.

3. Rollwitz, William L. and Claassen, John P., "Special Techniques for Measuring Material Properties," ML-TDR-64-123, April, 1964, AFML-TR-65-17, January, 1965, and AFML-TR-66-76, October, 1966.

4. Shelton, William L., "Electron Radiography," AFML-TR-67-114, June, 1967.

5. Stinebring, R.C. and Sturiale, T., "Development of Nondestructive Methods for Evaluating Diffusion Formed Coatings on Metallic Substrates," AFML-TR-66-221, September, 1966.

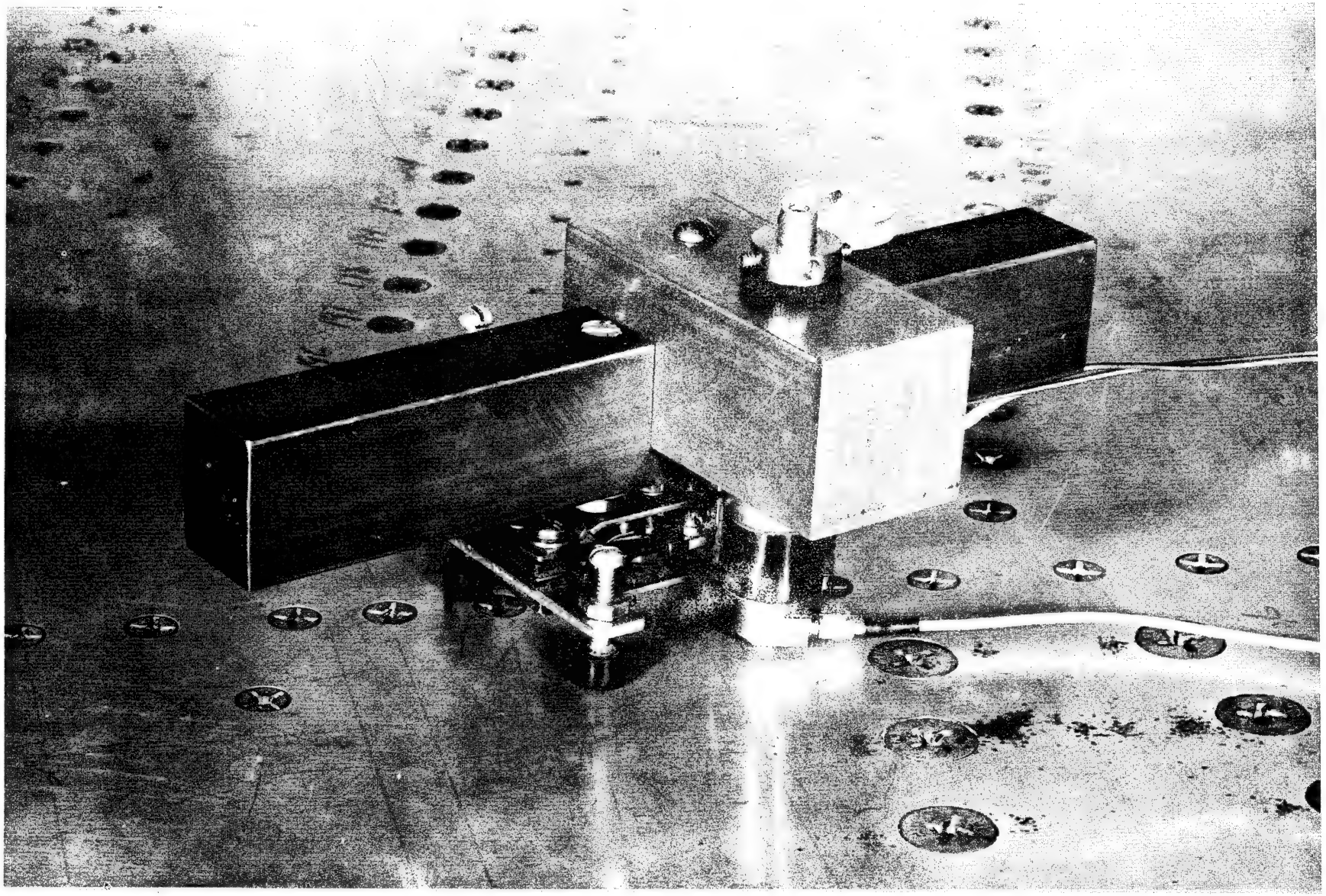

FIGURE I VIBRATOR/ACCELEROMETER ASSEMBLY USED FOR ACOUSTIC TECHNIQUE

NO CRACK

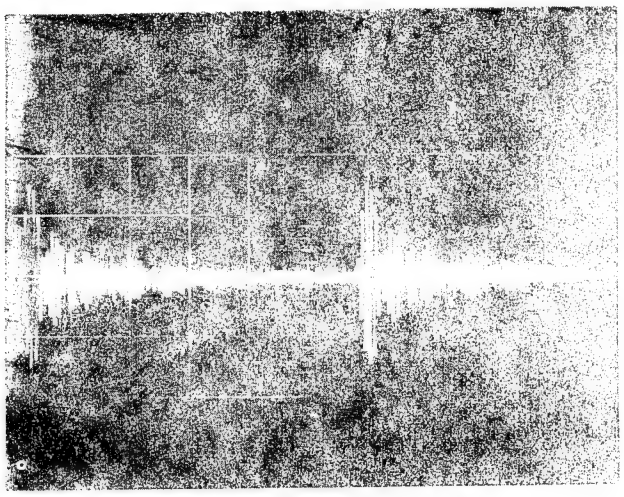

WITH CRACK

FIGURE 2 PULSE PATTERN FROM NON-CRACKED AND CRACKED SAMPLES 6KHZ - 12.8 KHZ FREQUENCY BAND

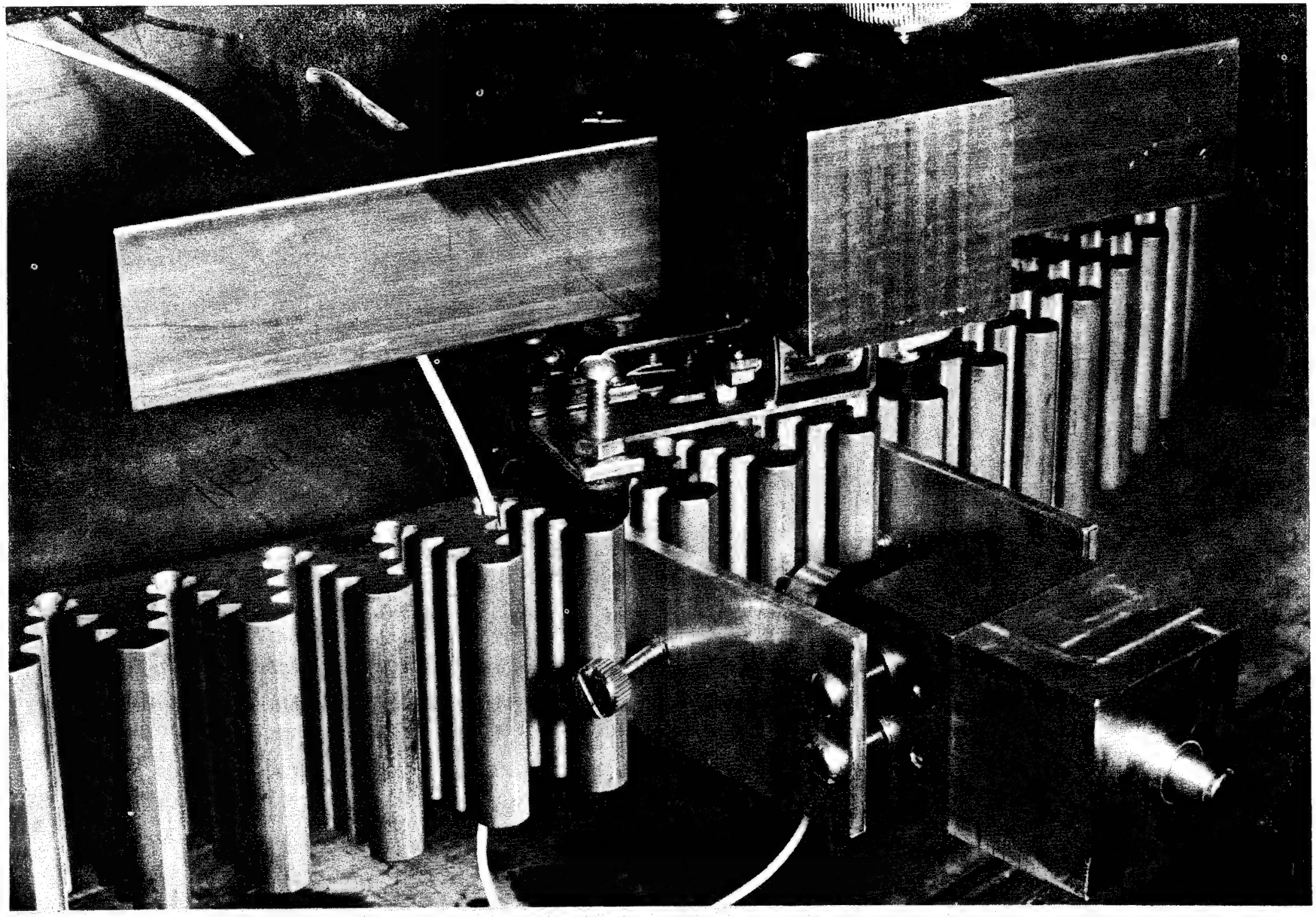

FIGURE 3 EQUIPMENT ARRANGED FOR TESTING COMPRESSOR DISC

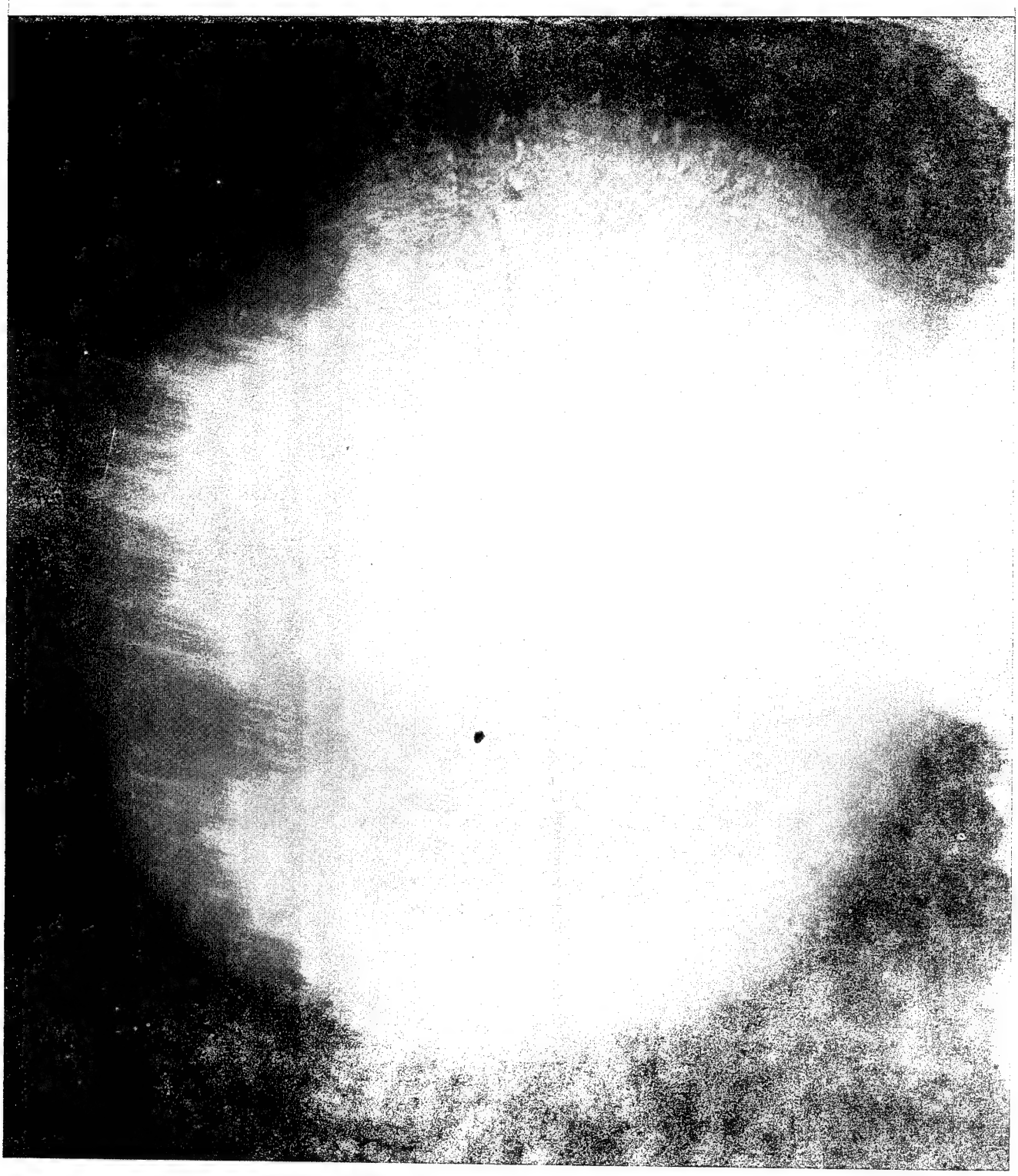

FIGURE 4 38 X OPTICAL VIEW OF ROOT CRACK IN TURBINE DISC.

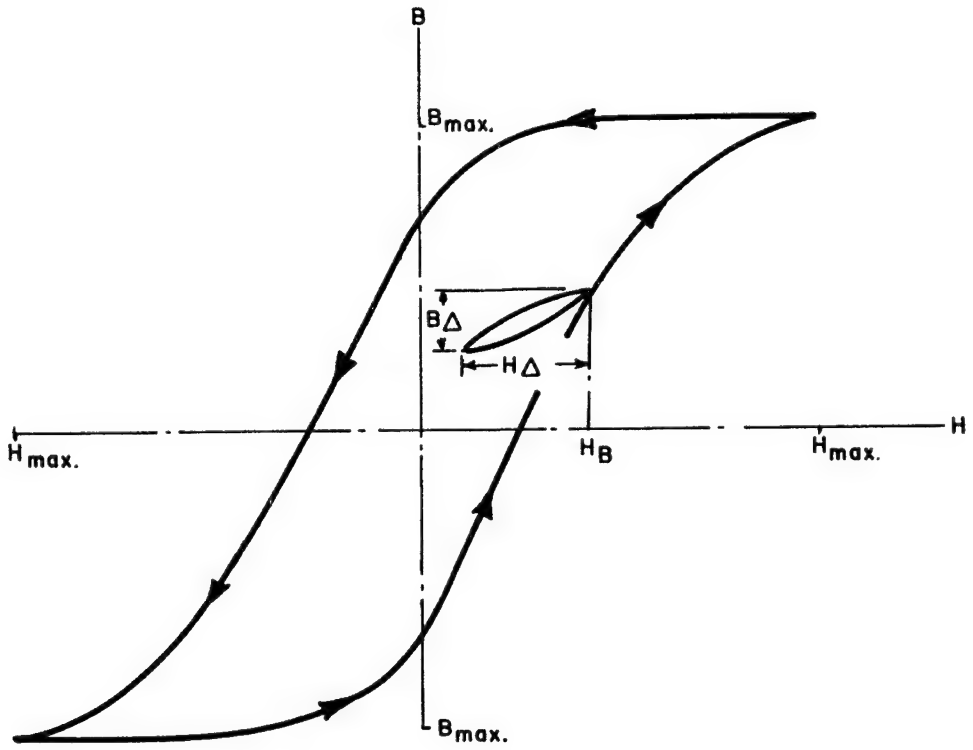

FIGURE 5 B VS H CURVE - MAGNETOABSORPTION

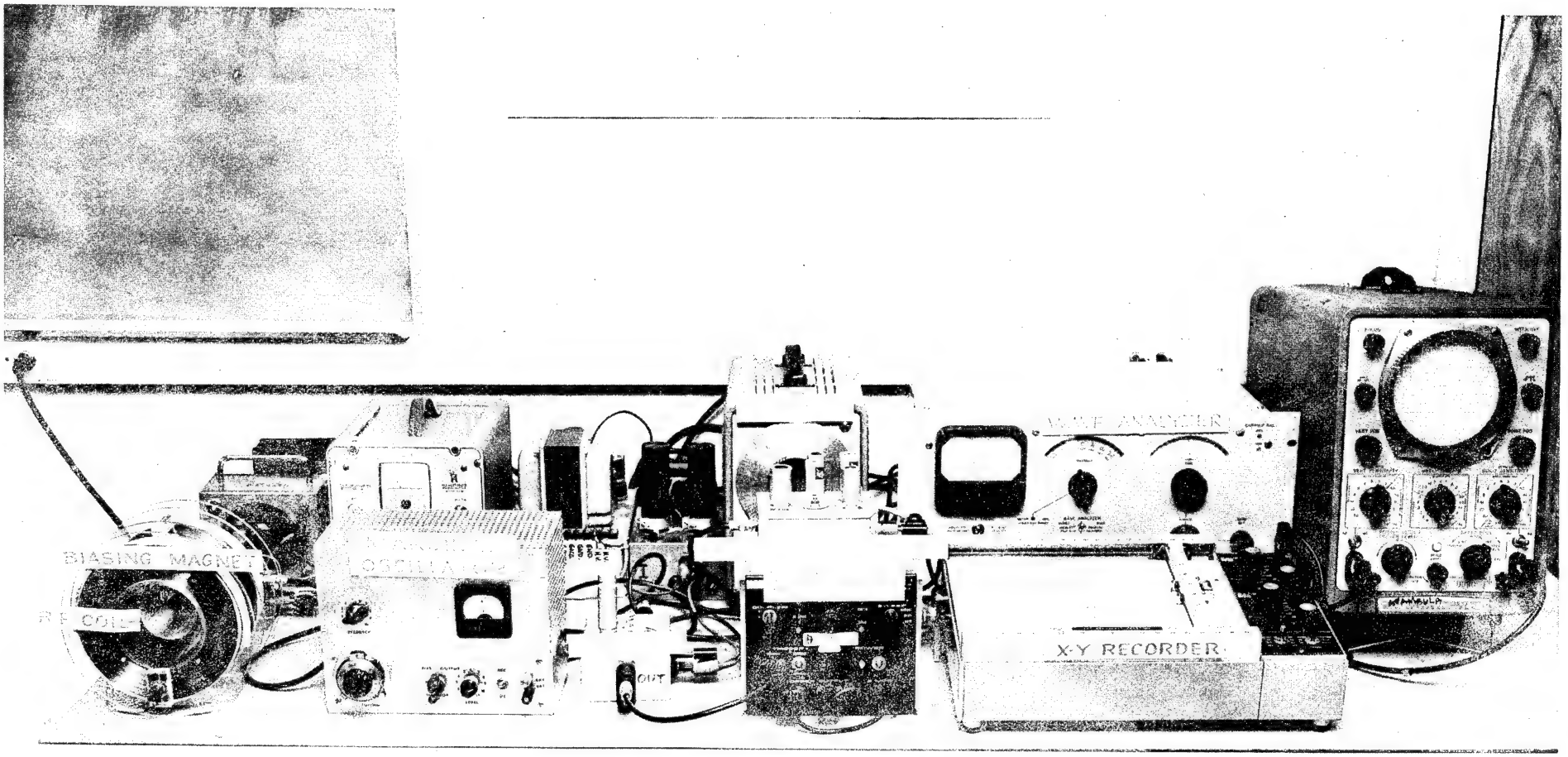

FIGURE 6 MAGNETOABSORPTION INSTRUMENTATION

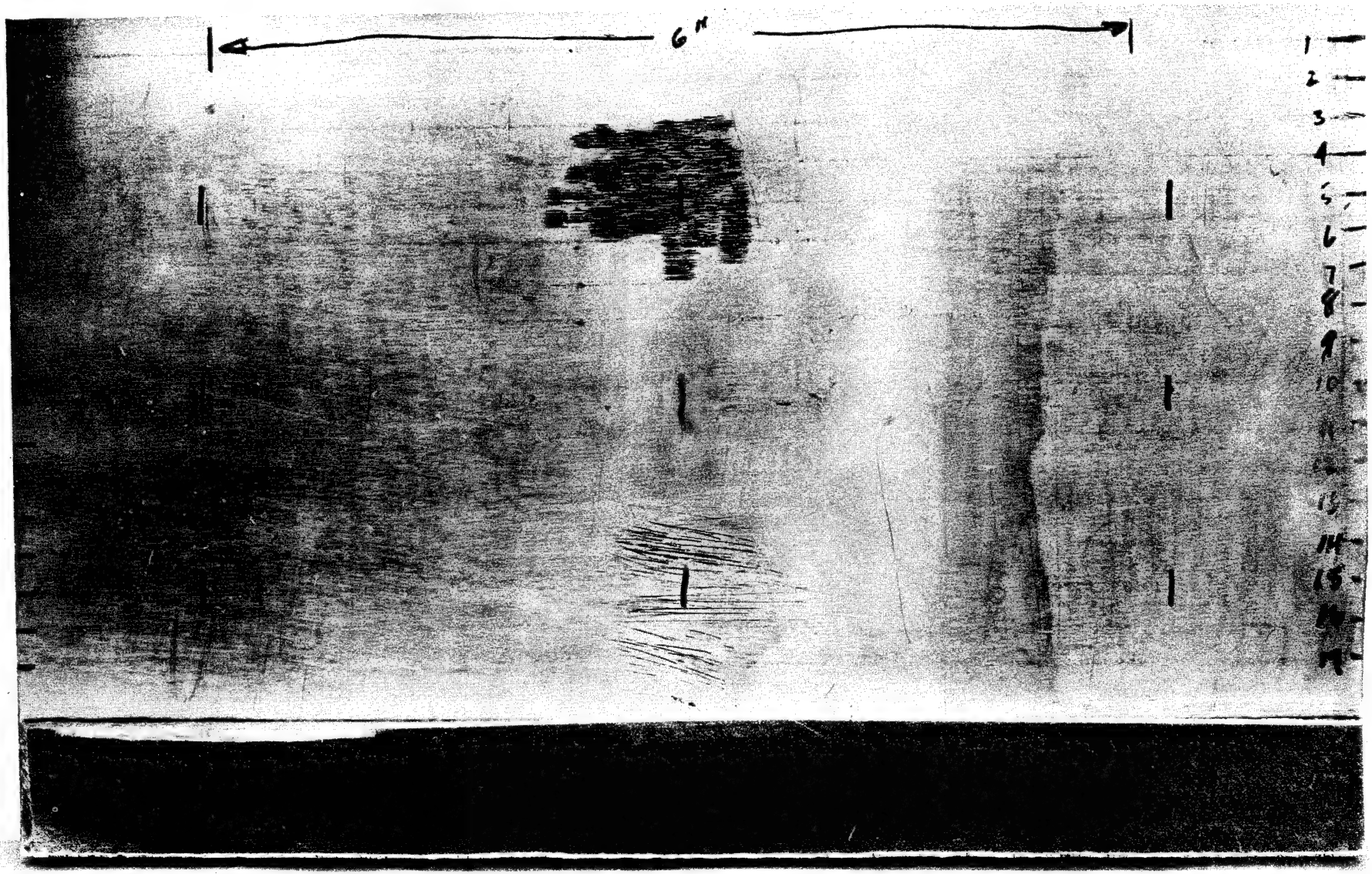

FIGURE 7 MARAGING STEEL PLATE WITH EDM SLOTS

FIGURE 8 DOUBLE - D R-F COIL

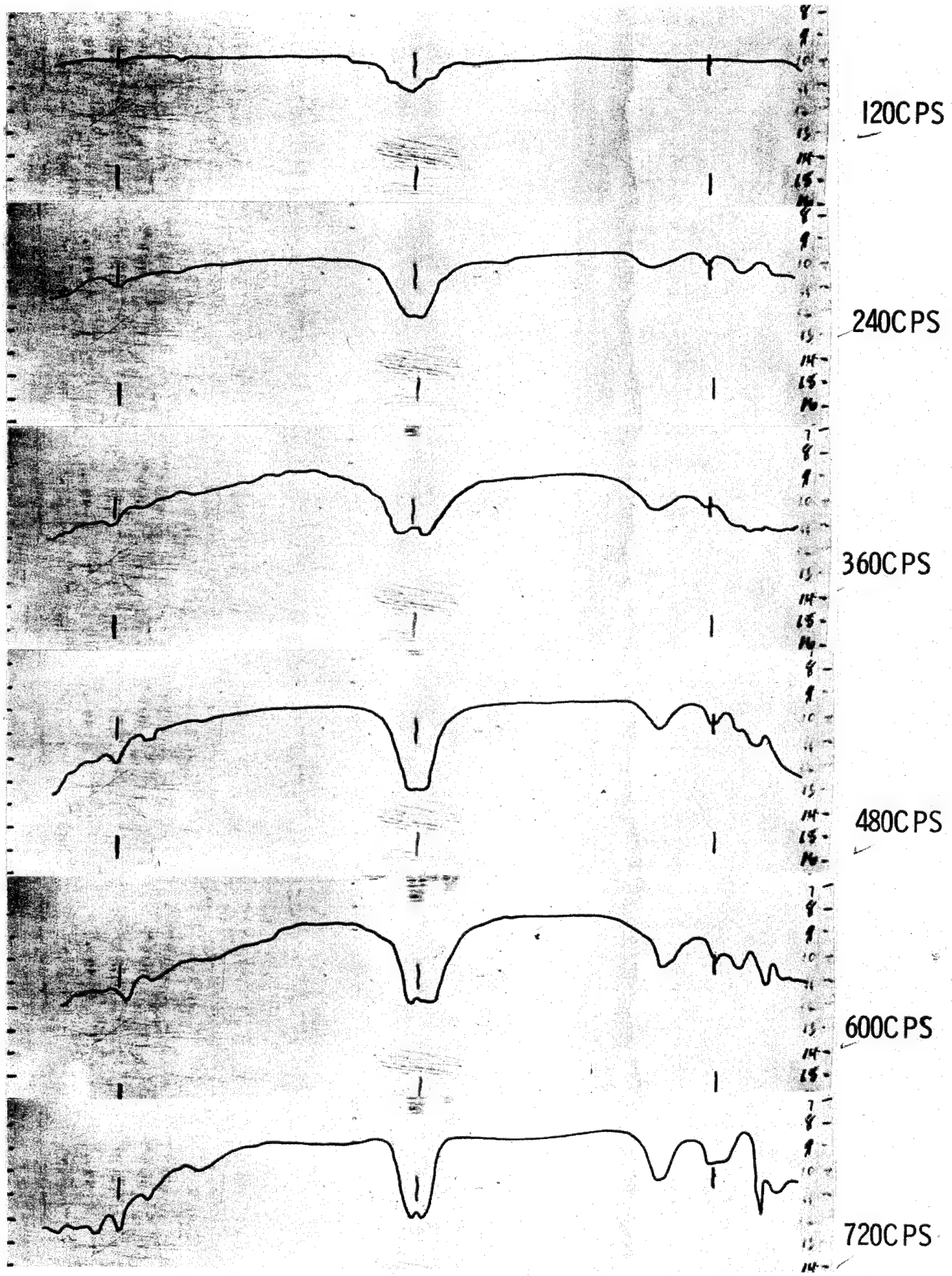

FIGURE 9 AMPLITUDE VARIATION OF MAGNETOABSORPTION SIGNA I HARMONICS FOR ONE SCAN LINE ACROSS MARAGING STEEL PLATE

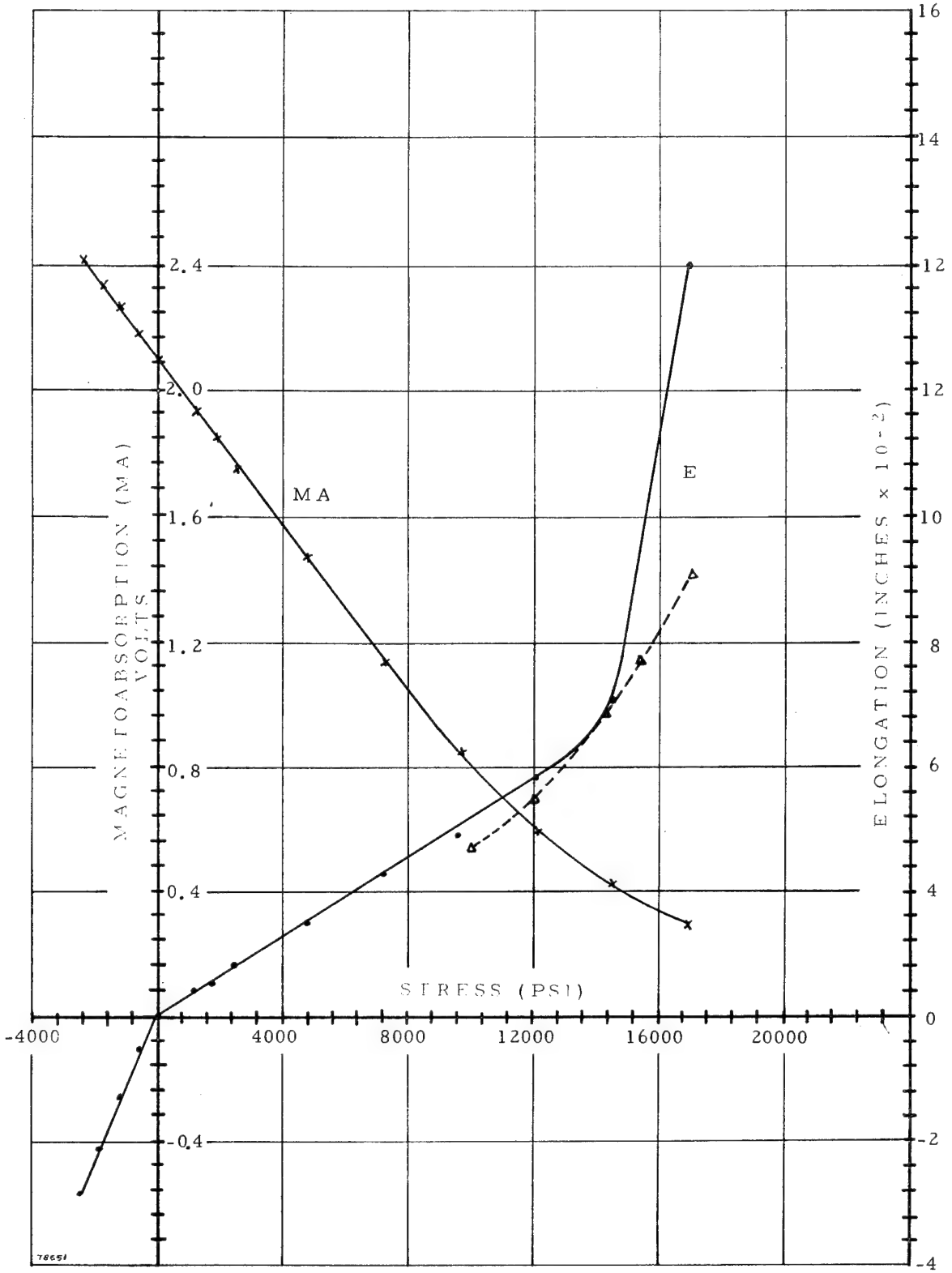

FIGURE 10 MAGNETOABSORPTION AMPLITUDE VERSUS STRESS AND STRAIN FOR ANNEALED NICKEL PLATED ALUMINUM ROD

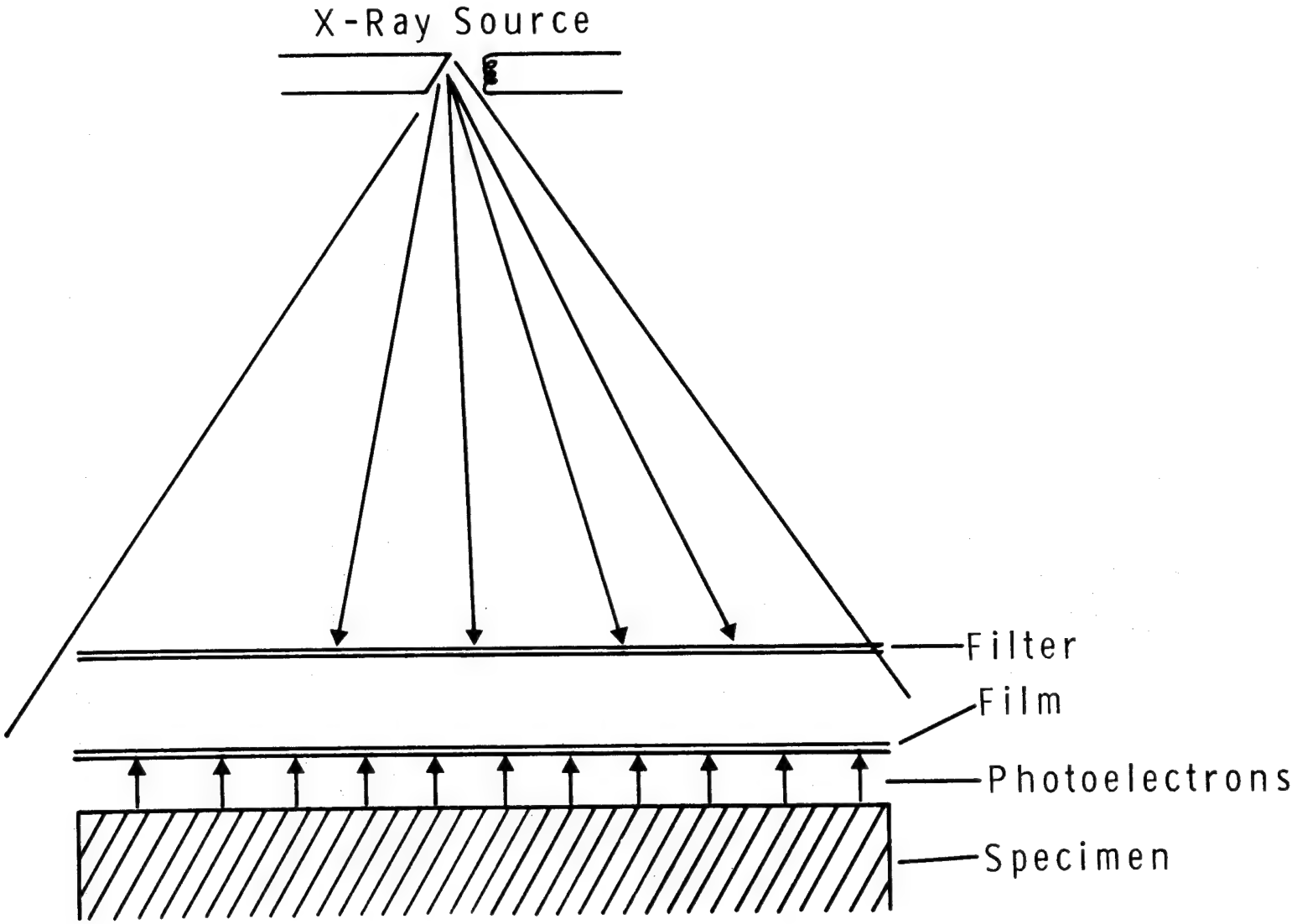

Fig. 11 - Back Emission Electron Radiography

X-rays are filtered, passes through the photographic emulsion, strikes the specimen, Photoelectrons are emitted which return and penetrate the film emulsion making an image.

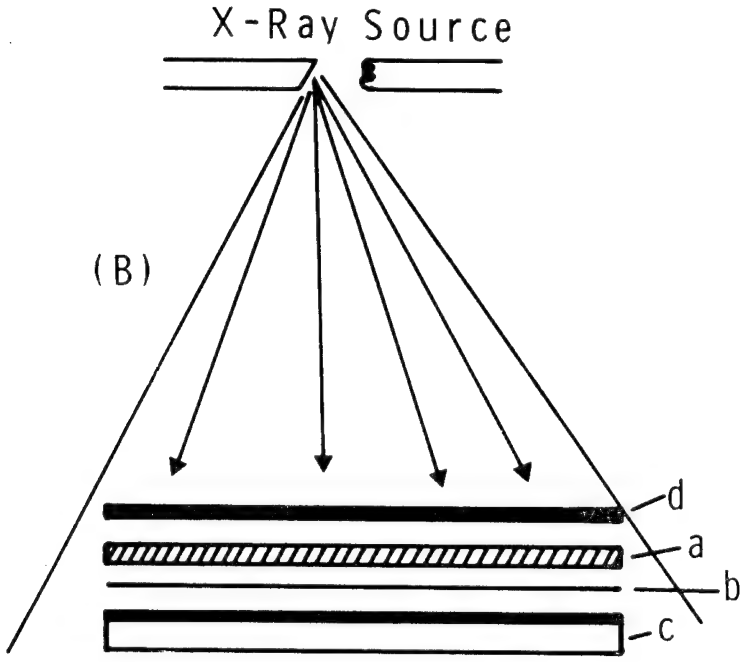

a. Radiator (High atomic number material)
b. Specimen (thin)
c. Photographic Emulsion
d. Filters (Al, Cu)

FIGURE 12 FORWARD EMISSION ELECTRON RADIOGRAPHY

FIGURE 13 FORWARD EMISSION ELECTRON RADIOGRAPH

FIGURE 14 FPG FILM DENSITY VERSUS ATOMIC NUMBER AT 175 KVCP

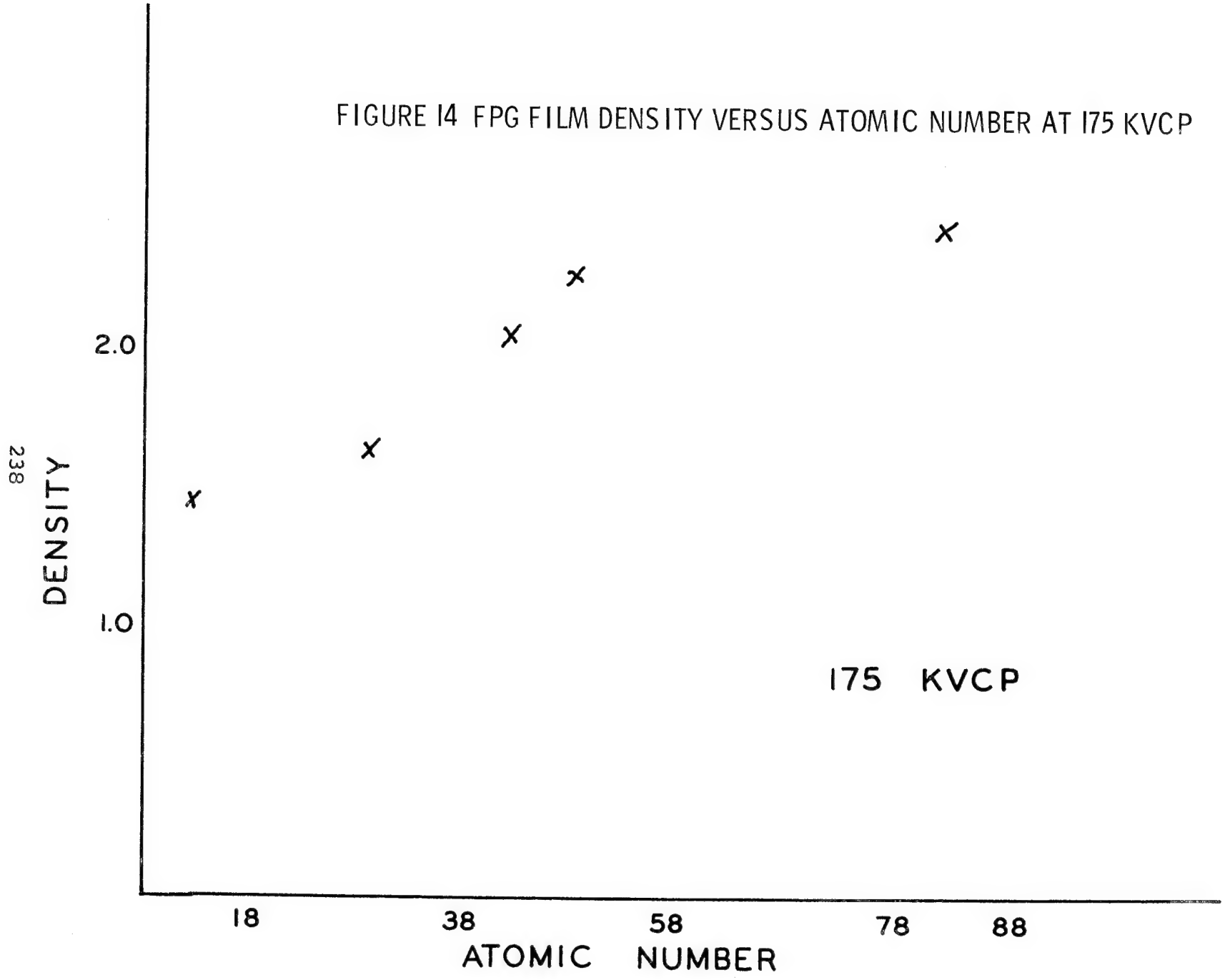

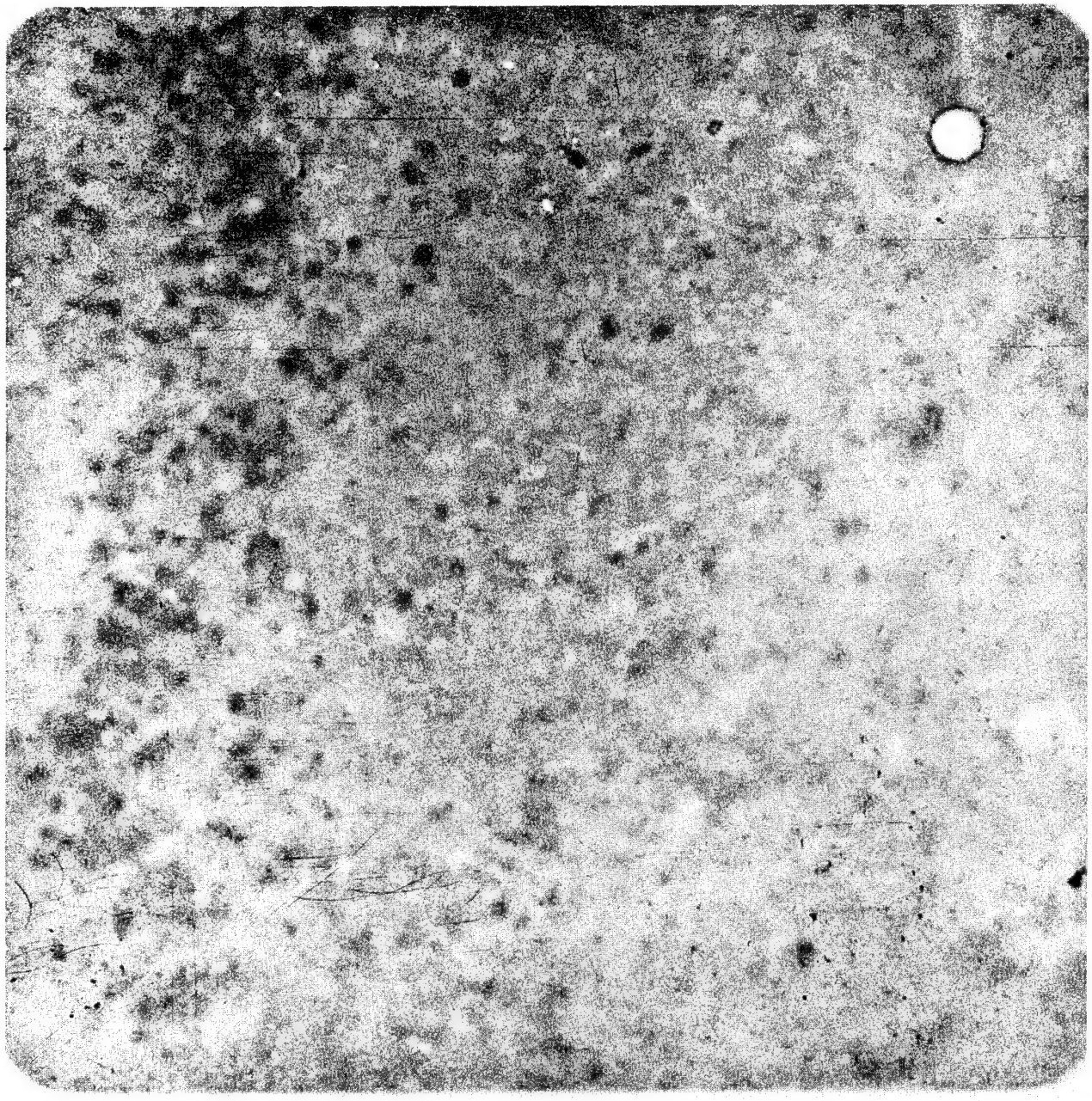

FIGURE 15 BACK EMISSION ELECTRON RADIOGRAPH OF SILICIDE COATED SAMPLE

ADDITIONAL PRESENTATIONS AND HANDOUT MATERIAL*

PAPER - DATA AND EQUIPMENT FOR PROCESS CONTROL OF EXPANDED PAPER HONEYCOMB ENERGY DISSIPATER MATERIALS - Morris L. Budnick, U. S. Army Natick Laboratories, Natick, Massachusetts

PAPER - ACCEPTANCE OF RADIOGRAPHY FROM A PROCESS IN CONTROL - W. E. Medinger, W. R. Schmechel and A. C. Malchiodi, Quality Assurance Dept., Supervisor of Shipbuilding Conversion and Repair, USN, Groton, Connecticut

PROBLEM - DETECTION OF UNBONDED AREAS BETWEEN TANK WALL AND ROLLING BLADDER - Robert A. Gould, Naval Weapons Center, China Lake, California

*Not discussed during Conference.
It is requested that any information or comments that could aid the authors be forwarded to them.

DATA AND EQUIPMENT FOR PROCESS CONTROL OF EXPANDED PAPER HONEYCOMB ENERGY DISSIPATER MATERIAL

MORRIS L. BUDNICK
U. S. ARMY NATICK LABORATORIES

Expanded paper honeycomb is the current standard energy dissipater material used in military airdrop operations. This paper describes what was done to assure that expanded paper honeycomb panels with the required dynamic crushing stress property are furnished for airdrop operations. Tests of commercially available expanded paper honeycomb panels disclosed that this material crushes at an essentially constant stress of 6000 pounds per square foot, plus or minus 10 percent, through zero to 70 percent strain and that the crushing stress increases rapidly beyond the 70 percent.

The short film I shall show now will give you a better understanding of how expanded paper honeycomb is used as an energy dissipater material to provide protection against damage on ground impact to airdropped materiel. The first sequence will show the airdrop of a vehicle loaded platform from an aircraft in flight, the second will show the free fall drop of a vehicle loaded platform and the third will show the impact testing of expanded paper honeycomb samples on the horizontal impact tester at the U. S. Army Natick Laboratories.

MATERIALS AND METHODS

MATERIALS

The material I have in my hand is a sample of commercially expanded paper honeycomb panel. The core of the original commercial paper honeycomb material under discussion is 80-pound kraft paper. The cells of the expanded, double faced panels have parallel faces, are hexagonal and 1/2-inch in size, nominal. The size is the dimension between any two parallel faces. The panel thickness is 3 inches. The facing sheets may be either 80- or 126-pound kraft paper. Both the core and facing papers are 100 percent unbleached kraft fiber. The adhesive is water resistant, urea formaldahyde emulsion type. The size of the panels procured normally for military airdrop operations is 3 x 8 feet. Specification MIL-H-9884, Honeycomb Material, Cushioning, Paper, prepared and issued to permit competitive procurement of expanded paper honeycomb panels, is a detailed specification which calls for certain chemical and physical properties in the core and facing papers, certain physical properties in the adhesive, and dimensional requirements for the cell structure and the expanded, double faced panels.

TEST CRITERIA

Testing of standard Army vehicles using the expanded paper honeycomb material as the standard energy dissipater developed data used in the preparation and promulgation of Standard MIL-STD-669, Loading Environment and Related Requirements for Platform Rigged Airdrop Materiel. MIL-STD-669 is a reference document covering detailed technical airdrop requirements which are to be used during the development of military vehicles and equipment which have an airdrop requirement. Specifically, MIL-STD-669 requires that each military equipment which has an airdrop requirement be designed to accommodate the current standard expanded paper honeycomb energy dissipater system and, typically, shall withstand a deceleration force of 19.5 times, plus or minus 10 percent, its airdrop weight when decelerated from a velocity of 28.5 feet per second to zero feet per second upon ground impact. The airdrop weight is defined as the weight of the equipment including that of external or internal loads such as fuel, ammunition or field gear. Also, this standard states that the deceleration force of 19.5 times the airdrop weight will be met by using 3.1 square feet of expanded paper honeycomb crushing area for each 1000 pounds of the airdrop vehicle weight, the thickness of the crushing stacks to be 12 inches, composed of 4 layers of 3-inch thick expanded paper honeycomb panels. The values in MIL-STD-669 are based upon a nominal average dynamic crushing stress value of 6000 pounds per square foot, plus or minus 10 percent through zero to 70 percent strain. The appendix to MIL-STD-669 lists three energy dissipater configuration design equations: these are used to calculate values necessary to design energy dissipater configurations. The equation of particular significance as regards the dynamic crushing stress property of expanded paper honeycomb panels is

$$A = \frac{W\ (G/1)}{S_a}$$

This equation is used to determine the total energy dissipater area required (A) with the vehicle airdrop weight (W), the average dynamic crushing stress (S_a), and the design deceleration ratio (G) given. The typical deceleration ratio has been established as 18.5. This value is based upon the desired maximum energy dissipater crushing stack height of 12 inches and the results of an investigation of standard military vehicles. It can be readily seen that the dynamic crushing stress property is significant to the design of an effective energy dissipater system. If the total energy dissipater area for a particular piece of military equipment is computed, based upon an average dynamic crushing stress value of 6000 pounds per square foot, and the actual value, for some reason, is but 4000 pounds per square foot, the resulting computed

energy dissipater area will be too small. Upon ground impact, the energy dissipater will bottom out before the energy has been dissipated at the desired deceleration level. This means that the expanded paper honeycomb will crush beyond the 70 percent strain and the crushing stress will rise rapidly resulting, in many instances, in damage to the airdropped vehicle or equipment. Conversely, if the average dynamic crushing stress value of the expanded paper honeycomb is significantly greater than 6000 pounds per square foot, the deceleration level increases proportionately. This, again, could result in severe damage to the vehicle or equipment. The above facts demonstrate the importance of controlling the average dynamic crushing stress property of expanded paper honeycomb which is currently the energy dissipater material for military airdrop operations.

DISCUSSION

Specification MIL-H-9884, mentioned previously in this paper, is a detailed specification which controls some properties of the materials and the geometry requirements, but which does not make reference to or control the average dynamic crushing stress of the expanded paper honeycomb panel. It had been recognized, conclusively, that the average dynamic crushing stress property of the energy dissipater material is of major functional significance to airdrop operations. It had been considered that by controlling some properties of the materials and the geometry requirements of the expanded paper honeycomb panel, the average dynamic crushing stress property would be controlled. Testing of expanded paper honeycomb panels from several sources disclosed a wide variation in the average dynamic crushing stress value despite the fact that the panels conformed to the material and geometric requirements, essentially. It was self-evident that Specification MIL-H-9884 must be changed at once to effect control of the average dynamic crushing stress property of expanded paper honeycomb panels being procured for energy dissipater use. Exceptions to Specification MIL-H-9884 were issued. The average dynamic crushing stress property was made a requirement of the expanded paper honeycomb panels. Paper basis weight, cell size, panel density, and glue line spacing and thickness become reference data. These changes in the specification require the suppliers of expanded paper honeycomb panels to establish and control both the processes used to produce the honeycomb cores and to expand and double face the honeycomb cores into panels.

The average dynamic crushing stress value for the expanded paper honeycomb panels, the method of performing the dynamic crushing stress test, and the quality assurance and acceptance data are set forth in the

proposed revision of Specification MIL-H-9884. This proposed revision is now in the Department of Defense and Industry Coordination Phase. For the test, two specimens, each 16 x 18 inches, are selected from 5 randomly selected expanded paper honeycomb panels, each 3 x 8 feet, to make 5 samples. The two specimens from each panel make one sample which is subjected to an impact test to determine the average dynamic crushing stress value for each of the panels. The 16 x 18 inch size is used to minimize blowout and other edge effects, the double thickness to reduce the possibilities of bottoming out upon impact. The impacting mass shall insure at least 70 percent strain at velocity of 24 to 29 feet per second. If testing is done by means of a drop tower, the sample is stationary and the impacting mass free falls at the velocity noted above. If testing is done on the horizontal impact tester, the impacting mass and the sample move toward each other at a velocity of 15-feet per second or a relative velocity of 30-feet per second. On the basis of data furnished by instrumentation, a stress strain curve is made. If the average dynamic crushing stress value from each test conforms to specification requirement, the lot of expanded paper honeycomb panels is acceptable as regards the dynamic crushing stress requirement. If only four out of five values conform, a retest is made. For the retest, 16 specimens are selected to make 8 samples. If the value for 7 of the 8 samples are in conformity, the lot is considered to meet the specification requirement. The sampling plan and the related acceptance criteria are essentially those specified by Standard MIL-STD-105, inspection level S-1, AQL-2.5, normal inspection. It is a source of satisfaction that expanded paper honeycomb panels accepted to date, using the above quality assurance criteria are performing effectively as energy dissipater material for airdrop operations.

TEST EQUIPMENT

The inclusion of the dynamic crushing stress requirement in Specification MIL-H-9884 generated a new problem - that of the availability of test equipment. Evaluation of expanded paper honeycomb panels from a number of sources indicated that there is a greater correlation between the expanded cell size and the dynamic crushing stress property than there is between any of the material and dimensional requirements. This means that a change in the extent of expansion of the paper honeycomb core has the greatest effect on the nominal average dynamic crushing stress value. It is not to be implied that glue line thickness and spacing, the type of the adhesive, or the paper physical and chemical properties are to be ignored. Each has an effect, but the extent of expansion has the greatest. At the time the average dynamic crushing test property was made a requirement for expanded, double faced paper honeycomb panels, there were but two facilities which had the equipment

to conduct dynamic crushing stress tests. One is located at the Engineering Mechanics Research Laboratory, the University of Texas, the other at the Research and Development Laboratory, Airdrop Engineering Laboratory, U. S. Army Natick Laboratories. It is obvious from the picture of the drop tower on the screen that this equipment is highly specialized, and not the type that could be set up and the cost amortized on a contract by contract basis. The same is true of the horizontal impact tester located at the U. S. Army Natick Laboratories. Both pieces of equipment are complex and expensive to install, require extensive space, and must take environmental factors into consideration.

It was recognized that industry must have readily available either equipment or sources for dynamic crushing stress testing of expanded paper honeycomb panels. As static testing facilities are usually available, an attempt was made to establish a correlation between static crushing tests and dynamic crushing tests. This was not successful. Although a satisfactory correlation could be obtained by some plants, an industry wide conversion formula could not be established. The conversion factor for one source would not necessarily be true for another. The only practical solution to this problem was the development of a low cost dynamic crushing stress tester, easy to calibrate and maintain, and simple to operate.

The U. S. Army Natick Laboratories, therefore, placed a contract with the Engineering Mechanics Research Laboratory, the University of Texas to develop test equipment of this type. The equipment was to be simple in design, small in height, size, and weight, easy to operate, maintain, and calibrate, and, in addition, have a high degree of reliability as regards reproducibility of results. A further consideration was ease of readout of data; that is, no extensive or complicated computations to make or interpret before judgements could be made. The final consideration was cost: - the target was $2500.00. As you can see from the photograph on the screen, the Engineering Mechanics Research Laboratory developed such a tester. The team that worked on this development was comprised of students guided by the director of the Laboratory, Dr. Ripperger. The leader of the student group was a graduate student working for his Ph D. The other members were all undergraduates who, as composite, included quite a variety of skills and knowledge. Among them was an Aeronautical Engineer, Electronic Engineer, and a Psychology Major to assure consideration was given to human factors.

The equipment you see on the screen was developed and built in a matter of months. The overall height of the tester is approximately 12 feet. Its components are a free fall mass of a predetermined weight,

four steel guide rods to guide the movement of the mass, a catch and release device to be used in securing and releasing the mass, and electric hoist to raise the mass, a strain gage accelerometer, and oscilloscope, two plastic resistance strips, and a rapid development type camera. The strain gage accelerometer measures the stress. The two plastic resistance strips, one on the mass, the other on one of the guide rods, provide the voltage to drive the X axis or strain axis of the oscilloscope; the stress strain curve thus generated is recorded by the rapid development, polaroid type, camera. Each test record contains a 12,000 pounds per square foot calibration mark on the Y axis and a 100 percent strain calibration mark on the X axis. Readout of the average dynamic crushing stress of the sample tested is merely a matter of comparing the average height of the curve to the 70 percent strain mark with the Y axis calibration mark, or alternatively, by calculating the average height of the curve in relation to a strain of 70 percent, using a standard planimeter. The latter method is more precise than that obtained by using the Y axis calibration mark. The second method results in a more reliable value. Yet another method of readout is to compare the curve resulting from a specific test against a standard curve which has been recorded on a transparent film. As regards the time required to make the test and complete the readout, it is of interest that the Engineering Mechanics Research Laboratory made 16 tests and the readouts in two hours.

To check reproducibility of results from this test equipment, a drop is made using a material, such as styrofoam, for which the dynamic crushing stress value is known. As a check on the reliability of this test equipment to reproduce results, tests were made on samples composed of adjacent specimens from the same expanded paper honeycomb panels. The results indicated that the variation was not greater than 1-1/2 percent between the maximum and minimum results obtained. Since this same degree of variation was found in production lots of expanded paper honeycomb panels being furnished under a contract with the Army and tested on the other test equipment, the performance of the low cost simplified tester was demonstrated to be satisfactory. It can, therefore, be concluded that the University of Texas developed tester will reproduce results, consistently, with samples from homogeneous lots of expanded paper honeycomb.

The method of test for this equipment is the same as that used with the drop tower and the horizontal impact tester facilities. The sample is made of two specimens, each 16 x 18 inches. The mass is raised to the maximum height by the hoist and is released by pressing a button. The free falling mass impacts the sample, the stress strain curve is recorded on the oscilloscope and photographed by the preset polaroid

camera. All that remains is to readout and interpret the resulting curve. It might be of interest to note that the equipment, including all instrumentation, costs $2395.00, which is less than the established target cost of $2500.00.

The inclusion of the dynamic crushing stress requirement in Specification MIL-H-9884 presupposed that industry should have a means of determining the major performance capacity of expanded paper honeycomb panels and whether or not these panels meet the specification as an effective energy dissipater material for airdrop operations. The development of the low cost dynamic crushing stress tester, easy to operate, maintain, and interpret results provides industry with just that - a means of assuring that expanded paper honeycomb panels furnished as energy dissipater for use in airdrop operations meet the requirements and are operationally acceptable. It also makes available to industry and government an easy to operate and reliable test device for use in acceptance and surveillance testing of energy dissipater materials. It is gratifying to be able to say that the U. S. Army Natick Laboratories consider that it has essentially solved the problem of providing data and equipment to determine what is and what is not an operationally acceptable energy dissipater material for military airdrop use.

I will close this paper with a short film on the University of Texas developed dynamic crushing stress tester.

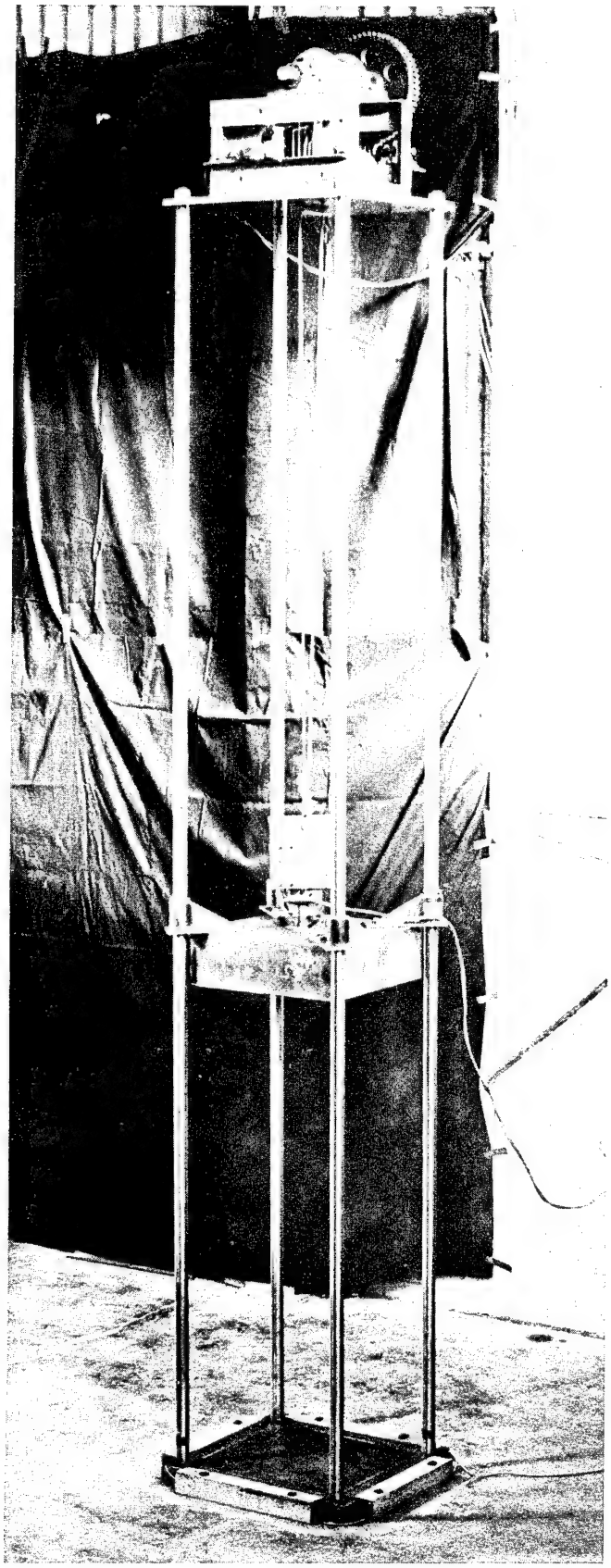

FIGURE 1. LOW COST DYNAMIC CRUSHING STRESS TESTER

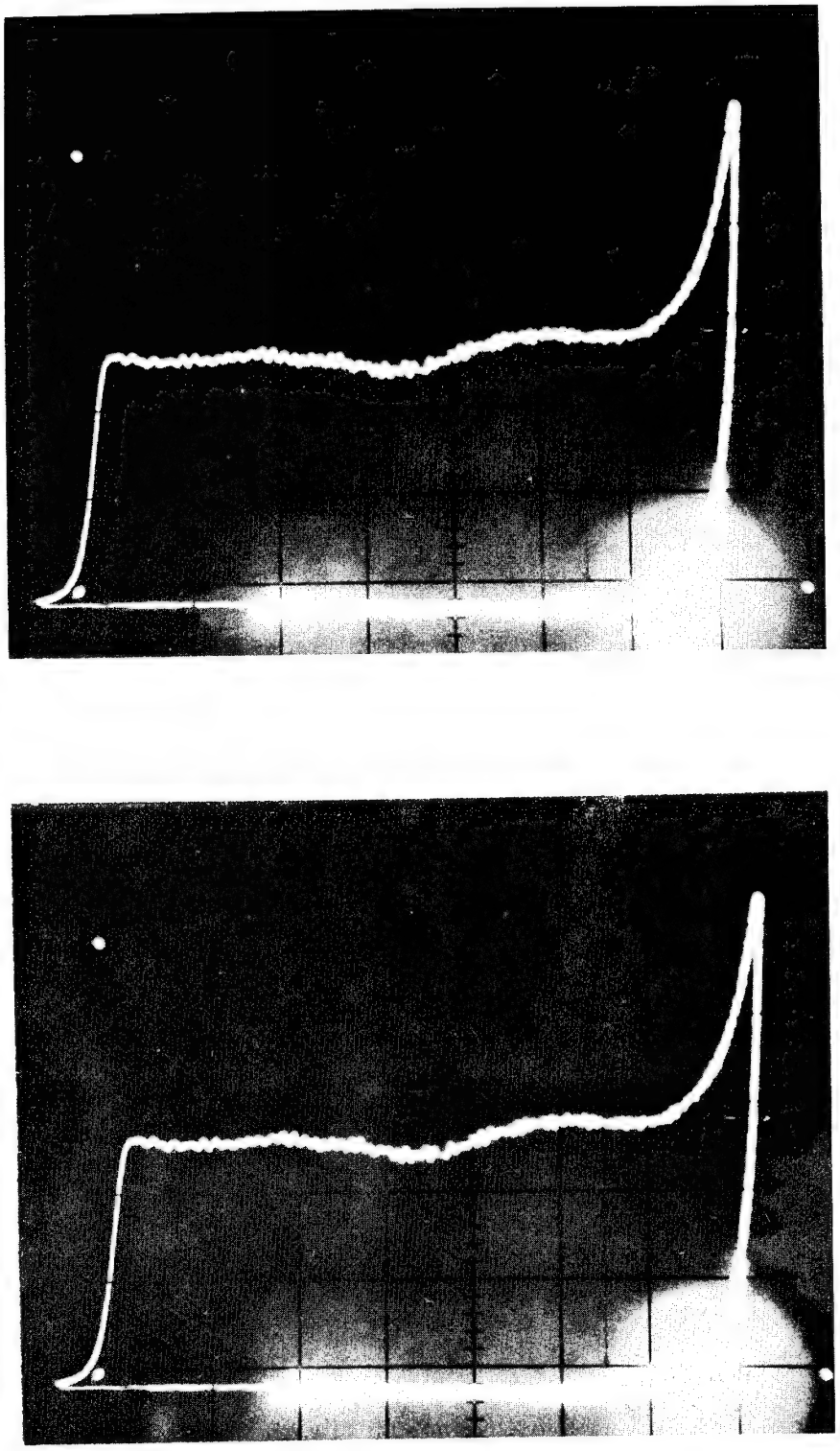

FIGURE 2. TYPICAL STRESS STRAIN CURVES

ACCEPTANCE OF RADIOGRAPHY FROM A PROCESS IN CONTROL

By

W. E. Medinger, W. R. Schmechel and A. C. Malchiodi
Quality Assurance Department, Supervisor of Shipbuilding
Conversion and Repair, USN, Groton, Connecticut

ABSTRACT

This paper is intended to convey a logical technique developed as a tool for Government acceptance of nondestructive testing on products of high production volume and critical in nature.

The nondestructive test problem which generated the solution presented in this paper was one of how the Government could best accept the radiographed products being produced by a private shipbuilder on a large number of nuclear submarines being constructed on a continuous basis. The critical nature of these products comes from the fact that they constitute pressure hull weldments, nuclear systems pipe welds, and castings in high pressure or critical systems.

All things being considered, the art of performing radiography and evaluating the results therefrom for purposes of nondestructive test acceptance of products has been considered to be a process. This process is continuous in nature and produces a homogeneous product that can be measured to determine the process average with regard to defectiveness being produced.

The scientific principle of radiography is not dwelled upon in this paper. Instead, the variability of application of this nondestructive test method is discussed as a part of the process used on ferrous and non-ferrous castings and pipe joints or on heavy hull structures. These variables are explained as they relate to the process and measure of process acceptability.

The principle of finding homogeneity of products from a continuous process performing at the point of inherent process capability has been well substantiated as has the probability of being able to determine the defectiveness in a finite lot of products by random sampling from the lot. The use of these principles is explained as they relate to the measure of control of the process of nondestructive test acceptance of products.

Since the technique requires a measure of the control of the process, then all radiographic products coming from the process will be considered as acceptable when the process exhibits a pre-defined acceptable state of control; and conversely, the products will all be considered unacceptable when the process goes beyond stated limits. This requires a refined measure of the parts of the process; and these measures are explained as they relate to the risks, probabilities, and limitations involved.

The data-keeping and decision-making functions of this technique are very important facets and take the form of standard control charts and Binominal Probability graphs. These tools are discussed as they relate to the measure of product characteristics distribution and ability to provide decisions to act in behalf of the Government in the acceptance of nondestructive testing.

ADDITIONAL PROBLEM

DETECTION OF UNBONDED AREAS BETWEEN TANK WALL AND ROLLING BLADDER
Naval Weapons Center, China Lake, California

Name of Product to be Evaluated - Missile liquid propellant tanks and positive expulsion bladders.

Kind of Material Involved - Tank wall -- .060 to .070 18% Ni, 250 grade maraging steel; rolling bladder -- .040 to .080 1100-0 aluminum bonded with .005 to .007 FEP Teflon.

Type of Process Involved - Bladder precoated with Teflon is placed in steel tank, heated to 600°F and expanded against steel tank with 100 psi internal pressure to obtain bond. Internal diaphragms bonded to steel sleeves using mechanical clamping pressure.

Design of Product - See figure below.

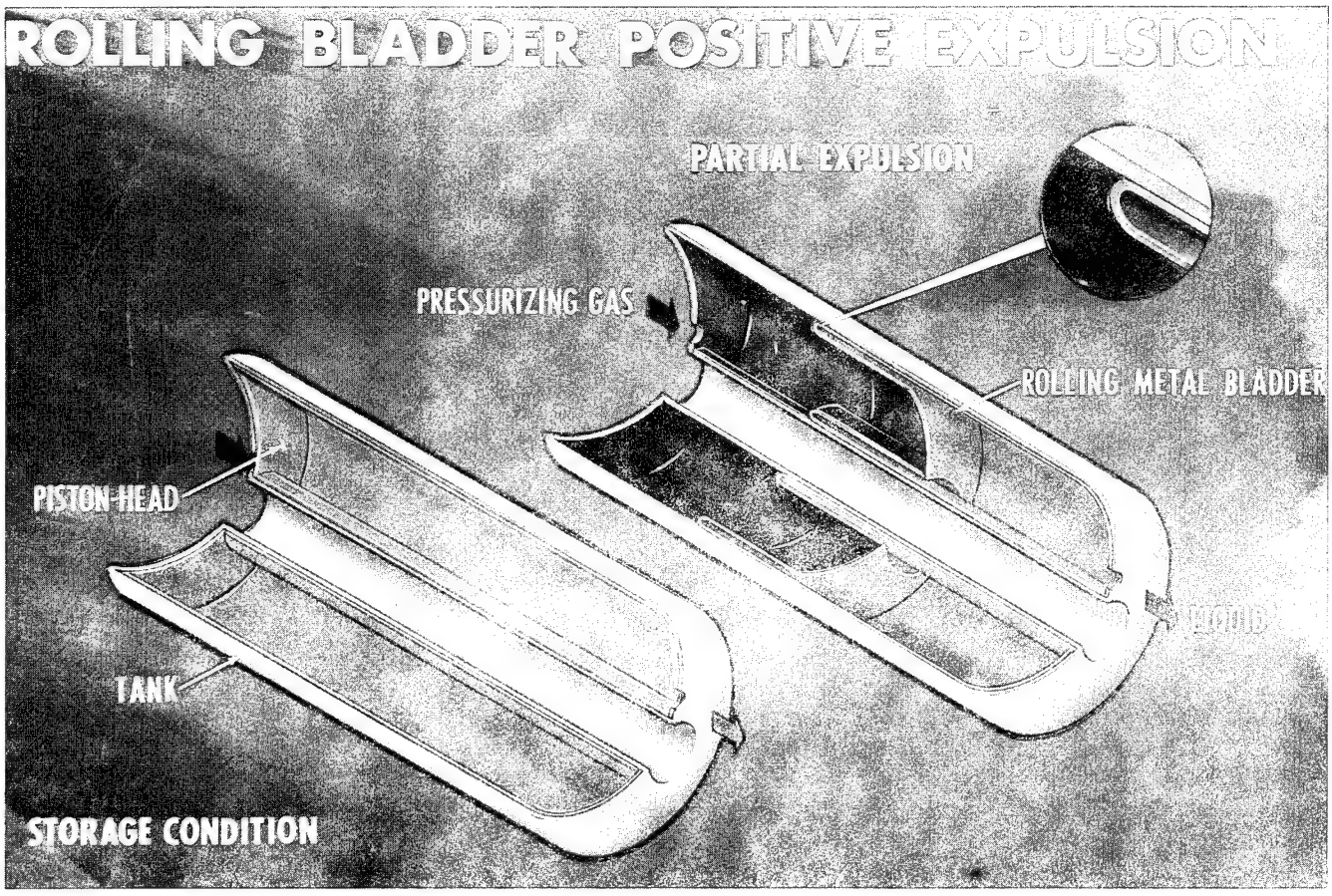

Quantity Involved - Will be used on tactical missile systems in quantities into thousands.

Kind of Quality Characteristic to be Evaluated - To assure proper operation of rolling diaphragm, quality must be controlled to assure bond of diaphragm to tank.

Magnitude of Quality Characteristics: At this time it is not known how large an unbonded area is permissible, however, it is believed that areas 0.25-inch or smaller are permissible. Unbonded areas larger than 0.25-inch must be detected and the assembly rejected.

Basis for Acceptance - The bond must now allow diaphragm to pull away from tank wall prior to operation of expulsion system or stoppage of the expulsion cycle may result. Rips in the diaphragm may also occur, causing catastrophic failure of the missile.

Urgency - Local Priority - This system is proposed as a back-up design for a missile now in development.

Feasibility of Redesign - Redesign could not eliminate the laminated wall design due to requirements placed on propulsion system, i.e., positive expulsion, five-year storage requirement of highly reactive propellants (all-welded containment).

Present Inspection Method - No method tried by contractor to date has been successful.

Limitations of Test Equipment - Either portable or stationary equipment.

Security Classification - Unclassified.

LIST OF ATTENDEES

SIXTEENTH DEFENSE CONFERENCE ON NONDESTRUCTIVE TESTING

Stanley J. Alster
U.S.Army Munitions Command
Bldg. 171, AMSMU-QC
Dover, New Jersey 07801
201 328-3223/3228

Eugene M. Ashton, SPL 3113
NavPlant Representative Office
Lockheed Missile & Space Co.
P. O. Box 504
Sunnyvale, California 94088
408 742-0831

William H. Baer
U.S.Army Mobility Equipment
Research & Development Center
Materials Research Laboratory
Bldg. 363
Fort Belvoir, Virginia 22060

Nicholas T. Baldanza
Plastec, Bldg. 3401
Picatinny Arsenal
Dover, New Jersey 07801

TSgt. Floyd W. Baker
NDI Monitor
HQ ADC(ADMME-B/NDI)
Ent Air Force Base
Colorado 80912
Autovon ext. 7208/7209

A. L. Baldridge
U.S.Army Test & Eval.Command
Attn: AMSTE-TA-A
Aberdeen Proving Ground,
Maryland 21005

Douglas W. Ballard
Supervisor of Mfg. Personnel
Sandia Laboratory
Sandia Base
Albuquerque, New Mexico 87115

Emmett G. Barnes
Radiographic Section
Bldg. 908 (SMUPA-NI-5)
Picatinny Arsenal
Dover, New Jersey 07801

E. R. Bartholomew
Federal Aviation Administration
Office of Supersonic Transport
SS-110
800 Independence Avenue, S. W.
Washington, D. C. 20590

Arthur D. Beatrice
Manufacture & Repair Inspection
3245 C.A.M. Sqdn.
ESBMH-4-2
L. G. Hanscom Field
Bedford, Massachusetts 01730

Richard J. Bedford
Headquarters
Defense Supply Agency
DSAH-PRQ
Cameron Station
Alexandria, Virginia 22314
OX 8 1448

LtCol. William F. Bennett
SAAMA(SANET)
Kelly Air Force Base, Texas 78254
Autovon 755 6400

TSgt. Richard A. Berg
1st CAMRON,c/o NDI Shop
Selfridge Air Force Base
Michigan 48045

Richard W. Blake AIR 09H33C
Naval Air Systems Command
Engr.& Integrated Support Office
Naval Air Station
Patuxent River, Maryland 20670
Autovon 555 1660 ext 7807

Lewis Bogdanoff
Philadelphia Naval Shipyard
Philadelphia, Pennsylvania
19112

Captain Louis S. Bodony
FU 3146582
4500th Air Base Wing (TAC)
Langley Air Force Base
Virginia 23365

Bernard W. Boisvert
Hq. SAAMA (SANTEP)
Kelly Air Force Base
Texas 78241
Autovon 755 6400

Eugene S. Bosinski
Met. Eng. Sect.T.S.L.
Bldg. 352
SMUPA-DT
Picatinny Arsenal
Dover, New Jersey 07801

Ellis J. Boudreaux
Naval Ordnance Station
Indian Head, Maryland 20640

Robert F. Boyd
WRAMA(WRMQQC)
Robins Air Force Base
Georgia 31093
Autovon 468-5887/4097

Robert R. Brauer
Page Aircraft Maintenance,Inc.
Dir. of Engr. and QA
P. O. Box 518
Fort Rucker, Alabama 36360
205 774-5131 x2877

Doyle L. Braun
SCASR/LA DCRL-QES
11099 S. LaCienega Blvd.
Los Angeles, California 90045
Autovon 833 1214

John F. Britt (DCRB-QES)
Defense Contract Admin.
Services Region
666 Summer Street
Boston, Massachusetts 02210

B. J. Brunty
Head, Test Section
Quality Evaluation Laboratory
Naval Weapons Station
Concord, California 94520

Dr. James I. Bryant
Army Research Office
Physical Sciences Division
3045 Columbia Pike
Arlington, Virginia 20370

Charles Brzesinski
Office of the Assistant
Secretary of Defense
The Pentagon
Washington, D. C. 20301

Garr J. Burt
SMULC-IE-Q
Lake City Army Ammo. Plant
Independence, Missouri 64050
816 SY6-3900 x57

Carl J. Bysura, Code 550A
Navav Weapons Services Office
U. S. Naval Base
Philadelphia, Pennsylvania 19112

Herbert F. Campbell
AMXMR-TMS
Army Materials and Mechanics
Research Center
Watertown
Massachusetts 02172
Autovon 956 1465

Louis C. Cardinal, Code 8434
Ocean Technology Division
U.S. Naval Research Laboratory
Washington, D. C. 20390

George D. Carney
Naval Plant Representative
Goodyear Aerospace Corporation
Akron, Ohio 44305

John Carosiello
Philadelphia Naval Shipyard
Philadelphia, Pennsylvania 19112

George A. Carver, Engineer
U.S. Army Weapons Command
AMSWE-QA 34400
Rock Island, Illinois 60201

Henry W. Caughman
Navy Plant Rep. Office (ENAA)
McDonnell-Douglas Corporation
P. O. Box 516
St. Louis, Missouri 63166
314 PE1 2121 ext 2665

Herbert W. Chandler
Director, Engineering Division
Naval Plant Rep. Office
Baltimore, Maryland
c/o Westinghouse Electric Corp.
Box 1693, Baltimore, Md. 21203

Henry H. Chaskelis, Code 8434
U. S. Naval Research Laboratory
Washington, D. C. 20390

Albert L. Chick, Code 934
U. S. Naval Applied Science Lab
Brooklyn, New York 11251

MSgt. Victor H. Christenson
363 FMS
Shaw Air Force Base
Sumter, South Carolina 29152

Eugene S. Cocsinski
Picatinny Arsenal
Dover, New Jersey 07801

James A. Conway
Army Materials & Mechanics
Research Center
Arsenal Street
Watertown, Massachusetts 02172
Attn: AMXMR-TMS
Autovon 956 1465

Joseph E. Costello
Code 305B Lab Branch
Quality Assurance Division
Building 121
Philadelphia Naval Shipyard
Philadelphia, Pennsylvania 19112

Christy W. Cottrill QALT-2
Quality Evaluation Laboratory
Naval Ammunition Depot
St. Juliens Creek
Portsmouth, Virginia 23702
Autovon 555 1670 ext 3236

Edward L. Criscuolo, Code 223
U. S. Naval Ordnance Laboratory
White Oak
Silver Spring, Maryland 20910

Maurice J. Curtis, Code 5503
Naval Weapons Center
China Lake, California 93555
Autovon 898 1700

Stanley Dabrowski, NXED
Picatinny Arsenal
Dover, New Jersey 07801

Henry C. Dade, SAVAE-QL
ARADMAC(Laboratory)
U. S. Naval Air Station
Corpus Christi, Texas 78419

James A. Davis
OCAMA (OCNCTS)
Tinker Air Force Base
Oklahoma 73145

Charles F. Dieter, Jr. ORD-03322
Naval Ordnance Systems Command
Navy Department
Washington, D. C. 20360

John R. Edgar
Defense Contract Admin. Services
1580 East Grand Blvd.
Detroit, Michigan 48211
Attn: DCRD-QES

William N, Ember
NASA Hqs.
400 Maryland Avenue, S. W.
Washington, D. C. 20546

D. E. Evans
DCASD (DIQE), Bldg. 1
Fort Benjamin Harrison
Indianapolis, Indiana 46249
317 546-9211 ext 2183

Dwight O. Fearnow
Air Force Flight Dynamics Lab
Experimental Mechanics Branch
AFFDL/FDTE
Wright-Patterson Air Force Base
Ohio 45433

Patrick J. Fetta, Code P 4522
Naval Undersea Warfare Center
3202 E. Foothill Blvd.
Pasadena, California 91107
Autovon 873-1318

MSgt. Donald E. Findlay
438 Stockton Street
4500 CAMSgt
Langley Air Force Base
Hampton, Virginia 23369
764-2961

Kenneth A. Fowler
U.S. Army Materials & Mechanics
Research Center
Federal Street
Watertown, Massachusetts 02172
AMXMR-TMT
Autovon 956 1445

Harold U. Frazes
DCASR-Chicago
DCRI-QES
O'Hare International Airport
P. O. Box 8758
Chicago, Illinois 60666
Autovon 930 6247

Donald V. Gallagher
Code 130M2
San Francisco Bay Naval Shipyard
Vallejo, California 94590
646 2224

David L. Gamache
Army Tank-Automotive Command
Attn: AMSTA-QED
Warren, Michigan 48090

John E. Garriss
Physical Test Laboratory
Field Evaluation Division
Technical Sup't Dir.
Edgewood Arsenal, Maryland 21010

William H. Geatty
Naval Plant Rep. Office
c/o Westinghouse Electric Corp.
Box 1693, Baltimore, Md. 21203

Calvin S. George
Dir/QA SMUFD-QA
Fort Detrick
Frederick, Maryland 21701

Kenneth H. Gerred
Naval Air Systems Command 09144
Weapons Personnel Research Div.
Engr. & Integrated Support Off.
Patuxent River, Maryland 20670
301 863-3111 ext 454

John Gleim, SEC 6101D
Naval Ships Engineering Center
Room 3613
Navy Department
Washington, D. C. 20360

Truman D. Glenn
Head, Tech. Unit
Code 1346 NDT-2, Bldg. 13
Charleston Naval Shipyard
Charleston, South Carolina 29408

Donald R. Glodoski
DSA DCRI-DMQ03
144 North 4th Street
Milwaukee, Wisconsin 53203

S. Goldspiel
U. S. Naval Applied Science Lab
Metallurgy Branch, Code 952
Flushing and Washington Ave.
Brooklyn, New York 11251

Robert A. Gould, Code 4582
Naval Weapons Center
China Lake, California 93555
Autovon 898 1700 ext 9358

John J. Gurtowski
Naval Air Systems Command
Washington, D. C. 20360
201 OXford 6-2158

Charles E. Haire
DCASR, Atlanta
Attn: DCRA-QES
3100 Maple Drive
Atlanta, Georgia 30314

MSgt. R. W. Hamilton
Andrews Air Force Base
Washington, D. C. 20331

B. Lyle Hansen
U.S.Army Cold Regions Research
and Engineering Laboratory
Hanover, New Hampshire 03755
Autovon 552-3470 ext 245

Alex Harrison, Jr.
P. O. Box 94
White Sands Missile Range
New Mexico 88002

Stephen D. Hart, Code 8430
U.S. Naval Research Laboratory
Washington, D. C. 20390
Autovon 851 3400 ext 613

Otis D. Hartley
Army Missile Command
Redstone Arsenal
AMSMI-RTR, Bldg. 7290
Alabama 35809
876-0217

Harold P. Hatch
AMMRC
Watertown, Massachusetts 02172
AMXMR-TMT
Autovon 956-1241

George N. Hathaway, Code 342
Supervisor of NDT
Sup-Ships Conversion & Repair
Newport News, Virginia 23607
247-1211 ext 8403

George F. Hazelton
Sikorsky Aircraft
Main Street
Stratford, Connecticut 06497

Col. Charles C. Heckel
Shaw Air Force Base,363 FMS
Sumter, South Carolina 29152

Paul J. Heger
Air Force Plant Representative
North American Aviation Autonetics
Anaheim, California 92803

Clen M. Henderson, Jr., Code 134
Metallurgy Section
Norfolk Naval Shipyard
Portsmouth, Virginia 23701

Harold D. Henry
NDI Laboratory
Vance Air Force Base
Enid, Oklahoma 73701

Howard Heffan, Code 60500
QE Laboratory
Naval Weapons Station
Concord, California 94520

Lindley E. Hiatt
Naval Tech. Representative
P. O. Box 157
Magna, Utah 84044

Charles H. Hickok, III
Army Materiel Command
Harry Diamond Labs
Quality Assurance Branch 740
Code AMXDO-ED-742, Bldg. 16-328
Washington, D. C. 20438
202 696-9957 Autovon 226-9957

W. Theodore Highberger, Code 52031
Metallurgist
Naval Air Systems Command
Navy Department
Washington, D. C. 20360

Jack L. Hile
University of California
Lawrence Radiation Laboratory
P. O. Box 808
Livermore, California 94550
415 447-1100, ext 7601

L. O. Hines, Code 303
Quality Assurance Branch
U.S.N. Ship Repair Fac (Guam)
F.P.O. San Francisco
California 96630

J. A. Holloway
Processing & NDT Branch MAMN
Air Force Materials Laboratory
Wright-Patterson Air Force Base
Ohio 45433

Robert L. Huddleston
STEAP-DS-EP
Aberdeen Proving Ground
Maryland 21005
301 278-3258

L. C. Huggard, Code 4003
Naval Ship Missile System
Port Hueneme, California 93041

Melvin H. Hughes
Attn: AMXNC-M
New Cumberland Army Depot
New Cumberland, Pennsylvania 17070

Warren W. Inglis
SMUFA Q3300
Inspection Equipment Branch
Quality Assurance Directorate
Frankford Arsenal
Philadelphia, Pennsylvania 19137
215 JE5 2900 ext 24123

Taylor H. Jefferson
Chief, Fuels Decontamination Br.
Mobility Equipment Research
and Development Center
Fort Belvoir, Virginia 22060
703 780-1100 ext 45746

Harry P. John
DCASR-QES.3
2800 South 20th Street
Philadelphia, Pennsylvania 19101
237 271-3574

James E. Johnson
Naval Air Rework Facility
Code 344, Bldg. 341
Naval Air Station, North Island
San Diego, California 92135
Autovon ext 67111

Abner I. Kayser
Weapons Engr. Standardization Off.
Naval Air Engineering Center
Philadelphia, Pennsylvania 19112
Autovon 243-3892

Harold S. Kean, Code 305
Quality Assurance Division
Philadelphia Naval Shipyard
Philadelphia, Pennsylvania 19112

Frank M. Kelly, Sr.
Head, NDT Branch, Code 134N
Metallurgical Division
Norfolk Naval Shipyard
Portsmouth, Virginia 23701
Autovon 555-1670 ext 2449

Gerald R. Kerins, QE-3
Naval Underwater Weapons
Research & Engineering Station
Newport, Rhode Island 02840

Alfred S. Kress
Army Tank-Automotive Command
AMSTA-QE
Warren, Michigan 48090

J. Fred Kreissig
Chief, P & M Division
Bldg. 722
Fort Detrick
Frederick, Maryland 21701

R. A. Lampi
Packaging Division
General Equipment and
Packaging Laboratory
U. S. Army Natick Labs.
Natick, Massachusetts 01760

Harvey B. Legrone
Quality Evaluation Laboratory
U. S. Naval Ammo. Depot
Oahu, Hawaii
FPO, San Francisco, Cal. 96612

Gene Link
OCNATB
Tinker Air Force Base
Oklahoma, 73145

John A. Lolo
DCAS, Baltimore
Fort Holabird, Maryland 21219

Joe H. Lopez
SWMMF Nondestructive Insp.
Kirtland Air Force Base
Albuquerque, New Mexico 87117

Regis J. Mack, Code TCN
Naval Ordnance Station
Indian Head, Maryland 20640
743-5511, ext 520

James L. Madara
1001 FMS(DMMFM)
Andrews Air Force Base
Washington, D. C. 20331

Alfred C. Malchiodi, Code 304G
Supervisor of Shipbuilding
Conversion and Repair
Groton, Connecticut 06340

Donald P. Manahan, Air 09H3A
Naval Air Systems Command
Engineering & Integrated
Support Office
Naval Air Station
Patuxent River, Maryland 20670

Charles E. Martens
AVCOM Maint. Engr. Division
Naval Air Station
Corpus Christi, Texas 78419
C/o AMSAV-EM

James G. Massey, Code 342A
Supervisor of Shipbuilding
Conversion and Repair
Newport News, Virginia 23607

Edward Matzkanin
STEYP-TTS
Yuma Proving Ground
Yuma, Arizona 85364

Louis T. Mazza
USA-AVLABS
Physical Sciences Division
Fort Eustis, Virginia 23604

Edward W. McKelvey
Air Force Materials Laboratory
Wright-Patterson Air Force Base
Ohio 45433

James M. McKinley
STEAP-DS-EP
Aberdeen Proving Ground
Aberdeen, Maryland 21005
278-3409

William J. McNair
Federal Aviation Administration
FS-300
800 Independence Avenue
Washington, D. C. 20590

William E. Medinger, Code 304
Supervisor of Shipbuilding
Conversion and Repair
Eastern Point Road
Groton, Connecticut 06340

Albert D. Meeks
Harry Diamond Labs
Quality Assurance Branch
Washington, D. C. 20438

LCDR. Roland O. Melcher
Repair Officer
USS Nereus AS-17
c/o FPO San Francisco
California 96601
Autovon 742-0111 ext 225-3209

Charles P. Merhib
Army Materials & Mechanics
Research Center
Attn: AMXMR-TMT
Watertown, Massachusetts 02172
Autovon 956-1265/1507

Milburn P. Meriwether
Maintenance Division DCSLOG
USA AVNC, Fort Rucker
Alabama 36360

Alfred R. Millien
Long Beach Naval Shipyard
Q/RA Department, Code 133N
NDT Supervisor
Long Beach, California 90801

Harry L. Millward, Jr.
Quality Assurance Division
Dir/QUAL (AMXNC-Q)
New Cumberland Army Depot
New Cumberland, Penna. 17070

Lawrence E. Moore
62 FMS/NDI Lab
McChord Air Force Base
Washington 98438
984 2014/2946

SSgt. Leister D. Moore
Tech. Sub. Section
U. S. Army Trans. School
Fort Eustis, Virginia 23604
878-5016

Louis J. Moore
Director of Technical Services
USA GETA
Fort Lee, Virginia 23801

R. E. Moore
Naval Ships Engineering Center
Navy Department
Washington, D. C. 20360

David M. Moses
DCAS-QES, Cameron Station
Alexandria, Virginia 22314

John J. Mozart
108th TFW NJANG
McGuire Air Force Base
New Jersey 08614
Attn: NDT Laboratory
Autovon 363-4157

Robert T. Muse
USA GETA
Fort Lee, Virginia 23801
734-4424

Daniel E. Negola, Code KR
National Aeronautics and
Space Administration, Hqs.
Washington, D. C. 20546
WO 2-4932

John Neuner, Jr.
Naval Plant Rep. Office
Westinghouse Defense
and Space Center
P. O. Box 746
Baltimore, Maryland 21203
301 765-3055

Salvatore A. Norod
Attn: SMUPA-I, Bldg. 6
Picatinny Arsenal
Dover, New Jersey 07801

LtCdr. William O'Halloran
Naval Ships Systems Command
Washington, D. C. 20360

Milton S. Orysh, Code 6765
Head, Radiographic Branch
Naval Ships Engr. Center
Philadelphia, Penna. 19112
Autovon 243-3922

James F. Pack
Arnold Engr. Dev. Center
ARO Inc.
Arnold Air Force Station
Tennessee 37389

Jay S. Pasman
NRD, QAD, Bldg. 65
Picatinny Arsenal
Dover, New Jersey 07801

John H. Penrose
SWEWV-QAR
Watervliet Arsenal
Watervliet, New York 12189

Earl H. Pergande
Chief, DMQE
DCASD, Milwaukee
744 N. 4th Street
Milwaukee, Wisconsin 53202
Autovon 551-3640

Albert J. Perry
Federal Aviation Administration
800 Independence Avenue
Washington, D. C. 20590

Ralph A. Petraglia
Materials Laboratory
Bldg. 34, Code 134
Boston Naval Shipyard
Boston, Massachusetts 02129
617 242-1400 ext 691/692

Kee J. Pon
Naval Ships Engineering Center
Code 6101D
Navy Department
Washington, D. C. 20360
OX 6-4226

Edward A. Reulecke
Attn: AMXGC-QA
Granite City Army Depot
Granite City, Illinois 62040

Carl A. Rich
Harry Diamond Labs
Quality Assurance Branch
Washington, D. C. 20438

Ernest H. Rodgers
Army Materials & Mechanics
Research Center
Attn: AMXMR-TMT
Watertown, Massachusetts 02172
Autovon 956-1113/1356

Eugene Roffman, N3100 202-1
Frankford Arsenal
Philadelphia, Penna. 19137
578-3300 x5112

Bernard Rosenbaum
Naval Ships Systems Command
Navy Department
Washington, D. C. 20360

Saul Schiff, SMUPA-DA-2
Anti-Armor Section, AMAL
Bldg. 351
Picatinny Arsenal
Dover, New Jersey 07801

Paul Schindler, SMUPA-DC5
Picatinny Arsenal
Dover, New Jersey 07801

William R. Schmechel, Code 304A
Supervisor of Shipbuilding
Conversion and Repair USN
Eartern Point Road
Groton, Connecticut 06340

Donald F. Schlosman
Defense Contracts Admin.
Service District, DCRP-DRQE
750 Penn Street
Reading, Pennsylvania 19602

Alfred E. Schnell
Technical Division, Code 1035
Naval Supply Center
Norfolk, Virginia 23512

Ltjg. Victor D. Segal
USS Nereus (AS-17)
NDT Officer, Repair Dept.
c/o FPO San Francisco
California 96601
Autovon 742-0111

F. Kent Serkland (AMSWE-QAT)
Chief, Test Evaluation &
Data Analysis Division
U. S. Army Weapons Command
Rock Island Arsenal
Rock Island, Illinois 61201

Stephen Sharan
Naval Plant Rep. Office, Bethpage
c/o Grumman Aircraft Engr. Corp.
Quality Assurance QAME, Plant 35
Bethpage, New York 11714

Louis Shaywitz
U. S. Army Aviation Command
RD&E Directorate AMSAV-EGSM
12th and Spruce Streets
Saint Louis, Missouri 63103

Richard S. Shelor
Production & Maintenance Div.
Department of the Army
Fort Detrick
Frederick, Maryland 21701

George E. Smeltzer
DCAS AMF York
Metal Treatment Processes
York, Pennsylvania 17405

David E. Smith
Code 6101D
Naval Ship Engineering Center
Navy Department
Washington, D. C. 20360
OS 6 4224

James T. Smith, Code QE.2
NDT Coordinator
DCAS Reading
750 Penn Street
Reading, Penna. 19601
215 374-5194 ext 249

Lt. Howard W. Sorenson
Asst. Repair Officer
USS Bushnell (AS-15)
Key West, Florida 33040
Autovon 899-3400 ext 526

John J. Spicer, Jr.
GE-DCASO Rm. 2455
3198 Chestnut Street
Philadelphia, Penna 19104

Joseph Stea
Philadelphia Naval Shipyard
Philadelphia, Penna. 19112

David Stein
SMUPA-ND1
Quality Assurance Directorate
Picatinny Arsenal
Dover, New Jersey 07801
201 328-2123

Michael L. Stellabotte
Code MAMM
Naval Air Development Center
Johnsville, Warminister
Pennsylvania 18974
Autovon 243-3580

William Stuart, SNEWV-QA
Chief, QAO
Watervliet Arsenal
Watervliet, New York 12189

James L. Studdard
U. S. Army Missile Command
Attn: AMCPM-LCC
Redstone Arsenal
Alabama 35809
Autovon 266-5211

Johnny W. Summey
Head NDT Branch, Code 135A
Bldg. 18
Portsmouth Naval Shipyard
Portsmouth, New Hampshire 03808
Autovon 881-1550 ext 1380/1369

Alan S. Tetelman*
Deputy Director Matl. Sciences
ARPA
Office of Asst. Secy of Defense
Washington, D. C. 20301

Caspar Tootgooshian
GE-DCASO
3198 Chestnut Street
Philadelphia, Penna. 19104

Frederick Thompson
Physical Lab Branch
Inspection Operations Div.
Edgewood Arsenal
Edgewood, Maryland 21010

Col. F. N. Thompson
Seymour Johnson Air Force Base
North Carolina 27530

John G. Turbitt, Code 335
Naval Torpedo Station
Keyport, Washington 98345
Autovon 554-1510 ext 8873

Capt. Elee W. Tyler
Hq. ATC (ATMME-A)
Randolph Air Force Base
Texas 78248

Eleanor Th. Vadala
Aero. Materials Department
Naval Air Development Center
Johnsville
Warminister, Penna. 18974

E. J. VanArnhem
U. S. Army Materiel Command
Bldg. T-7, Rm 2440
AMCQA-E
Washington, D. C. 20315

Howard B. Ward, DSQ
Defense Contract Admin Services
4297 Pacific Highway
San Diego, California 92110
714 225-4275

Hartwell K. Webber
USA ECOM, P&P Directorate
Fort Monmouth, New Jersey 07703

*Did not attend

John M. Wenke 09H33D
Naval Air Systems Command
Engr. & Integrated Support Off.
Naval Air Station
Patuxent River, Maryland 20670
Autovon 555-1660 x7806

E. J. Wheelahan
AMSMI-RSM
U. S. Army Missile Command
Redstone Arsenal, Alabama 35809
205 876-6628

Lt. D. D. Whitney
64th TAW (DMM)
Stewart Air Force Base
Tennessee 37168
Autovon ext 4201

W-1 Clark D. Yates
USS Bushnell (AS-15)
c/o FPO New York
New York 09501

Additional Distribution List - Minutes 16th DOD Conference on NDT

Cdr. R. L. Abbott
Naval Air Development Center
Johnsville
Warminister, Penna. 18974

John Atzberger, QAMP
Naval Plant Rep. Office
Sperry Gyroscope Company
Great Neck, Long Island
New York 11020

George Compton, SP 27422
Special Projects Office
Navy Department, Rm 3337
Washington, D. C. 20360

Anthony F. Chaikowski
Logistic Ship Project
Naval Ship Engineering Center
Navy Department
Washington, D. C. 20360

Alden P. Cowles
Naval Air Systems Command
Navy Department
Washington, D. C. 20360

SSgt. Robert Dubiel
Andrews Air Force Base
Washington, D. C. 20331

John B. Ferguson
Harry Diamond Labs
Washington, D. C. 20438

E. H. Garrett
Naval Ships Engineering Center
Navy Department
Washington, D. C. 20360

Furman Hare
Andrews Air Force Base
Washington, D. C. 20331

John W. Harrop
Naval Underwater Weapons
Research & Engr. Station
Newport, Rhode Island 02840

Holger Hellemalm
Logistic Ship Project
Naval Ships Engineering Center
Navy Department
Washington, D. C. 20360

Richard D. Klinedinst
Harry Diamond Labs
Washington, D. C. 20438

Peter R. Kosting
Army Materiel Command
Washington, D. C. 20315

Theresa M. Lavelle
N5100-201-3
Frankford Arsenal
Philadelphia, Penna. 19137

Bernard A. Litchfield
Harry Diamond Labs
Washington, D. C. 20438

Howard H. Lebo
Andrews Air Force Base
Washington, D. C. 20331

Homer L. Manning
Andrews Air Force Base
Washington, D. C. 20331

S. Matesky, ORD-0333
Naval Ordnance Systems Command
Navy Department, Rm 2223
Washington, D. C. 20360

Gene Morin
Logistic Ship Project
Navy Department
Washington, D. C. 20360

Robert E. Muncy, Jr.
Chanute Air Force Base
Illinois 61866

Robert S. Norte
Naval Air Systems Command
Navy Department
Washington, D. C. 20360

Fred J. Peck, Jr.
Federal Aviation Administration
800 Independence Avenue
Washington, D. C. 20590

W. B. Powell
Supervisor of Shipbuilding
Conversion and Repair Facility
New Orleans, Louisiana 70140

John D. Powers
Naval Underwater Weapons
Research & Engineering Station
Newport, Rhode Island 02840

TSgt. James W. Reinke
Andrews Air Force Base
Washington, D. C. 20331

Leo F. Risko
Naval Underwater Weapons
Research & Engineering Station
Newport, Rhode Island 02840

TSgt. Roland H. Roy
Andrews Air Force Base
Washington, D. C. 20331

Ira Smith
Harry Diamond Labs
Washington, D. C. 20348

William J. Williams
Harry Diamond Labs
Washington, D. C. 20348

J. P. Zaluski
Naval Air Systems Command
Representative Atlantic
U. S. Naval Air Station
Norfolk, Virginia 23511

Commander
Hq 140th Tactical Fighter Gr.
Buckley Air National Guard Base
Colorado
Attn: Major V. T. Marooney, DMM

Commander
Hq Military Airlift Command
Scott Air Force Base, Illinois 62225
Attn: LtCol. A. L. Littman MAMMEAA

Everett C. Iverson, TSDT
3345th Tech. Training School
Chanute Air Force Base
Illinois 61866

Commander
Hq Strategic Air Command
Offutt Air Force Base
Nebraska 68113
Attn: AM4B (Major Nokes/5001)

Ralph M. Morstad
Chief, Quality Assurance Div.
U.S. Army Maintenance Plant Mainz
APO New York 09185
Attn: AEZMZ-Q

Commander
Hq Air Force Contract Management
Division (AFSC)
Air Force Unit Post Office
Los Angeles, California 90015
Attn: R. E. Meoli, CMQE

Commander
Hq Tactical Air Command
Langley Air Force Base
Virginia 23365
Attn: LtCol. J. I. Cottle
DMEMS

M. Greenstine, Chief
Quality Assurance Engr. Div.
DSASR, P. O. Box 7478
Philadelphia, Penna. 19101

Commander
Hq OCAMA (AFLC)
Tinker Air Force Base
Oklahoma 73145
Attn: Albert R. Snawder OCM

Commander
Naval Air Maintenance Group
Naval Air Station (71)
Memphis, Tennessee 38115
Attn: TRBD-G. T. Maxwell

Commanding Officer
U.S.Army Training School
Fort Eustic, Virginia 23604
Attn: Col. T. A. Roller

Commanding Officer
DCASO-FMC Corp.
P. O. Box 367
San Jose, California 95103
Attn: W. L. Perry, DCRC-RFQ

Commander
Hq 3525th Pilot Training Wing (ATC)
Williams Air Force Base
Arizona 85224
Attn: MCM(386) LtCol. R. J. Hubka

Commander
Pearl Harbor Naval Shipyard
Box 400
FPO San Francisco 96610
Attn: K. F. Casey

Supervisor of Shipbuilding
Conversion and Repair
USN Ninth Naval District
Bay City, Michigan 48706
Attn: R. N. Anger

Col. James R. Mills, Jr.
Northwest Procurement Agency
U. S. Army
P. O. Box 1029
Oakland, California 94604

Asaf Benderly
Harry Diamond Laboratories
Washington, D. C. 20438

M. L. Budnick, AMXRE-AS
U. S. Army Natick Labs
Natick, Massachusetts 01760